JOHANNES GUTENBERG UNIVERSITÄT MAINZ

Deconstructing the Proximate Drivers of the Germline Mutation Rate in *Chironomus riparius*

Dissertation

Zur Erlangung des Grades

Doktor der Naturwissenschaften

Am Fachbereich Biologie

Der Johannes Gutenberg-Universität Mainz

Burak Bulut

geb. am 18.08.1995 in İstanbul

Mainz, 2026

Tag der mündlichen Prüfung: 15/06/2026

Dekan: Prof. Dr. Eckhard Thines

1. Berichterstatter: Prof. Dr. Markus Pfenninger

2. Berichterstatter: Prof. Dr. Thomas Hankeln

Tag der mündlichen Prüfung:

To the eyes of Darwin; the eyes that seek knowledge before they can bear the beauty of a peacock's feather.

Table of Contents

Table of Figures

Zusammenfassung

Mutationen entstehen im Kern als zufällige Fehler in den normalerweise hochpräzisen Prozessen der DNA-Replikation und -Reparatur. Dadurch verändert sich die Primärsequenz der genetischen Information eines Organismus. Diese Fehler reichen von einzelnen Nukleotidsubstitutionen bis hin zu großflächigen Chromosomenumlagerungen. Sie haben vielfältige Ursachen: Endogene Ursachen umfassen spontane chemische Instabilitäten der DNA-Basen und Schäden durch Stoffwechselprodukte wie reaktive Sauerstoffspezies; exogene Ursachen sind beispielsweise Umweltmutagene wie chemische Produkte. Aus evolutionärer Sicht stellt diese molekulare Unvollkommenheit ein zweischneidiges Schwert dar: Sie ist die einzige Quelle neuer genetischer Variationen, die die Anpassung antreibt. Gleichzeitig sind die meisten phänotypverändernden Mutationen schädlich und belasten die Fitness kontinuierlich, was biologische Funktionen beeinträchtigen kann. Angesichts dieser ständigen Bedrohung durch Degradation haben Organismen komplexe und energieintensive Korrektur- und Reparaturmechanismen entwickelt. Die Tatsache, dass alle Keimbahnmutationen an die nächste Generation weitergegeben werden, unterstreicht, dass diese Systeme nicht unfehlbar sind und ihre Wirksamkeit durch interne und externe Faktoren beeinträchtigt werden kann.

Die Rate, mit der diese Fehler in der Keimbahn auftreten (die Mutationsrate), ist ein fundamentaler Parameter der Evolutionsbiologie. Historisch gesehen wurde die Mutationsrate als relativ stabile, artspezifische Konstante betrachtet. Dieses Paradigma wurde jedoch durch ein differenzierteres Verständnis, die Drift-Barriere-Hypothese, abgelöst. Diese besagt, dass die Mutationsrate ein evolvierbares Merkmal ist, dessen untere Grenze durch die Stärke der natürlichen Selektion im Verhältnis zur genetischen Drift begrenzt wird. Diese moderne Sichtweise wurde durch das Aufkommen von Mutationsakkumulationslinien-Experimenten in Verbindung mit der Sequenzierung des gesamten Genoms ermöglicht. Diese erlauben die direkte, unverzerrte Schätzung von Mutationsraten und -spektren und haben das Feld von indirekten Schlussfolgerungen zu direkten empirischen Messungen geführt.

Eine zentrale Herausforderung in der Mutationsratenforschung besteht darin, dass die wichtigsten unmittelbaren Einflussfaktoren auf die Plastizität der Mutationsrate typischerweise isoliert untersucht werden, wodurch die Auswirkungen von Störvariablen unberücksichtigt bleiben. Diese Dissertation schließt diese Lücke durch eine gezielte, mehrstufige Dekonstruktion der Mutationsrate in der Modellzuckmücke Chironomus riparius. Dabei werden die Beiträge intrinsischer Lebenszyklusbeschränkungen, natürlicher Umweltfaktoren und anthropogener Stressoren systematisch getrennt betrachtet. Durch den Aufbau eines hierarchischen Rahmens, ausgehend von der intrinsischen biologischen Basislinie bis hin zu zunehmend komplexen Umweltbelastungen, geht diese Arbeit über monofaktorielle Erklärungen hinaus und entwickelt ein mechanistisch fundiertes, vielschichtiges Verständnis der Mutagenese.

In Kapitel 1 habe ich durch die Auswahl von Individuen an den Extremen der natürlichen Generationszeitverteilung unter konstanten thermischen Bedingungen gezeigt, dass das Entwicklungstempo ein Mutationsminimum bei der häufigsten Generationszeit der Population erzeugt, wo replikationsabhängige und zeitabhängige mutagene Kräfte gemeinsam minimiert werden. In Kapitel 2 isolierte ich direkt den thermischen Effekt auf das endogene oxidative Milieu und zeigte ein U-förmiges ROS-Profil entlang des ökologisch relevanten

Temperaturgradienten. Ich konnte nachweisen, dass extreme Kälte und Hitze mechanistisch unterschiedliche oxidative Belastungen darstellen, die zusammensetzungsspezifische antioxidative Reaktionen erfordern. Kapitel 3 stellt diesen natürlichen Faktoren einen anthropogenen gegenüber und zeigt, dass chronische BaP-Exposition die Mutationsrate in der Keimbahn erhöht und die Fitness über einen ROS-unabhängigen Adduktionsweg reduziert, für den sich über drei Generationen keine adaptive Toleranz entwickelte.

Ich integrierte diese Ergebnisse in der Allgemeinen Diskussion unter drei konzeptionellen Themen. Abschnitt 1 synthetisiert Kapitel 1 und Kapitel 2 und schlägt die Hypothese der „Konvergenz von Optima“ vor. Diese besagt, dass die Mutationslast in einem ökologischen Fenster minimiert werden kann, in dem die Wirkung mehrerer unabhängiger mutagener Faktoren gleichzeitig reduziert ist. Abschnitt 2 analysiert die molekularen Fingerabdrücke verschiedener mutagener Faktoren, indem er die Ergebnisse aus Kapitel 1, Kapitel 2 und Kapitel 3 zusammenführt und zeigt, dass unterschiedliche Stressoren charakteristische molekulare Signaturen erzeugen. Abschnitt 3 vergleicht die Reaktionen von Organismen auf wiederkehrende und neuartige Selektionsdrücke und zeigt so eine grundlegende Asymmetrie in der evolutionären Kapazität auf.

Diese Dissertation schließt die Lücke zwischen den durch die Drift-Barriere definierten evolutionären Beschränkungen und den proximaten Mechanismen, die die tatsächliche Mutationsrate in der Natur bestimmen. Um die Variation der Mutationsrate zu verstehen, ist es letztlich notwendig zu wissen, warum sie entsteht, wie sie über unabhängige molekulare Mechanismen wirkt und welche Populationen am stärksten betroffen sind, wenn die Evolutionsgeschichte keine optimierte Verteidigung bietet.

Summary

At its most fundamental level, mutation originates as a random error in the general and overall high-fidelity processes of DNA replication and repair, altering the primary sequence of an organism's genetic information. These errors can range from single nucleotide substitutions to large-scale chromosomal rearrangements. They arise from multiple sources: endogenous sources include spontaneous chemical instabilities in DNA bases, damage from metabolic by-products like reactive oxygen species, and exogenous sources including environmental mutagens such as chemical products. From an evolutionary perspective, this molecular imperfection represents a profound double-edged sword: it is the sole source of the novel genetic variation that fuels adaptation, yet the vast majority of phenotype altering new mutations are deleterious, imposing a constant fitness load that can disrupt biological function. Given this constant threat of degradation, organisms have evolved complex and energy-intensive proofreading and repair pathways. The fact that all germline mutations persist to be passed to the next generation underscores that these systems are not infallible, and their efficacy can be compromised by both internal and external factors.

The rate at which these errors occur in the germline (the mutation rate) is a fundamental parameter in evolutionary biology. Historically, the mutation rate was treated as a relatively stable, species-specific constant. This paradigm, however, has been superseded by a more nuanced understanding, the Drift-Barrier hypothesis, which posits that the mutation rate is an evolvable trait whose lower limit is constrained by the power of natural selection relative to genetic drift. This contemporary view was made possible by the advent of mutation accumulation lines experiments coupled with whole-genome sequencing, which allow for the direct, unbiased estimation of mutation rates and spectra, moving the field from indirect inference to direct empirical measurement.

A primary challenge in mutation rate research is that the key proximate drivers of mutation rate plasticity are typically studied in isolation, failing to resolve the effects of confounding variables. This dissertation addresses this gap through a targeted, multi-stage deconstruction of the mutation rate in the model non-biting midge *Chironomus riparius*, systematically partitioning the contributions of intrinsic life-history constraints, natural environmental modulators, and anthropogenic stressors. By building a hierarchical framework from the intrinsic biological baseline outward to increasingly complex environmental challenges, this work moves beyond single-factor explanations toward a mechanistically grounded, multi-layered understanding of mutagenesis.

By selecting individuals at the extremes of the natural generation time distribution under constant thermal conditions, in **Chapter 1** I demonstrated that developmental tempo creates a mutational minimum at the population's modal generation time, where replication-dependent and time-dependent mutagenic forces are jointly minimized. In **Chapter 2** I directly isolated the thermal effect on the endogenous oxidative environment, demonstrating a U-shaped ROS profile across the ecologically relevant thermal gradient and revealed that cold and heat extremes impose mechanistically distinct oxidative challenges requiring composition-specific antioxidant responses. **Chapter 3** contrasts these natural drivers with an anthropogenic one, showing that chronic BaP exposure elevates the germline mutation rate and reduces fitness through a ROS-independent adduction pathway, for which no adaptive tolerance emerged over three generations.

I integrated these findings under three conceptual themes in the General Discussion. **Section 1** synthesises **Chapter 1** and **Chapter 2** to propose a "Convergence of Optima" hypothesis, suggesting that mutational load may be minimized in an ecological window where the effect of

multiple independent mutagenic drivers are simultaneously reduced. **Section 2** deconstructs the molecular fingerprints of distinct mutagenic drivers by synthesizing the findings from **Chapter 1**, **Chapter 2,** and **Chapter 3**, demonstrating that different stressors generate characteristic molecular signatures. **Section 3** contrasts organismal responses to recurrent versus novel selective pressures, demonstrating fundamental asymmetry in evolutionary capacity.

This dissertation bridges the gap between the ultimate evolutionary constraints defined by the Drift-Barrier and the proximate mechanistic drivers that determine the realised mutation rate in nature. Ultimately, understanding mutation rate variation requires knowing why it arises, how it operates across independent molecular pathways, and which populations are most exposed when evolutionary history provides no optimised defence.

General Introduction

1. Foundational Role of Mutation in Evolution

1.1. Mutation as the Ultimate Source of Genetic Variation

Mutation is a fundamental biological process defined as a permanent, heritable alteration to the nucleotide sequence of an organism's genome (Crow, 1970). For these alterations to be evolutionarily significant, they must occur in the germline, allowing for their transmission to subsequent generations. This distinguishes them from somatic mutations, which are restricted to the individual and do not contribute to the heritable variation of a population (Lesecque et al., 2012). As the sole process that generates novel alleles, germline mutation provides the essential raw material upon which evolutionary forces such as natural selection and genetic drift act. The process is inherently stochastic with respect to fitness; mutations do not arise in response to an organism's needs but rather provide a random spectrum of genetic possibilities that is the prerequisite for all adaptive change (Raynes and Sniegowski, 2014).

The spectrum of mutational events is vast, encompassing a range of molecular scales. The most frequent are small-scale events, primarily single base substitutions where one nucleotide is replaced by another (Sniegowski et al., 2000). These are further classified as transitions (purine to purine or pyrimidine to pyrimidine) or transversions (purine to pyrimidine or pyrimidine to purine). Small insertions and deletions (indels) also contribute significantly to variation and can cause frameshifts within coding regions or disrupt key functional elements, such as splice sites, in non-coding DNA (Eyre-Walker et al., 2006). At the broadest scale are large-scale structural variations, such as chromosomal duplications, deletions, inversions, and translocations (Agarwal et al., 2023). These substantial rearrangements can have profound phenotypic consequences by altering gene dosage, disrupting gene function, modifying regulatory architecture, or creating novel gene fusions. These alterations arise from a combination of endogenous sources, such as errors in DNA replication and repair, and exogenous sources, such as environmental mutagens (Maki, 2002). This continuous influx of variation, from the smallest point mutation to the rearrangement of entire chromosome arms, is the foundational prerequisite for evolution.

1.2 The Evolutionary Paradox of Mutation: A Double-edged Sword

1.2.1 The Cost of Mutation

While mutation is the indispensable engine of adaptation, it presents a profound evolutionary paradox. Organisms are complex, highly integrated systems whose genetic architecture has been optimised by long-term natural selection for robust physiological function. Consequently, random perturbations to this architecture are statistically far more likely to disrupt function than to improve it (Eyre-Walker et al., 2006). The direct consequence is that the vast majority of new mutations with discernible phenotypic effects are deleterious, ranging from mildly detrimental to unconditionally lethal (Keightley and Lynch, 2003).

This constant, unavoidable influx of harmful alleles imposes a persistent fitness burden on populations, a concept formalized as mutational load (Agrawal and Whitlock, 2012; Haldane, 1937). Mutational load quantifies the proportional reduction in a population's mean fitness relative to a hypothetical, mutation-free genotype. This load, arising from the continuous input of new deleterious

mutations, is a primary component of the broader "genetic load" and represents one of the most persistent evolutionary challenges faced by all organisms (Baer et al., 2007; Lynch et al., 1999). This inescapable burden establishes a powerful and persistent selective pressure, the response to which has fundamentally shaped the evolution of molecular systems.

1.2.2 Genomic Defence: The Architecture of DNA Repair

In response to the persistent selective pressure imposed by mutational load, organisms have evolved a sophisticated and multi-layered defence system dedicated to maintaining genomic integrity (Marteijn et al., 2014). These DNA repair pathways are among the most ancient and conserved cellular mechanisms, with origins tracing back to the “Last Universal Common Ancestor”, underscoring their fundamental importance (Aravind et al., 1999; Makarova et al., 1999). Life has responded not by eliminating mutation entirely but by evolving complex, energy-intensive molecular machinery to minimize its rate.

The first line of defence is intrinsic to the process of DNA replication. DNA polymerases possess a 3' to 5' exonuclease (proofreading) activity that detects and excises mis-incorporated nucleotides, increasing replication fidelity by several orders of magnitude (Kunkel, 2004a). For errors that escape this initial surveillance, or for damage arising from other sources, a suite of dedicated repair pathways exists. The mismatch repair (MMR) system scans newly synthesised DNA to correct base-base mismatches and small indels (Kunkel and Erie, 2015). To counteract DNA damage, pathways such as base excision repair (BER) remove single damaged bases, nucleotide excision repair (NER) removes bulkier lesions, and homologous recombination (HR) provides high-fidelity repair for double-strand breaks (Hoeijmakers, 2001).

The construction, maintenance, and operation of this entire enzymatic arsenal represent a significant energetic investment (Lynch, 2012). This significant metabolic expenditure underscores that genomic fidelity is a complex, multi-component trait under strong selective maintenance, purchased at a high cellular cost.

1.2.3 Constraints on a Zero Mutation Rate

Despite the remarkable sophistication of these genomic maintenance systems, they remain inherently imperfect, ensuring that a non-zero mutation rate persists across all life. This imperfection arises from fundamental physical and cellular constraints that operate at two distinct levels. First, at the molecular level, DNA polymerases and repair enzymes face inherent kinetic constraints rooted in the biophysics of kinetic proofreading (Kunkel, 2004b). The chemical mechanisms governing nucleotide discrimination operate through multiple sequential checkpoints, each requiring finite time for thermodynamic discrimination between correct and incorrect base pairs (Hopfield, 1974). This creates an unavoidable speed-accuracy trade-off: achieving higher fidelity demands slower catalysis to allow sufficient time for proofreading steps, while rapid replication necessarily reduces discrimination time and increases error rates. These intrinsic error rates cannot be eliminated without severely reducing catalytic speed to levels incompatible with cellular function. Second, at the cellular level, genomic fidelity systems impose substantial metabolic costs (Lynch, 2011). DNA replication and repair machinery consume an estimated ~2-10% of total cellular energy budgets in rapidly dividing cells (Lynch and Marinov, 2015), and the material investment required to build and maintain increasingly sophisticated repair pathways eventually outweighs the fitness benefit gained from marginal improvements in accuracy. Together,

these physical and metabolic constraints ensure that mutation rates remain above zero even under strong purifying selection.

Beyond these metabolic and kinetic constraints, a non-zero mutation rate is an evolutionary necessity (Sniegowski et al., 2000). A hypothetical organism with perfect DNA repair (i.e., $\mu = 0$) would have a mutation rate of zero, effectively halting the input of new genetic variation. While this would maximise current fitness by eliminating the mutational load, it would create an evolutionary dead end, leaving the population with no capacity to adapt to future environmental changes (evolvability) (Kirschner and Gerhart, 1998).

Therefore, the persistence of mutation is the result of a complex balance. The effectiveness of DNA repair is not maximised but is instead optimised to a point where the benefits of maintaining current genomic integrity are weighed against the costs of repair and the long-term necessity of generating novel variation (de Vries, 1914). It is this small but persistent stream of mutations, escaping the grasp of even the most efficient repair systems, that ensures the raw material for evolution is never fully exhausted.

2. The Evolving Concept of the Mutation Rate

The spontaneous mutation rate (μ), which quantifies the rate at which new mutations arise per unit of time (e.g., per site per generation), is one of the most fundamental parameters in evolutionary biology (Baer et al., 2007). As the ultimate source of all genetic variation, this rate dictates the amount of raw material available for natural selection and genetic drift, thereby setting the pace for adaptation and evolutionary change. In contrast, given that the vast majority of mutations with phenotypic effects are deleterious, μ also determines the constant influx of harmful alleles that imposes a mutational load on populations (Lynch et al., 1999). Consequently, understanding the forces that govern this critical parameter has been a central goal of the field, and its conceptualisation has undergone a profound transformation, from a static constant to a dynamic and evolvable trait.

2.1 Classical View of μ: A Species-Specific Constant

The modern, dynamic view of the mutation rate represents a significant shift from earlier paradigms. The intellectual groundwork for treating mutation rate as a measurable parameter was laid by the classic experiment of Luria and Delbrück (1943), which addressed whether mutations arise spontaneously or as a directed response to environmental pressures (Luria and Delbrück, 1943). Their landmark fluctuation test demonstrated that resistance mutations arise spontaneously and randomly before any selective pressure is applied. This established the fundamental principle of mutation as a stochastic, undirected process, yet one that could be treated as a measurable statistical parameter at the population level.

This concept was later integrated into a powerful theoretical framework by Motoo Kimura with his Neutral Theory of Molecular Evolution (Kimura, 1983, 1968). Kimura proposed that the vast majority of evolutionary change at the molecular level is driven by the random genetic drift of selectively neutral mutations. A critical consequence of this theory is that for neutral alleles, the rate of substitution (the rate at which new variants become fixed in a population) is precisely equal to μ. This provided a profound theoretical link between the microevolutionary process of mutation and

macroevolutionary patterns, reinforcing the idea that a relatively constant rate of evolution implied a relatively constant underlying mutation rate.

Empirical support for this constant rate paradigm was synthesised by John Drake in 1991 (Drake, 1991). By surveying a diverse array of DNA-based microbes, Drake discovered a surprising consistency: the mutation rate per genome per replication was remarkably stable, clustering around a value of ~0.003. This observation, known as Drake's Rule, suggested that natural selection had driven mutation rates down to an evolutionarily optimised constant, reflecting a fundamental trade-off between the fitness costs of deleterious mutations and the metabolic costs of maintaining high-fidelity DNA replication and repair machinery. Within this consensus framework, μ was treated as a fixed parameter inversely correlated with genome size.

However, this classical paradigm faced a crisis of empirical inadequacy as genomic data accumulated from the 1990s onward. The assumption of constant rates was systematically violated by the discovery of massive mutation rate heterogeneity (Hodgkinson and Eyre-Walker, 2011). Rates were found to vary by orders of magnitude across different phylogenetic lineages, far exceeding what could be explained by genome size or physiological constraints. Crucially, studies revealed that multicellular eukaryotes maintain mutation rates substantially above Drake's constant and far above their apparent physiological minimums (Baer et al., 2007). Furthermore, mutation rates showed systematic correlations with life-history traits (e.g., generation time, fecundity, size at maturity, lifespan) and exhibited significant variation between species, populations, and even sexes within species (Kong et al., 2012; Martin and Palumbi, 1993), as well as substantial intra-genomic variation across chromosomes and genomic regions, demonstrating that μ is not a fixed constant but a highly flexible and plastic trait (Sung et al., 2012).

2.2 The Drift-Barrier Hypothesis

The systematic failure of the classical paradigm to account for the vast heterogeneity in mutation rates necessitated a new theoretical framework, which was provided by Michael Lynch's Drift-Barrier Hypothesis (Lynch, 2010; Lynch et al., 2016). While some prior studies had documented mutation rate variation across taxa (Kondrashov, 2003; Sniegowski et al., 2000), the Drift-Barrier hypothesis provided a unifying population-genetic framework that quantitatively predicted the equilibrium mutation rate based on the balance between natural selection and random genetic drift. This hypothesis posited that the lower limit of the mutation rate is determined not solely by physiological constraints, but fundamentally by the efficacy of selection relative to drift, which is inversely proportional to effective population size (N_e).

The hypothesis treats the mutation rate as a quantitative trait, where anti-mutator alleles that increase fidelity are beneficial due to the reduction in deleterious mutations. However, the key insight is that the fitness advantage conferred by each successive improvement in fidelity shows diminishing returns; as the mutation rate gets lower, the selective advantage of a slightly better anti-mutator allele becomes so small that it is effectively neutral. Eventually, as mutation rates decline and repair fidelity improves, the fitness advantage conferred by each successive anti-mutator allele becomes vanishingly small. When this advantage falls below a critical threshold ($s \approx 1/(2N_e)$), selection becomes too weak relative to drift to reliably fix beneficial alleles. This threshold, inversely proportional to N_e, constitutes the "drift barrier." In small populations (low N_e), this drift barrier is high: genetic drift dominates whenever $s \approx 1/(2N_e)$, meaning that selection cannot efficiently fix anti-mutator alleles unless their fitness benefit is large. In large populations (high N_e), the threshold is

low, allowing selection to detect and fix alleles with even tiny fitness advantages. Consequently, species with large effective population sizes, such as bacteria and unicellular eukaryotes, can evolve exceptionally low mutation rates, while multicellular eukaryotes with chronically smaller N_e equilibrate at mutation rates orders of magnitude higher (Lynch et al., 2016).

This paradigm changed the understanding of mutation rate variation across taxa. The central, testable prediction of the Drift-Barrier hypothesis is that per-nucleotide mutation rate should correlate negatively with effective population size across species. This prediction has been robustly supported by empirical data (Sung et al., 2012), explaining the patterns the classical paradigm could not. It clarifies why species with enormous effective population sizes, like bacteria, face a weak drift barrier and can evolve exceptionally low mutation rates. Conversely, it explains why most multicellular eukaryotes, with their chronically smaller effective population sizes, face a strong drift barrier and equilibrate at mutation rates orders of magnitude higher. The Drift-Barrier hypothesis thus provides the modern foundation for treating μ not as a fixed parameter, but as a dynamic, evolvable trait whose equilibrium is dictated by the population-genetic environment.

2.3 Direct Measurement of Mutation Rate

The paradigm shift from viewing μ as a static parameter to an evolvable trait was driven by a methodological revolution that moved the field from indirect inference to direct empirical measurement. Historically, mutation rates were estimated via indirect methods that fell into two main categories (Kondrashov and Kondrashov, 2010). The first approach used phylogenetic inference, which estimates mutation rates indirectly by calculating the rate of nucleotide substitutions between species over evolutionary time. This method assumes a molecular clock, which hypothesises that substitution rates remain approximately constant over time, and divides the observed sequence divergence by the estimated divergence time to infer the average mutation rate (Bromham and Penny, 2003). The second approach, pioneered by Luria and Delbrück and refined by Drake, employed phenotypic screens using reporter loci, specific genes (such as antibiotic resistance markers in bacteria or coat color loci in model organisms), where mutations produce easily scorable phenotypic changes (Drake, 1991; Luria and Delbrück, 1943). By counting the frequency of mutant phenotypes in large populations and applying fluctuation analysis, researchers could estimate mutation rates at these specific loci, which were then extrapolated to genome-wide rates. However, phylogenetic approaches suffer from a critical and unavoidable flaw: they measure substitution rates (the rate at which new mutations become fixed in a population) rather than the raw mutation rate (the rate at which all non-lethal mutations initially occur in the germline) (Bromham and Penny, 2003). Reporter loci methods are similarly biased, as they can only detect mutations with detectable phenotypic effects, missing the vast majority of silent and synonymous mutations (Bromham and Leys, 2005). This introduces a profound selection bias, as purifying selection systematically removes deleterious mutations, causing substitution rates to underestimate the true mutation rate. This created a fundamental attribution problem, making it impossible to disentangle observed rate variation caused by true differences in mutation from that caused by differences in selection intensity or demographic history.

The conceptual and technological breakthrough that resolved this impasse was the coupling of mutation accumulation (MA) experiments with whole-genome sequencing (WGS). The MA method involves propagating numerous parallel lineages through extreme, single-individual bottlenecks for many generations. This experimental design creates conditions where genetic drift becomes the overwhelming evolutionary force, rendering natural selection almost completely ineffective at

filtering out mutations. In standard MA experiments, where each generation passes through a single individual ($N_e \approx 1$), the power of drift is maximised. Under these conditions, mutations that would normally be eliminated by selection in natural populations which including mildly and moderately deleterious alleles can instead accumulate randomly via genetic drift, regardless of their fitness effects (Halligan and Keightley, 2009; Lynch et al., 2016). By uncoupling the process of mutation from the filtering effects of selection, MA lines allow nearly all non-lethal mutations to accumulate, providing an unbiased sample of the mutational spectrum that would be invisible to phylogenetic methods.

The MA experimental design itself predates genomic sequencing, but the advent of WGS transformed it into the modern gold standard by enabling the direct, unbiased detection of all mutations across the genome. By sequencing the genomes of the founding ancestor and the evolved MA lines, researchers can directly count the *de novo* mutations that have accumulated. This MA-WGS approach provides several critical advantages (Katju and Bergthorsson, 2019) over phylogenetic methods:

- Unbiased Rate Estimates: It measures the instantaneous mutation rate, free from the confounding filter of natural selection (Lynch et al., 2016).
- Complete Mutational Spectra: It captures the full spectrum of mutational events except the lethal mutations but including the deleterious mutations that would be purged in nature and thus are invisible to phylogenetic analysis (Keightley et al., 2009).
- Mechanistic Insight: It reveals characteristic mutational signatures (e.g., strand-specific patterns, context-dependent rates) that provide direct insights into the underlying molecular processes of mutation (Schrider et al., 2013; Uchimura et al., 2015).

This methodological advancement provided the high-resolution, unbiased data necessary to rigorously test modern hypotheses. By enabling direct measurement of the instantaneous mutation rate free from selection bias, MA-WGS made it possible to test the Drift-Barrier hypothesis's core prediction: a negative correlation between effective population size and per-site mutation rate across taxa (Lynch, 2010; Lynch et al., 2016). Empirical studies using this approach have robustly confirmed this prediction (Sung et al., 2012), while also revealing the true extent of mutation rate heterogeneity and plasticity, cementing the modern paradigm of μ as a dynamic, evolvable, and environmentally responsive trait.

3. Mechanistic Drivers of Mutation Rate Plasticity

The Drift-Barrier hypothesis provides a powerful population-genetic framework for understanding the ultimate evolutionary equilibrium of the mutation rate, explaining broad-scale patterns of variation across the tree of life. However, this paradigm treats μ as a unified parameter and does not, by itself, detail the proximate molecular and physiological processes (Wei et al., 2022). To understand the observed plasticity of this trait, it is necessary to deconstruct it into its component drivers. The logical starting point for this deconstruction is to establish the baseline mutation rate governed by intrinsic drivers inherent to an organism's life history and developmental strategy (Martin and Palumbi, 1993; Thomas et al., 2010). Only after this intrinsic baseline is characterised can the modulatory effects of extrinsic factors, such as natural environmental variables and anthropogenic pressures, be accurately contextualized and assessed.

3.1 Intrinsic drivers: Life-History and the Replication-Time Damage

Beyond the Drift-Barrier constraint, the realised mutation rate in any organism at any moment is shaped by proximate mechanistic forces. These forces arise from the fundamental biological processes required for development, survival, and reproduction (Roff and D. A., 2002; Stearns and S. C., 1992). Generation time, a core life-history parameter and physiological constraint, is subject to two simultaneous mutagenic components: replication-dependent errors that scale with the number of cell divisions, and time-dependent damage that accumulates as a function of chronological exposure (Maki, 2002). These forces exert distinct pressures on the germline, yet experimentally disentangling their relative contributions has remained a major challenge.

It is critical to distinguish between physiological constraints and environmental stressors when discussing mutagenic drivers. Physiological constraints (such as generation time and cell cycle dynamics) are intrinsic properties of the organism's developmental program (Sniegowski, 1997), whereas environmental stressors (such as temperature extremes and chemical pollutants) are extrinsic challenges imposed by external conditions (Bickham et al., 2000; Nauman et al., 1978). Generation time is not a stressor acting upon the organism but rather a life-history parameter that reflects the organism's evolved developmental strategy under selection.

3.1.1 Replication-Dependent Mutagenesis and the Generation Time Effect

The first intrinsic mechanism governing mutation rate plasticity is replication-dependent mutagenesis, formalized as the Generation Length Hypothesis (GLH) (Douzery et al., 1995; Ohta, 1992). This model posits that because germline mutations arise primarily from copy errors during DNA replication, organisms with shorter generation times (which require more cell divisions per unit of time) will exhibit a higher mutation rate per year (Martin and Palumbi, 1993). This prediction arises from the fundamental observation that DNA polymerase errors occur at each replication cycle, meaning the total mutational burden scales with the number of germline cell divisions (Coop et al., 2008).

The proximate mechanism underlying replication-dependent mutagenesis is the speed-fidelity trade-off in DNA replication itself (Fitzsimmons et al., 2018). This trade-off is rooted in the biophysics of kinetic proofreading: high-fidelity DNA polymerases perform multiple, sequential quality control steps, each of which requires a finite amount of time (Kunkel, 2004b). At the organismal level, rapid development compresses the cell cycle, particularly the S-phase (DNA synthesis phase), which in turn reduces the time available for these proofreading mechanisms to operate effectively. This temporal pressure can increase polymerase error rates and allows more misincorporated bases to escape post-replicative MMR surveillance before being fixed as permanent mutations (Lynch, 2010).

The GLH therefore predicts that rapid development will lead to a higher mutation rate per unit of time (μ/day or μ/year) and may produce a distinct mutational signature biased towards replication-associated errors (Niccum et al., 2018). Specifically, transition mutations (A↔G, C↔T) preserve Watson-Crick-like purine-pyrimidine geometry because both purines and both pyrimidines share similar base sizes, causing minimal helical distortion. In contrast, transversions (purine to pyrimidine) introduce major geometric distortions that are more readily detected by proofreading exonucleases (Kunkel, 2004b). Under accelerated cell cycles, when proofreading time is

compressed, the already-subtle transitions become even more likely to escape detection, leading to an elevated transition-to-transversion ratio (Ts/Tv) (Alexandrov et al., 2013).

3.1.2 Time-dependent Mutagenesis: Chronological Accumulation of DNA Damage

In contrast to replication-dependent errors, the time-dependent model of mutagenesis proposes that a significant component of the germline mutation rate accumulates as a function of chronological time, independent of the number of cell divisions (Lindahl, 1993; Maki, 2002). This model posits that the germline is constantly exposed to damage from endogenous mutagens such as reactive oxygen species (ROS), spontaneous hydrolytic degradation, and background radiation, with a longer window of exposure leading to a greater mutational load (Ames, 1983; Halliwell and Gutteridge, 1990). Critically, these time-dependent processes operate continuously in both mitotically active and quiescent cells, meaning their contribution to mutagenesis is decoupled from replication cycles (Gao et al., 2016).

Time-dependent damage arises from two major endogenous sources. First, spontaneous hydrolytic reactions, such as depurination and deamination, continuously degrade DNA even in the absence of replication (Pak, 2008). These processes follow first-order reaction kinetics and proceed at rates determined primarily by temperature and pH. Consequently, a germline cell that exists for a longer chronological duration accumulates proportionally more baseline damage (Lindahl, 1993). The second major source is oxidative damage from ROS, which are unavoidable byproducts of mitochondrial respiration (Poetsch, 2020). The most mutagenic lesion is 8-oxo-7,8-dihydroguanine (8-oxoG), formed by ROS-mediated oxidation of guanine. During replication, 8-oxoG frequently mispairs with adenine rather than cytosine, resulting in a G→T transversion if the lesion escapes repair mechanisms (David et al., 2007a). Because ROS production is continuous and metabolically driven, oxidative DNA damage accumulates over chronological time even in non-replicating cells.

The time-dependent model, therefore predicts that organisms with prolonged generation times will accumulate a higher mutation rate per generation (μ/generation) due to extended chronological exposure. The mutational spectrum under time-dependent damage is expected to show an elevated proportion of transversions, particularly C→A and G→T mutations resulting from oxidative lesions, leading to a lower Ts/Tv ratio compared to replication-dominated regimes (Bush and Goriely, 2023; Wang and Obbard, 2023).

These two mechanistic forces operate simultaneously, and their relative contribution depends on repair efficiency: when DNA repair is fast, mutations primarily arise during replication, whereas when repair is slow, lesions persist and mutations accumulate over chronological time (Gao et al., 2016). The total mutational burden is therefore the integrated product of both replication-dependent and time-dependent processes, with generation time determining which force dominates (Beichman et al., 2024).

3.2 Extrinsic Drivers I: Natural Environmental Modulation

The intrinsic, life-history-dependent mutations do not operate in isolation but are continuously modulated by the organism's external environment. These extrinsic drivers can be broadly categorised into biotic and abiotic components (Hoffmann and Hercus, 2000; Parsons et al., 2005). Biotic pressures, such as competition, predation, and parasitism, act as potent physiological stressors that can force a reallocation of metabolic energy away from high-fidelity DNA maintenance

(Cucchi et al., n.d.; Kirkwood, 1977). In contrast, it is often the abiotic environment that dictates the fundamental baseline for physiological operation and genomic integrity. These non-living drivers encompass a vast range of physicochemical stressors that can be directly mutagenic, including ionizing radiation, ultraviolet (UV) radiation, and genotoxic chemicals such as heavy metals (Ellegren, 2006). Among this constellation of abiotic factors, ambient temperature represents arguably the most fundamental and pervasive driver influencing mutagenesis (Bestion et al., 2015).

3.2.1 Temperature as a Key Abiotic Driver

The significance of temperature is exceptionally pronounced in ectotherms, organisms whose internal physiological state is inextricably linked to ambient thermal conditions (Angilletta and M. J., 2009; Gillooly et al., 2001). Unlike endotherms, which maintain thermal homeostasis, the core body temperature of an ectotherm fluctuates with its environment. This makes temperature a uniquely powerful driver of mutation rate plasticity because it simultaneously influences mutagenesis through two distinct but interconnected pathways: an indirect pathway mediated by life-history modulation and a direct pathway mediated by cellular physiology (Waldvogel and Pfenninger, 2021).

The indirect pathway operates over developmental timescales (de Souza et al., 2025). Ambient temperature governs the rate of development and thus determines generation time, linking temperature directly to the intrinsic mutagenic forces discussed previously. Higher temperatures accelerate development, increasing cell division rates and thereby amplifying replication-dependent mutagenesis, while simultaneously reducing chronological exposure time and thus minimizing time-dependent damage accumulation. Conversely, lower temperatures prolong development, reducing the rate of cell divisions per unit time but extending the window for time-dependent damage from oxidative stress and spontaneous degradation (Gao et al., 2016). Temperature thus acts as an external modulator that simultaneously affects both replication-dependent and time-dependent mutagenic pathways.

Independent of this life-history modulation, temperature exerts a powerful, direct influence over the biochemistry of organisms. The kinetics of virtually all biochemical processes, from the rate of spontaneous DNA degradation to the efficiency of enzymatic DNA repair, are temperature-dependent (Dohnalová et al., 2024; Pohl et al., 1982). Furthermore, temperature governs the overall metabolic rate, which in turn controls the production of endogenous mutagens (Abele et al., 2002; Lushchak et al., 2005). For an ectotherm, ambient temperature is therefore a master variable that simultaneously modulates the rate of DNA damage, the efficiency of DNA repair, and the tempo of life history. The primary molecular mechanism mediating this direct effect is the production of ROS.

3.2.2 The Mechanism of Oxidative Stress

Reactive Oxygen Species (ROS) are a group of highly reactive oxygen-containing molecules that are the unavoidable byproducts of normal aerobic metabolism (Balaban et al., 2005; Halliwell and Gutteridge, 2015). The principal endogenous source of ROS in most non-photosynthetic eukaryotes is the mitochondrial electron transport chain (ETC) (Murphy, 2009). From ETC I and III an estimated ~1-2% of consumed oxygen "leaks" and prematurely reacts with molecular oxygen, generating the superoxide radical (Turrens, 2003). This primary radical initiates a biochemical cascade that produces other ROS species. Superoxide radical converted by *superoxide dismutase* (SOD) to the more stable, membrane-permeable hydrogen peroxide (Wong et al., 2017). In the presence of reduced transition metals (Fe^{2+}, Cu^{+}), hydrogen peroxide can undergo the Fenton reaction to

generate the highly reactive hydroxyl radical, which is the most damaging ROS species (Halliwell and Gutteridge, 2015).

It is critical to understand that ROS are not exclusively detrimental; their role in the cell is context-dependent. At low, controlled concentrations, they are essential components of cellular functioning (Sies, 2017). Hydrogen peroxide, for instance, acts as a critical second messenger in numerous signaling pathways by reversibly oxidizing specific protein residues, thereby regulating metabolism, stress responses, and development (D'Autréaux and Toledano, 2007). Furthermore, a controlled "oxidative burst" is a cornerstone of the innate immune system: phagocytic cells such as neutrophils and macrophages deliberately generate large quantities of ROS to destroy invading pathogens, oxidizing their cellular components and DNA (Nathan and Cunningham-Bussel, 2013). A mild elevation in ROS can also trigger a beneficial hormetic response, leading to the upregulation of protective mechanisms that can increase an organism's resilience to subsequent stress (Costantini, 2014).

The damaging nature of ROS emerges only when this homeostatic system is imbalanced. Oxidative stress occurs when the rate of ROS production chronically overwhelms the cell's capacity to neutralize them. In this state, excess ROS indiscriminately attack all major classes of biomolecules: lipid peroxidation degrades cellular and organellar membranes, protein oxidation causes misfolding and inactivation of critical enzymes, including those involved in DNA repair itself, and, most critically for mutagenesis, ROS directly attack DNA (Shokolenko et al., 2009). While oxidative stress causes a wide spectrum of DNA lesions, the most critical for mutagenesis is the oxidation of guanine bases. Among these, oxidized purine bases are particularly mutagenic because they frequently mispair during DNA replication, leading to transversion mutations if not corrected by the DNA repair system (David et al., 2007b). The characteristic mutational signature of oxidative stress is an elevated proportion of transversions, particularly C→A and G→T substitutions, resulting in a reduced Ts/Tv ratio (Alexandrov et al., 2013).

To manage this constant threat and maintain redox homeostasis, organisms have evolved a complex, multi-layered antioxidant defence system. This system includes non-enzymatic and enzymatic components (Monaghan et al., 2009). The non-enzymatic layer consists of small-molecule scavengers that directly neutralize ROS. The most important of these is the tripeptide glutathione (GSH), the primary intracellular redox buffer, which is complemented by dietary antioxidants like vitamins C and E (Surai et al., 2016). The second, enzymatic layer is a dedicated protein machinery that catalytically detoxifies specific ROS in a multi-step process (Fridovich, 1995). The primary line of defence is SOD, which converts the initial superoxide radical into hydrogen peroxide (Wong et al., 2017). The resulting hydrogen peroxide is then neutralized to water by two major enzyme classes: *Catalase* (CAT) and the *Glutathione Peroxidase* (GPx) family (Hewitt and Degnan, 2023). Additional enzymatic defences include the *thioredoxin* and *peroxiredoxin* systems, which provide further ROS scavenging capacity and maintain cellular redox balance (Rhee et al., 2005). This intricate system provides the mechanistic link between environmental stress, such as non-optimal temperatures, and mutagenesis.

3.3 Extrinsic Drivers II: Anthropogenic Stressors

Beyond the natural drivers to which populations have co-evolved, organisms now face an escalating class of extrinsic pressures: anthropogenic environmental pollutants (Bickham et al., 2000). These compounds, including industrial chemicals, pesticides, and byproducts of combustion,

represent evolutionarily novel mutagens (Hendry et al., 2017). While life has had billions of years to develop sophisticated defences against natural mutagens, it has no such deep evolutionary history with the thousands of synthetic compounds released in the last two centuries. This lack of pre-existing, specific defence pathways means that these novel mutagens can be uniquely potent, capable of overwhelming or bypassing an organism's established genomic maintenance systems. The resulting elevation in germline mutation rate not only increases mutational load and reduces immediate fitness through the accumulation of deleterious alleles, but also has long-term evolutionary consequences by increasing the supply of genetic variation, which may facilitate adaptation under changing environments but more commonly imposes a mutational load (Oziolor et al., 2019). In populations exposed to pollutants, elevated mutation rates may create a genetic load that reduces fitness, but whether this leads to mutational meltdown or provides raw material for adaptive evolution depends critically on N_e, the strength of selection, and the distribution of mutational effects.

Among the most widespread of these pollutants are Polycyclic Aromatic Hydrocarbons (PAHs), a class of persistent organic contaminants formed during the incomplete combustion of fossil fuels, tobacco, and organic matter. PAHs are ubiquitous in industrialized environments, accumulating in air, water, and soil (Abdel-Shafy and Mansour, 2016). The archetypal PAH is Benzo[a]pyrene (BaP), a potent and ubiquitous environmental mutagen (Xue and Warshawsky, 2005). BaP itself is chemically inert; it is a pro-mutagen that requires metabolic activation by the organism's own *Cytochrome P450* enzymes (Nebert and Dalton, 2006). This process, which evolved to detoxify natural compounds, paradoxically converts BaP into its ultimate carcinogenic form: (+)-anti-benzo[a]pyrene-7,8-diol-9,10-epoxide (BPDE) (Baird et al., 2005).

It is critical to distinguish temporal novelty (recent anthropogenic introduction) from mechanistic novelty (unprecedented biochemical challenge). PAHs as a chemical class are not temporally novel since they also arise naturally from wildfires and volcanic activity, exposing organisms sporadically over evolutionary history (Balmer et al., 2019). Nonetheless, industrial-scale PAH pollution introduces two distinct forms of novelty. First, concentration novelty: anthropogenic PAH exposure involves mutagenic doses orders of magnitude above natural background levels, overwhelming detoxification and repair systems evolved for sporadic, low-level exposure. Second, mechanistic novelty: the metabolic activation of BaP generates stereochemically complex bulky DNA adducts (BPDE-dG) that impose distinct structural challenges to nucleotide excision repair (NER). While NER is the evolutionarily conserved pathway for bulky lesion recognition, the efficiency of BPDE adduct removal is highly sequence-context dependent and often inefficient (Pfeifer et al., 2002). The precise structural features of BPDE adducts that impair NER recognition remain incompletely understood, suggesting that these lesions present an evolutionarily unprecedented repair challenge distinct from the small base modifications (e.g., oxidative damage, depurination) that constitute the majority of endogenous DNA damage (Geacintov et al., 2002; Schärer, 2003). Thus, while PAHs themselves are not evolutionarily novel, the scale and biochemical specificity of industrial BaP exposure constitute a mechanistically unprecedented mutagenic pressure (Baird et al., 2005; Pfeifer et al., 2002).

3.3.1 Differentiating Mechanisms of Action

The mutagenicity of BaP highlights the critical importance of differentiating the molecular mechanisms of anthropogenic pollutants. While BaP metabolism can generate secondary ROS-mediated effects (Burczynski et al., 2000; Miller et al., 2010), its primary mutagenic action occurs

via a direct DNA adduction pathway (Pfeifer et al., 2002). This mechanistic distinction is critical, as the work in this dissertation demonstrates that mutagenic concentrations of BaP increase the germline mutation rate in *C. riparius* without a corresponding increase in organismal ROS production (Chapter 3), highlighting its molecular pathway (Kucab et al., 2019). The highly reactive BPDE metabolite physically and covalently binds to DNA, predominantly at the N² position of guanine, forming a large, helix-distorting BPDE-N²-dG adduct (Geacintov et al., 2002; Hess et al., 1997). This bulky lesion stalls high-fidelity DNA polymerases, forcing the engagement of error-prone translesion synthesis (TLS) polymerases to bypass the damage. The mutational outcome of TLS bypass is polymerase-specific and context-dependent. While mammalian somatic studies predominantly report G→T transversions (Petljak and Alexandrov, 2016), germline systems and alternative TLS polymerase repertoires can produce transition-biased spectra depending on which polymerase (e.g., Pol η vs. Pol ζ) is recruited and the sequence context surrounding the adduct (Prakash et al., 2005; Waters et al., 2009).

This mechanistic distinction is fundamental for assessing the evolutionary impact of anthropogenic pollution. The natural stressors discussed previously, such as temperature, primarily modulate the rate of endogenous, ROS-mediated damage, a threat for which organisms have evolved robust and adaptable defences (e.g., antioxidant systems, base excision repair) (Costantini, 2014; Halliwell and Gutteridge, 2015). In contrast, the direct adduction pathway of BaP presents an evolutionarily novel challenge. The bulky adducts generated by BaP are repaired by the NER pathway, which recognizes helix-distorting lesions. Unlike BER, which is highly specific for small base modifications, NER must accommodate a diverse array of bulky lesions, making it less substrate-specific and also less efficient for any single lesion type (Lankoff et al., 2008). Notably, adaptive evolution in response to PAH pollution has been documented in some populations (e.g., Atlantic killifish in Elizabeth River; (Reid et al., 2016)), demonstrating that resistance is possible but likely requires specific genetic variation and large population sizes. Consequently, an organism's capacity to evolve resistance to adduct-forming mutagens is far more constrained than its ability to adapt to oxidative stress. Failing to differentiate these pathways risks severely underestimating the persistent mutational load imposed by such pollutants, as their primary impact is invisible to assays that only measure oxidative damage.

4. The Model System and Research Gap

4.1 Justification of *Chironomus riparius* as a Model System

The theoretical framework established in the preceding sections requires a model organism that is not merely convenient, but one that possesses a specific combination of ecological, biological, and experimental attributes. To deconstruct the mutation rate into its intrinsic, natural, and anthropogenic drivers, a system is needed that bridges environmental realism with genomic tractability. The non-biting midge *Chironomus riparius* has emerged as a model system particularly well-suited for this multi-layered investigation.

Its ecological relevance is paramount. As a ubiquitous, sediment-dwelling larva in freshwater ecosystems, *C. riparius* is widely used as a model organism for toxicological research and is an OECD-recommended bioindicator for sediment toxicity (OECD, 2010; Vogt et al., 2007). Its ecological niche in benthic habitats, where pollutants such as PAHs accumulate, makes it an ecologically relevant system for studying the mutagenic impacts of anthropogenic contamination. Biologically, *C. riparius* is an ectotherm whose physiology is inextricably linked to ambient

temperature. This makes it an ideal subject for disentangling the dual influence of temperature on mutagenesis. Crucially, the species exhibits significant natural variation in its generation time under constant thermal conditions, providing the exact experimental leverage needed to isolate generation time from temperature and disentangle the relative contributions of replication-dependent and time-dependent mutagenic processes.

Finally, these attributes are matched by profound experimental tractability. A short generation time (~3-4 weeks) and high fecundity (300-1,000 eggs/female) (Oppold et al., 2016; Pfenninger and Nowak, 2008) make multi-generational MA experiments feasible, providing the statistical power necessary to detect subtle changes in mutation rates. This is supported by the availability of a high-quality, annotated reference genome (~200 Mb) (Pettrich and Waldvogel, 2025) and extensive transcriptomic resources (Foucault et al., 2019), which are the essential prerequisites for the whole-genome sequencing approaches central to this work. In summary, *C. riparius* occupies a unique niche, combining the environmental realism of an aquatic bioindicator with the genomic and experimental tractability of a classic laboratory model, making it the ideal system to execute the systematic deconstruction of the mutation rate that this dissertation proposes.

4.2 The Central Research Gap: A Systematic Deconstruction of Mutagenic Drivers

Despite a growing body of research on mutation rate plasticity, our understanding of the proximate mechanisms remains critically fragmented. The primary limitation of the current literature is that different classes of mutagenic drivers (e.g., intrinsic life-history constraints, natural environmental modulators, and anthropogenic perturbations) have been studied largely in isolation or confounded with one another (Green et al., 2024; Krašovec et al., 2017; Monroe, 2023; Oman et al., 2022). This creates three fundamental gaps in our mechanistic understanding.

First, the relative contribution of replication-dependent versus time-dependent mutagenesis to the baseline germline mutation rate remains empirically unresolved, particularly in ectotherms where generation time and temperature are naturally confounded. While theoretical models propose that both processes contribute under some conditions (Gao et al., 2016), direct experimental tests that isolate generation time from environmental variables are lacking. Without establishing this intrinsic baseline, it is impossible to accurately interpret mutation rate variation in natural populations. Second, even for well-studied natural environmental drivers like temperature, the mechanistic pathways remain poorly resolved. Temperature can affect mutation rates through multiple routes: indirectly by modulating generation time (linking to the intrinsic drivers discussed above), and directly by altering the biochemical kinetics of DNA damage and repair (Gillooly et al., 2001). The "U-shaped" temperature-mutation rate relationship observed in *C. riparius (Waldvogel and Pfenninger, 2021)* exemplifies this mechanistic ambiguity; without disentangling indirect (generation time) from direct (physiological) effects, the causality remains unresolved. Third, the mutagenic impact of anthropogenic pollutants cannot be properly contextualized without first characterizing the natural baseline and understanding which molecular pathways they perturb. For instance, do pollutants increase mutation rates by amplifying existing ROS-mediated oxidative stress, or do they act through entirely distinct mechanisms such as direct DNA adduction? This distinction is critical for predicting long-term evolutionary consequences and adaptation potential.

Therefore, the central research gap is the lack of a systematic, hierarchical deconstruction that establishes the intrinsic baseline of mutagenesis, then layers on natural environmental modulators while disentangling their pathways, and finally contextualizes anthropogenic impacts against this

well-defined mechanistic foundation. Such a framework is necessary to move from descriptive observations of mutation rate variation to a predictive, mechanistic understanding of mutagenesis.

5. Dissertation Aims and Chapter Outline

This dissertation bridges the gap between ultimate evolutionary constraints and proximate mechanistic drivers of mutation rate variation. While the Drift-Barrier hypothesis predicts that effective population size determines the minimum mutation rate a species can achieve through evolutionary optimization of anti-mutator alleles, it does not explain the mechanistic processes generating variation within this evolutionary ceiling (Figure 1). The realised mutation rate at any moment reflects how cellular machinery responds to immediate physiological demands, a question of proximate causation (Baer et al., 2007).

By systematically deconstructing the drivers of mutagenesis in the model ectotherm *Chironomus riparius* across three empirical studies, this work reveals the proximate mechanisms generating the patterns of mutation rate variation that evolutionary theory predicts but does not mechanistically explain. Mutation rate variation occurs within the evolutionary ceiling imposed by the drift barrier and is driven mechanistically by three distinct forces: (1) intrinsic variation in organismal life history (generation time), (2) environmental variations in a key abiotic factor (temperature), and (3) exposure to anthropogenic chemicals.

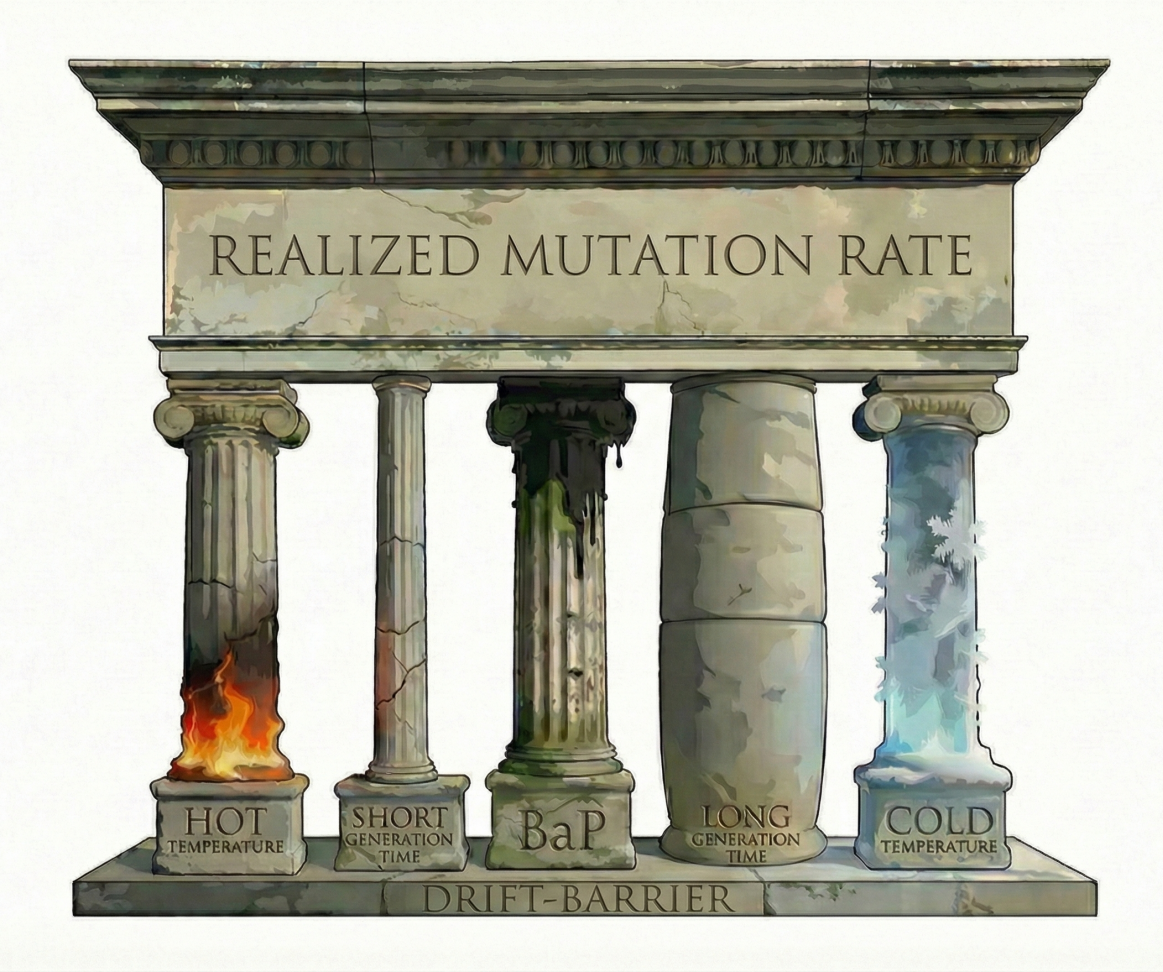

Figure 1: A conceptual framework for the proximate drivers of the realized germline mutation rate. The Drift-Barrier hypothesis defines the evolutionary lower limit of the mutation rate, below which selection cannot overcome genetic drift given finite effective population size (N_e). Within this constraint, the realized mutation rate is shaped by distinct proximate drivers as intrinsic life-history parameters (generation time), natural abiotic modulators (temperature), and anthropogenic stressors (benzo[a]pyrene, BaP). Each pillar represents a mechanistically independent mutagenic axis studied in this dissertation; their combined influence determines the realized mutation rate. This work systematically deconstructs these drivers to reveal that mutation rate variation above the Drift-Barrier limit is mechanistically structured rather than stochastic.

Chapter 1 establishes the intrinsic biological baseline by experimentally isolating developmental tempo from thermal stress. Rearing individuals at constant temperature (20 °C) while exploiting natural variation in generation time revealed a U-shaped mutation rate relationship, with the minimum coinciding with the population's mean generation time (~26 days). Distinct mutational signatures emerged at extremes: rapid development elevated daily mutation rates with replication-associated fingerprints, while prolonged development elevated per-generation rates with oxidative damage signatures.

Chapter 2 characterised the direct physiological impact of temperature. Reactive oxygen species production exhibited a U-shaped relationship across an ecologically relevant thermal gradient (4-28 °C), with minimum ROS production at 12-18 °C. Cold and heat extremes impose mechanistically

distinct oxidative challenges, each eliciting composition-specific antioxidant responses, demonstrating that temperature extremes generate compositionally distinct ROS profiles and corresponding antioxidant responses.

Chapter 3 contrasts these natural processes with an anthropogenic pollutant, benzo[a]pyrene (BaP). Chronic BaP exposure across five generations increased germline mutation rates (1.2-fold at 100 µg/L) while simultaneously reducing survival and fecundity, demonstrating that elevated mutagenesis directly compromises fitness. Critically, no evidence of adaptive tolerance emerged over three generations, suggesting that either the population lacked the necessary standing genetic variation or that selection was insufficient to overcome the mutational load imposed by BaP. Most importantly, BaP exposure did not elevate ROS levels under our *in vivo* assay, arguing against elevated organismal oxidative stress as the primary proximate mechanism in this setup, and supporting a ROS-independent pathway.

Collectively, these chapters execute a systematic deconstruction of the germline mutation rate, moving from intrinsic biological constraints to extrinsic environmental modulators. By integrating these distinct layers of causality, this dissertation aims to disentangle the mechanistic layers under the ceiling set by the Drift-Barrier hypothesis. This approach is fundamental for predicting evolutionary trajectories, as it reveals not only how mutation rates vary, but why specific environmental futures pose distinct challenges to genomic integrity.

Chapter 1

Developmental Speed and Chronological Time Exert Opposing Effects on the Spontaneous Mutation Rate in *Chironomus riparius*

Burak Bulut[1], Markus Pfenninger

[1] first author

Accepted in: Evolution Letters

Acknowledgements: The authors are grateful for support by a DFG grant to M.P. (PF 390/15-1).

Funding: This work was supported by Deutsche Forschungsgemeinschaft, PF 390/15-1.

Conflict of Interest: The authors declare no conflicts of interest.

Data Availability: The data is accessible at the European Nucleotide Archive (ENA) under accession number PRJEB92091. Raw data for the analyses were made available at Zenodo doi: doi.org/10.5281/zenodo.18621629

Evolution Letters, 2026, **0**(0), qrag010
https://doi.org/10.1093/evlett/qrag010
Letter

OXFORD

Developmental speed and chronological time exert opposing effects on the spontaneous mutation rate in *Chironomus riparius*

Burak Bulut [1], **Markus Pfenninger** [1,2]

[1]Department of Molecular Ecology, Senckenberg Biodiversity and Climate Research Centre, Georg-Voigt-Str. 14-16, D-60325 Frankfurt am Main, Germany
[2]Institute for Molecular and Organismic Evolution, Johannes Gutenberg University, Johann-Joachim-Becker-Weg 7, D-55128 Mainz, Germany
Corresponding author: Department of Molecular Ecology, Senckenberg Biodiversity and Climate Research Centre, Georg-Voigt-Str. 14-16, D-60325 Frankfurt am Main, Germany. Email: markus.pfenninger@senckenberg.de

Abstract

The spontaneous mutation rate (μ) is shaped by two distinct forces: the passage of chronological time, inevitably associated with mutation accumulation, and the speed of development, where rapid replication contributes to error rates. Disentangling these forces has been a major challenge, particularly in ectotherms. Testing the distinct predictions of the classic replication-dependent generation length hypothesis and the time-dependent accumulation model, we experimentally assessed individuals with naturally short (15 days) and long (38 days) generation time (GT), which is mainly determined by differences in developmental speed in the midge *Chironomus riparius*. To overcome the challenges of swarm-mating, we employed a parent-offspring pedigree reconstruction approach using pooled sequencing of siblings to infer parental allelic composition. We estimated the *de novo* mutation rates by whole genome sequencing. We found that Long-GT groups accumulated 1.2-fold more total mutations per generation (μ/gen), consistent with time-dependent mutagenic processes. Conversely, Short-GT groups exhibited a nearly two-fold higher mutation rate per day (μ/day) and a trend toward a transition-biased mutational spectrum (*Ts*/*Tv* ratio = 1.14 vs. 0.89), a pattern consistent with a replication-dependent errors in DNA. These results suggest that the overall mutation load is the product of these two interacting processes. Integrating our data with previous studies and life-history data, we show that the daily mutation rate followed a non-linear relationship with respect to developmental speed, and that the species' generation time mode coincides with its minimum. This suggests that the developmental speed is, amongst other factors, selected to optimize the mutational load by balancing between replication accuracy and developmental speed.

Keywords germline mutation rate, molecular clock, drift-barrier hypothesis, fitness costs, deleterious mutations

Introduction

Spontaneous mutations are the ultimate source of all genetic variation, yet the forces that govern their rate (μ) remain a central topic in evolutionary biology (Lynch et al., 2016). Historically, the mutation rate was often treated as a stable constant, a view foundational to the molecular clock hypothesis (Zuckerkandl & Pauling, 1965). However, it is now clear that μ varies substantially between species, individuals, and even sexes (Lynch et al., 2023; Wang & Obbard, 2023; Zhu et al., 2024). The drift-barrier hypothesis provides the current evolutionary framework for this variation, proposing that selection acts to lower μ only until the cost of further optimization outweighs the benefit, a threshold determined by the power of genetic drift (Lynch, 2010; Lynch et al., 2016). While this hypothesis sets the expectation for the ultimate lower limit of μ in a species, the proximate physiological mechanisms that generate mutations and how they scale with life history remain debated.

Two primary mechanisms are hypothesized to explain the generation time (GT)-dependent mutation rate variation. The first mechanism is a replication-dependent model (Drake, 1991), often formalized as the generation length hypothesis (Li et al., 1987; Ohta, 1995). This model posits that because germline mutations arise primarily from copy errors during DNA replication, organisms with shorter GTs will therefore exhibit a higher mutation rate per time unit. In contrast, the "time-dependent" model, proposes that the rate of development is a critical factor (Lindahl, 1993; Maki, 2002). This model suggests that the germline DNA is constantly exposed to damage from endogenous mutagens such as reactive oxygen species (ROS), radiation, and spontaneous chemical modification of DNA bases (e.g., deamination, oxidation), with a longer window of exposure leading to a greater mutational load (Ames,

Received: 15 December 2025. **Revised:** 12 February 2026. **Accepted:** 19 February 2026

1983; Halliwell & Gutteridge, 1990; Shokolenko et al., 2009). These two forces, replication-dependent and time-dependent error, exert distinct pressures on the germline, but experimentally disentangling their relative contributions has remained a major challenge. In part because theoretical models show that both processes can, under different assumptions about repair efficiency, lead to mutation accumulation that scales with cell divisions (Gao et al., 2016), which in turn contributes to a broader scaling conflict where evolutionary predictions differ depending on the time units used (Beichman et al., 2024).

Ectotherms exemplify the difficulty of separating these forces because their life-history schedules are inextricably linked to ambient temperature. In these organisms, environmental temperature dictates developmental speed: warmer conditions compress GT, while colder conditions prolong it (Gillooly et al., 2001). This environmental control complicates the interpretation of mutation rate variation, as illustrated by the recently described "U-shaped" relationship between temperature and mutation rate in the midge *Chironomus riparius* (Waldvogel & Pfenninger, 2021). While elevated mutation rates in the heat are readily explained by metabolic stress, the high mutation rates observed in the cold are puzzling. Crucially, these cold-reared individuals exhibit drastically prolonged GTs. This raises a critical causality dilemma: Is the high mutation rate in the cold a direct physiological consequence of thermal (cold) stress, or is it simply the indirect effect of the extended chronological time allowing for greater mutation accumulation, as predicted by the time-dependent damage?

Here, we address this question by experimentally disentangling the effects of chronological time and developmental speed on the germline mutation rate. We utilized the non-biting midge *C. riparius* lives as major component of the benthos communities in small streams and ditches. As ectothermic organisms, their GT strongly depends on the ambient temperature Oppold et al. 2016. The species is multivoltine, with, in dependence of local climatic conditions, as much as 15 generations per year (Oppold et al., 2016). The species has no winter resting stage or diapause; development of larvae is stalled below ∼10–12 °C and development continues if this temperature is exceeded (Pfenninger et al. 2023). Most of their life time (>90%) the midges spend on going through four larval stages after hatching from an egg-rope. After pupation and emergence, mating almost immediately takes places by females flying into swarms of males, which makes identification of parent pairs difficult. The adult midges live only a few days; both sexes usually die shortly after a single reproduction. Their life-span is therefore nearly identical to their GT and any difference in GT is determined by the developmental speed of the larvae (Foucault et al., 2019), and not in a differential life span as fully developed adults. Their short GT in conjunction with a large number of offspring [400–800] and a high effective population size (Waldvogel et al. 2018) permits rapid adaptation (Pfenninger, 2017), which results in adaptive tracking of environmental variation (Pfenninger & Foucault 2022). For the experiment *C. riparius* reared under identical, benign thermal conditions were employed, drawing on the significant natural intrinsic variation in GT (Foucault et al., 2019). By selecting the earliest and latest reproducing individuals from a single cohort, we created "short" and "long" GT groups at a constant, stress-reduced temperature. This design allowed us to isolate the mutational consequences of developmental speed driven GT from those of ambient temperature. We simultaneously tested the predictions of both replication-dependent and time-dependent models, with the former predicting to affect the mutation rate per generation, mutation rate and the mutational spectrum.

Material and methods

Experimental design and rearing

This study employed a modified parent-offspring triad design to assess the effect of reproductive timing on germline mutation rates in *Chironomus riparius*. Because the species' swarm-mating behavior prevents direct identification of parents, their genotypes were instead reconstructed from pooled sequencing of their offspring (Oppold & Pfenninger, 2017). The experiment was initiated with 10 egg ropes, ensuring a genetically diverse starting cohort. To control for environmental variation, the resulting larvae were reared at a constant 20 °C with a 16:8 hr light/dark cycle and *ad libitum* feeding and constant aeration (Foucault et al., 2019).

From this mixed sample with several thousand individuals, two experimental groups were established based on the reproductive timing of the adults. The Short-GT group was founded using the first 10 egg ropes produced by the earliest emerging adults (14–17 days post-hatching, mean = 15.6). The Long-GT group was founded using 10 egg ropes produced by late-emerging adults (38 days post-hatching) (Sup. Data). We established 20 independent biological lines (10 Short-GT, 10 Long-GT), each representing a distinct genetic background, because all were descending from different parental pairs.

For each line, the offspring were reared under standardized conditions to the third larval instar stage (L3), at which point 10 individual larvae were sampled for individual sequencing from each line ($n = 200$). The remaining siblings from each line (several hundred) were pooled to generate a "parental pool" for *in silico* parental genotype reconstruction ($n = 20$ pools, Figure 1A). While this pooling approach precludes the identification of individual parents' genotypes, it is a robust method for accurately reconstructing parental allele occurrences at each locus in species with a large number of offspring, with potential biases mitigated by high sequencing depth and stringent variant filtering criteria (Oppold & Pfenninger, 2017).

Integration with external life-history data

To contextualize our findings in relation to the species' typical life history, we compiled generation length data from 1,796 control individuals from previous experiments (Bulut et al., 2024; Rigano et al., 2025; Waldvogel & Pfenninger, 2021). This distribution was plotted to visualize the most frequent GT of *C. riparius* under standard laboratory conditions. As a visual inspection of the plot suggested the mixture of two normal distributions, we used the R-module mixtools (Benaglia et al., 2009) to assess the statistical significance and estimate parameters.

Whole-genome sequencing and bioinformatic analysis

We extracted genomic DNA from the 200 individual L3 larvae (100 per group) and the 20 corresponding sibling pools.

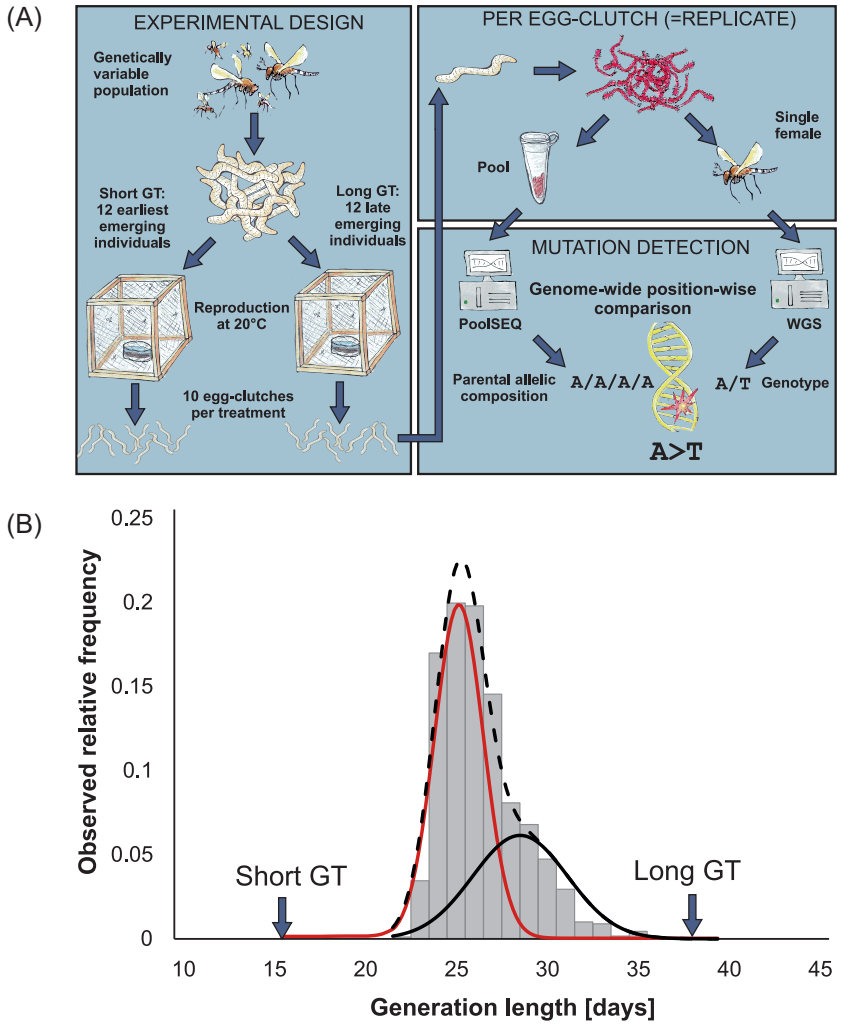

Figure 1. Experiment and natural variation in GTs. (A) Schematic representation of the experimental design and the mutation detection process. (B) Frequency distribution of 1796 GT measurements. The red and black solid lines represent the inferred distinct underlying normal distributions, and the dashed line is the inferred mixed distribution. The blue arrows indicate the GT of the Short and Long GT groups.

Paired-end whole-genome sequencing was conducted on an Illumina platform at Novogene following the methodology of Waldvogel & Pfenninger (2021). Raw read quality was assessed using FastQC. The raw reads then processed using a bioinformatics pipeline based on GATK Best Practices (Van der Auwera et al., 2013). Forward and reverse reads were first merged using PEAR v0.9.6 (Zhang et al., 2014). Merged reads were then mapped to the *C. riparius* reference genome v.4 (Pettrich et al., 2024) using the BWA-MEM algorithm (Li, 2013). To ensure high data quality, duplicate reads were identified and removed using Picard tools v1.123 ("Picard Tools—By Broad Institute," n.d.), and low-quality reads were filtered with SAMtools (Li et al., 2009).

To identify de novo mutations, we analyzed the BAM files from each triad (pooled parents and their 10 individual offspring) with the mutation caller accuMUlate (Winter et al., 2018). The resulting candidate mutations were filtered using a custom script with the following criteria: mutation probability ≥ 0.90; probability of exactly one mutation in the triad ≥ 0.90; probability of correct descendant genotype ≥ 0.90; number of mutant reads in the parental pool $= 0$; mapping quality difference ≤ 2.95; and strand bias or pair-mapping rate difference ≥ 0.05. This multi-layered filtering strategy generates a high-confidence set of de novo single-nucleotide mutations (SNMs). Finally, all candidate mutations passing the filtering were manually inspected using the IGV to confirm the mutations (Robinson et al., 2011).

To detect small insertions and deletions (indels) (DePristo et al., 2011), we utilized the GATK HaplotypeCaller on the processed BAM files (Keightley et al., 2009; A. Oppold & Pfenninger, 2017). Candidate indels were filtered using GATK's standard hard-filtering recommendations [QualByDepth (QD) < 3.0, FisherStrand (FS) > 200.0, ReadPosRankSum < -20.0, StrandOddsRatio (SOR) > 3.00]. To ensure high confidence, we applied the same pedigree constraints used for SNMs. Finally, all candidate indels were manually curated by visual inspection of read alignments using the IGV to rule out mapping artifacts or alignment errors.

Table 1. Overview of results per GT group.

Group	Mean callable sites	Mean generation time [days]	Total mutations	Total per generation μ	Total per day μ	SNMs	SNM μ	Indels	Indel μ	*Ts*/*Tv* ratio
Short GT	6.08E + 09	15	67	1.1E-08	1.5E-11	57	9.40E-09	10	1.70E-09	1.14
Long GT	5.83E + 09	37.7	79	1.4E-08	7.9E-12	72	1.20E-08	7	1.20E-09	0.89

Note. Mean number of callable sites, mean GT in days, total mutations, total per generation μ, total per day μ, (SNMs) number of single nucleotide mutations, (SNM μ) single nucleotide mutation rate, (Indels) total number of indels, (Indel μ) indel rate, and (*Ts*/*Tv* ratio) transition vs. transversion rate.

Statistical analysis of mutation rates and spectra

We used a Bayesian implementation of a Poisson test (BayesianFirstAid R package) (Bååth, 2014) to estimate the respective median mutation rates along with their 95% high-density interval (HDI) and statistically compare mutation rates between the short and long GT groups. The spontaneous mutation rate (μ) per site per generation was estimated by dividing the number of validated SNMs by the total number of callable genomic sites times the generational passages. The mutation rate per day (μ/day) was calculated by dividing the mutation number by the mean number of callable sites multiplied by the cumulated number of days from egg-laying to reproduction for each line. The mutational spectrum was analysed by calculating the transition-to-transversion (*Ts*/*Tv*) ratio and comparing the proportion of transitions between groups with a Bayesian proportion test (Bååth, 2014). To compare the mutation rates obtained from short and long GTs with those from GTs of average length, we combined our data with previously published mutation rate estimates under control conditions for *C. riparius* (Bulut et al., 2024; Rigano et al., 2025; Waldvogel & Pfenninger, 2021). The pooling of these datasets is justified by the highly standardized experimental conditions employed across all studies, including identical rearing temperatures (20 °C), light cycles, feeding protocols, and the use of the same bioinformatics pipeline (accuMUlate) with identical parameters for mutation calling. While we cannot completely rule out subtle batch effects from separate experiments, use of several studies, highly standardized rearing protocols and identical bioinformatic pipelines minimize this possibility and provide the best available data for assessing the mutation rate at intermediate GTs.

We used the same additional data sets to test whether the mutation spectrum of intrinsically slow or fast reproducing individuals is similar to the mutation spectrum of individuals whose developmental speed is forced by temperature. We included data on the mutational spectra of the three controls mentioned above in addition to the temperatures 12, 14, 17, and 23 °C from (Waldvogel & Pfenninger, 2021). Data for 26 °C was left out as this temperature is already highly stressful for the midges and was shown to bias the spectrum strongly. We used the normalized (mean = 0, s.d. = 1) per generation rates for each of the six spectral categories as input for a Principle Component Analysis (PCA). We assessed significance of the resulting axes with a broken stick model. Since only the first axis was above random expectations, we calculated Euclidean distances of the PCA1 scores and clustered the resulting distance matrix with the neighbor-joining algorithm. Calculations were performed with PAST 4.07b (Hammer, 2001).

Results

Experimental groups fall into the extreme tails of the population GT distribution

An analysis of 1,796 individuals from control conditions of previous experiments revealed that the mean GT for *C. riparius* under standard laboratory conditions was 26.4 (s.d. 2.3) days (Figure 1B). However, the GT data were much better described by a mixture of two normal distributions (p single mode $< 1 \times 10^{-16}$). The estimated parameters of these two distributions were a mean GT of 25.3 ± 1.2 days for the first mode and 28.3 ± 2.3 days for the second, with relative proportions of 0.62 and 0.38, respectively. The distribution showed that the individuals recruited for the Short-GT and Long-GT group fall into the extremes of the natural GT variation (Figure 1A).

Per-generation mutation rate is higher in the long-GT group

The mean GT difference between the first and the last reproducing individuals from the same cohort was 22.5 (1.6 s.d.) days. From overall over $1.1 \times 10^{1\circ}$ callable genomic sites, we identified 146 high-confidence de novo mutations (129 SNMs and 17 indels). Offspring from the short generation group accumulated 67 mutations (57 SNMs and 10 indels), while the long generation group accumulated 79 mutations (72 SNMs and 7 indels). The estimated total mutation rate (μ) for the short generation group was 1.1×10^{-8} per site per generation (95% HDI = $8.6 \times 10^{-}$–1.4×10^{-8}). The rate for the long generation group was 1.4×10^{-8} per site per generation (95% HDI = 1.1×10^{-8}–1.7×10^{-8}) (Table 1). This represents, with a posterior probability of 89.2% an increase (median = 1.2-fold increase) in the germline mutation rate per generation in the offspring of parents that reproduced later (Figure 2A).

To assess the sensitivity of our pipeline to germline mosaicism (mutations arising early in gametogenesis and thus present in multiple siblings) (Latta et al., 2013; Rahbari et al., 2016), we performed a secondary analysis removing the "probability of exactly one mutation in the triad" filter. We re-screened the data allowing for variant calls to appear in more than one individual offspring within a triad. This sensitivity analysis yielded no additional high-confidence de novo mutations, indicating that early germline

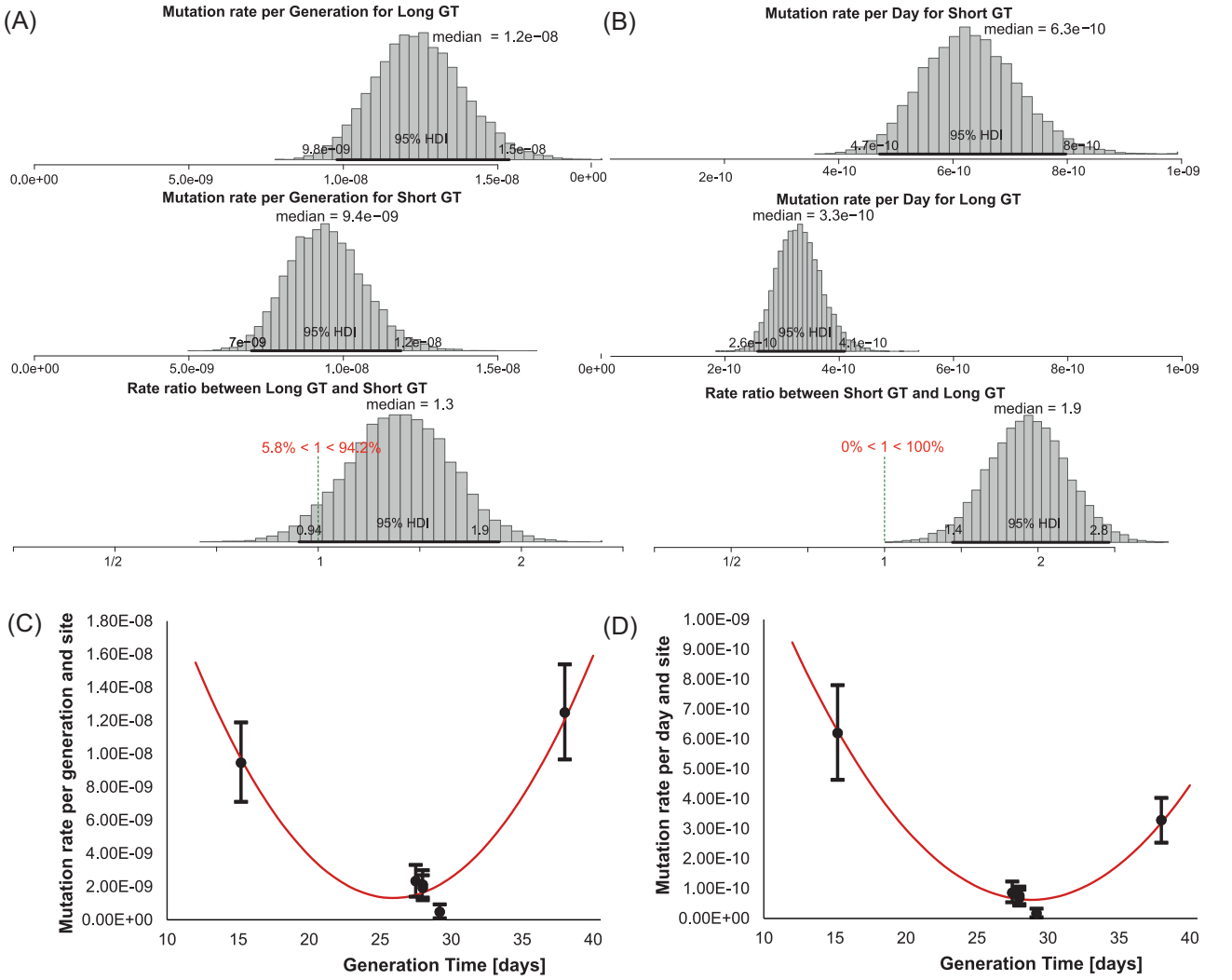

Figure 2. The effect of GT on the per-generation mutation rate. (A) Posterior probability distribution of the rate ratio (λ_long/λ_short) of the per-generation mutation rate between the long and short GT groups. The median rate ratio is 1.2, indicating a 1.2-fold higher rate in the Long-GT group. The 95% HDI is [0.89, 1.7]. The posterior probability that the rate in the Long-GT group is higher than in the Short-GT group (ratio >1) is 89.2%. (B) In contrast, the per-day mutation rate ratio between short and long generation groups has a median of 1.9, signifying a 1.9-fold higher rate in the short group. The 95% HDI is [1.4, 2.7]. The posterior probability that the rate in the short group is higher than in the long group (ratio >1) is 100%. (C) Mutation rate per generation. (D) Mutations per day. Error bars correspond to 95% HDI. The solid red line shows the best-fit quadratic functions.

events are rare in our dataset and that the singleton filter did not artificially deflate the mutation rate estimates.

Per-day mutation rate is higher in the Short-GT group

In contrast to the per-generation rate, the mutation rate per day was nearly two-fold higher in the Short-GT group. The estimated daily rate (μ/day) for the Short-GT group was 1.5×10^{-11} per site per day (95% HDI = 1.2×10^{-11}–1.9×10^{-11}), while the rate for the Long-GT group was 7.9×10^{-12} per site per day (95% HDI = 6.3×10^{-12}–9.8×10^{-12}) (Table 1). Bayesian analysis showed a posterior probability of 100% that the daily rate in the Short-GT group was higher than in the Long-GT group, with a median rate ratio of 1.9 (Figure 2B).

The relationship between daily μ and GT is non-linear

Using the mutation rates inferred under stress-free control conditions for intermediate generation length in other studies (Bulut et al., 2024; Rigano et al., 2025; Waldvogel & Pfenninger, 2021) and unpublished data suggested that the relationship between GT and mutation rate is non-linear, as evidenced by the non-overlap of the 95% HDI intervals to both short and long GT groups (Figure 2C and D). To visualize the potential non-linear relationship between mutation rate and GT, we plotted a quadratic curve, which suggested

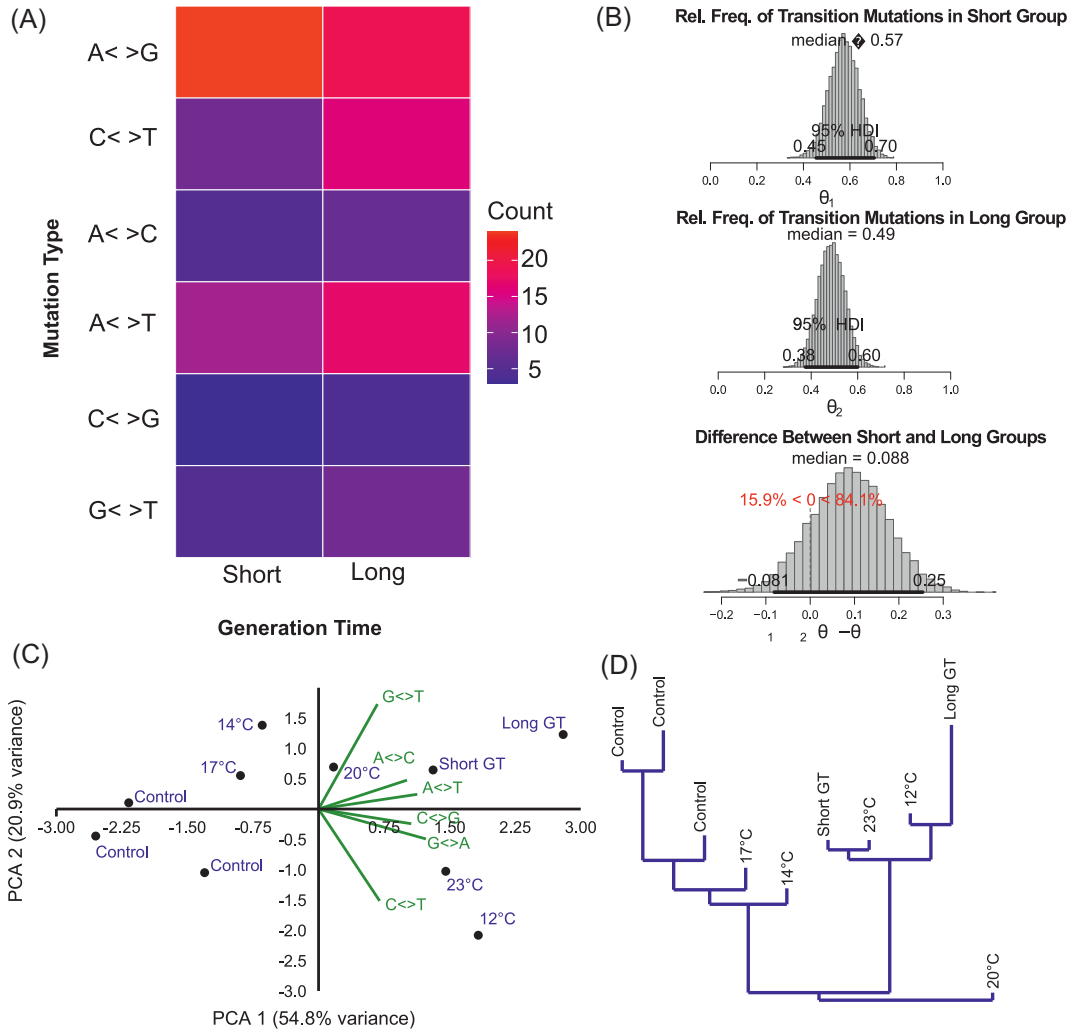

Figure 3. Analysis of mutational spectra. (A) Heatmap showing the absolute counts of the six SNM types. The *y*-axis categorizes mutation types, with transitions (C > T, T > C) in the third and fifth rows and transversions. The *x*-axis separates the two experimental groups. The spectrum is biased toward transitions in the Short-GT group (*Ts*/*Tv* = 1.14) and is more balanced in the Long-GT group (*Ts*/*Tv* = 0.89). (B) The relative frequencies of specific mutation types. Bayesian proportion test indicated an 79.0% posterior probability that the proportion of transition mutations was higher in the short group (95% CI for difference: −0.098, 0.24). (C) Biplot of principal component analysis of the per generation mutation rates for each mutation spectrum class for current data along with controls and different temperatures taken from previous studies (see text). Please note that only the first PCA summarized more variation than expected from random expectations. (D) Neighbor-joining tree of Euclidian distance among mutational spectra along PCA1, rooted with the spectrum at 20 °C.

a nadir around 26 days for the per day rate and 29 days per generation (Figure 2C and D).

Mutational spectra and indels differ between GT groups

There was evidence that the single nucleotide mutational spectrum was shifted between the two groups. The short-generation group exhibited a *Ts*/*Tv* ratio of 1.14, while the long-generation group had a *Ts*/*Tv* ratio of 0.89 (Figure 3A). A Bayesian proportion test indicated an 79.0% posterior probability that the proportion of transitions was higher in the short-generation group (estimated group difference 95% CI: −0.10–0.23). This was driven by C > A transversions which showed a trend toward being more frequent in the long-generation group (posterior probability = 0.858) (Figure 3B).

To further test for signatures of replication-dependent stress, we analyzed the accumulation of small insertions and deletions (indels) up to 5 base pairs (Sun et al., 2012; Tanay & Siggia, 2008). We identified a total of 17 validated de novo indels. The Short-GT group accumulated 10 indels (1.64×10^{-9} per site/gen), while the Long-GT group accumulated 7 (1.20×10^{-9} per site/gen, posterior probability 86.6%). However, indels constituted a larger fraction of the total mutations in the Short-GT group (17.5%) compared to the Long-GT group (9.7%, posterior probability 86.6% of being different). More importantly, in the Short-GT group, the daily influx of indels was 3.4 times higher in the rapidly developing groups (1.1×10^{-10} vs. 3.2×10^{-11} per day and site, posterior probability 99.4%), consistent with the hypothesis that compressed replication schedules increase the propensity for polymerase slippage.

Only PCA1 summarized more variance than expected, accounting for 54.8% (Figure 3C). The axis was most highly (0.91)

correlated to the G<>A transition, but all other classes except G<>T and C<>T were also important determinants. It divided mutational spectra from all controls and moderately low temperatures on the left part (G<>A transition deficient) from the extreme warm and cold temperatures and the long and short GTs on the right (G<>A enriched), with 20 °C close to the center. Clustering the Euclidean distances along PCA1 and rooting it with 20 °C reproduced the pattern, but clustered the mutational spectrum of the short generation with 23 °C and those of the long generation with 12 °C (Figure 3D).

Discussion

Our study provides direct experimental evidence that the germline mutation rate is shaped by the interaction between two distinct forces tied to GT. By isolating GT, driven by developmental speed from temperature in *Chironomus riparius*, we demonstrate that a "replication-dependent" mutational regime, hinting to a speed-fidelity trade-off, dominates at short GTs, while a "time-dependent" regime, governed by mutation accumulation over time, prevails at long GTs. This finding helps resolve the dichotomy between time and replication-dependent models of mutagenesis. It provides empirical support for theoretical frameworks predicting that mutation accumulation depends on the interplay between mutation accumulation and repair efficiency (Gao et al., 2016). While the current study is restricted to our model system, there is little reason to believe that these processes should act principally differently in other ectotherms.

A replication-dependent model drives mutagenesis at short GTs

The mutational signature of the Short-GT group is a pattern consistent with replication-dependent errors. These individuals exhibited a nearly two-fold higher mutation rate per day than the Long-GT group, likely a direct cost of their compressed developmental schedule. The elevated daily mutation rate, combined with a bias toward transitions ($Ts/Tv = 1.14$) and a higher relative frequency of indels, are molecular signatures frequently associated with replicative polymerase errors, which are expected to occur more often when developmental processes are accelerated (Kunkel, 2004; Lindahl, 1993; Lynch, 2010). This happens potentially by altering DNA replication dynamics; for instance, mutation rates are known to be higher in genomic regions that replicate late in S-phase (the DNA synthesis phase of the cell cycle), a state that may be more prevalent under temporal pressure (Stamatoyannopoulos et al., 2009). In systems ranging from viruses to yeast, such errors are a known constraint on rapid growth (Liu & Zhang, 2021; Regoes et al., 2013), and our results demonstrate this principle operating in the germline of a complex animal as well, providing strong evidence for a replication-dependent mutational load due to overly fast reproduction. Although the shift in the mutational spectrum was subtle, the daily rate of *de novo* indels was significantly higher in the Short-GT group (posterior probability = 99.4%). This elevated daily influx of replication errors is consistent with the molecular signatures of high-speed DNA synthesis and supports our mechanistic interpretation.

Time-dependent DNA decay increases the mutational load at long GTs

Conversely, the Long-GT group exemplifies the time-dependent accumulation, but with a critical temporal nuance. These groups accumulated a 1.2-fold higher mutation rate per generation, confirming that a longer chronological window allows for a greater total accumulation of mutations (Latta et al., 2013; Thomas et al., 2010). Despite this higher generational total, however, the daily influx of mutations was significantly lower than in the Short-GT group. The mutational spectrum gave a hint on the resolution of this apparent paradox. The shift to a lower *Ts*/*Tv* ratio (0.89) is indicative of a greater relative contribution from time-dependent DNA damage, such as oxidative lesions that are known to produce transversions (La et al., 2023; Wang & Obbard, 2023). This indicates that while the chronological clock of mutation accumulation is always ticking, its daily rate is substantially lower than the rate of error introduction during rapid replication. This demonstrates that while the chronological "clock" is a persistent source of mutations, its per-day impact on the total mutation rate is small compared to the errors introduced by the "replication fidelity clock" when development is accelerated.

Resolving the scaling conflict

Recent models in vertebrates propose that GT effects can be explained by a "weighted average" of rapid embryonic mutation rates and slower germline stem cell rates (Thomas et al., 2018; Venn et al., 2014). In mammals, GT differences often result from extending the adult phase (where cell division is slow). In *C. riparius*, the adult phase is inherently short (1–2 days) and of relatively fixed duration compared to the larval stages. Consequently, the observed difference in GT was entirely caused by the speed of larval development. Therefore, the "weighted average" model of embryonic vs. adult rates cannot explain our data. Instead, the physiological process of rapid larval growth itself appears to incur a cost in replication fidelity. The "U-shaped" relationship where the population mean GT coincides with the mutational minimum (Figure 3), likely reflects the crossover point where the costs of rapid replication errors and the costs of slow development (time-dependent accumulation) are jointly minimized.

The population's mean developmental time coincides with the mutational minimum

Bayesian analysis showed that the 95% HDI for the mutation rates at intermediate generation lengths did not overlap with those from either the short or the long GT groups. This indicated a posterior probability of nearly 100% that the mutation rate at the nadir is truly lower than at the extremes. These distinct mutational regimes predict that the daily mutational burden should be a nonlinear (perhaps quadratic) function of GT, but the evolutionary relevance of this pattern hinges on whether the species' natural life history coincides with this minimum.

The distribution of GT of over 1,700 individuals from earlier studies (see above) revealed that the mean of the GT for *C. riparius* under these experimental conditions lies between the nadirs of

both the daily mutation rate (Figure 2C) and the generational mutation rate (Figure 2D). Even more interestingly, the analysis of the GT distribution revealed that it is significantly better described by a mixture of two normal distributions (Figure 1B). The two-modal distribution is consistent with a model where an allele of large effect segregates in the population in addition to polygenic variation (Jain & Stephan, 2015). Crucially, because these groups were reared under identical conditions, the observed differences reflect intrinsic variation, driven by genetic background or developmental noise rather than phenotypic plasticity. This polygenic basis implies that there is substantial phenotypic variation of this trait in natural populations (Barghi et al., 2019) if not all contributing loci are fixed. The non-linear reaction norm of the mutation rate in relation to GT found here therefore means that the mean mutation rate in natural populations is likely to be higher than that measured in the laboratory at optimal GT, regardless of other natural (Waldvogel & Pfenninger, 2021) and anthropogenic (Bulut et al., 2024; Rigano et al., 2025) factors that may increase it.

In principle, earlier reproduction should increase individual fitness by producing more direct and later generation offspring faster, particularly in a species with a predominantly semelparous life history such as *C. riparius*, where fitness is largely determined by a single, successful reproductive event following maturation (Brommer et al., 2002). If there is genetic variation in developmental speed, there should be a selective pressure toward early reproduction. Experimental evolution on developmental time clearly showed a strong and rapid selective response, indicating a broad, polygenic basis for GT variation (Caliendo, 2025). However, a shorter developmental time is inevitably associated with costs, and the mutational load associated with a higher mutation rate is likely one of them (Leslie et al., 2017). While some theories propose that higher mutation rates could be adaptive under stressful conditions by increasing "evolvability" (Metzgar & Wills, 2000), theoretical and empirical evidence show that mutational load tends to overall decrease population fitness (Grossen & Ramakrishnan, 2024; Lynch et al., 2016). Our data reveal a striking concordance: the population's modal GT (∼26 days) coincides with the nadir of the mutation rate. While ecological drivers such as predation risk, resource availability, and temperature are undoubtedly selective forces determining GT (Luhring et al., 2018; Twardochleb et al., 2023), this coincidence suggests that the species' molecular machinery has co-evolved to minimize mutational load at its most frequent developmental pace. At this optimum, development is slow enough to maintain high replication fidelity, mitigating the costs of speed, yet rapid enough to avoid the substantial accumulation of time-dependent mutations, mitigating the costs of time. A first step toward demonstrating this would be to prove that individuals with extreme GTs are less fit than individuals at the supposed optimum. It would also be interesting to see whether individual mutation rates along the GT gradient exhibit dynamic cryptic genetic variation, as is the case with temperature (Pfenninger et al., 2025).

Mutational spectra suggest that deviation from optimal GT *per se* influences mutation rates

Our findings hint at a surprising resolution of the temperature-mutation paradox previously described in ectotherms. A prior study in *C. riparius* reported a U-shaped relationship between temperature and mutation rate, where μ increased significantly under both heat stress and cold conditions (Waldvogel & Pfenninger, 2021). While the elevated rate in the heat was explained by metabolic stress and increased ROS production, the high mutation rate in the cold has remained puzzling, as lower temperatures where reproduction is still possible typically suppress metabolic rate and ROS generation in this species (Bulut et al., 2025; Lalouette et al., 2011). According to expectations, the placements of mutational spectra along the significant first PCA axis grouped the mutational spectrum of the Long-GT group with the spectrum of the coldest temperature (12 °C), while the Short-GT group clustered with the highest temperature (23 °C). However, the largest separation of mutational spectra existed between this group of extreme temperatures/GTs on the one hand and all spectra recorded at evolutionary optimal temperatures/GTs (14 and 17 °C) on the other. Under the assumption that similar spectra signify similar mutational processes (Rahbari et al., 2016), this suggested that the either intrinsically or thermally driven deviation from the evolutionary optimal GT per se might govern mutation rates. The divide along the (insignificant) PCA2 indicated, however, that the mutational processes for external temperature and intrinsically driven GT extremes were not completely identical. However, the similar spectral pattern found for extreme GTs calls into question the hypothesis that ROS caused by metabolic stress is the major reason for an increased mutation rate at moderately elevated temperatures.

Methodological implications for non-model organisms

A significant challenge in estimating spontaneous mutation rates in non-model organisms is the difficulty of isolating mating pairs in species with complex reproductive behaviors, such as swarming (Downe & Caspary, 1973; Foucault et al., 2019). Our study validates a parent-offspring triangulation design where parental allelic compositions are reconstructed *in silico* from pooled offspring sequencing. This approach successfully identified high-confidence de novo mutations without requiring physical isolation of the parents, nor the sequencing of the parents themselves. This methodology offers a robust framework for future mutation rate studies in a wide range of organisms where standard parent-offspring trio sequencing is logistically unfeasible but many siblings are available.

Implications for life-history evolution

The current view of mutation rate evolution acknowledges that while ultimate limits may be set by the drift-barrier (Lynch et al., 2016), the realized rate is a highly plastic trait shaped by an organism's internal and external environment (Sharp & Agrawal, 2018). Our dual-mechanism optimization model provides a novel hypothesis for an environmentally independent part of this lability by suggesting a direct link between an organism's GT and its mutational load.

Data and code availability

All nucleotide sequences used in this study are deposited in the European Nucleotide Archive (ENA) under the project number PRJEB89193. Raw data for the analyses were made available at Zenodo: doi.org/10.5281/zenodo.18621629

Funding

We gratefully acknowledge the support of this study by a grant of the Deutsche Forschungsgemeinschaft (PF 390/15-1) to M.P.

Conflicts of interest

The authors declare no conflict of interest.

References

Ames, B. N. (1983). Dietary carcinogens and anticarcinogens. Oxygen radicals and degenerative diseases. *Science*, *221*, 1256–1264. https://doi.org/10.1126/science.6351251.

Pfenninger, M., Foucault, Q., Waldvogel, AM., & Feldmeyer, B. (2023). Selective effects of a short transient environmental fluctuation on a natural population. *Mol Ecol*, *32*, 335–349. https://doi.org/10.1111/mec.16748

Pfenninger, M. (2017). The effect of offspring number on the adaptation speed of a polygenic trait. *bioRxiv* 212613. https://doi.org/10.1101/212613

Pfenninger, M., & Foucault, Q. (2022). Population Genomic Time Series Data of a Natural Population Suggests Adaptive Tracking of Fluctuating Environmental Changes. *Integr Comp Biol*, *62*, 1812–1826. https://doi.org/10.1093/icb/icac098

Waldvogel, AM., Wieser, A., Schell, T., Patel, S., Schmidt, H., Hankeln, T., Feldmeyer, B., & Pfenninger, M. (2018). The genomic footprint of climate adaptation in Chironomus riparius. *Mol Ecol*, *27*, 1439–1456. https://doi.org/10.1111/mec.14543

Bååth, R. (2014). Bayesian first aid: A package that implements Bayesian alternatives to the classical∗. test functions in R. *Proc. UseR*, *2014*, 2.

Barghi, N., Tobler, R., Nolte, V., Jakšić, A. M., Mallard, F., Otte, K. A., Dolezal, M., Taus, T., Kofler, R., & Schlötterer, C. (2019). Genetic redundancy fuels polygenic adaptation in *Drosophila*. *PLOS Biology*, *17*, e3000128. https://doi.org/10.1371/journal.pbio.3000128.

Beichman, A. C., Zhu, L., & Harris, K. (2024). The evolutionary interplay of somatic and germline mutation rates. *Annu. Rev. Biomed. Data Sci.*, *7*, 83–105. https://doi.org/10.1146/annurev-biodatasci-102523-104225.

Benaglia, T., Chauveau, D., Hunter, D. R., & Young, D. S. (2009). mixtools: an R package for analyzing mixture models. *Journal of Statistical Software*, *32*, 1–29. https://doi.org/10.18637/jss.v032.i06.

Brommer, J. E., Merilä, J., & Kokko, H. (2002). Reproductive timing and individual fitness. *Ecology Letters*, *5*, 802–810. https://doi.org/10.1046/j.1461-0248.2002.00369.x.

Bulut, B., Geiss, M., Bernard, M., Doria, H. B., Feldmeyer, B., & Pfenninger, M. (2025). Dissecting oxidative stress and organismic response to various temperature regimes in the midge *C. riparius*. *Ecology and Evolution*, *15*(12), e72625. https://doi.org/10.1002/ece3.72625.

Bulut, B., Rigano, L., Doria, H. B., Gemüth, G., & Pfenninger, M. (2024). A multigenerational study can detect the evolutionary response to BaP exposure in the non-biting freshwater midge *Chironomus riparius*. *Chemosphere*, *358*, 142242. https://doi.org/10.1016/j.chemosphere.2024.142242.

Caliendo, C. (2025). Insights into rapid adaptation patterns in *Chironomus riparius* through advanced bioinformatics. https://doi.org/10.25358/openscience-13319.

DePristo, M. A., Banks, E., Poplin, R., Garimella, K. V., Maguire, J. R., Hartl, C., Philippakis, A. A., del Angel, G., Rivas, M. A., Hanna, M., McKenna, A., Fennell, T. J., Kernytsky, A. M., Sivachenko, A. Y., Cibulskis, K., Gabriel, S. B., Altshuler, D., & Daly, M. J. (2011). A framework for variation discovery and genotyping using next-generation DNA sequencing data. *Nature Genetics*, *43*, 491–498. https://doi.org/10.1038/ng.806.

Downe, A. E. R., & Caspary, V. G. (1973). The swarming behaviour of *Chironomus riparius* (DIPTERA: CHIRONOMIDAE) in the laboratory. *Canadian Entomologist*, *105*, 165–171. https://doi.org/10.4039/Ent105165-1.

Drake, J. W. (1991). A constant rate of spontaneous mutation in DNA-based microbes. *Proceedings of the National Academy of Sciences 88*, 7160–7164. https://doi.org/10.1073/pnas.88.16.7160.

Foucault, Q., Wieser, A., Waldvogel, A., & Pfenninger, M. (2019). Establishing laboratory cultures and performing ecological and evolutionary experiments with the emerging model species *Chironomus riparius*. *Journal of Applied Entomology*, *143*, 584–592. https://doi.org/10.1111/jen.12606.

Gao, Z., Wyman, M. J., Sella, G., & Przeworski, M. (2016). Interpreting the dependence of mutation rates on age and time. *PLoS Biology*, *14*, e1002355. https://doi.org/10.1371/journal.pbio.1002355.

Gillooly, J. F., Brown, J. H., West, G. B., Savage, V. M., & Charnov, E. L. (2001). Effects of size and temperature on metabolic rate. *Science*, *293*, 2248–2251. https://doi.org/10.1126/science.1061967 .

Grossen, C., & Ramakrishnan, U. (2024). Genetic load. *Current Biology*, *34*, R1216–R1220. https://doi.org/10.1016/j.cub.2024.11.004.

Halliwell, B., & Gutteridge, J. M. (1990). Role of free radicals and catalytic metal ions in human disease: an overview. *Methods in Enzymology*, *186*, 1–85. https://doi.org/10.1016/0076-6879(90)86093-b .

Hammer, Ø. (2001). PAST-Palaeontological statistics, *Palaeontologia electronica*, *4*, 1–9.

Jain, K., & Stephan, W. (2015). Response of polygenic traits under stabilizing selection and mutation when loci have unequal effects. *G3 GenesGenomesGenetics*, *5*, 1065–1074. https://doi.org/10.1534/g3.115.017970.

Keightley, P. D., Trivedi, U., Thomson, M., Oliver, F., Kumar, S., & Blaxter, M. L. (2009). Analysis of the genome sequences of three *Drosophila melanogaster* spontaneous mutation accumulation lines. *Genome Research*, *19*, 1195–1201. https://doi.org/10.1101/gr.091231.109.

Kunkel, T. A. (2004). DNA replication fidelity. *Journal of Biological Chemistry*, *279*, 16895–16898. https://doi.org/10.1074/jbc.R400006200.

La, B., Besenbacher, S., Zheng, J., Li, P., Bertelsen, M.F., Quintard, B., Hoffman, J.I., Li, Z., St Leger, J., Shao, C., Stiller, J., Gilbert, M.T.P., Schierup, M.H., & Zhang, G., (2023). Evolution of the germline mutation rate across vertebrates. *Nature*, *615*, 285–291. https://doi.org/10.1038/s41586-023-05752-y.

Lalouette, L., Williams, C. M., Hervant, F., Sinclair, B. J., & Renault, D. (2011). Metabolic rate and oxidative stress in insects exposed to low temperature thermal fluctuations. *Comparative Biochemistry and Physiology Part A: Molecular & Integrative Physiology*, *158*, 229–234. https://doi.org/10.1016/j.cbpa.2010.11.007.

Latta, L. C., Morgan, K. K., Weaver, C. S., Allen, D., Schaack, S., & Lynch, M. (2013). Genomic background and generation time influence deleterious mutation rates in *Daphnia*. *Genetics*, *193*, 539–544. https://doi.org/10.1534/genetics.112.146571 .

Leslie, M. P., Shelton, D. E., & Michod, R. E. (2017). Generation time and fitness tradeoffs during the evolution of multicellularity. *Journal of Theoretical Biology*, *430*, 92–102. https://doi.org/10.1016/j.jtbi.2017.07.007.

Li, H. (2013). Aligning sequence reads, clone sequences and assembly contigs with BWA-MEM. https://doi.org/10.48550/arXiv.1303.3997.

Li, H., Handsaker, B., Wysoker, A., Fennell, T., Ruan, J., Homer, N., Marth, G., Abecasis, G., & Durbin, R., 1000 Genome Project Data Processing Subgroup (2009). The sequence alignment/map format and SAMtools. *Bioinformatics Oxford English*, *25*, 2078–2079. https://doi.org/10.1093/bioinformatics/btp352.

Li, W.-H., Tanimura, M., & Sharp, P. M. (1987). An evaluation of the molecular clock hypothesis using mammalian DNA sequences. *Journal of Molecular Evolution*, *25*, 330–342. https://doi.org/10.1007/BF02603118.

Lindahl, T. (1993). Instability and decay of the primary structure of DNA. *Nature*, *362*, 709–715. https://doi.org/10.1038/362709a0.

Liu, H., & Zhang, J. (2021). The rate and molecular spectrum of mutation are selectively maintained in yeast. *Nature Communications*, *12, 4044*. https://doi.org/10.1038/s41467-021-24364-6.

Luhring, T. M., Vavra, J. M., Cressler, C. E., & DeLong, J. P. (2018). Predators modify the temperature dependence of life-history trade-offs. *Ecology & Evolution*, *8*, 8818–8830. https://doi.org/10.1002/ece3.4381.

Lynch, M. (2010). Evolution of the mutation rate. *Trends in Genetics*, *26*, 345–352. https://doi.org/10.1016/j.tig.2010.05.003.

Lynch, M., Ackerman, M. S., Gout, J.-F., Long, H., Sung, W., Thomas, W. K., & Foster, P. L. (2016). Genetic drift, selection and the evolution of the mutation rate. *Nature Reviews Genetics*, *17*, 704–714. https://doi.org/10.1038/nrg.2016.104.

Lynch, M., Ali, F., Lin, T., Wang, Y., Ni, J., & Long, H. (2023). The divergence of mutation rates and spectra across the Tree of Life. *EMBO Reports*, *24, EMBR202357561*. https://doi.org/10.15252/embr.202357561.

Maki, H. (2002). Origins of spontaneous mutations: specificity and directionality of base-substitution, frameshift, and sequence-substitution mutageneses. *Annual Review of Genetics*, *36*, 279–303. https://doi.org/10.1146/annurev.genet.36.042602.094806.

Metzgar, D., & Wills, C. (2000). Evidence for the adaptive evolution of mutation rates. *Cell*, *101*, 581–584. https://doi.org/10.1016/s0092-8674(00)80869-7 .

Ohta, T. (1995). Synonymous and nonsynonymous substitutions in mammalian genes and the nearly neutral theory. *Journal of Molecular Evolution*, *40*, 56–63. https://doi.org/10.1007/BF00166595.

Oppold, AM., Pedrosa, JA., Bálint, M., Diogo, JB., Ilkova, J., Pestana, JL., & Pfenninger, M. (2016). Support for the evolutionary speed hypothesis from intraspecific population genetic data in the non-biting midge Chironomus riparius.. *Proc Biol Sci*, *283*, 20152413. 20152413

Oppold, A., & Pfenninger, M. (2017). Direct estimation of the spontaneous mutation rate by short-term mutation accumulation lines in *Chironomus riparius*. *Evolution Letters*, *1*, 86–92. https://doi.org/10.1002/evl3.8.

Pettrich, L. C., King, R., Field, L. M., & Waldvogel, A.-M. (2024). The interplay of recombination landscape, a transposable element and population history in European populations of *Chironomus riparius*. https://doi.org/10.1101/2024.04.04.588075 bioRxiv.

Pfenninger, M., Nieto-Blazquez, M.-E., Schell, T., Geiss, M., Bulut, B., Eberhardt, L., & Feldmeyer, B. (2025). Pervasive and dynamic release of Cryptic Genetic Variation in *Chironomus riparius*: rethinking adaptation in fluctuating environments. https://doi.org/10.1101/2025.07.01.661462 bioRxiv.

Rahbari, R., Wuster, A., Lindsay, S. J., Hardwick, R. J., Alexandrov, L. B., Turki, S. A., Dominiczak, A., Morris, A., Porteous, D., Smith, B., Stratton, M. R., UK10K ConsortiumHurles, M. E. (UK10K Consortium, 2016). Timing, rates and spectra of human germline mutation. *Nature Genetics*, *48*, 126–133. https://doi.org/10.1038/ng.3469.

Regoes, R., Hamblin, S., & Tanaka, M. M. (2013). Viral mutation rates: modelling the roles of within-host viral dynamics and the trade-off between replication fidelity and speed. *Proceedings of the Royal Society B: Biological Sciences*, *280, 1750*. https://doi.org/10.1098/rspb.2012.2047.

Rigano, L., Schmitz, M., Linnemann, V., Krauss, M., Hollert, H., & Pfenninger, M. (2025). Exposure to complex mixtures of urban sediments containing Tyre and Road Wear particles (TRWPs) increases the germ-line mutation rate in *Chironomus riparius*. *Aquatic Toxicology*, *281*, 107292. https://doi.org/10.1016/j.aquatox.2025.107292.

Robinson, J. T., Thorvaldsdóttir, H., Winckler, W., Guttman, M., Lander, E. S., Getz, G., & Mesirov, J. P. (2011). Integrative genomics viewer. *Nature Biotechnology*, *29*, 24–26. https://doi.org/10.1038/nbt.1754.

Sharp, N. P., & Agrawal, A. F. (2018). An experimental test of the mutation-selection balance model for the maintenance of genetic variance in fitness components. *Proceedings of the Royal Society B: Biological Sciences*, *285*, 20181864. https://doi.org/10.1098/rspb.2018.1864.

Shokolenko, I., Venediktova, N., Bochkareva, A., Wilson, G. L., & Alexeyev, M. F. (2009). Oxidative stress induces degradation of mitochondrial DNA. *Nucleic Acids Research*, *37*, 2539–2548. https://doi.org/10.1093/nar/gkp100.

Stamatoyannopoulos, J. A., Adzhubei, I., Thurman, R. E., Kryukov, G. V., Mirkin, S. M., & Sunyaev, S. R. (2009). Human mutation rate associated with DNA replication timing. *Nature Genetics*, *41*, 393–395. https://doi.org/10.1038/ng.363.

Sun, C., López Arriaza, J. R., & Mueller, R. L. (2012). Slow DNA loss in the gigantic genomes of salamanders. *Genome Biology and Evolution*, *4*, 1340–1348. https://doi.org/10.1093/gbe/evs103.

Tanay, A., & Siggia, E. D. (2008). Sequence context affects the rate of short insertions and deletions in flies and primates. *Genome Biology*, *9*, R37. https://doi.org/10.1186/gb-2008-9-2-r37.

Thomas, G. W. C., Wang, R. J., Puri, A., Harris, R. A., Raveendran, M., Hughes, D. S. T., Murali, S. C., Williams, L. E., Doddapaneni, H., Muzny, D. M., Gibbs, R. A., Abee, C. R., Galinski, M. R., Worley, K. C., Rogers, J., Radivojac, P., & Hahn, M. W. (2018). Reproductive longevity predicts mutation rates in primates. *Current Biology*, *28*, 3193–3197.e5. https://doi.org/10.1016/j.cub.2018.08.050.

Thomas, J. A., Welch, J. J., Lanfear, R., & Bromham, L. (2010). A generation time effect on the rate of molecular evolution in invertebrates. *Molecular Biology and Evolution*, *27*, 1173–1180. https://doi.org/10.1093/molbev/msq009.

Twardochleb, L. A., Zarnetske, P. L., & Klausmeier, C. A. (2023). Life-history responses to temperature and seasonality mediate ectotherm consumer–resource dynamics under climate warming. *Proceedings of the Royal Society B: Biological Sciences*, *290*, 20222377. https://doi.org/10.1098/rspb.2022.2377.

Van der Auwera, G. A., Carneiro, M. O., Hartl, C., Poplin, R., Del Angel, G., Levy-Moonshine, A., Jordan, T., Shakir, K., Roazen, D., Thibault, J., Banks, E., Garimella, K. V., Altshuler, D., Gabriel, S., & DePristo, M. A. (2013). From FastQ data to high confidence variant calls: the Genome Analysis Toolkit best practices pipeline. *Current Protocols in Bioinformatics*, *43*, 11.10.1–11.10.33. https://doi.org/10.1002/0471250953.bi1110s43.

Venn, O., Turner, I., Mathieson, I., de Groot, N., Bontrop, R., & McVean, G. (2014). Strong male bias drives germline mutation in chimpanzees. *Science*, *344*, 1272–1275. https://doi.org/10.1126/science.344.6189.1272 .

Waldvogel, A.-M., & Pfenninger, M. (2021). Temperature dependence of spontaneous mutation rates. *Genome Research*, *31*, 1582–1589. https://doi.org/10.1101/gr.275168.120.

Wang, Y., & Obbard, D. J. (2023). Experimental estimates of germline mutation rate in eukaryotes: a phylogenetic meta-analysis. *Evolution Letters*, *7*, 216–226. https://doi.org/10.1093/evlett/qrad027.

Winter, D. J., Wu, S. H., Howell, A. A., Azevedo, R. B. R., Zufall, R. A., & Cartwright, R. A. (2018). accuMUlate: a mutation caller designed for mutation accumulation experiments. *Bioinformatics*, *34*, 2659–2660. https://doi.org/10.1093/bioinformatics/bty165 .

Zhang, J., Kobert, K., Flouri, T., & Stamatakis, A. (2014). PEAR: a fast and accurate Illumina Paired-end reAd mergeR. *Bioinformatics*, *30*, 614–620. https://doi.org/10.1093/bioinformatics/btt593 .

Zhu, L., Beichman, A., & Harris, K. (2024). Population size interacts with reproductive longevity to shape the germline mutation rate. *Proceedings of the National Academy of Sciences*, *122* (21), e2423311122. https://doi.org/10.1073/pnas.2423311122

Zuckerkandl, E., & Pauling, L. (1965). Evolutionary divergence and convergence in proteins. In V. Bryson, & H.J. Vogel (Eds.), *Evolving genes and proteins* (pp. 97–166). Academic Press. https://doi.org/10.1016/B978-1-4832-2734-4.50017-6.

Received: 15 December 2025. **Revised:** 12 February 2026. **Accepted:** 19 February 2026

Chapter 2

Dissecting Oxidative Stress and Organismic Response to a Temperature Gradient in the Midge *Chironomus riparius*

Burak Bulut[1], Maximillian Geiss, Markus Bernard, Halina Binde Doria, Barbara Feldmeyer, Markus Pfenninger

[1] first author

Published as: Bulut, B., M. Geiss, M. Bernard, H. B. Doria, B. Feldmeyer, and M. Pfenninger. 2025. “Dissecting Oxidative Stress and Organismic Response to a Temperature Gradient in the Midge *Chironomus riparius*.” Ecology and Evolution 15, no. 12: e72625. https://doi.org/10.1002/ece3.72625.

Acknowledgements: The authors are grateful for support by a DFG grant to M.P. (PF 390/15-1). Open Access funding enabled and organized by Projekt DEAL.

Funding: This work was supported by Deutsche Forschungsgemeinschaft, PF 390/15-1.

Conflict of Interest: The authors declare no conflicts of interest.

Data Availability: The data is accessible at the European Nucleotide Archive (ENA) under accession number PRJEB89193. All other primary data supporting the results of this study, including raw fluorescence intensity measurements and sample metadata, can be found at Zenodo doi: doi.org/10.5281/zenodo.17184450

Ecology and Evolution

WILEY

Ecology and Evolution Open Access

RESEARCH ARTICLE OPEN ACCESS

Dissecting Oxidative Stress and Organismic Response to a Temperature Gradient in the Midge *Chironomus riparius*

Burak Bulut[1] | Maximilian Geiss[2] | Markus Bernard[3] | Halina Binde Doria[3] | Barbara Feldmeyer[1] | Markus Pfenninger[1,2,3]

[1]Department of Molecular Ecology, Senckenberg Biodiversity and Climate Research Centre, Frankfurt am Main, Germany | [2]Institute for Molecular and Organismic Evolution, Johannes Gutenberg University, Mainz, Germany | [3]LOEWE Centre of Translational Biodiversity Genomics, Senckenberg Biodiversity and Climate Research Centre, Frankfurt am Main, Germany

Correspondence: Markus Pfenninger (markus.pfenninger@senckenberg.de)

Received: 26 September 2025 | **Revised:** 11 November 2025 | **Accepted:** 24 November 2025

Keywords: antioxidant response | climate change | insect | oxidative stress | temperature stress

ABSTRACT

Oxidative stress, caused by reactive oxygen species (ROS), poses a major challenge for organisms facing temperature fluctuations. This study provides the first direct in vivo measurements of ROS production together with transcriptome analysis of oxidative stress genes across a broad range of ecologically relevant temperatures in insect larvae of the dipteran midge *Chironomus riparius*. We observed a U-shaped pattern of oxidative stress, with minimal ROS levels within an optimal thermal window (12°C–18°C) and significantly elevated stress at both cold and warm extremes. Crucially, our findings reveal distinct underlying molecular mechanisms for ROS generation at these extremes: at low temperatures, predominantly ROS produced is of the superoxide group, linked to hypoxia-induced hemoglobin autoxidation. Conversely, at high temperatures, the hydrogen peroxide group dominates, associated with increased metabolic rate and heat stress signaling pathways. Transcriptomic analysis shows that *C. riparius*'s antioxidant defense system adapts accordingly, selectively upregulating mechanisms to counteract the specific dominant ROS type at different temperatures. This mechanistically differentiated oxidative stress at different temperatures and the modulated organismic response reflect the ecological niche and evolution of *C. riparius*.

1 | Introduction

In their natural habitats, most organisms are subjected to a range of temperatures throughout their lifespan. Temperature can vary across multiple temporal and spatial scales, ranging from gradual changes across seasons overlain by multiday weather periods and rapid fluctuations over the course of a single day, as well as spatial thermal heterogeneity within the habitat. These fluctuations are especially pronounced in temperate regions, where seasonal shifts in temperature can be substantial, requiring organisms to cope with prolonged periods of suboptimal or stressful conditions (Heise et al. 2007). Given that temperature influences the rate of all chemical reactions, each temperature represents a distinct environmental condition that ultimately affects organismal fitness (Kiekebusch et al. 2024). Deviations from the optimal temperature range that the organism is adapted to may therefore result in increased stress, diminished fitness, and in the extreme, mortality (Gasparrini et al. 2015).

A primary consequence of temperature-related stress is the disruption of cellular homeostasis, which elicits a complex, integrated stress response. This response is multifaceted, involving an array of protective mechanisms. A key component is the upregulation of *heat shock proteins* (HSPs), which function as molecular chaperones to refold denatured proteins and maintain cellular integrity under thermal duress (Hagymasi et al. 2022). Concurrently, organisms often engage in membrane remodeling, adjusting the lipid composition of cellular membranes to maintain optimal fluidity and function across different

temperatures, a process known as homeoviscous adaptation (Los and Leusenko 2025). Another reason for temperature-related stress is the production of reactive oxygen species (ROS) (Szechyńska-Hebda et al. 2022). ROS are highly reactive molecules that necessarily occur in every living cell. The majority of ROS generated within cells is produced by mitochondria as an unavoidable by-product of the electron transport chain, primarily by complexes I and III (Hernansanz-Agustín and Enríquez 2021; Pfenninger and Foucault 2020). The actual ROS composition produced depends strongly on the stress-inducing conditions and the organism's condition and may thus vary widely (Das and Roychoudhury 2014). While the broader cellular stress response is critical for survival, this study focuses on providing a mechanistic understanding of the oxidative stress component of thermotolerance.

To prevent the damage caused by ROS, cells have evolved sophisticated antioxidant defense systems that include both non-enzymatic and enzymatic components. The non-enzymatic antioxidant system, whose basic concept is to produce bait substances that are oxidized by ROS instead of essential cell components (e.g., vitamin C, glutathione, etc.; Chinta and Andersen 2008; Liu et al. 2020). On the other hand, the enzymatic antioxidant system produces diverse enzymes to directly turn ROS into less harmful substances. This system encompasses superoxide dismutase, catalase, glutathione peroxidase, thioredoxin, peroxiredoxin, and glutathione transferase (Jomova et al. 2024). Antioxidant enzymes are distributed throughout various cellular compartments to counteract ROS wherever they occur (Nwachukwu et al. 2021). However, ROS molecules are not only harmful; they are essential for a multitude of cellular processes, including signaling and the defense against xenobiotic agents. As a result, cells attempt to maintain a delicate equilibrium between ROS production and removal by the antioxidant systems (Mackova et al. 2024; Sikder et al. 2025).

If ROS molecules are not swiftly scavenged, they cause widespread damage to macromolecules, which translates directly into fitness costs. The oxidation of metabolic enzymes (proteins) can impair energetic efficiency, while damage to cell membranes (lipids) can disrupt cellular transport and signaling, directly impacting growth and survival (Ntawubizi and Mukamuhirwa 2024). Crucially, oxidative damage to DNA not only compromises somatic cell function but can also introduce mutations into the germline, a link that is a powerful mechanism for evolutionary change (Dowling and Simmons 2009). Therefore, understanding how organisms manage oxidative stress is fundamental to explaining variation in key life history traits such as metabolic efficiency, growth rate, and transgenerational genomic integrity.

Studies of temperature-induced ROS effects have predominantly focused on plant systems, resulting in a substantial body of literature on the mechanisms and impacts of oxidative stress (Devireddy et al. 2021). The few prior studies in animals examining temperature-related oxidative stress employed indirect methods, such as measuring enzyme activity and/or gene expression of antioxidative genes (Yang et al. 2024; Zhang et al. 2015). Moreover, previous studies investigating ROS production have predominantly focused on high (Farahani et al. 2020; Zhang et al. 2014) or low (El-Saadi et al. 2023; Lebenzon et al. 2023) temperature conditions, and only a few have examined both thermal extremes within the same framework (Cui et al. 2011; Yang et al. 2010).

To our knowledge, no study has yet systematically measured ROS production in vivo across a continuous, ecologically relevant temperature gradient in an insect model. This represents a significant research gap, particularly because physiological responses to temperature are rarely linear. Thermal performance curves typically show that stress is minimized within an optimal window and overproportionally increases at both colder and warmer extremes (Pörtner et al. 2006). In *C. riparius* specifically, this U-shaped pattern has been documented for spontaneous mutation rates (Waldvogel and Pfenninger 2021). Based on these theoretical grounds and empirical observations, we hypothesize that overall ROS levels will also exhibit a U-shaped pattern, with minimal production within an optimal thermal window and significantly elevated levels at both cold and warm extremes.

This study aims to test this hypothesis by providing the first direct in vivo measurements of ROS production across a broad thermal gradient in *C. riparius*, alongside a transcriptomic analysis of its antioxidant defense system. Characterizing this relationship is critical for understanding the evolutionary implications of thermal stress. Variation among individuals in their ability to manage ROS can create fitness differentials, providing the raw material for natural selection to act upon (Huchzermeyer et al. 2022). Therefore, by dissecting the mechanistic underpinnings of temperature-induced oxidative stress, we are investigating a key physiological process that can determine a population's capacity to adapt to rising average temperatures and increased thermal extremes, or conversely, highlight its vulnerability in the face of climate change (Said and Nassar 2022).

2 | Material and Method

2.1 | Test Animal and Experimental Design

We selected the nonbiting midge *Chironomus riparius* for this study due to a combination of its ecological, practical, and physiological attributes. Ecologically, it is a widespread freshwater insect in temperate regions, central to benthic food webs, where its aquatic larvae are naturally exposed to significant daily and seasonal temperature fluctuations (Oppold et al. 2016). Practically, it is a well-established model organism in ecotoxicology and evolutionary biology, with standardized rearing protocols and extensive genomic resources available (Foucault et al. 2019; Pettrich et al. 2024). Physiologically, *C. riparius* possesses a unique hemoglobin-based respiratory system that makes it highly tolerant of hypoxia but also particularly susceptible to specific forms of oxidative stress linked to hemoglobin autoxidation, providing a useful system for investigating these mechanisms.

As a widespread freshwater insect, *C. riparius* inhabits rivers, lakes, and ponds across diverse climatic zones, including Hessen, Germany, where our lab population originates. In this region, temperature fluctuates seasonally and geographically, with an annual mean of approximately 9.74°C (Waldvogel and

Pfenninger 2021). Seasonal averages provide a more nuanced perspective: during spring and summer (May to September), the main reproductive period temperatures typically range from 13°C to 18°C, while occasional summer heatwaves or warmer microhabitats may push temperatures higher. In contrast, winter temperatures (November to February) often drop below 5°C, sometimes approaching 2°C (Oppold et al. 2016).

All experimental animals originated from a long-term laboratory culture established in 2015 (Oppold et al. 2016) with individuals from the Hasselbach stream in Hessen, Germany (50°12′N, 8°37′E). The stock population is maintained under controlled conditions at 20°C on a 16:8 light:dark photoperiod. Cultures are housed in plastic tray aquaria containing a 1.5 cm layer of fine sand (> 0.2 μm) and are supplied with constant aeration. Larvae are fed *ad libitum* with commercial fish food (TetraMin). To minimize inbreeding and prevent significant laboratory adaptation, the culture is maintained with a large breeding population size (> 500 individuals per generation) and is refreshed every 2 years with new wild-caught individuals from the source population. All larvae used in the experiments were reared under these standard conditions until the start of the thermal treatments.

For all experiments, L3-stage larvae were selected from this stock culture, due to their established physiological robustness and active metabolic state, making them highly responsive to thermal stressors. This stage avoids the practical challenges associated with handling smaller L1 and L2 larvae and the confounding physiological and transcriptomic changes related to beginning metamorphosis in L4 larvae (Eberhardt et al. 2025). A total of 20 L3-stage larvae were collected from this laboratory culture for each treatment and placed in 24-well plates. The plates were filled with 2.5 mL of the medium described in detail in (Foucault et al. 2018; Oppold et al. 2016).

We used a relatively recently developed method to measure ROS levels in living organisms (Kang et al. 2013). The use of cell-permeable fluorogenic probes allows for the measurement of ROS-related fluorescence intensity within the cells of living organisms. Two different reagents were used to identify the different ROS under different temperatures: CellROX Orange (Thermo Fisher cat. no. C10443) and CellROX Red reagents (Thermo Fisher cat. no. C10422). In the reduced state, the reagents are nonfluorescent. However, following oxidation by ROS, they exhibit fluorogenic signals at 545/565 nm for CellROX Orange and 640/665 nm excitation/emission wavelengths for CellROX Red. CellROX Orange is capable of detecting five distinct ROS, including hydrogen peroxide, hydroxyl radical, nitric oxide, peroxynitrite anion, and superoxide anion. In contrast, CellROX Red only detects two ROS, namely the hydroxyl radical and superoxide anion, which are also part of CellROX Orange. The difference between the CellROX Red and the CellROX Orange signal thus gives a hint at the relative proportion of the two ROS groups produced. Even though these substances are present in excess in the cells, they cannot scavenge all ROS molecules upon their emergence; the method nevertheless allows an accurate relative estimation of ROS production (Wu et al. 2019).

Single L3 larvae were placed in a single well of a 24 well-plate (Greiner Bio-One 662,160) in a climate chamber with a 16:8 light/dark cycle and a light intensity of 550 lx, without active aeration. The relatively large surface-to-volume ratio of the 2.5 mL medium in the wells allowed for sufficient passive oxygen diffusion to support larval respiration over the 24-h experimental period, minimizing systemic hypoxia as a confounding factor. The 24-h exposure duration was specifically chosen to capture the acute oxidative stress response to temperature shifts, reflecting ecologically relevant rapid fluctuations experienced by *C. riparius* larvae in their natural habitats. Experiments were conducted under a 16:8 light/dark cycle to account for potential influences of circadian rhythm on physiological responses. The study employed seven distinct consecutive temperature regimes, encompassing 4°C, 8°C, 12°C, 16°C, 20°C, 24°C, and 28°C. In total, we measured 20 larvae per temperature treatment. Larvae were randomly selected from a continuously breeding population pool, and due to the asynchronous nature of the population, individuals likely originated from different females. Consequently, sampling on consecutive days is not expected to introduce systematic variation.

2.2 | Reactive Oxygen Species Measurement

Following 24 h of treatment, the well plates were placed in a styrofoam box for transportation to the microscope to prevent any abrupt temperature change. ROS levels were estimated for a total of 20 larvae per temperature and CellROX dye type. Two larvae had to be excluded from further analysis because they died in the process (one from the 20°C treatment group and one from the 28°C treatment group for CellROX Orange).

A preliminary experiment with different concentrations of CellROX stock solution (0.5–2.5 μL per 2.5 mL of medium; results not shown) helped us to determine the final working concentrations for the main experiments. Each larva was stained with CellROX Orange at a final concentration of 1.5 μM (0.75 μL of 5 mM stock per 2.5 mL medium) and CellROX Red at a final concentration of 2.5 μM (1.25 μL of 5 mM stock per 2.5 mL medium). These concentrations were optimized to provide detectable signals with a non-detrimental concentration.

ROS levels were quantified in live larvae using a ZEISS Axio Imager 2 microscope with 10× magnification. The images were captured using AxioVision Rel. (v. 4.8) with an HXP 120 C fluorescence lamp (Item Number: 423013-9010-000), with maximum light intensity and 1-s exposure time. We furthermore employed the "43 HE" (BP 550/25 HE, FT 570 HE, BP 605/70 HE, Item Number 489043-9901-000) filter, which excites blue light at approximately 550 nm, transmitting emitted red fluorescence above 570 nm and filtering out the remaining blue excitation light, thus registering only red fluorescence around 605 nm. As the L3 larvae were too large for complete body imaging, fluorescence measurements were consistently performed in the first abdominal segment (Figure S2). This segment was selected due to its identifiability, accessibility, and suitability for consistent fluorescence measurement across all individuals.

The fluorescence field images were analyzed using the ImageJ Fiji software (version 2.15.0). Images were converted to 8-bit grayscale from RGB color images to eliminate color differences, to be able to solely calculate light intensity. The

CellROX Orange and CellROX Red dyes exhibited differential brightness under identical fluorescence illumination conditions. Consequently, distinct thresholds were applied to the respective reagent treatments. Because the maximum fluorescence light intensity was applied, consequently the background noise (background light) was elevated. Therefore, the auto threshold was set too high to lower the background noise. The mean values were taken as a measure of fluorescence intensity. It should be noted that the fluorescence intensity measured represents the relative amount of reagent that has entered the cell and undergone oxidation by binding to ROS, rather than an absolute quantification of ROS present within the cell. However, the optimized concentration of CellROX reagents used was sufficient to capture the ROS present within the cells across all conditions, ensuring that our measurements reflect true differences in ROS production. While direct quantification of dye uptake or its intrinsic temperature sensitivity was not performed, the optimized nonlethal concentrations of reagents were applied uniformly across all temperature treatments to ensure consistent and relative measurements of ROS dynamics in vivo.

2.3 | Gene Expression Analysis

For gene expression analysis, a distinct experimental setup was employed compared to the acute ROS measurements, designed to capture transcriptional responses and adaptive changes over longer periods. A total of 45 L3 larvae were collected from the lab culture for each temperature treatment. The larvae were exposed to specific temperature treatments in glass bowls filled with sand and medium, as previously described (Foucault et al. 2019). Unlike the CellROX experiments, the temperatures used for transcriptomics were 5°C, 10°C, 15°C, 20°C, and 25°C. This difference in temperature ranges between the CellROX and transcriptomic experiments was due to logistical constraints and financial considerations inherent to each distinct experimental setup, though both ranges effectively cover ecologically relevant thermal conditions for *C. riparius*. Larvae were provided with aeration and permitted to feed at their discretion, which was essential for these longer-term exposures (2–5 days) to allow for complete transcriptional responses and to account for temperature-dependent developmental rates. As developmental time depends on temperature in this ectothermic organism, the duration of exposure varied accordingly: 2 days for 25°C, 3 days for 20°C, 4 days for 15°C and 10°C, and 5 days for 5°C.

For each temperature treatment, multiple replicates of larvae were utilized, with 12 individuals per 25°C, 15°C, and 10°C groups, and 11 individuals per 20°C and 5°C groups. For each individual larva, a separate RNA library was prepared. RNA was extracted using the Direct-zol RNA Miniprep Kits (R2053; Zymo Research) according to the manufacturer's manual. Library preparation and sequencing were conducted at Novogene on a NovaSeq X Plus instrument.

2.4 | RNA Data Analysis

The FASTQ files were aligned to the *C. riparius* reference genome v4 (Pettrich et al. 2024) which was pre-indexed for efficient mapping. Alignment was performed using HISAT2 (v. 2.1.0; Kim et al. 2019). Subsequently, the resulting SAM files were sorted and converted to BAM format using Samtools (v. 1.20; Li et al. 2009). Finally, read counts for each gene per individual sample were quantified using FeatureCounts (version 2.0.6; Liao et al. 2014).

Raw counts were subsequently normalized using DESeq2 (v. 3.19; Love et al. 2014) with read counts <10 in at least 4/5 of all tested temperatures were excluded to remove lowly expressed genes and reduce noise, resulting in the selection of 118 genes. In this study, we focused on ROS-related genes and their specific reaction norms to different temperatures only. To this end, protein sequences of 134 ROS-related proteins from the model organism *Drosophila melanogaster* were downloaded from UniProt on 30 June 2024. *Drosophila* was selected as a well-annotated insect model, which is a dipteran and a close phylogenetic relative of *C. riparius*, making its ROS-related protein set a highly relevant reference (Akinyemi et al. 2018; Bag and Mishra 2020; Yang et al. 2024). Subsequently, the *C. riparius* genome was queried against the downloaded protein database using BLASTx (v. 2.12.0; Camacho et al. 2009) to identify and extract the corresponding genes, including those related to mitochondrial ETC components. With this approach, nine previously annotated genes were discovered in the *C. riparius* genome and incorporated into the analysis. The *C. riparius* protein set was queried against the UniProtKB protein database using the InterProScan (v. 5.52) software to obtain the gene name.

2.5 | Statistical Analysis

All statistical analyses and data visualizations were performed in R version 4.4.1 ("R: A Language and Environment for Statistical Computing | BibSonomy" n.d.).

2.6 | Analysis of ROS Data

To test for a significant effect of temperature on overall ROS levels (Relative Fluorescence Intensity, RFI), we performed an Analysis of Variance (ANOVA). To test our hypothesis of a U-shaped relationship between temperature and ROS, we fitted a second-order polynomial regression model to the data. The fit of this model was compared to a linear model using the Akaike Information Criterion (AIC) to confirm that the polynomial model provided a better description of the data.

2.7 | Differential Gene Expression Analysis

Differential gene expression analysis was performed to identify genes with significant expression changes between the temperature (15°C) and each of the other thermal treatments (5°C, 10°C, 20°C, and 25°C). The analysis was conducted in R, using the DESeq2-normalized count data for the 118 selected ROS-related genes as input. The limma package (v. 3.60.2) was employed for its robust statistical framework (Ritchie et al. 2015). Prior to modeling, the normalized expression values were log2-transformed, with a pseudocount of 1 added to accommodate zero values. A linear model was then fitted

for each gene, and empirical Bayes moderation was applied to increase statistical power. Contrasts were established to compare each temperature group against the 15°C, since it is close to the optimal temperature. p values were adjusted for multiple testing using the Benjamini-Hochberg method to control the false discovery rate. The results were visualized as volcano plots using the ggplot2 package, where the x-axis represents the $\log_2$ fold change and the y-axis represents the negative $\log_{10}$ of the adjusted p value. Genes were colored according to their ROS target classification (superoxide, hydrogen peroxide, general ROS) to highlight the response patterns of different functional groups.

2.8 | Principal Component Analysis (PCA)

To explore coordinated temperature-dependent responses in the antioxidant system, we conducted a principal component analysis (PCA) exclusively on 23 genes known to be directly involved in ROS production or scavenging (Ryan et al. 2020). The goal was to identify dominant patterns of variation in gene expression across the temperature gradient and to uncover how antioxidant systems respond collectively under thermal stress. The normalized gene expression data for these antioxidant genes were imported into R and preprocessed by applying z-score normalization. PCA was performed using the "prcomp()" function to capture the major axes of variation in antioxidant gene expression across temperature treatments. Gene loadings obtained from the PCA rotation matrix were combined with ROS target annotations, where the sign and magnitude of the loading indicate the direction and strength of a gene's contribution to the variance along a principal component, providing insight into its expression pattern across temperatures. Sample metadata, including temperature, were extracted from sample identifiers and merged with PCA scores. Additionally, a broken stick model was used to assess the significance of the variance explained by each principal component.

Visualization of the PCA results was carried out using the ggplot2 package (Wickham et al. 2019). A biplot was generated, displaying samples in the PC1–PC2 space with points colored by temperature and gene loadings represented as scaled arrows. Complementary boxplots were also created to compare the distribution of principal component scores across temperature treatments, with custom color scales applied for clarity.

3 | Results

3.1 | Temperature Dependent Stress Levels Across Temperatures Detected via ROS

The stress levels of larvae as measured by the relative fluorescence intensity (RFI) of ROS exhibited a significant temperature dependence (ANOVA, $F(6, 133) = 64.02$, $p < 0.001$), indicating relative changes in oxidative activity across the thermal gradient. RFI was highest at the two temperature extremes and lowest between 12°C and 18°C, which indicates an optimal temperature range (Figure 1). Fitting a second-order polynomial regression model to the data revealed a U-shaped relationship between temperature and RFI (goodness of fit: $R^2 = 0.6$, p value $< 2.2e\text{-}16$; formula: $44.91672 + 30.85863*x + 298.3746*x^2$). The polynomial regression model fitted better to the data compared to the linear model, according to AIC values of 1250 and 1377, respectively.

3.2 | Characterization of ROS Types Under Different Temperature Conditions

When assessing the relative abundance of ROS species across temperatures, it becomes evident that the qualitative contribution of different ROS groups, inferred from the differential sensitivity of the CellROX probes, changes with temperature. At 4°C, the superoxide group (detected by CellROX Red) predominated, indicating a higher relative contribution of these species. In contrast, at 24°C and 28°C, there was an elevated level of the hydrogen peroxide group (inferred from the CellROX Orange signal, encompassing hydrogen peroxide, nitric oxide, and peroxynitrite), suggesting their increased relative contribution at warmer temperatures (Figure 2). At optimal temperatures, the overall amount of ROS was lower than at the extremes, and the superoxide group appeared to be more prominent. It is important to note that Figure 2 serves as a qualitative illustration of the shifting ROS profiles; the quantitative data showing the distribution and variance of total ROS and the statistical support for the significant effect of temperature are presented in Figure 1.

A key observation emerged when analyzing the normalized data (Figure 2). At 12°C and 20°C, the relative signal from CellROX Red, which detects superoxide and hydroxyl radicals, surpassed that of the broader-spectrum CellROX Orange probe. As this is a mathematical consequence of normalizing two probes with different baseline signals and sensitivities, we further explored the biological meaning of this signal crossover.

3.3 | Principal Component Analysis of ROS Associated Genes Under Different Temperature Conditions

To investigate the overall transcriptional response to temperature, we first analyzed the gene expression profiles from our 58 individual larva samples (11–12 biological replicates per temperature treatment). Principal component analysis (PCA) was performed on normalized read counts of 23 antioxidant genes directly related to either ROS production or scavenging to determine temperature-dependent expression patterns. Significant PCs were revealed using the Broken Stick model (Data S1), where the first three principal components (PCs) capture different aspects of gene expression variation, with PC1, PC2, and PC3 explaining 24.2%, 16.2%, and 10.8%, respectively. Together, they explained more than 50% of the data (Figure 3A).

The PCA biplot showed a clear temperature-dependent clustering of the samples. The low-temperature samples (5°C–10°C) formed distinct clusters in the negative PC1 region, while the high-temperature samples (20°C–25°C) clustered in the positive PC1 region. Intermediate temperature samples (15°C) occupied transitional positions between these clusters, indicating a gradual shift in gene expression patterns across the temperature gradient.

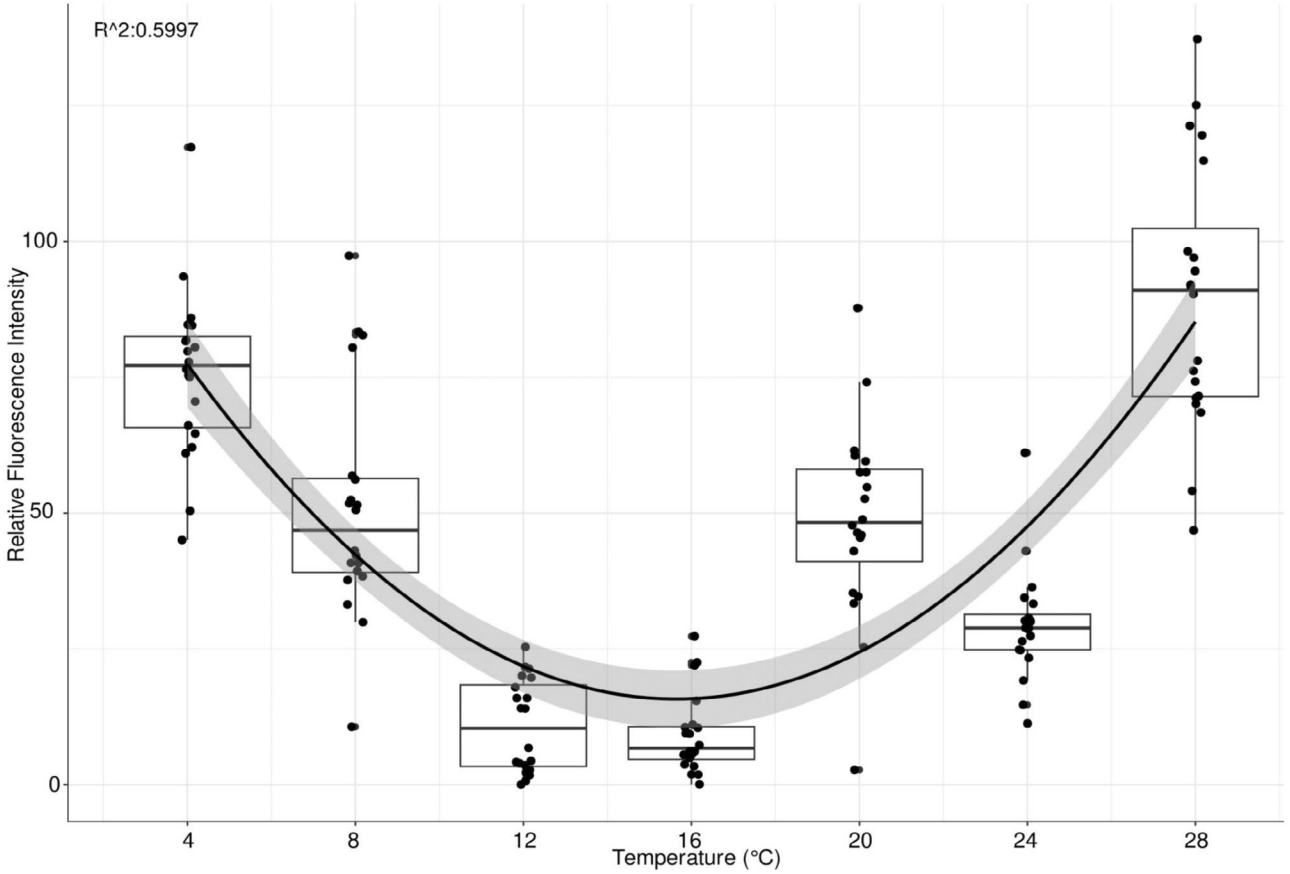

FIGURE 1 | Boxplot depicting the relative fluorescence intensity (RFI) across different temperatures based on CellROX Orange measurements, which detects a broader spectrum of ROS. The distribution of RFI across temperatures fits a parabolic distribution ($R^2 = 0.5997$; *F*-statistic: 105.1 on 2 and 137 DF, *p* value: < 2.2e-16). The line shows the fitted regression with a 95% confidence interval (shaded area).

Analysis of PC scores across temperatures revealed systematic variation in gene expression patterns. PC1 scores showed a strong correlation with temperature, transitioning from negative values at low temperatures to positive values at high temperatures, indicating that genes with positive loadings on PC1 are increasingly expressed at higher temperatures, and vice versa. PC2 scores showed another clear distinction between low temperature (5°C) and high temperature (20°C–25°C), while the 10°C and 15°C data sets fell in the middle. This suggests a threshold of regulation in the antioxidant response system. PC3 provided additional information on cold-temperature-specific responses, particularly in the 5°C data (Figure 3B; Data S1).

3.4 | Differential Gene Expression Highlights a Strong Cold-Stress Response

To investigate the expression changes of individual genes, we compared each temperature treatment to the 15°C baseline. Genes were considered significantly differentially expressed if they had a False Discovery Rate (FDR) *p* value < 0.05. This analysis revealed a starkly asymmetric transcriptional response to thermal stress (Figure S1). The most profound and widespread changes occurred at the cold extreme (5°C), where numerous antioxidant genes were significantly up- or downregulated, indicating a large-scale transcriptomic reprogramming. In striking contrast, the responses to milder cold (10°C) and warm temperatures (20°C and 25°C) were far more subdued at the individual gene level. Very few genes passed the stringent threshold for statistical significance, suggesting a different regulatory mechanism is at play in response to moderate versus extreme cold stress.

3.5 | Gene Contributions to Temperature Response

Based on the PCA (Figure 3A), gene loadings were obtained to determine the contribution of the 23 antioxidant genes directly related to either ROS production or scavenging to the temperature response. In PC1, *thioredoxin-2*, two *mitochondrial thioredoxin isoforms*, two *sup*eroxide *dismutase* variants, *peroxiredoxin-6*, *catalase isoform X2*, and *mpv17-like protein 3* showed strong positive loadings (0.2–0.4), indicating higher expression levels at elevated temperatures. In contrast, *dual oxidase* exhibited a negative loading, suggesting increased expression at lower temperatures.

PC2 and PC3 captured variation associated with cold responses. Strong positive loadings in PC2 were observed for *superoxide dismutases, mpv17-like protein 2, mitochondrial glutathione peroxidase, and peroxiredoxin-5*, indicating their greater contribution under cold conditions. Negative PC2 loadings for *catalase isoform X2* and *sestrin homologs* suggested differential antioxidant activation at intermediate temperatures. PC3 was dominated by

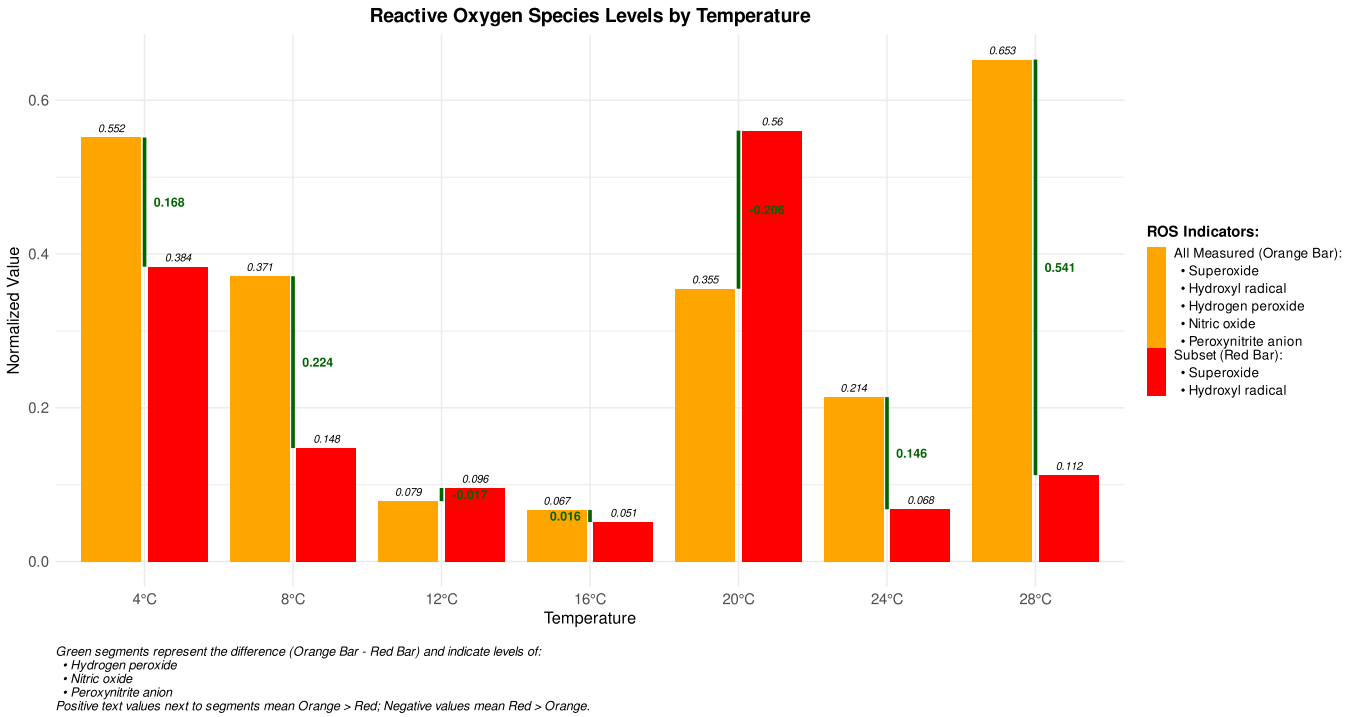

FIGURE 2 | Normalized fluorescence intensity of ROS indicated by orange bars (total measured ROS by CellROX Orange) and red bars (subset of ROS by CellROX Red) at temperatures ranging from 4°C to 28°C. This figure illustrates the relative abundance and qualitative shifts of different ROS species across temperatures, inferred from the differential sensitivity of CellROX Orange and CellROX Red. Total measured ROS includes superoxide, hydroxyl radical, hydrogen peroxide, nitric oxide, and peroxynitrite anion. The subset of ROS consists of superoxide and hydroxyl radicals. The figure is based on normalized fluorescence intensity data, with orange bars representing total ROS pool and red bars representing the superoxide and hydroxyl radical subset. Green segments, with corresponding numerical values, illustrate the difference between total and subset ROS levels (CellROX Orange—CellROX Red), representing the combined contribution of hydrogen peroxide, nitric oxide, and peroxynitrite anion. For quantitative data and statistical validation of the overall temperature effect, refer to Figure 1.

high negative loadings from *sestrin isoforms*, *peroxiredoxin-5*, and *thioredoxin domain-containing protein 15*, indicating a specific role for hydrogen peroxide detoxification at low temperatures (Figure 3C; Data S1).

4 | Discussion

Organisms need to be able to cope with a variety of different temperatures across different time scales and magnitudes. Even though water bodies may buffer temperature fluctuations to a certain extent, in water bodies of temperate regions, and especially small water bodies, temperatures may change on a seasonal, daily, and even minute time scale. Thus, organisms inhabiting these regions need to be adapted to cope with varying conditions, but they may still be vulnerable to temperature extremes. Temperature extremes can exert strong stress on organisms; however, the detection and quantification of this stress are not always easy. This study presents the first direct in vivo measurements of ROS under a broad range of temperatures in an insect. In contrast to earlier studies that employed indirect methods, such as enzyme activity assays or in vitro ROS measurements (Cui et al. 2011; Jia et al. 2011; Yang et al. 2010; Zhang et al. 2015), our direct in vivo measurements of ROS provide a more comprehensive and precise understanding of ROS production in response to a range of temperatures encountered by the species in their natural habitat. While acknowledging the theoretical potential for CellROX compounds to induce minor background oxidative responses, our optimized nonlethal concentrations and consistent application across all treatments ensured that the observed temperature-dependent differences accurately reflected biological variation rather than probe-induced artifacts.

4.1 | Temperature-Dependent Stress Response

Our findings demonstrated that ROS levels in *C. riparius* followed a U-shaped pattern across the temperature gradient, with potentially elevated oxidative stress at both upper and lower temperature extremes. The increased ROS levels at the extreme temperatures aligned with observations in other ectotherms, where temperature extremes challenge cellular homeostasis. For instance, in ectothermic species like fish and amphibians, either heat or cold stress can lead to increased ROS (Paital and Chainy 2014).

In ectotherms at high temperatures, the metabolic rate increases, leading to higher oxygen consumption and elevated ROS production as a metabolic by-product (Rollins-Smith and Le Sage 2023). Consistent with the generally increased metabolic rate observed at higher temperatures (Holden et al. 2022; Payne et al. 2025), our transcriptomic analysis identified a linearly increasing expression pattern for five *NADH dehydrogenase* genes and an exponential increase for a *cytochrome c reductase* gene with increasing temperature, which

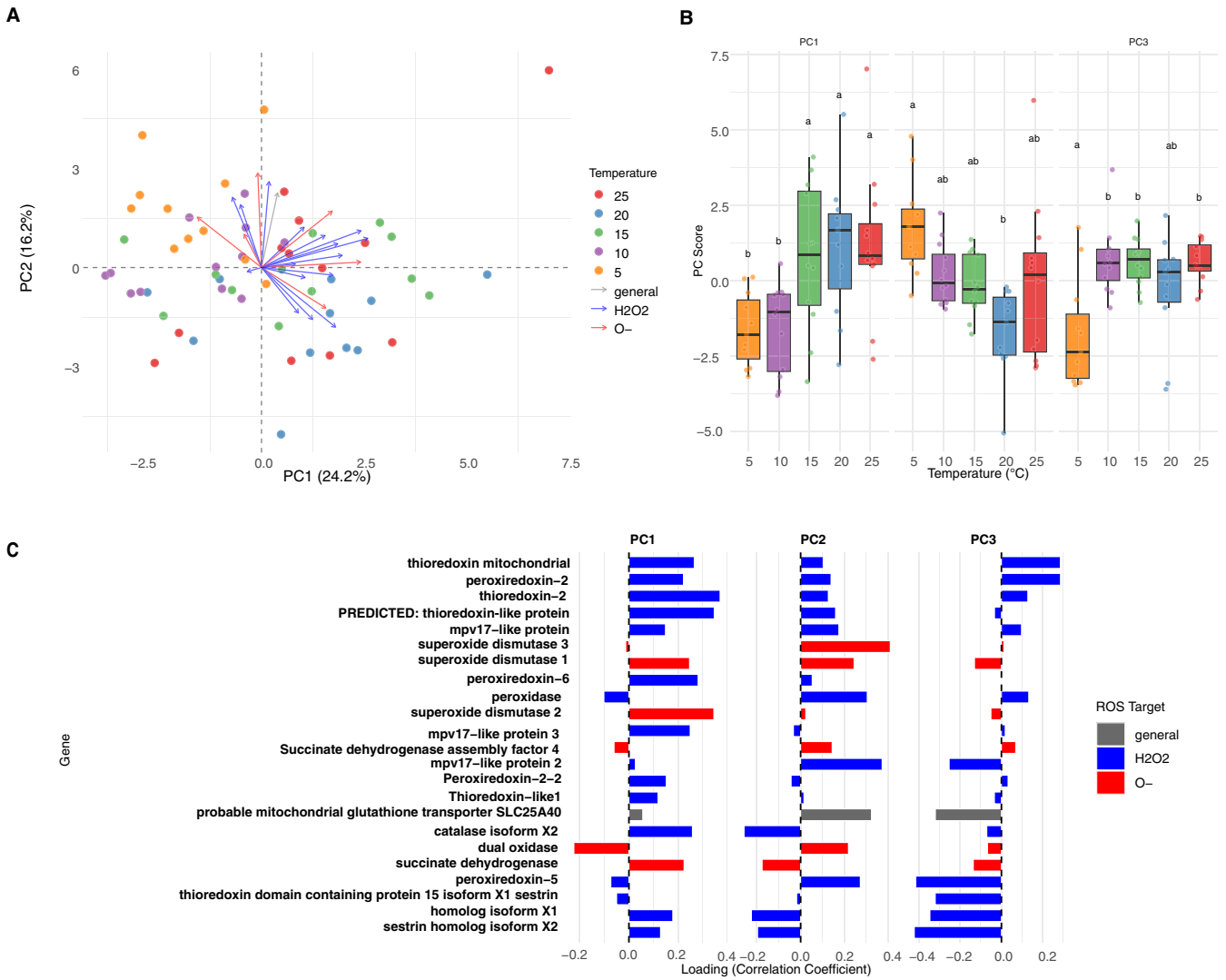

FIGURE 3 | PCA of antioxidant gene expression across five temperatures, showing temperature-specific patterns and the contribution of ROS-targeted genes to variation along principal components. (A) Biplot of the first two principal components derived from a principal component analysis (PCA) of 23 antioxidant gene expression profiles across five temperature treatments (5°C, 10°C, 15°C, 20°C, 25°C). Samples are color coded by temperature, and vectors indicate each gene's contribution to the observed variation along PC1 and PC2; the direction of the arrow indicates the temperature range where that gene's expression is higher. Genes are labeled and colored according to their primary ROS target, with gray for general (non-specific) antioxidants, blue for hydrogen peroxide-related antioxidants, and red for superoxide-related antioxidants. (B) Boxplots of sample scores for PC1, PC2, and PC3 across all temperature treatments, illustrating shifts in overall gene expression patterns. Letters indicate statistically significant differences among temperatures within each principal component (Tukey's HSD test, $p < 0.05$) (Data S1). (C) Contribution of 23 ROS production or scavenging candidate genes to PC1, PC2, and PC3. Genes are again categorized by primary ROS target, using the same color scheme as in panel A.

is consistent with enhanced expression of components within complexes I and III of the electron transport chain. This pattern likely reflected a response to elevated energy demands. As temperatures rise, cellular ATP requirements increase, driving the need for efficient mitochondrial ATP production (Twardochleb et al. 2023). The observed increasing pattern in mitochondrial gene transcription may therefore serve to increase the flow of electrons through the electron transport chain to meet these heightened energy demands under thermal stress (Park and Kwak 2014).

On the other hand, at lower temperatures, mitochondrial function is disrupted as enzyme function slows down and oxygen consumption is decreased, leading to increased electron leakage from the mitochondrial electron transport chain and subsequent enhancement of ROS production (Jørgensen et al. 2023). In accordance with this, we observed a general decreasing pattern of complex I and III genes at lower temperatures, which may represent a compensatory metabolic adjustment rather than dysfunction, aligning with diminished energy requirements in cold conditions. This decreasing trend of the specific genes in cold conditions might be a strategy to conserve energy and minimize ROS production specifically from the electron transport chain's activity, which is particularly useful in low-temperature environments where ATP demand decreases (Colinet et al. 2017).

While our direct in vivo ROS measurements provided an unprecedented view of real-time oxidative activity, future studies

should complement these findings by quantifying specific oxidative damage biomarkers to fully assess the consequences of this stress.

4.2 | Different ROS Profiles Across the Temperature Gradient

Beyond the observed U-shaped stress response, our approach of using different CellROX reagents further disentangled these responses: at low temperatures, the superoxide group (superoxide and hydroxyl radical) appears to predominate, whereas at high temperatures, the hydrogen peroxide group (hydrogen peroxide, peroxynitrite anion, and nitric oxide) suggests a greater contribution.

We propose that the signal crossover at 12°C and 20°C, where the normalized CellROX Red signal surpassed the Orange, reflects a significant, temperature-specific shift in the ROS composition. At 20°C, a temperature supporting high metabolic activity, the targeted production of superoxide is a critical component of cellular signaling pathways (Averill-Bates 2023; Sies and Jones 2020). The elevated CellROX Red signal here is powerfully substantiated by our transcriptomic data, which reveal that expression loadings for key superoxide-scavenging genes are significantly correlated with the higher Red signal at this exact temperature (Park et al. 2012). This indicates a direct biological response: the cell is actively enhancing its defense machinery to manage a higher, physiologically relevant flux of superoxide. Conversely, the crossover at the mild cold-stress temperature of 12°C likely results from altered mitochondrial electron transport efficiency, leading to increased superoxide leakage (Zhao et al. 2019). Therefore, we interpret this signal crossover not as a methodological artifact, but as a key finding that distinguishes between two distinct modes of ROS production: a managed flux for cellular signaling near optimal temperatures and mitochondrial leakage in response to cold.

At low temperatures (e.g., 4°C), the elevated ROS production was largely driven by hypoxia-induced hemoglobin autoxidation. In *C. riparius* larvae, hemoglobin levels are known to be high and increase further under hypoxic conditions (Choi et al. 2000). Under such low-oxygen environments, reduced oxygen diffusion promotes autoxidation of oxyhemoglobin to methemoglobin (Lushchak 2011), a process that generates superoxide radicals and, to a lesser extent, hydrogen peroxide (Yan et al. 2020). Furthermore, diminished peroxidase activity under these hypoxic conditions favors the Fenton reaction, thereby forming hydroxyl radicals. Such molecular mechanisms not only explain the ROS profile observed at low temperatures but may also account for the associated developmental delays observed below 15°C (Alter et al. 2024).

At elevated temperatures, the predominance of the hydrogen peroxide group aligns directly with our transcriptomic findings. We observed a general trend of temperature-dependent upregulation for genes encoding key components of the mitochondrial electron transport chain. This transcriptional response suggests an increased capacity for mitochondrial respiration, which would elevate the rate of electron flow and, consequently, the leakage of superoxide anions from the ETC (Messina et al. 2023). Upregulated *superoxide dismutase* activity then converts these anions into hydrogen peroxide (Murphy 2009). Beyond this general metabolic response, heat stress triggers additional molecular responses such as increased nitric oxide production through the modulation of *nitric oxide synthase* that promote the formation of peroxynitrite when superoxide reacts with nitric oxide (Piacenza et al. 2022; Figure S3).

The observed molecular processes reflect the knowledge about the ecology of *C. riparius* populations. Elevated temperatures accelerate larval development, thereby reducing generation time, which principally increases fitness (Foucault et al. 2019). However, the trade-offs are significant: increasing temperatures increasingly compromise larval survival, reduce pupation success, and thus overall impair adult reproductive fitness (Foucault et al. 2018; Nemec et al. 2013). Experiments have shown that while optimal growth and relatively short generation times are maintained between 16°C and 23°C (Oppold et al. 2016), exposure to temperatures around 28°C leads to a notable decline in population growth (Nemec et al. 2013). This suggests that the benefits of accelerated growth rates at elevated temperatures are counterbalanced, among others, by the physiological costs of the increased ROS production shown here.

Our findings may also have evolutionary implications for the species. The mutation rate response across temperatures reported by Waldvogel and Pfenninger (2021) exhibited an optimality pattern, superficially similar to the one observed in our ROS measurements. Observed mutation rates had their minimum at ~18°C and increased with increasing temperatures, but also towards colder temperatures, reaching a maximum at 12°C (Waldvogel and Pfenninger 2021). Below this temperature, reproduction is not possible anymore in *C. riparius*, and therefore, transgenerational mutation rates could not be measured. However, the current study has shown that ROS levels had their minimum at 12°C and therefore may not be the sole or primary driver for the increased mutation rate observed at this temperature. One plausible hypothesis is that the extended generation times at cold temperatures (Oppold et al. 2016) allow even low ROS levels or other mechanisms more time to inflict DNA damage (Beal et al. 2019) and thus increase mutation rates. However, the overwintering generation of *C. riparius* in nature is exposed for several months to much lower temperatures down to 4°C (Pfenninger et al. 2023). The increased ROS level at these cold temperatures observed here could thus still be a major driver of mutagenesis in natural populations, due to the interplay of increased oxidative cold stress and extended exposure time during hibernation.

It is crucial to interpret these findings in the context of our study design, which utilized a single laboratory population originating from a temperate climate in Germany. Given the broad geographical distribution of *C. riparius* across diverse climatic regimes, from the Mediterranean to Northern Europe, local adaptation in thermal physiology is highly probable (Waldvogel et al. 2018). Therefore, the specific thermal optima and stress thresholds we report here are certainly not universal for the species. This underscores that population-specific variation is a critical factor, and our study provides a foundational baseline for

future comparative population studies aimed at dissecting the genetic basis of local thermal adaptation.

Furthermore, the responses documented in this study represent the acute plastic response to a novel thermal environment, as all larvae were reared at a constant 20°C. It is well established that an organism's thermal history can profoundly shape its physiological and molecular responses to stress. For example, acclimation history, through which an individual gradually adjusts to a new thermal regime, can lead to the restructuring of metabolic pathways or the accumulation of protective molecules, potentially dampening the acute ROS production we observed upon a sudden temperature shift (Shama et al. 2014). Similarly, transgenerational plasticity, often mediated by maternal effects, can preprogram offspring for the environment their parents experienced (Bonzi et al. 2025). A mother exposed to colder conditions might provision its eggs with specific antioxidants or transcripts that alter the baseline stress response of its larval offspring, leading to a different oxidative stress profile than the one we measured (Marks and Lailvaux 2024). Therefore, while our results provide a crucial baseline for understanding the immediate mechanisms of thermal stress, they should be interpreted as one component of the broader thermal biology of *C. riparius*.

4.3 | Molecular Mechanisms of Antioxidant Defense Across Temperature Gradients

Our RNA-Seq approach, which analyzed individual larvae, allowed us to capture interindividual variation in gene expression, which is crucial for understanding the full spectrum of plastic responses and genetic variation within a population (Pfenninger et al. 2025). This analysis revealed a targeted gene expression response by which *C. riparius* reacted to temperature-induced oxidative stress, corroborating the physiological level results observed above. At higher temperatures (20°C–25°C), our analysis revealed a response favoring the management of hydrogen peroxide. Our transcriptomic data provide a direct mechanistic basis for this observation. We saw a general trend of upregulation for genes encoding key components of the mitochondrial electron transport chain (ETC), such as *NADH dehydrogenases* (Complex I) and *cytochrome c reductase* (Complex III). This suggests an increased metabolic rate and electron flow to meet higher energy demands, which inevitably increases the leakage of superoxide from the ETC (Murphy 2009). The cellular response to this primary challenge was evident in the concurrent positive contribution of *superoxide dismutase* variants, whose function is to convert this excess superoxide into hydrogen peroxide. Consequently, the system then activated defenses to manage this secondary product, as shown by the strong contribution of hydrogen peroxide-neutralizing enzymes like *thioredoxins*, *peroxiredoxin-6*, and *catalase isoform X2* to the variance in gene expression at warm temperatures, as revealed by our PCA (Figure 3C). Thus, the ROS profile at high temperatures appears to be a direct consequence of an elevated metabolic rate (Pamenter et al. 2018), followed by a coordinated, two-step enzymatic defense. However, it is important to note that our transcriptomic analysis did not include the 28°C treatment, which elicited the highest physiological ROS production. Future studies incorporating this upper thermal limit would be valuable for elucidating the transcriptional signatures associated with the transition from adaptive response to acute heat stress.

Conversely, the response to colder conditions (5°C–10°C) was mechanistically distinct. Physiologically, these temperatures were dominated by superoxide anion oxidant, a pattern that cannot be explained by an elevated metabolic rate. Our transcriptomic analysis, however, provides a compelling molecular explanation. The transcriptional reprogramming at cold temperatures was the most pronounced observed across the entire gradient, with a large number of genes being significantly differentially expressed at 5°C (Figure S1). Central to this response was the significant upregulation of *dual oxidase*, a membrane-bound enzyme known to be a potent producer of superoxide (Donkó et al. 2005). This specific gene induction offers a direct molecular source for the observed superoxide surge, fitting the physiological data perfectly. Furthermore the antioxidant system, in turn, mounted a complex defense tailored to this specific threat. The primary challenge of superoxide under cold temperatures, was met with a complex regulation of *superoxide dismutase* variants (Figure 3C), whose role is to convert superoxide to the less reactive hydrogen peroxide. However, this enzymatic conversion creates a secondary oxidative challenge. Accordingly, the cold response also involved the regulation of hydrogen peroxide scavengers, as indicated by the strong contribution of genes like *peroxiredoxin-5* and *mpv17-like protein 2* to the variance observed in the PCA at low temperatures (Figure 3C). This reveals a sophisticated, multi-step defensive strategy. The cold-temperature response, therefore, appropriately emphasizes primary superoxide management, but also prepares for its secondary byproducts. This seemingly counterintuitive production and management of multiple ROS species at low temperatures may serve critical signaling functions, potentially activating cold-adaptive pathways or maintaining cellular redox homeostasis despite reduced metabolic activity (Jørgensen et al. 2023; Murphy 2009).

5 | Conclusion and Future Directions

This study provides the first direct in vivo evidence for a U-shaped pattern of oxidative stress across a broad temperature range in the insect *C. riparius*, with minimal ROS levels observed within a thermal window of 12°C–18°C. We demonstrate that this pattern arises from mechanistically distinct challenges: superoxide predominance at low temperatures, linked to hemoglobin autoxidation, and hydrogen peroxide predominance at high temperatures, driven by increased metabolic rate. Correspondingly, the transcriptional response of antioxidant genes is tailored to counter the specific ROS type prevalent at each thermal extreme. These findings establish that temperature extremes impose distinct forms of oxidative stress, a mechanism that plausibly impacts organismal fitness and likely influences the ecology and evolution of the species by exerting complex selective pressures. While our results provide a crucial mechanistic baseline, future work is needed to explore how these responses are modulated by factors such as local adaptation, as our findings are based on a single population. Further studies should also investigate the transcriptional tipping point at extreme high temperatures and how long-term acclimation and developmental plasticity alter

these acute stress responses. Such research will be critical for predicting the vulnerability and adaptive potential of freshwater ectotherms in a changing world.

Author Contributions

Burak Bulut: conceptualization (equal), data curation (equal), formal analysis (equal), methodology (equal), visualization (equal), writing – original draft (equal). **Maximilian Geiss:** conceptualization (equal), data curation (equal), formal analysis (equal). **Markus Bernard:** methodology (equal). **Halina Binde Doria:** conceptualization (equal), methodology (equal). **Barbara Feldmeyer:** conceptualization (equal), data curation (equal), writing – review and editing (equal). **Markus Pfenninger:** conceptualization (equal), funding acquisition (equal), methodology (equal), project administration (equal), resources (equal), validation (equal), writing – review and editing (equal).

Acknowledgments

The authors are grateful for support by a DFG grant to M.P. (PF 390/15-1). Open Access funding enabled and organized by Projekt DEAL.

Funding

This work was supported by Deutsche Forschungsgemeinschaft, PF 390/15-1.

Conflicts of Interest

The authors declare no conflicts of interest.

Data Availability Statement

The data is accessible at the European Nucleotide Archive (ENA) under accession number PRJEB89193. All other primary data supporting the results of this study, including raw fluorescence intensity measurements and sample metadata, can be found at Zenodo doi: https://doi.org/10.5281/zenodo.17184450.

References

Akinyemi, A. J., G. Oboh, O. Ogunsuyi, A. O. Abolaji, and A. Udofia. 2018. "Curcumin-Supplemented Diets Improve Antioxidant Enzymes and Alter Acetylcholinesterase Genes Expression Level in *Drosophila melanogaster* Model." *Metabolic Brain Disease* 33: 369–375. https://doi.org/10.1007/s11011-017-0100-7.

Alter, K., J. Jacquemont, J. Claudet, et al. 2024. "Hidden Impacts of Ocean Warming and Acidification on Biological Responses of Marine Animals Revealed Through Meta-Analysis." *Nature Communications* 15: 2885. https://doi.org/10.1038/s41467-024-47064-3.

Averill-Bates, D. 2023. "Reactive Oxygen Species and Cell Signaling." *Biochimica et Biophysica Acta, Molecular Cell Research* 279: L1005–L1028. https://doi.org/10.1016/j.bbamcr.2023.119573.

Bag, J., and M. Mishra. 2020. "Biochemical Assays to Detect the Antioxidant Level in *Drosophila melanogaster*." In *Fundamental Approaches to Screen Abnormalities in Drosophila*, edited by M. Mishra, 151–168. Springer US. https://doi.org/10.1007/978-1-4939-9756-5_13.

Beal, M. A., M. J. Meier, A. Williams, et al. 2019. "Paternal Exposure to Benzo(a)pyrene Induces Genome-Wide Mutations in Mouse Offspring." *Communications Biology* 2: 228. https://doi.org/10.1038/s42003-019-0476-5.

Bonzi, L. C., J. M. Donelson, R. K. Spinks, P. L. Munday, T. Ravasi, and C. Schunter. 2025. "Matching Maternal and Paternal Experiences Underpin Molecular Thermal Acclimation." *Molecular Ecology* 34: e17328. https://doi.org/10.1111/mec.17328.

Camacho, C., G. Coulouris, V. Avagyan, et al. 2009. "BLAST+: Architecture and Applications." *BMC Bioinformatics* 10: 421. https://doi.org/10.1186/1471-2105-10-421.

Chinta, S. J., and J. K. Andersen. 2008. "Redox Imbalance in Parkinson's Disease." *Biochimica et Biophysica Acta* 1780: 1362–1367. https://doi.org/10.1016/j.bbagen.2008.02.005.

Choi, J., H. Roche, and T. Caquet. 2000. "Effects of Physical (Hypoxia, Hyperoxia) and Chemical (Potassium Dichromate, Fenitrothion) Stress on Antioxidant Enzyme Activities in *Chironomus riparius* Mg. (Diptera, Chironomidae) Larvae: Potential Biomarkers." *Environmental Toxicology and Chemistry* 19: 495–500. https://doi.org/10.1002/etc.5620190231.

Colinet, H., D. Renault, and D. Roussel. 2017. "Cold Acclimation Allows Drosophila Flies to Maintain Mitochondrial Functioning Under Cold Stress." *Insect Biochemistry and Molecular Biology* 80: 52–60. https://doi.org/10.1016/j.ibmb.2016.11.007.

Cui, Y., Y. Du, M. Lu, and C. Qiang. 2011. "Antioxidant Responses of Chilo Suppressalis (Lepidoptera: Pyralidae) Larvae Exposed to Thermal Stress." *Journal of Thermal Biology* 36: 292–297. https://doi.org/10.1016/j.jtherbio.2011.04.003.

Das, K., and A. Roychoudhury. 2014. "Reactive Oxygen Species (ROS) and Response of Antioxidants as ROS-Scavengers During Environmental Stress in Plants." *Frontiers in Environmental Science* 2: 53. https://doi.org/10.3389/fenvs.2014.00053.

Devireddy, A. R., T. J. Tschaplinski, G. A. Tuskan, W. Muchero, and J.-G. Chen. 2021. "Role of Reactive Oxygen Species and Hormones in Plant Responses to Temperature Changes." *International Journal of Molecular Sciences* 22: 8843. https://doi.org/10.3390/ijms22168843.

Donkó, Á., Z. Péterfi, A. Sum, T. Leto, and M. Geiszt. 2005. "Dual Oxidases." *Philosophical Transactions of the Royal Society, B: Biological Sciences* 360: 2301–2308. https://doi.org/10.1098/rstb.2005.1767.

Dowling, D. K., and L. W. Simmons. 2009. "Reactive Oxygen Species as Universal Constraints in Life-History Evolution." *Proceedings of the Royal Society B: Biological Sciences* 276: 1737–1745. https://doi.org/10.1098/rspb.2008.1791.

Eberhardt, L., H. B. Doria, B. Bulut, B. Feldmeyer, and M. Pfenninger. 2025. "Transcriptomics Predicts Artificial Light at Night's (ALAN) Negative Fitness Effects and Altered Gene Expression Patterns in the Midge *Chironomus riparius* (Diptera:Chironomidae)." *Environmental Pollution* 369: 125827. https://doi.org/10.1016/j.envpol.2025.125827.

El-Saadi, M. I., H. A. MacMillan, and L. V. Ferguson. 2023. "Cold-Induced Immune Activation in Chill-Susceptible Insects." *Current Opinion in Insect Science* 58: 101054. https://doi.org/10.1016/j.cois.2023.101054.

Farahani, S., A. R. Bandani, H. Alizadeh, S. H. Goldansaz, and S. Whyard. 2020. "Differential Expression of Heat Shock Proteins and Antioxidant Enzymes in Response to Temperature, Starvation, and Parasitism in the Carob Moth Larvae, Ectomyelois Ceratoniae (Lepidoptera: Pyralidae)." *PLoS One* 15: e0228104. https://doi.org/10.1371/journal.pone.0228104.

Foucault, Q., A. Wieser, A. Waldvogel, and M. Pfenninger. 2019. "Establishing Laboratory Cultures and Performing Ecological and Evolutionary Experiments With the Emerging Model Species *Chironomus riparius*." *Journal of Applied Entomology* 143: 584–592. https://doi.org/10.1111/jen.12606.

Foucault, Q., A. Wieser, A.-M. Waldvogel, B. Feldmeyer, and M. Pfenninger. 2018. "Rapid Adaptation to High Temperatures in *Chironomus riparius*." *Ecology and Evolution* 8: 12780–12789. https://doi.org/10.1002/ece3.4706.

Gasparrini, A., Y. Guo, M. Hashizume, et al. 2015. "Mortality Risk Attributable to High and Low Ambient Temperature: A Multicountry Observational Study." *Lancet* 386: 369–375. https://doi.org/10.1016/S0140-6736(14)62114-0.

Hagymasi, A. T., J. P. Dempsey, and P. K. Srivastava. 2022. "Heat-Shock Proteins." *Current Protocols* 2: e592. https://doi.org/10.1002/cpz1.592.

Heise, K., M. S. Estevez, S. Puntarulo, et al. 2007. "Effects of Seasonal and Latitudinal Cold on Oxidative Stress Parameters and Activation of Hypoxia Inducible Factor (HIF-1) in Zoarcid Fish." *Journal of Comparative Physiology B* 177: 765–777. https://doi.org/10.1007/s00360-007-0173-4.

Hernansanz-Agustín, P., and J. A. Enríquez. 2021. "Generation of Reactive Oxygen Species by Mitochondria." *Antioxidants* 10: 415. https://doi.org/10.3390/antiox10030415.

Holden, K. G., A. R. Hedrick, E. J. Gangloff, S. J. Hall, and A. M. Bronikowski. 2022. "Temperature-Dependence of Metabolism and Fuel Selection From Cells to Whole Organisms." *Journal of Experimental Zoology Part A: Ecological and Integrative Physiology* 337: 199–205. https://doi.org/10.1002/jez.2564.

Huchzermeyer, B., E. Menghani, P. Khardia, and A. Shilu. 2022. "Metabolic Pathway of Natural Antioxidants, Antioxidant Enzymes and ROS Providence." *Antioxidants* 11: 761. https://doi.org/10.3390/antiox11040761.

Jia, F.-X., W. Dou, F. Hu, and J.-J. Wang. 2011. "Effects of Thermal Stress on Lipid Peroxidation and Antioxidant Enzyme Activities of Oriental Fruit Fly, *Bactrocera dorsalis* (Diptera: Tephritidae)." *Florida Entomologist* 94: 956–963. https://doi.org/10.1653/024.094.0432.

Jomova, K., S. Y. Alomar, S. H. Alwasel, E. Nepovimova, K. Kuca, and M. Valko. 2024. "Several Lines of Antioxidant Defense Against Oxidative Stress: Antioxidant Enzymes, Nanomaterials With Multiple Enzyme-Mimicking Activities, and Low-Molecular-Weight Antioxidants." *Archives of Toxicology* 98: 1323–1367. https://doi.org/10.1007/s00204-024-03696-4.

Jørgensen, L. B., A. M. Hansen, Q. Willot, and J. Overgaard. 2023. "Balanced Mitochondrial Function at Low Temperature Is Linked to Cold Adaptation in *Drosophila* Species." *Journal of Experimental Biology* 226: jeb245439. https://doi.org/10.1242/jeb.245439.

Kang, T., W. Lu, W. Xu, et al. 2013. "MicroRNA-27 (miR-27) Targets Prohibitin and Impairs Adipocyte Differentiation and Mitochondrial Function in Human Adipose-Derived Stem Cells." *Journal of Biological Chemistry* 288: 34394–34402. https://doi.org/10.1074/jbc.M113.514372.

Kiekebusch, E., A. M. Louthan, W. F. Morris, B. R. Hudgens, and N. M. Haddad. 2024. "Vital Rate Responses to Temperature Lead to Butterfly Population Declines Under Future Warming Scenarios." *Journal of Insect Conservation* 28: 1079–1091. https://doi.org/10.1007/s10841-024-00626-8.

Kim, D., J. M. Paggi, C. Park, C. Bennett, and S. L. Salzberg. 2019. "Graph-Based Genome Alignment and Genotyping With HISAT2 and HISAT-Genotype." *Nature Biotechnology* 37: 907–915. https://doi.org/10.1038/s41587-019-0201-4.

Lebenzon, J. E., J. Overgaard, and L. B. Jørgensen. 2023. "Chilled, Starved or Frozen: Insect Mitochondrial Adaptations to Overcome the Cold." *Current Opinion in Insect Science* 58: 101076. https://doi.org/10.1016/j.cois.2023.101076.

Li, H., B. Handsaker, A. Wysoker, et al. 2009. "The Sequence Alignment/Map Format and SAMtools." *Bioinformatics* 25: 2078–2079. https://doi.org/10.1093/bioinformatics/btp352.

Liao, Y., G. K. Smyth, and W. Shi. 2014. "featureCounts: An Efficient General Purpose Program for Assigning Sequence Reads to Genomic Features." *Bioinformatics* 30: 923–930. https://doi.org/10.1093/bioinformatics/btt656.

Liu, L., B. Wang, D. Liu, et al. 2020. "Transcriptomic and Metabolomic Analyses Reveal Mechanisms of Adaptation to Salinity in Which Carbon and Nitrogen Metabolism Is Altered in Sugar Beet Roots." *BMC Plant Biology* 20: 138. https://doi.org/10.1186/s12870-020-02349-9.

Los, D. A., and A. V. Leusenko. 2025. "50 Years Since the Concept of Homeoviscous Adaptation." *Biochimie* 231: 98–103. https://doi.org/10.1016/j.biochi.2024.12.008.

Love, M. I., W. Huber, and S. Anders. 2014. "Moderated Estimation of Fold Change and Dispersion for RNA-Seq Data With DESeq2." *Genome Biology* 15: 550.

Lushchak, V. I. 2011. "Environmentally Induced Oxidative Stress in Aquatic Animals." *Aquatic Toxicology* 101: 13–30. https://doi.org/10.1016/j.aquatox.2010.10.006.

Mackova, V., M. Raudenska, H. H. Polanska, M. Jakubek, and M. Masarik. 2024. "Navigating the Redox Landscape: Reactive Oxygen Species in Regulation of Cell Cycle." *Redox Report* 29: 2371173. https://doi.org/10.1080/13510002.2024.2371173.

Marks, J. R., and S. P. Lailvaux. 2024. "The Integrative Life History of Maternal Effects." *Integrative and Comparative Biology* 64: 1623–1632. https://doi.org/10.1093/icb/icae117.

Messina, S., D. Costantini, and M. Eens. 2023. "Impacts of Rising Temperatures and Water Acidification on the Oxidative Status and Immune System of Aquatic Ectothermic Vertebrates: A Meta-Analysis." *Science of the Total Environment* 868: 161580. https://doi.org/10.1016/j.scitotenv.2023.161580.

Murphy, M. P. 2009. "How Mitochondria Produce Reactive Oxygen Species." *Biochemical Journal* 417: 1–13. https://doi.org/10.1042/BJ20081386.

Nemec, S., S. Patel, C. Nowak, and M. Pfenninger. 2013. "Evolutionary Determinants of Population Differences in Population Growth Rate × Habitat Temperature Interactions in *Chironomus riparius*." *Oecologia* 172: 585–594. https://doi.org/10.1007/s00442-012-2517-3.

Ntawubizi, M., and M. L. Mukamuhirwa. 2024. "A Reflexion on the Oxidative Stress and Animal Welfare: A Review." *Tropical Animal Health and Production* 56: 396. https://doi.org/10.1007/s11250-024-04238-x.

Nwachukwu, I. D., R. A. Sarteshnizi, C. C. Udenigwe, and R. E. Aluko. 2021. "A Concise Review of Current in Vitro Chemical and Cell-Based Antioxidant Assay Methods." *Molecules* 26: 4865. https://doi.org/10.3390/molecules26164865.

Oppold, A.-M., J. A. M. Pedrosa, M. Bálint, et al. 2016. "Support for the Evolutionary Speed Hypothesis From Intraspecific Population Genetic Data in the Non-Biting Midge *Chironomus riparius*." *Proceedings of the Royal Society B: Biological Sciences* 283: 20152413. https://doi.org/10.1098/rspb.2015.2413.

Paital, B., and G. B. N. Chainy. 2014. "Effects of Temperature on Complexes I and II Mediated Respiration, ROS Generation and Oxidative Stress Status in Isolated Gill Mitochondria of the Mud Crab *Scylla serrata*." *Journal of Thermal Biology* 41: 104–111. https://doi.org/10.1016/j.jtherbio.2014.02.013.

Pamenter, M. E., G. Y. Lau, and J. G. Richards. 2018. "Effects of Cold on Murine Brain Mitochondrial Function." *PLoS One* 13: e0208453. https://doi.org/10.1371/journal.pone.0208453.

Park, K., and I.-S. Kwak. 2014. "The Effect of Temperature Gradients on Endocrine Signaling and Antioxidant Gene Expression During *Chironomus riparius* Development." *Science of the Total Environment* 470: 1003–1011. https://doi.org/10.1016/j.scitotenv.2013.10.052.

Park, S.-Y., P. M. G. Nair, and J. Choi. 2012. "Characterization and Expression of Superoxide Dismutase Genes in *Chironomus riparius* (Diptera, Chironomidae) Larvae as a Potential Biomarker of Ecotoxicity." *Comparative Biochemistry and Physiology, Part C:*

Toxicology & Pharmacology 156, no. 3–4: 187–194. https://doi.org/10.1016/j.cbpc.2012.06.003.

Payne, N. L., J. D. Kong, A. L. Jackson, et al. 2025. "Heat Limits Scale With Metabolism in Ectothermic Animals." *Journal of Animal Ecology* 94: 1307–1316. https://doi.org/10.1111/1365-2656.70042.

Pettrich, L. C., R. King, L. M. Field, and A.-M. Waldvogel. 2024. "The Interplay of Recombination Landscape, a Transposable Element and Population History in European Populations of *Chironomus riparius*." https://doi.org/10.1101/2024.04.04.588075.

Pfenninger, M., and Q. Foucault. 2020. "Genomic Processes Underlying Rapid Adaptation of a Natural *Chironomus riparius* Population to Unintendedly Applied Experimental Selection Pressures." *Molecular Ecology* 29: 536–548. https://doi.org/10.1111/mec.15347.

Pfenninger, M., Q. Foucault, A.-M. Waldvogel, and B. Feldmeyer. 2023. "Selective Effects of a Short Transient Environmental Fluctuation on a Natural Population." *Molecular Ecology* 32: 335–349. https://doi.org/10.1111/mec.16748.

Pfenninger, M., M.-E. Nieto-Blazquez, T. Schell, et al. 2025. "Pervasive and Dynamic Release of Cryptic Genetic Variation in *Chironomus riparius*: Rethinking Adaptation in Fluctuating Environments." https://doi.org/10.1101/2025.07.01.661462.

Piacenza, L., A. Zeida, M. Trujillo, and R. Radi. 2022. "The Superoxide Radical Switch in the Biology of Nitric Oxide and Peroxynitrite." *Physiological Reviews* 102: 1881–1906. https://doi.org/10.1152/physrev.00005.2022.

Pörtner, H. O., A. F. Bennett, F. Bozinovic, et al. 2006. "Trade-Offs in Thermal Adaptation: The Need for a Molecular to Ecological Integration." *Physiological and Biochemical Zoology* 79: 295–313. https://doi.org/10.1086/499986.

R: A Language and Environment for Statistical Computing | BibSonomy. n.d. https://www.bibsonomy.org/bibtex/7469ffee3b07f9167cf47e7555041ee7.

Ritchie, M. E., B. Phipson, D. Wu, et al. 2015. "Limma Powers Differential Expression Analyses for RNA-Sequencing and Microarray Studies." *Nucleic Acids Research* 43: e47. https://doi.org/10.1093/nar/gkv007.

Rollins-Smith, L. A., and E. H. Le Sage. 2023. "Heat Stress and Amphibian Immunity in a Time of Climate Change." *Philosophical Transactions of the Royal Society, B: Biological Sciences* 378: 20220132. https://doi.org/10.1098/rstb.2022.0132.

Ryan, S. M., K. Wildman, B. Oceguera-Perez, S. Barbee, N. T. Mortimer, and A. D. Vrailas-Mortimer. 2020. "Evolutionarily Conserved Transcription Factors Drive the Oxidative Stress Response in Drosophila." *Journal of Experimental Biology* 223: jeb221622. https://doi.org/10.1242/jeb.221622.

Said, R. M., and S. E. Nassar. 2022. "Mortality, Energy Reserves, and Oxidative Stress Responses of Three Native Freshwater Mussels to Temperature as an Indicator of Potential Impacts of Climate Change: A Laboratory Experimental Approach." *Journal of Thermal Biology* 104: 103154. https://doi.org/10.1016/j.jtherbio.2021.103154.

Shama, L. N. S., A. Strobel, F. C. Mark, and K. M. Wegner. 2014. "Transgenerational Plasticity in Marine Sticklebacks: Maternal Effects Mediate Impacts of a Warming Ocean." *Functional Ecology* 28: 1482–1493. https://doi.org/10.1111/1365-2435.12280.

Sies, H., and D. P. Jones. 2020. "Reactive Oxygen Species (ROS) as Pleiotropic Physiological Signalling Agents." *Nature Reviews. Molecular Cell Biology* 21: 363–383. https://doi.org/10.1038/s41580-020-0230-3.

Sikder, M. M., X. Li, S. Akumwami, and S. A. Labony. 2025. "Reactive Oxygen Species: Role in Pathophysiology, and Mechanism of Endogenous and Dietary Antioxidants During Oxidative Stress." *Chonnam Medical Journal* 61: 32–45. https://doi.org/10.4068/cmj.2025.61.1.32.

Szechyńska-Hebda, M., R. Z. Ghalami, M. Kamran, F. Van Breusegem, and S. Karpiński. 2022. "To be or Not to be? Are Reactive Oxygen Species, Antioxidants, and Stress Signalling Universal Determinants of Life or Death?" *Cells* 11: 4105. https://doi.org/10.3390/cells11244105.

Twardochleb, L. A., P. L. Zarnetske, and C. A. Klausmeier. 2023. "Life-History Responses to Temperature and Seasonality Mediate Ectotherm Consumer–Resource Dynamics Under Climate Warming." *Proceedings of the Royal Society B: Biological Sciences* 290: 20222377. https://doi.org/10.1098/rspb.2022.2377.

Waldvogel, A.-M., and M. Pfenninger. 2021. "Temperature Dependence of Spontaneous Mutation Rates." *Genome Research* 31: 1582–1589. https://doi.org/10.1101/gr.275168.120.

Waldvogel, A.-M., A. Wieser, T. Schell, et al. 2018. "The Genomic Footprint of Climate Adaptation in *Chironomus riparius*." *Molecular Ecology* 27: 1439–1456. https://doi.org/10.1111/mec.14543.

Wickham, H., M. Averick, J. Bryan, et al. 2019. "Welcome to the Tidyverse." *Journal of Open Source Software* 4: 1686. https://doi.org/10.21105/joss.01686.

Wu, L., A. C. Sedgwick, X. Sun, S. D. Bull, X.-P. He, and T. D. James. 2019. "Reaction-Based Fluorescent Probes for the Detection and Imaging of Reactive Oxygen, Nitrogen, and Sulfur Species." *Accounts of Chemical Research* 52: 2582–2597. https://doi.org/10.1021/acs.accounts.9b00302.

Yan, J., J. Jiang, L. He, and L. Chen. 2020. "Mitochondrial Superoxide/Hydrogen Peroxide: An Emerging Therapeutic Target for Metabolic Diseases." *Free Radical Biology & Medicine* 152: 33–42. https://doi.org/10.1016/j.freeradbiomed.2020.02.029.

Yang, L.-H., H. Huang, and J.-J. Wang. 2010. "Antioxidant Responses of Citrus Red Mite, Panonychus Citri (McGregor) (Acari: Tetranychidae), Exposed to Thermal Stress." *Journal of Insect Physiology* 56: 1871–1876. https://doi.org/10.1016/j.jinsphys.2010.08.006.

Yang, Y., Y. Cao, J. Zhang, et al. 2024. "Artemisia Argyi Extract Exerts Antioxidant Properties and Extends the Lifespan of *Drosophila melanogaster*." *Journal of the Science of Food and Agriculture* 104: 3926–3935. https://doi.org/10.1002/jsfa.13273.

Zhang, G.-H., H. Liu, J.-J. Wang, and Z.-Y. Wang. 2014. "Effects of Thermal Stress on Lipid Peroxidation and Antioxidant Enzyme Activities of the Predatory Mite, *Neoseiulus cucumeris* (Acari: Phytoseiidae)." *Experimental & Applied Acarology* 64: 73–85. https://doi.org/10.1007/s10493-014-9806-y.

Zhang, S., W. Fu, N. Li, F. Zhang, and T.-X. Liu. 2015. "Antioxidant Responses of *Propylaea japonica* (Coleoptera: Coccinellidae) Exposed to High Temperature Stress." *Journal of Insect Physiology* 73: 47–52. https://doi.org/10.1016/j.jinsphys.2015.01.004.

Zhao, R., S. Jiang, L. Zhang, and Z.-B. Yu. 2019. "Mitochondrial Electron Transport Chain, ROS Generation and Uncoupling (Review)." *International Journal of Molecular Medicine* 44: 3–15. https://doi.org/10.3892/ijmm.2019.4188.

Supporting Information

Additional supporting information can be found online in the Supporting Information section. **Data S1:** ece372625-sup-0001-DataS1.xlsx. **Data S2:** ece372625-sup-0002-Appendix.docx.

Chapter 3

A multigenerational study can detect the evolutionary response to BaP exposure in the non-biting freshwater midge *Chironomus riparius*

Burak Bulut[1], Lorenzo Rigano[1], Halina Binde Doria, Gajana Gemüth, Markus Pfenninger

[1] shared first author

Published as: Bulut, B., Rigano, L., Doria, H.B., Gemüth, G. and Pfenninger, M., 2024. A multigenerational study can detect the evolutionary response to BaP exposure in the non-biting freshwater midge *Chironomus riparius*. Chemosphere, 358, p.142242.

Acknowledgements: The authors are grateful for support by a DFG grant to M.P. (PF 390/15-1). Open Access funding enabled and organized by Projekt DEAL.

Funding: This work was supported by Deutsche Forschungsgemeinschaft, PF 390/15-1.

Conflict of Interest: The authors declare no conflicts of interest.

Data Availability: The data is accessible at the European Nucleotide Archive (ENA) under accession number PRJEB89420. Supplementary data to this article can be found at Zenodo doi: doi.org/10.1016/j.chemosphere.2024.142242

Chemosphere 358 (2024) 142242

Contents lists available at ScienceDirect

Chemosphere

journal homepage: www.elsevier.com/locate/chemosphere

A multigenerational study can detect the evolutionary response to BaP exposure in the non-biting freshwater midge Chironomus riparius

Burak Bulut [a,1], Lorenzo Rigano [a,b,*,1], Halina Binde Doria [b], Gajana Gemüth [b], Markus Pfenninger [a,b,c]

[a] Department of Molecular Ecology, Senckenberg Biodiversity and Climate Research Centre, Georg-Voigt-Str. 14-16, D-60325, Frankfurt am Main, Germany
[b] LOEWE Centre of Translational Biodiversity Genomics, Senckenberg Biodiversity and Climate Research Centre, Georg-Voigt-Str. 14-16, D-60325, Frankfurt am Main, Germany
[c] Institute for Molecular and Organismic Evolution, Johannes Gutenberg University, Johann-Joachim-Becker-Weg 7, D-55128, Mainz, Germany

HIGHLIGHTS

- BaP exposure increases the mutation rate of *C. riparius*.
- BaP exposure is detrimental for the fitness and the population dynamics of *C. riparius*.
- Multi-generational studies are essential to assess evolutionary implications of anthropogenic substances on biodiversity.

GRAPHICAL ABSTRACT

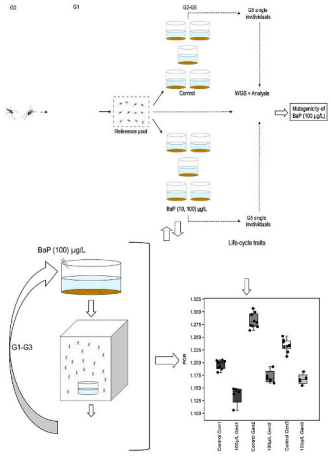

ARTICLE INFO

Handling editor: Marisa Passos

Keywords:
Multigeneration life-cycle test
Reactive oxygen species
Evolutionary ecotoxicology
Oxidative stress

ABSTRACT

The release of polycyclic aromatic hydrocarbons (PAHs) into the environment is posing a threat to ecosystems and human health. Benzo(*a*)pyrene (BaP) is considered a biomarker of PAH exposure and is classified as a Group 1 carcinogen. However, it was not known whether BaP is mutagenic, i.e. induces inherited germline mutations. In this study, we used a recently established method, which combines short-term mutation accumulation lines (MAL) with whole genome sequencing (WGS) to assess mutagenicity in the non-biting midge *Chironomus riparius*. The mutagenicity analysis was supplemented by an evaluation of the development of population fitness in three successive generations in the case of chronic exposure to BaP at a high concentration (100 µg/L). In addition, the level of ROS-induced oxidative stress was examined *in vivo*. Exposure to the higher BaP concentration led to an

* Corresponding author. Department of Molecular Ecology, Senckenberg Biodiversity and Climate Research Centre, Georg-Voigt-Str. 14-16, D-60325, Frankfurt am Main, Germany.
E-mail address: lorenzo.rigano@senckenberg.de (L. Rigano).
[1] Burak Bulut and Lorenzo Rigano contributed equally and should be considered joint first authors.

https://doi.org/10.1016/j.chemosphere.2024.142242
Received 4 August 2023; Received in revised form 18 March 2024; Accepted 2 May 2024
Available online 4 May 2024

increase in germline mutations relative to the control, while the lower concentration showed no mentionable effect. Against expectations, BaP exposure decreased ROS-level compared to the control and is thus probably not responsible for the increased mutation rate. Likewise, the higher BaP concentration decreased fitness measured as population growth rate per day (PGR) significantly over all generations, without signs of rapid evolutionary adaptations. Our results thus highlighted that high BaP exposure may influence the evolutionary trajectory of organisms.

1. Introduction

The release of anthropogenic substances into the environment usually causes negative effects at all levels of biological organization, from the molecule up to the community and ecosystem (Zhang et al., 2018). The unifying factor is their effect on population fitness, which on the one hand integrates all processes within individuals and on the other hand is decisive for the organism's role in the ecological community and thus for the ecosystem (Sæther and Engen, 2015; Shaw et al., 2008). However, as species are not static but evolve, anthropogenic stressors with a negative impact on population fitness also represent selection factors that can trigger evolutionary adaptation (Charlesworth, 1971; Murray, 1990). The same stressors can also induce mutations that, although essential for evolution, in the vast majority of cases have a negative impact on fitness (Baer et al., 2005; Eyre-Walker et al., 2006). These long-term consequences, which alter not only current demography but also the future evolutionary trajectory of species, are the focus of the emerging research field of evolutionary ecotoxicology.

Polycyclic aromatic hydrocarbons (PAH) represent one of the most important polluting compounds, ubiquitously present in all environmental compartments (Adeniji et al., 2019). Their heterocyclic aromatic ring structure, hydrophobicity, and thermostability make them highly persistent in the environment (Patel et al., 2020). Moreover, PAH represents a legacy of contemporary society as their increasing presence in the environment was associated with car use and urban sprawl (Van Metre et al., 2000). BaP is one of the most prevalent PAH pollutants in the urban environment. It is formed during the incomplete combustion of organic matter like wood and certain types of fossil fuels such as petrol and diesel and reaches the environment mainly in exhaust gasses, as well as in cigarette smoke (Bukowska et al., 2022; Phillips, 1983). It accumulates in the sediment carried by runoff water, particularly if the runoff encounters vehicles, road surfaces, or deposits of combustion byproducts. Moreover, it has been described as genotoxic and carcinogenic in mammalian cells and has already been proven to inhibit DNA repair, thereby likely promoting mutagenicity. It is the only PAH classified as carcinogenic in Group 1 (Baan et al., 2008). Benzo[*a*]pyrene has been shown to increase ROS production and induce oxidative stress (Baan et al., 2008). Under conditions of oxidative stress, ROS levels can become excessive and cause damage to biomolecules such as DNA, proteins, and lipids (Dröge, 2002). Its accumulation in tissue caused adverse metabolic, neuronal, and genotoxic effects in Chironomid and Aedes larvae (Kagan and Kagan, 1986; Vicentini et al., 2017).

However, it is not known whether BaP has a mutagenic effect on germ cells upon environmental exposure. Instead of mutations in somatic cells, mutations in germ cells are passed onto offspring for generations even if exposure to the substance has ceased. Despite being the "fuel of evolution", mutations have usually a detrimental effect on the fitness of organisms (Lynch and Gabriel, 1990). Thus, measuring the mutagenic effect of a toxic substance in germ cells is crucial because it can irreversibly change the evolutionary trajectory of the population under investigation. Indeed, mutagens behave differently from other toxicants, which may exert a genotoxic action, but without necessarily inducing an increased rate of mutagenicity. Ecotoxicological tests represent a key tool for determining the toxicity of a substance and its potential impact on the environment. However, these tests usually do not focus on the direct measurement of mutagenicity. In this regard, considering the evolutionary effects of anthropogenic emissions increases the scope of environmental assessments and allows for an integrated assessment of emerging pollution problems.

Although it is reliable to test mutation rates in microorganisms or in cell cultures, these do not consider the real complexity of a multicellular organism, let alone an organism as a living system (Kirkland et al., 2007; Knaap et al., 1988). However, the use of next-generation sequencing (NGS) technology for the direct assessment of the mutagenicity of chemicals is currently not yet widespread (Beal et al., 2019; Du et al., 2017; Wamucho et al., 2019). There is a lack of established and standardized protocols, which means that thousands of chemicals currently in use in Europe are not comprehensively evaluated for their potential health and environmental risks (Doria and Pfenninger, 2021). In the present study, we describe the application of a recently introduced mutation rate test (Oppold and Pfenninger, 2017) as an effective ecotoxicological mutagenicity test tool for metazoan organisms. The test is a combination of short-term mutation accumulation (MA) lines, whole genome sequencing (WGS), and dedicated data analysis. For this, we used *Chironomus riparius,* a non-biting freshwater midge that is widely distributed in Europe, Asia, and North America. It is used as a test species in ecotoxicological assessment of water and sediments and four validated tests are included in the OECD Guidelines for the Testing of Chemicals (OECD, 2010). *C. riparius* has already been used as a model organism for mutagenicity tests, evaluating the toxicity of Cadmium (Cd) in a multigenerational scenario (Doria and Pfenninger, 2021). In addition, the genomic analysis was complemented by a multigenerational study over three successive generations, assessing changes in population fitness over time, in particular, whether constant exposure leads to rapid adaptation, as has been shown for other stressors in *C. riparius* (Foucault et al., 2019; Nowak et al., 2009; Pfenninger and Foucault, 2020). Because oxidative stress is known as a major agent to induce mutations (Aitken and Krausz, 2001), we measured oxidative stress through the quantification of reactive oxygen species (ROS).

2. Materials and methods

2.1. Test compound

Benzo[*a*]pyrene (BaP) (Merck, Germany) was prepared by diluting it with dimethyl sulfoxide (DMSO) and kept as a 1% stock solution. The BaP exposure was continued for 5 generations at concentrations of 10 μg/L and 100 μg/L. The concentrations were chosen, because the lower value represents high environmentally relevant concentrations (Bukowska et al., 2022), and the higher was a just not yet lethal concentration in an exploratory 24 h acute test with freshly hatched larvae (data not shown). BaP was added to the medium in corresponding amounts at the beginning of every generation.

2.2. Chemical analysis

To determine the final concentration of BaP, sediment, and water samples were collected and sent to Fresenius SGS Institut GmbH laboratory for chemical analysis. Water samples were analyzed using gas chromatography combined with mass spectrometric detection (GC-MS) (DIN 38407-39:2011–09). Sediment samples were analyzed according to DIN EN 14346:2007–03 by gas chromatography and subsequent determination by mass spectrometry (GC-MS) (DIN IDO, 18287:2006–05).

2.3. Mutation accumulation lines experimental design

For the experiment, one egg rope was raised under optimal conditions to avoid premature selection pressure. After the successful reproduction of the G1 generation, egg ropes from the G2 generation were collected to establish the next generation. The hatched clutches were placed in glass bowls (20 cm diameter, 14 cm height) containing 1.5 cm of sand and 1.150 L of medium with a conductivity between 550 and 650, and a pH value of around 8. The four groups were Control, 10 μg/L, 100 μg/L, and Solvent, with 15 replicates each. For conducting the next generation, only one egg clutch was chosen. The mutation accumulation lines were kept at 22 ± 0.5 °C, 60% humidity, and 16:8 light and dark periods. The bowls were aerated 24 h a day, and evaporation of the medium was avoided by adding distilled water and adjusting the conductivity when necessary. Because of the swarm fertilization of *C. riparius* and the impossibility of determining the parents of specific egg clutches, adults of the first generation were collected and used as a pooled reference. At the end of the fifth generation, one randomly chosen female was collected for DNA extraction.

2.4. Life cycle test

A chronic toxicity test was conducted according to the OECD Guideline 233 to determine the toxicity of benzo[*a*]pyrene (BaP) to *C. riparius* over a test period of 28 days (OECD, 2010). The same experimental design was used with minor modifications to mutation accumulation lines. Five egg clutches were selected to initiate the experiment, and 30 first-instar larvae were placed in glass bowls. After placing 30 individuals, BaP was added to the medium at a final concentration of 100 μg/L. In every generation, the glass bowls were replaced with new sand, medium, and 100 μ/L BaP was freshly added, keeping the exposure concentration constant. Both the control and the treatment were subjected to a life cycle test every generation. The number of emerged adults was counted to determine mortality, which corresponds to the subtraction of the emerged from the exposed larvae. Adult sexes were recorded daily to determine the mean emergence time (EmT50), i.e. when 50% of the females emerged. The number of adults that emerged and their sexes were recorded daily to determine the mean emergence time (EmT50). For fertility determination, all emerged individuals were placed in breeding cages according to their experimental groups. The number of fertile laid eggs were counted, and the egg numbers were determined according to. Non-fertile eggs rarely occur in experiments, with the exception of certain experimental conditions that, for instance, strongly influence sex ratios. Finally, all measured parameters were summarized in the population growth rate (PGR) (Nemec et al., 2013).

2.5. Whole genome sequencing and bioinformatic analysis

DNA extraction was done with the Blood and Tissue QUIAGEN Kit by following the manufacturer's instructions. The whole genome sequencing of both the reference pool and individuals was established using the study (Doria and Pfenninger, 2021). Clean reads of individual females of each mutation accumulation line and ancestors were analyzed using the best practices of the GATK pipeline (McKenna et al., 2010). First, the reads were paired with Pear (Zhang et al., 2014). The reference genome v.4 (unpublished data) was used for mapping with bwa-mem. Picard v.1.123 (https://broadinstitute.github.io/picard/) was used for marking and removing duplicates, and low-quality reads were removed using samtools with default parameters. The target lists for realignments, vcf file creation, variant filtration, and base recalibration were created using GATK. The bam files were merged with samtools merge (Danecek et al., 2021), and accuMUlate (Winter et al., 2018) was used with the same reference genome and merged bam files. The output was filtered with a custom bash script using the following parameters: probability of a mutation (≥ 0.90), probability of one mutation (≥ 0.90), probability of correct descendant genotype (≥ 0.90), N mutant in wt (=0), mapping quality difference (≤ 2.95), and stand bias (≥ 0.05). The filtered mutation positions were then validated using IGV. The mutation rate was estimated by multiplying the number of mutations per generational passage by the callable sites. Finally, we used a Bayesian implementation of the Poisson test to compare the mutational rates between treatments with the R package BayesianFirstAid (Bååth, 2014).

2.6. ROS detection and image analysis

For each condition (control, 10μ/L, and 100μ/L), 10 L3 larvae were collected and placed in 24 well plates. Plates were filled with 2.5 ml medium as described in Foucault. CellROX Orange (Thermo Fisher cat. no. C10443) reagents were used to identify ROS products. CellROX is an oxidative stress reagent that is cell-permeable and suitable for live cell ROS measurements. Within the reduced state, they are non-fluorescent but after oxidation by ROS, they exhibit fluorogenic signals at 545/565 nm for CellROX Orange. The reagent is localized within the cytoplasm and can detect 5 different ROS types (hydrogen peroxide, hydroxyl radical, nitric oxide, peroxynitrite anion, and superoxide anion). After placing larvae on the well plates, 0.75 μl of CellROX Orange was used per larva.

Well-plates were placed in a climate chamber with a 16:8 light/dark cycle with 550 lux light intensity without aeration under 20 °C. After 24 h of treatment, well plates were placed in a styrofoam box to avoid the temperature change effect. The ROS was measured in a live larva with ZEISS Axio Imager 2 under 10× magnification. The images were taken with AxioVision Rel. v.4.8. For fluorescence images, an HXP 120C fluorescence lamp was used with maximum light intensity (Item Number: 423,013-9010-000). Fluorescence images were obtained from the larva under filter set "43 HE" (BP 550/25 HE, FT 570 HE, BP 605/70 HE, Item Number 489043-9901-000) with 1 s exposure. This specific filter excites blue light around 550 nm, transmitting emitted red fluorescence above 570 nm filtering out the remaining blue excitation light and allowing only red fluorescence around 605 nm.

The fluorescence field images were analyzed by ImageJ Fiji (v. 2.15.0). Images were uploaded to ImageJ as an image sequence and converted to 8-bit grayscale from RGB Color images to avoid color difference and only calculate light intensity. The same threshold was applied to all images (Threshold: 23). After setting the threshold measure function was used. The mean values of each image were taken as fluorescence intensity. The fluorescence intensity we measured is not the actual ROS amount within the cell but the current amount of reagent entered in the cell and oxidized by binding to ROS which is the remaining amount after the cell's antioxidant system scavenges ROS. The data were analyzed with the R package BayesianFirtsAid (Bååth, 2014).

2.7. Data analysis

The statistics program PAST® software (version 4.15) was used to create the graphs. The R package BayesianFirstAid (Bååth, 2014) was used for the *t*-test to compare life-cycle parameters between treatments.

3. Results

3.1. Final BaP concentration

Final BaP concentrations of group 100 μg/L resulted in a BaP sediment content of 0.63 μg/kg after the first generation. After the second generation, 0.19 μg/kg BaP, and after the third generation, 0.20 μg/kg was detected. The final concentration of BaP was undetectable in all generations of the 10 μg/L treatment.

3.2. Mutation rate and spectrum

The mean read coverage per MAL ranged from 41.61× to 87.83× and the number of callable sites ranged from 33,153,776 to 169,912,242 (Table 2). In total, 2104 candidate mutations were identified, which were subsequently filtered down to 104 credible mutations. In 100 μg/L BaP, 5 transversion, and 27 transition mutations were identified with TV/TS ratio of 0.19. In 10 μg/L BaP, 4 transversion, and 19 transition mutations were identified, and TV/TS ratio was 0.21. For the control and solvent groups, 6 transversion and 19 transition mutations, and 8 transversion and 16 transition mutations, respectively, were identified (Table 1). For control, the TV/TS ratio was 0.31, and for SOL 0.5. The ratio between the treatments and the control groups was not significantly different in Fisher's exact test ($p = 0.1292$).

The mutation rate estimate for the Control was $\mu = 3.16 \times 10^{-9}$ (95% HDI 2.1 × 10–9 and 4.6 × 10^{-9}), and for 100 μg/L BaP was $\mu = 3.51 \times 10^{-9}$ (95% HDI 2.6 × 10–9 and 5.3 × 10^{-9}). The control/100 μg/L BaP rate ratio was 1.2 as shown in Fig. 1, with 75.7% certainty this ratio being larger than 1. The rate estimate for 10 μg/L BaP was $\mu = 2.68 \times 10^{-9}$ (95% HDI 1.8 × 10–8 and 4.2 × 10–8). The control/10 μg/L BaP rate ratio (Fig. 1) was 1.1 (36.3% certainty). For the solvent group, the rate estimate was $\mu = 2.6 \times 10^{-9}$ (95% HDI 1.8 × 10–8 and 4.1 × 10–8) as well with a rate ratio of 1.1 (33.8% certainty).

3.3. Life cycle test

To increase statistical power, we combined the control and SOL groups, as there were no mentionable differences between the groups in any fitness parameters (mortality, EMT50, and fertility). In the first generation (G1), mortality differences were generally very low, with no evidence of significant differences between control and treatment (100 μg/L BaP) (median = −13, 95% HDI between −59 and 29). In the second generation (G2), a large difference of means (−11, 95% HDI -19 and −2.2) was found between control and treatment, with a posterior probability of 98.7% that control was smaller than treatment. This evidence had a large effect size of significantly increased mortality in treatment (Cohen's d = −2). The third generation (G3) also showed a large difference of means (−16, 95% HDI -24 and −8.1) between control and treatment, with a posterior probability of 99.7% that the control was had a lower mortality than the treatment (Fig. 2a). This evidence had a very large effect size (d = −2.8) (Table 3).

In the first generation no mentionable EmT50 difference was found between control and treatment (Fig. 2b) (−0.24, 95% HDI -1.4 and 0.91), as well as in the second and third generation (0.001, 95% HDI -1.9 and 1.7; −0.45, 95% HDI -1.7 and 0.86) (Table 3).

Regarding fertility, in all three generations small differences of means (G1 = 0.39, 95% HDI -0.13 and 0.87; G2 = 0.6, 95% HDI 0.15 and 1.1; G3 = 0.36, 95% HDI 0.19 and 0.54) were observed between control and treatment, with a posterior probability of 94.7%; 99.2% and 99.9% that control was bigger than treatment, respectively. This evidence had a large effect size of significantly reduced fertility in all generations in the treatment (G1 d = 1.2; G2 d = 1.7; G3 d = 2.3). (Fig. 2c) (Table 3).

In the first generation, differences in daily PGR were generally low, with no evidence of relevant differences between control and treatment (0.02, 95% HDI -0.2 and 0.05). In the second generation, a small difference of means (0.08, 95% HDI 0.03 and 0.12) was found between control and treatment, with a posterior probability of 99.7% that control was bigger than treatment (Fig. 2d). This evidence had a very large effect size (d = 2.7). In the third generation, again a small difference of means (0.07, 95% HDI 0.05 and 0.09) was found between control and treatment, with a posterior probability of 100% that control was bigger than treatment. This evidence had a huge effect size (d = 5.1) (Table 3).

Table 1
Mutation spectrum of *C. riparius* after 5 generations of 100 μg/L BaP exposure.

Treatments	Transitions		Transversion			
	G<>A	C<>T	A<>C	C<>G	A<>T	G<>T
100 μg/L	11	16	–	–	3	2
10 μg/L	6	13	1	1	1	1
CT	6	13	1	–	5	–
SOL	8	8	1	1	4	2

Table 2
Mean coverage, number of callable sites, number of single nucleotide mutations (SNM), and mutation rate (μ) per treatment of *C. riparius*.

Treatment	Mean Coverage	No. of Callable Sites	No. of SNM	Mean μ Rate
100 μg/L	49.9	1.7E+08	32	3.51E-09
10 μg/L	52.4	1.6E+08	23	2.68E-09
Control	51.6	1.6E+08	25	3.16E-09
Solvent	47.8	1.7E+08	24	2.60E-09

3.4. Reactive oxygen species measurements

The fluorescence images were analyzed with ImageJ to determine the red color density and intensity. The control group showed significantly higher fluorescence intensity than the treatment group 10 μg/L (30, 95% HDI 23 and 37, with posterior a probability of 100%, d = 4.3) and 100 μg/L (29, 95% HDI 23 and 37, with a posterior probability of 100%, d = 4.2). There was no significant difference between the BaP treatments (−0.53, 95% HDI -1.1 and 0.74) (Fig. 3).

4. Discussion

Our study investigated the microevolutionary responses of the midge *C. riparius* to BaP exposure, assessed by directly measuring mutagenicity and population fitness in a multigenerational setup. The results of our study showed that multigenerational exposure to BaP resulted in a non-significant increase in mutations at the lower exposure concentration (10 μg/L) and a 1.2-fold increase compared to the control at the higher concentration (100 μg/L). This concentration, however, exceeded the levels typically found in natural habitats (Bukowska et al., 2022) and was intended as the positive control. Nevertheless, the observed increase in mutation rate was 1.2-fold rather modest. Temperatures with which *C. riparius* is regularly confronted in their habitat (e.g. 12 °C and 26 °C), showed much more pronounced effects, leading to 2.79- and 4.54-fold increases in mutation rate, respectively (Waldvogel and Pfenninger, 2021). Analysis of the mutational spectrum in both control and treatment groups revealed a shift towards transitions at the expense of transversions in Fisher's exact test ($p = 0.1292$), while no significant difference in the mutation spectrum ratio was observed between the groups. Therefore, although BaP in environmentally unrealistically high concentrations induces an increased mutation rate, it is likely no important driver of the mutation rate in natural habitats. However, organisms like *C. riparius* are subjected to multiple environmental stressors in the wild (Pfenninger and Foucault, 2020). Such complex scenarios in natural populations may exert additive, interactive, or even inhibitory effects on mutation rates, thus warranting further investigation. Our results showed that exposure to BaP at higher concentrations (100 μg/L) exerted a mutagenic effect and that this rather modest effect can be reliably traced already after a few generations. As only the number of generational passages is relevant, the time necessary to perform the test could be shortened, if more MAL were used. Likewise, the test could also be adapted for different test species e.g. from other realms. We could thereby show that it is possible to develop a practical and easy-to-implement pipeline for rapid detection of germ cell mutagens in a metazoan test organism. Further multigenerational studies on the effect of BaP and other potentially mutagenic substances on mutational rates are essential to better assess evolutionary effects and influence on the living environment.

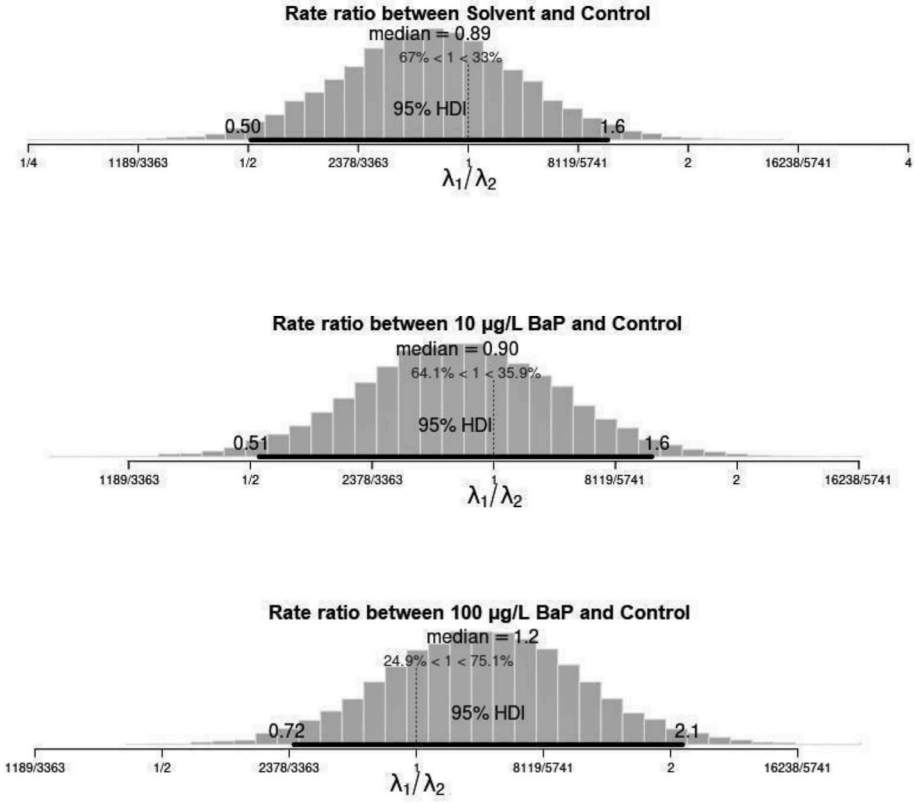

Fig. 1. Posterior distributions for rate ratios between solvent, 10 µg/L, and 100 µg/L BaP relative to the control group.

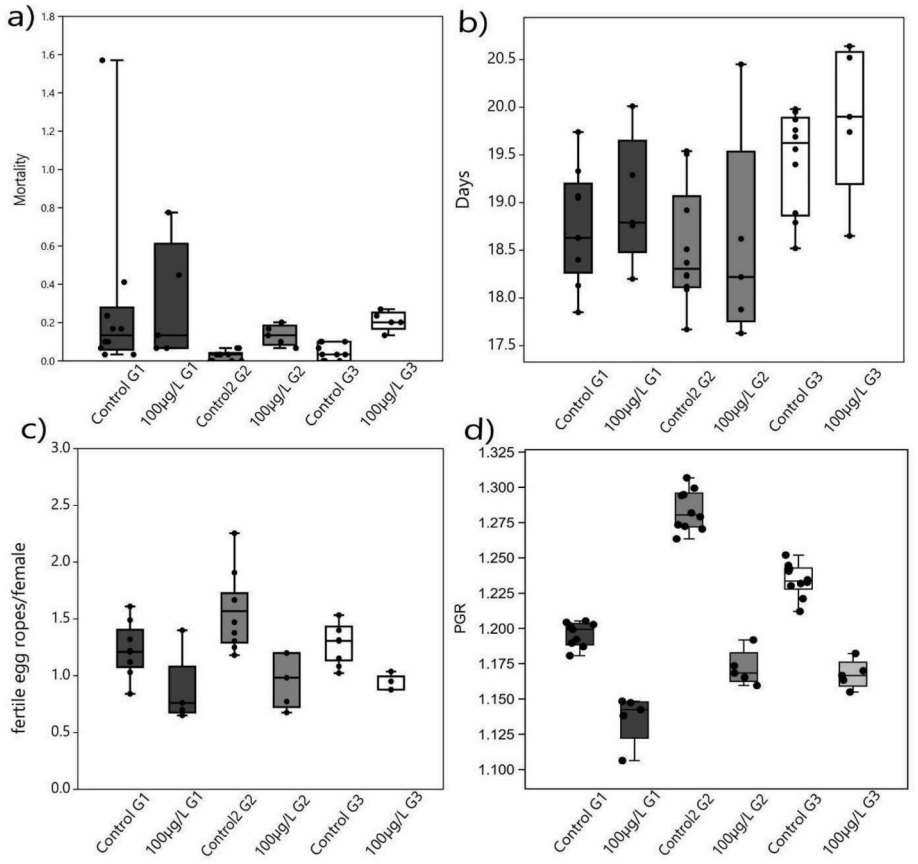

Fig. 2. *C. riparius* effects on a) mortality, b) Emt50, c) fertility, and d) PGR after exposure to control and 100µ/L of BaP for three consecutive generations.

Table 3
Summary of Bayesian statistics for Emerged Adults, EmT50, Fertility, and PGR within generations between the control group and 100 μg/L group.

Mortality					
Generation	Mean of Control (95% HDI)	Mean of 100 μg/L (95% HDI)	Mean Difference	PP (100 μg/L > Control)	Effect Size (95% HDI)
G1	14 (4.2–23)	27 (-14–71)	−13 (-59–29)	22.2%	−0.50 (−1.8–0.79
G2	2.6 (0.60–4.7)	13 (5.1–22)	−11 (−19–−2.2)	1.3%	−2 (−4–−0.17)
G3	4.6 (1.4–7.8)	21 (13–28)	−16 (−24–−8.1)	0.3%	−2.8 (−4.9–−0.76)
EmT50					
G1	19 (18–19)	19 (18–20)	−0.24 (−1.4–0.91)	30.4%	−0.31 (−1.5–0.89
G2	18 (18–19)	18 (17–20)	0.00077 (−1.9–1.7)	50.1%	0.00066 (−1.2–1.2)
G3	19 (19–20)	20 (19–21)	−0.45 (−1.7–0.86)	19.4%	−0.54 (−1.8–0.68)
Fertility					
G1	1.2 (1.0–1.3)	0.83 (0.39–1.3)	0.39 (−0.13–0.87)	94.7%	1.2 (−0.33–2.8)
G2	1.6 (1.3–1.8)	0.97 (0.57–1.3)	0.60 (0.15–1.1)	99.2%	1.7 (0.30–3.2)
G3	1.3 (1.1–1.4)	0.92 (0.81–1.0)	0.36 (0.19–0.54)	99.9%	2.3 (0.81–3.9)
PGR					
G1	1.2 (1.2–1.2)	1.2 (1.1–1.2)	0.016 (−0.023–0.054)	85.8%	0.73 (−0.64–2.1)
G2	1.2 (1.2–1.2)	1.1 (1.1–1.2)	0.08 (0.031–0.12)	99.7%	2.7 (0.46–4.8)
G3	1.2 (1.2–1.2)	1.2 (1.2–1.2)	0.067 (0.048–0.085)	100%	5.1 (1.9–8.3)

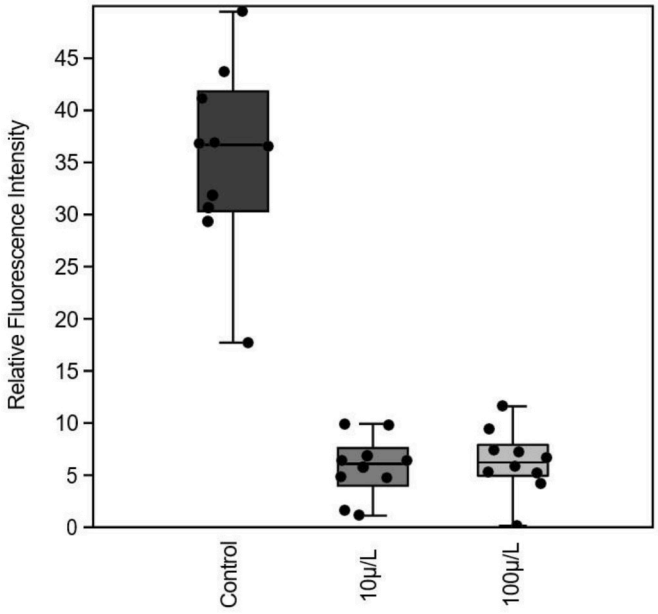

Fig. 3. Comparison of relative fluorescence intensity among control, 10μ/L, and 100μ/L.

While we could not show a mutagenic impact of environmentally relevant concentrations of BaP, the picture was different when the direct fitness effects of BaP were considered. Life cycle traits were assessed in a multi-generation test conducted with *C. riparius* exposed to nominal BaP concentrations of 0 (control) and 100 μg/L. Mortality, EmT50, fertility, and PGR of control and exposed groups fluctuated between generations. Despite the lack of significance, there was a tendency towards increased mortality in the first generation. Furthermore, there was a significant increase in mortality in the second and third generations. This effect could be due to the lipophilic properties of BaP, which is absorbed by the sediment (Leversee et al., 1982). Due to their sediment-bound lifestyle, chironomid larvae are exposed throughout the larval stage to pollutants in the sediment, thus absorbing the pollutant and accumulating it (Markert et al., 2003). During larval development, lipids are mobilized in the pupal stage and BaP previously stored in adipose tissue is released. Therefore, the release of BaP could be the cause of the observed increased adult mortality (Du et al., 2014).

The results of EmT50 showed no significant effects for the experimental groups compared to the control, for all generations analyzed. Therefore, no effect of BaP exposure on the developmental time of *C. riparius* was detected. However, fertility decreased significantly in all generations and was further significantly reduced in the third. Reduced fertility is a common consequence of exposure to various contaminants (Nowak et al., 2007). Regarding BaP, multigenerational studies with other organisms have yielded similar results, showing reduced fertility and reproduction in successive generations exposed to BaP (Mohamed et al., 2010; White et al., 1999). Mohamed et al. (2010) reported a decrease in sperm production in male mice exposed to BaP in the adult generation. In this case, the effects were even intergenerational, as the effect was felt up to the F2 generation without the G2 or G3 generation being exposed to BaP. In another study, larvae of the freshwater fish *Pimephales promelas* were exposed to BaP, and toxic effects on reproduction were observed in subsequent generations (White et al., 1999).

The PGR clearly decreased with BaP exposure, mainly due to the observed loss of fertility. In all generations, the BaP-exposed group had a significantly lower PGR value than the control. Although the effect of BaP as a stressor of *C. riparius* was confirmed, the PGR value was above the critical value of 1 d^{-1} despite the high stress. However, as we assessed the PGR per day, even a small decrease may have dramatic influences in the long run. For example, a population growing 8% less per day would have after only 14 days half the size of an undisturbed growing population.

While many organisms are unable to adapt to changing environmental conditions, *C. riparius* is known for its adaptability to environmental stressors (Doria et al., 2022; Khosrovyan et al., 2022). However, in the present study, we could not confirm an adaptation of *C. riparius* to BaP exposure. One reason might be that the effect of BaP exposure might not have been detrimental enough to trigger a rapid adaptation response, so detecting potential adaptation would have required more generations. Other, mutually non-exclusive reasons might have been i) lacking genetic variation for the particular trait in the laboratory population, ii) adaptation happened but the accumulation of mutations may have had an accumulating negative effect on fitness, thus veiling the adaptation. Further studies with a modified experimental design would be required to test this hypothesis.

The direct assessment of ROS activity by fluorescence intensity was performed with living *C. riparius* larvae exposed to nominal BaP concentrations of 0 μg/L (control), 10 μg/L, and 100 μg/L. Some studies on BaP exposure suggested that DNA damage is caused by ROS production (Saunders et al., 2006; Vicentini et al., 2017). In a study conducted on *Chironomus sancticaroli Strixino & Strixino* larvae, it was found that BaP

exposure caused genotoxic effects and biochemical changes usually associated with oxidative stress (Vicentini et al., 2017). Contrary to these results, our study, however, showed lower ROS levels in both treatments than in the control group. This discrepancy might have two reasons: First, the study by Vincentini et al. did not measure ROS activity directly, but antioxidative enzyme activity. However, such activity was shown to be time-dependent rather than concentration-related, as exposure to 10 μg/L and 100 μg/L BaP initially increased antioxidant enzyme activity in the first 24 h, but subsequently reduced to control level after 48 h (Guo et al., 2021). Second, the direct measurement as employed here presents the equilibrium between metabolic ROS production and antioxidant activity, it is possible that BaP either had a negative impact on metabolism or stimulated antioxidant activities to an extent that pushed the level under that of the control. In any case, our results suggested that the observed increase of mutation rate was not related to an increased ROS production, but rather involved other, unknown processes.

5. Conclusion

The results of our multigenerational study show that high BaP exposure led to an increased mutation rate and negatively impacted the demographic dynamics of *C. riparius*, thus altering the eco-evolutionary trajectory of the population. A rapid adaptive effect could not be observed but cannot be excluded over longer time frames. The results of this study thus demonstrated the importance of multigenerational studies for ecological risk assessment, as the evolutionary effects of most ecotoxicologically relevant chemical inputs such as BaP are still unknown.

CRediT authorship contribution statement

Burak Bulut: Conceptualization, Data curation, Formal analysis, Methodology, Visualization, Writing – original draft. **Lorenzo Rigano:** Conceptualization, Data curation, Formal analysis, Methodology, Visualization, Writing – original draft. **Halina Binde Doria:** Conceptualization, Data curation, Project administration, Writing – review & editing. **Gajana Gemüth:** Conceptualization, Data curation. **Markus Pfenninger:** Conceptualization, Funding acquisition, Methodology, Project administration, Resources, Validation, Writing – review & editing.

Declaration of competing interest

The authors declare that they have no known competing financial interests or personal relationships that could have appeared to influence the work reported in this paper.

Data availability

Data will be made available on request.

Acknowledgments

The study received support from the LOEWE-Centre Translational Biodiversity Genomics (TBG) (LOEWE/1/10/519/03/03.001(0014)/52) funded by Hessen State Ministry of Higher Education, Research and the Arts (HMWK). Burak Bulut was supported by a DFG grant to MP (PF 390/15-1).

Appendix A. Supplementary data

Supplementary data to this article can be found online at https://doi.org/10.1016/j.chemosphere.2024.142242.

References

Adeniji, A.O., Okoh, O.O., Okoh, A.I., 2019. Levels of polycyclic aromatic hydrocarbons in the water and sediment of Buffalo river Estuary, South Africa and their health risk assessment. Arch. Environ. Contam. Toxicol. 76, 657–669. https://doi.org/10.1007/s00244-019-00617-w.

Aitken, R.J., Krausz, C., 2001. Oxidative stress, DNA damage and the Y chromosome. Reprod. Camb. Engl. 122, 497–506. https://doi.org/10.1530/rep.0.1220497.

Bååth, R., 2014. Bayesian first aid: a package that implements Bayesian alternatives to the classical*. test functions in R. Proc. UseR 2014 (2).

Baer, C.F., Shaw, F., Steding, C., Baumgartner, M., Hawkins, A., Houppert, A., Mason, N., Reed, M., Simonelic, K., Woodard, W., Lynch, M., 2005. Comparative evolutionary genetics of spontaneous mutations affecting fitness in rhabditid nematodes. Proc. Natl. Acad. Sci. 102, 5785–5790. https://doi.org/10.1073/pnas.0406056102.

Beal, M.A., Meier, M.J., Williams, A., Rowan-Carroll, A., Gagné, R., Lindsay, S.J., Fitzgerald, T., Hurles, M.E., Marchetti, F., Yauk, C.L., 2019. Paternal exposure to benzo(a)pyrene induces genome-wide mutations in mouse offspring. Commun. Biol. 2, 228. https://doi.org/10.1038/s42003-019-0476-5.

Bukowska, B., Mokra, K., Michałowicz, J., 2022. Benzo[a]pyrene—environmental Occurrence, human exposure, and mechanisms of toxicity. Int. J. Mol. Sci. 23, 6348. https://doi.org/10.3390/ijms23116348.

Charlesworth, B., 1971. Selection in density-regulated populations. Ecology 52, 469–474. https://doi.org/10.2307/1937629.

Danecek, P., Bonfield, J.K., Liddle, J., Marshall, J., Ohan, V., Pollard, M.O., Whitwham, A., Keane, T., McCarthy, S.A., Davies, R.M., Li, H., 2021. Twelve years of SAMtools and BCFtools. GigaScience 10, giab008. https://doi.org/10.1093/gigascience/giab008.

Doria, H.B., Pfenninger, M., 2021. A multigenerational approach can detect early Cd pollution in Chironomus riparius. Chemosphere 262, 127815. https://doi.org/10.1016/j.chemosphere.2020.127815.

Doria, H.B., Hannappel, P., Pfenninger, M., 2022. Whole genome sequencing and RNA-seq evaluation allowed to detect Cd adaptation footprint in *Chironomus riparius*. Sci. Total Environ. 819, 152843 https://doi.org/10.1016/j.scitotenv.2021.152843.

Dröge, W., 2002. Free radicals in the physiological control of cell function. Physiol. Rev. 82, 47–95. https://doi.org/10.1152/physrev.00018.2001.

Du, H., Pan, B., Chen, T., 2017. Evaluation of chemical mutagenicity using next generation sequencing: a review. J. Environ. Sci. Health, Part A C 35, 140–158. https://doi.org/10.1080/10590501.2017.1328831.

Du, J., Li, Y., Huang, Z.C., You, J., 2014. Chronic toxicity thresholds for sediment-associated Benzo[a]pyrene in the Midge (Chironomus dilutus). Arch. Environ. Contam. Toxicol. 66, 370–378. https://doi.org/10.1007/s00244-014-0005-y.

Eyre-Walker, A., Woolfit, M., Phelps, T., 2006. The distribution of fitness effects of new deleterious amino acid mutations in humans. Genetics 173, 891–900. https://doi.org/10.1534/genetics.106.057570.

Foucault, Q., Wieser, A., Waldvogel, A., Pfenninger, M., 2019. Establishing laboratory cultures and performing ecological and evolutionary experiments with the emerging model species Chironomus riparius. J. Appl. Entomol. 143, 584–592. https://doi.org/10.1111/jen.12606.

Guo, B., Feng, D., Xu, Z., Qi, P., Yan, X., 2021. Acute benzo[a]pyrene exposure induced oxidative stress, neurotoxicity and epigenetic change in blood clam Tegillarca granosa. Sci. Rep. 11, 18744. https://doi.org/10.1038/s41598-021-98354-5.

Kagan, J., Kagan, E.D., 1986. The toxicity of benzo[a]pyrene and pyrene in the mosquito Aedes aegypti, in the dark and in the presence of ultraviolet light. Chemosphere 15, 243–251. https://doi.org/10.1016/0045-6535(86)90019-6.

Kirkland, D., Pfuhler, S., Tweats, D., Aardema, M., Corvi, R., Darroudi, F., Elhajouji, A., Glatt, H., Hastwell, P., Hayashi, M., Kasper, P., Kirchner, S., Lynch, A., Marzin, D., Maurici, D., Meunier, J.-R., Müller, L., Nohynek, G., Parry, J., Parry, E., Thybaud, V., Tice, R., van Benthem, J., Vanparys, P., White, P., 2007. How to reduce false positive results when undertaking in vitro genotoxicity testing and thus avoid unnecessary follow-up animal tests: report of an ECVAM Workshop. Mutat. Res. Toxicol. Environ. Mutagen. 628, 31–55. https://doi.org/10.1016/j.mrgentox.2006.11.008.

Knaap, A.G., Kramers, P.G., Voogd, C.E., Bergkamp, W.G., Groot, M.G., Langebroek, P.G., Mout, H.C., van der Stel, J.J., Verharen, H.W., 1988. Mutagenic activity of acrylamide in eukaryotic systems but not in bacteria. Mutagenesis 3, 263–268. https://doi.org/10.1093/mutage/3.3.263.

Khosrovyan, A., Doria, H.B., Kahru, A., Pfenninger, M., 2022. Polyamide microplastic exposure elicits rapid, strong and genome-wide evolutionary response in the freshwater non-biting midge *Chironomus riparius*. Chemosphere 299, 134452. https://doi.org/10.1016/j.chemosphere.2022.134452.

Leversee, G.J., Giesy, J.P., Landrum, P.F., Gerould, S., Bowling, J.W., Fannin, T.E., Haddock, J.D., Bartell, S.M., 1982. Kinetics and biotransformation of benzo(a) pyrene in Chironomus riparius. Arch. Environ. Contam. Toxicol. 11, 25–31. https://doi.org/10.1007/BF01055182.

Lynch, M., Gabriel, W., 1990. Mutation load and the survival of small populations. Evol. Int. J. Org. Evol. 44, 1725–1737. https://doi.org/10.1111/j.1558-5646.1990.tb05244.x.

Markert, B.A., Breure, A.M., Zechmeister, H.G., 2003. Chapter 1 Definitions, strategies and principles for bioindication/biomonitoring of the environment. In: Markert, B. A., Breure, A.M., Zechmeister, H.G. (Eds.), Trace Metals and Other Contaminants in the Environment, Bioindicators & Biomonitors. Elsevier, pp. 3–39. https://doi.org/10.1016/S0927-5215(03)80131-5.

McKenna, A., Hanna, M., Banks, E., Sivachenko, A., Cibulskis, K., Kernytsky, A., Garimella, K., Altshuler, D., Gabriel, S., Daly, M., DePristo, M.A., 2010. The Genome Analysis Toolkit: a MapReduce framework for analyzing next-generation DNA sequencing data. Genome Res. 20, 1297–1303. https://doi.org/10.1101/gr.107524.110.

Murray, B.G., 1990. Population dynamics, genetic change, and the measurement of fitness. Oikos 59, 189–199. https://doi.org/10.2307/3545534.
Mohamed, E.-S.A., Song, W.-H., Oh, S.-A., Park, Y.-J., You, Y.-A., Lee, S., Choi, J.-Y., Kim, Y.-J., Jo, I., Pang, M.-G., 2010. The transgenerational impact of benzo(a)pyrene on murine male fertility. Hum. Reprod. Oxf. Engl. 25, 2427–2433. https://doi.org/10.1093/humrep/deq205.
Nemec, S., Patel, S., Nowak, C., Pfenninger, M., 2013. Evolutionary determinants of population differences in population growth rate × habitat temperature interactions in Chironomus riparius. Oecologia 172, 585–594. https://doi.org/10.1007/s00442-012-2517-3.
Nowak, C., Jost, D., Vogt, C., Oetken, M., Schwenk, K., Oehlmann, J., 2007. Consequences of inbreeding and reduced genetic variation on tolerance to cadmium stress in the midge Chironomus riparius. Aquat. Toxicol. 85, 278–284. https://doi.org/10.1016/j.aquatox.2007.04.015.
Nowak, C., Vogt, C., Pfenninger, M., Schwenk, K., Oehlmann, J., Streit, B., Oetken, M., 2009. Rapid genetic erosion in pollutant-exposed experimental chironomid populations. Environ. Pollut. Barking Essex 157, 881–886. https://doi.org/10.1016/j.envpol.2008.11.005, 1987.
OECD, 2010. Test No. 233: Sediment-Water Chironomid Life-Cycle Toxicity Test Using Spiked Water or Spiked Sediment. Organisation for Economic Co-operation and Development, Paris.
Oppold, A.-M., Pfenninger, M., 2017. Direct estimation of the spontaneous mutation rate by short-term mutation accumulation lines in Chironomus riparius. Evol. Lett. 1 (8), 86–92. https://doi.org/10.1002/evl3.
Patel, A.B., Shaikh, S., Jain, K.R., Desai, C., Madamwar, D., 2020. Polycyclic aromatic hydrocarbons: sources, toxicity, and remediation approaches. Front. Microbiol. 11.
Pfenninger, M., Foucault, Q., 2020. Genomic processes underlying rapid adaptation of a natural Chironomus riparius population to unintendedly applied experimental selection pressures. Mol. Ecol. 29, 536–548. https://doi.org/10.1111/mec.15347.
Phillips, D.H., 1983. Fifty years of benzo(a)pyrene. Nature 303, 468–472. https://doi.org/10.1038/303468a0.
Sæther, B.-E., Engen, S., 2015. The concept of fitness in fluctuating environments. Trends Ecol. Evol. 30, 273–281. https://doi.org/10.1016/j.tree.2015.03.007.
Saunders, C.R., Das, S.K., Ramesh, A., Shockley, D.C., Mukherjee, S., 2006. Benzo(a) pyrene-induced acute neurotoxicity in the F-344 rat: role of oxidative stress. J. Appl. Toxicol. 26, 427–438. https://doi.org/10.1002/jat.1157.
Shaw, R.G., Geyer, C.J., Wagenius, S., Hangelbroek, H.H., Etterson, J.R., 2008. Unifying life-history analyses for inference of fitness and population growth. Am. Nat. 172, E35–E47. https://doi.org/10.1086/588063.
Van Metre, P., Mahler, B., Furlong, E., 2000. Urban sprawl leaves its PAH signature. Environ. Sci. Technol. 34. https://doi.org/10.1021/es991007n.
Vicentini, M., Morais, G.S., Rebechi-Baggio, D., Richardi, V.S., Santos, G.S., Cestari, M. M., Navarro-Silva, M.A., 2017. Benzo(a)pyrene exposure causes genotoxic and biochemical changes in the midge larvae of Chironomus sancticaroli Strixino & Strixino (Diptera: chironomidae). Neotrop. Entomol. 46, 658–665. https://doi.org/10.1007/s13744-017-0505-3.
Waldvogel, A.-M., Pfenninger, M., 2021. Temperature dependence of spontaneous mutation rates. Genome Res. 31, 1582–1589. https://doi.org/10.1101/gr.275168.120.
Wamucho, A., Unrine, J.M., Kieran, T.J., Glenn, T.C., Schultz, C.L., Farman, M., Svendsen, C., Spurgeon, D.J., Tsyusko, O.V., 2019. Genomic mutations after multigenerational exposure of Caenorhabditis elegans to pristine and sulfidized silver nanoparticles. Environ. Pollut. Barking Essex 254, 113078. https://doi.org/10.1016/j.envpol.2019.113078, 1987.
White, P.A., Robitaille, S., Rasmussen, J.B., 1999. Heritable reproductive effects of benzo [a]pyrene on the fathead minnow (Pimephales promelas). Environ. Toxicol. Chem. 18, 1843–1847. https://doi.org/10.1002/etc.5620180835.
Winter, D.J., Wu, S.H., Howell, A.A., Azevedo, R.B.R., Zufall, R.A., Cartwright, R.A., 2018. AccuMUlate: a mutation caller designed for mutation accumulation experiments. Bioinformatics 34, 2659–2660. https://doi.org/10.1093/bioinformatics/bty165.
Zhang, J., Kobert, K., Flouri, T., Stamatakis, A., 2014. PEAR: a fast and accurate Illumina Paired-End reAd mergeR. Bioinformatics 30, 614–620. https://doi.org/10.1093/bioinformatics/btt593.
Zhang, X., Xia, P., Wang, P., Yang, J., Baird, D.J., 2018. Omics advances in ecotoxicology. Environ. Sci. Technol. 52, 3842–3851. https://doi.org/10.1021/acs.est.7b06494.
Baan, R.A., Straif, K., Grosse, Y., Secretan, B., Ghissassi, F.E., Bouvard, V., Benbrahim-Tallaa, L., Cogliano, V., 2008. Carcinogenicity of some aromatic amines, organic dyes, and related exposures. Lancet Oncol. 9, 322–323. https://doi.org/10.1016/s1470-2045(08)70089-5Humans. I.W.G., 2010. Some aromatic amines, organic dyes, and related exposures. International Agency for Research on Cancer on the E. of C.R. to.

Supplementary Data

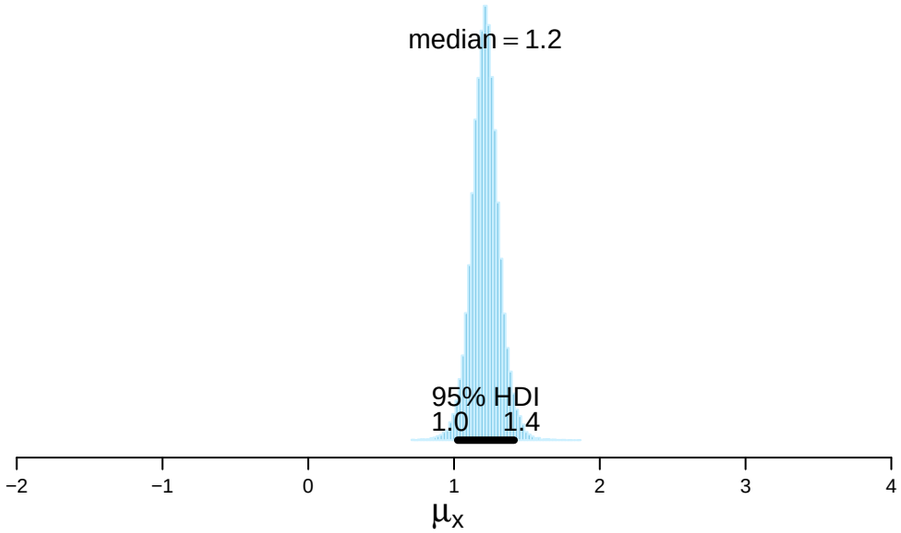
Fertility_Generation1_control Mean
median = 1.2
95% HDI
1.0
1.4
−2
−1
0
1
2
3
4
μx

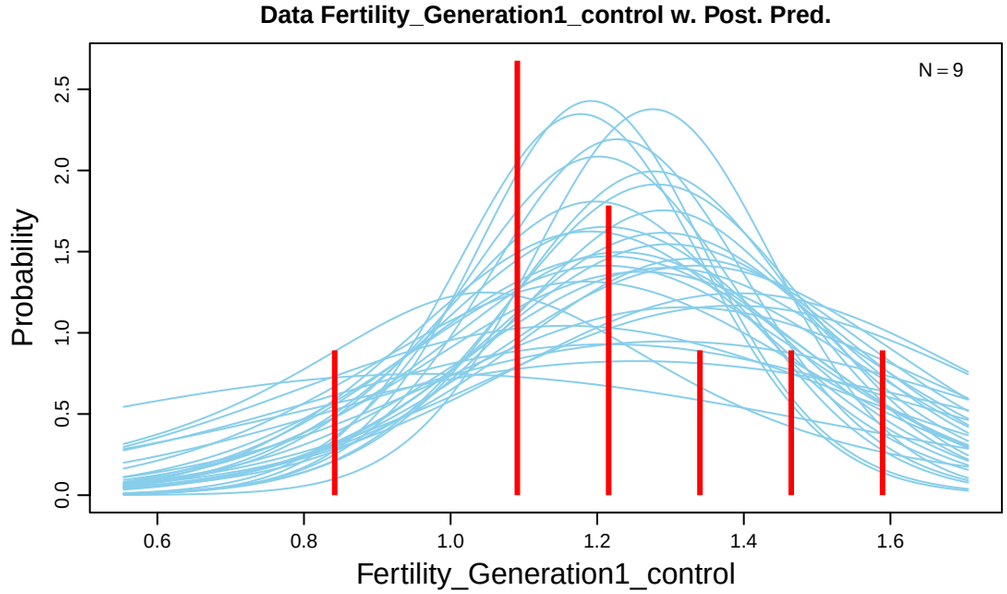
Data Fertility_Generation1_control w. Post. Pred.
N = 9
Probability
0.0
0.5
1.0
1.5
2.0
2.5
0.6
0.8
1.0
1.2
1.4
1.6
Fertility_Generation1_control

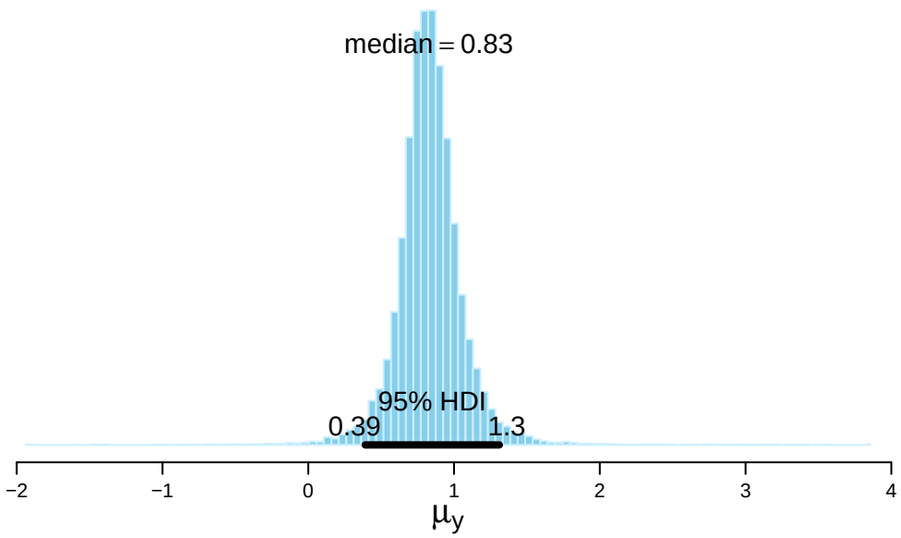
Fertility_Generation1_100 Mean
median = 0.83
95% HDI
0.39
1.3
−2
−1
0
1
2
3
4
μy

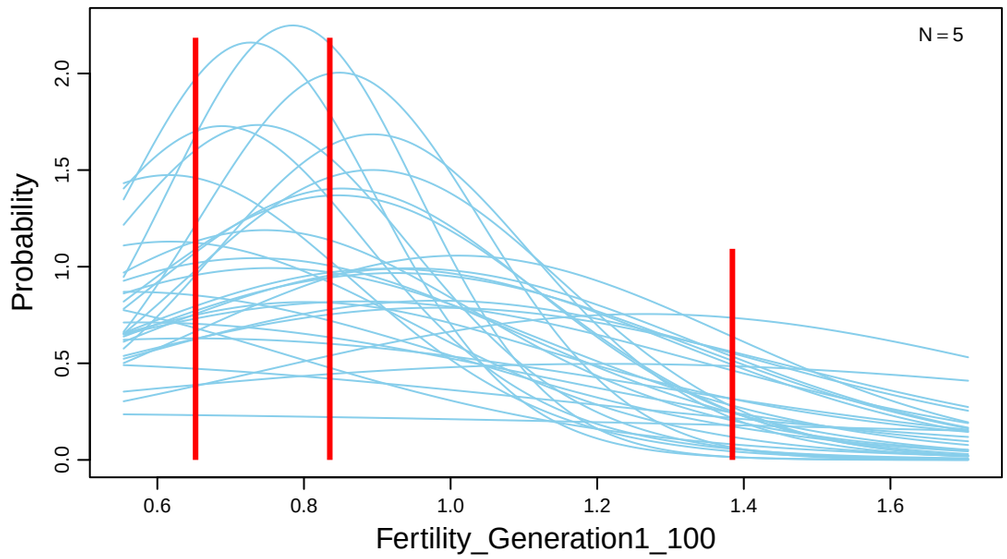
Data Fertility_Generation1_100 w. Post. Pred.
N = 5
Probability
0.0
0.5
1.0
1.5
2.0
0.6
0.8
1.0
1.2
1.4
1.6
Fertility_Generation1_100

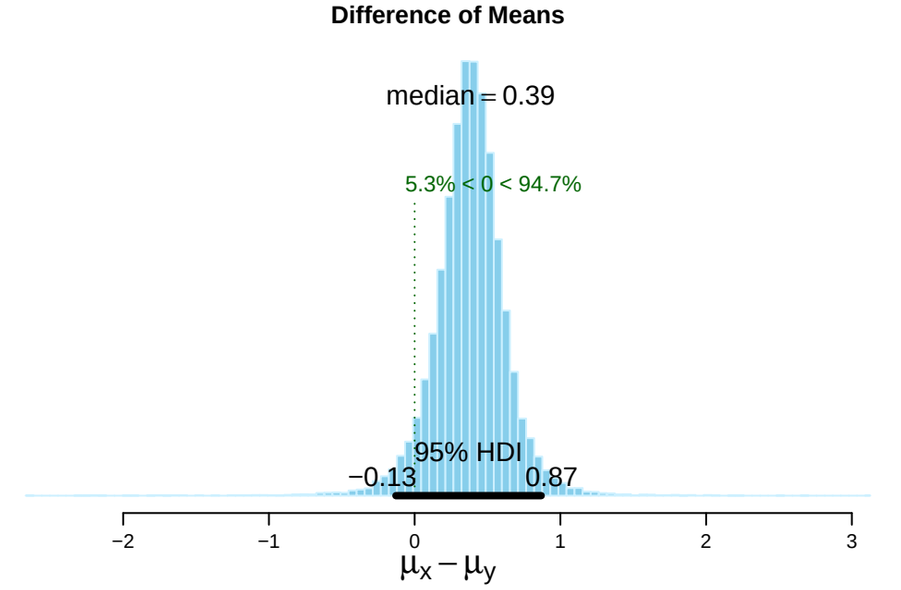
Difference of Means
median = 0.39
5.3% < 0 < 94.7%
95% HDI
−0.13
0.87
−2
−1
0
1
2
3
μx − μy

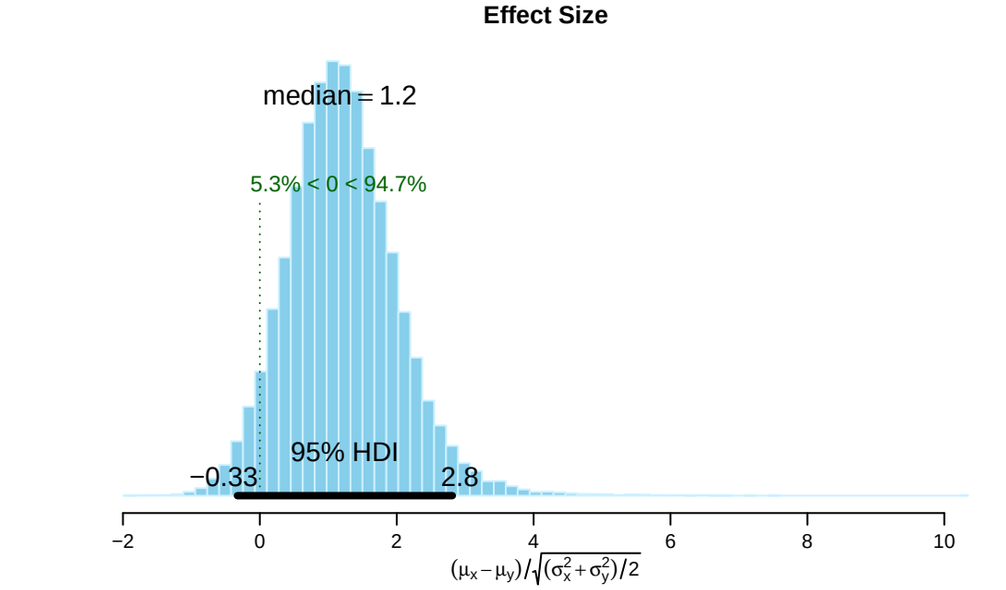
Effect Size
median = 1.2
5.3% < 0 < 94.7%
95% HDI
−0.33
2.8
−2
0
2
4
6
8
10
(μx − μy)/√((σx² + σy²)/2)

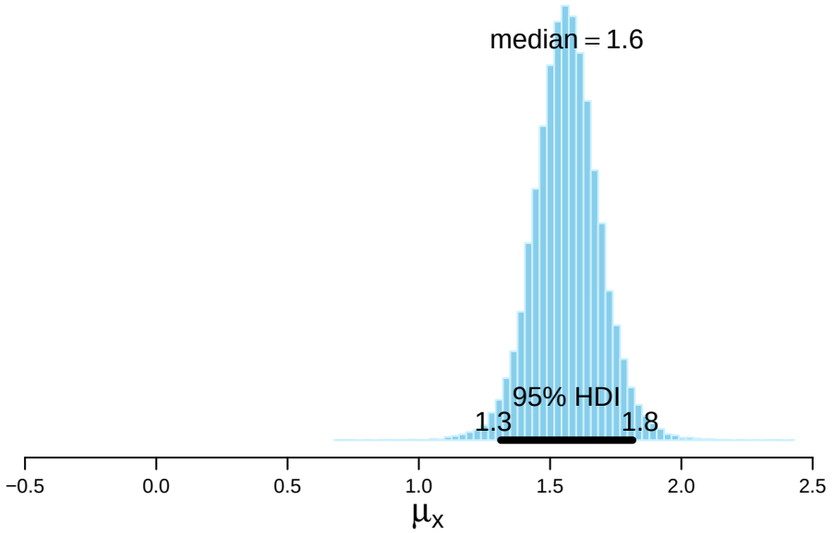
Fertility_Generation2_control Mean
median = 1.6
95% HDI
1.3
1.8
−0.5
0.0
0.5
1.0
1.5
2.0
2.5
μx

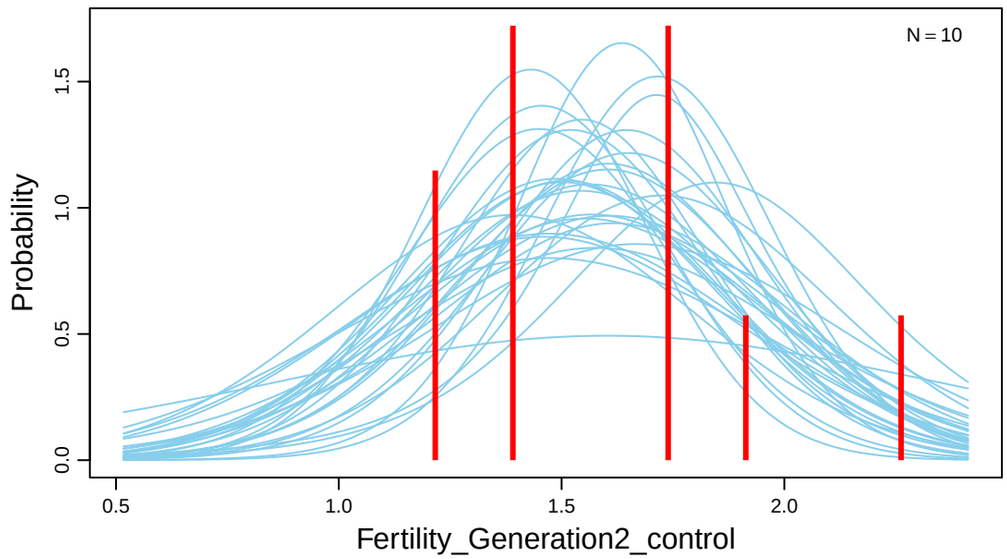
Data Fertility_Generation2_control w. Post. Pred.
N = 10
Probability
0.0
0.5
1.0
1.5
0.5
1.0
1.5
2.0
Fertility_Generation2_control

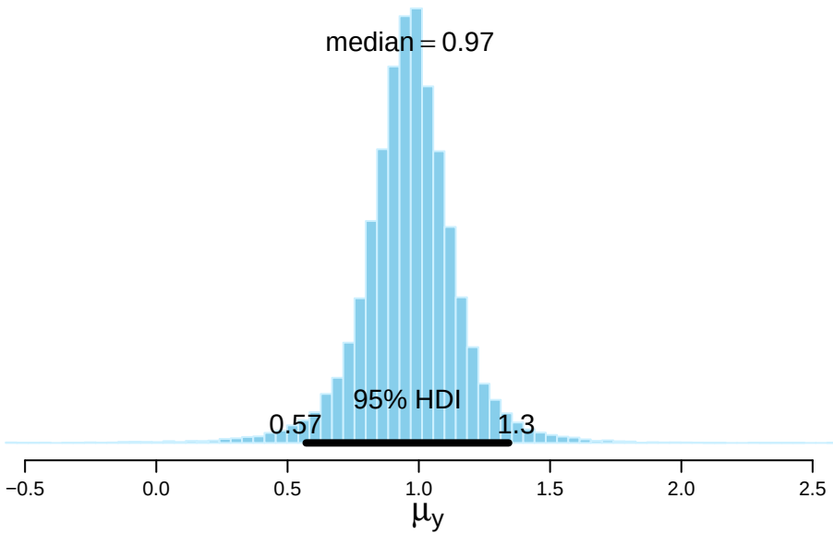
Fertility_Generation2_100 Mean
median = 0.97
95% HDI
0.57
1.3
−0.5
0.0
0.5
1.0
1.5
2.0
2.5
μy

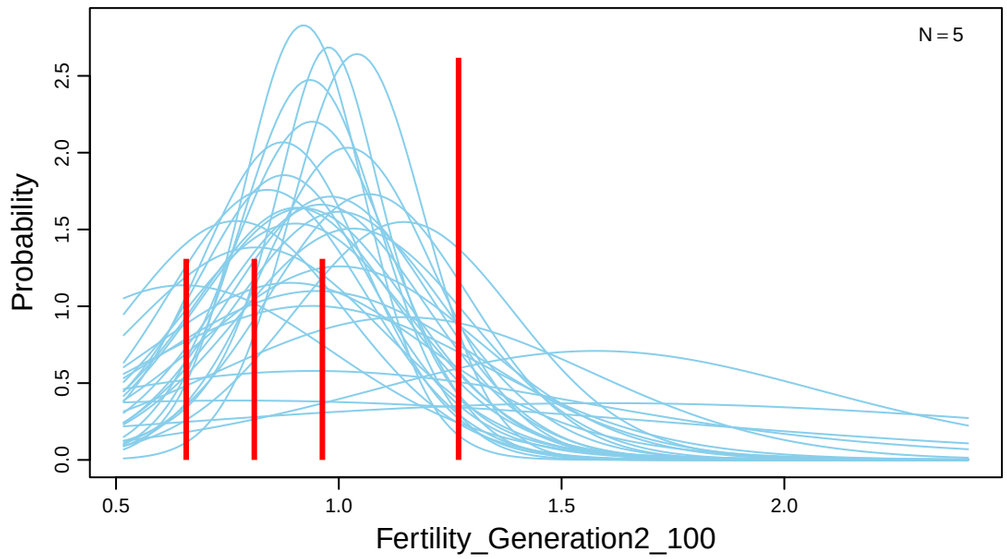
Data Fertility_Generation2_100 w. Post. Pred.
N = 5
Probability
0.0
0.5
1.0
1.5
2.0
2.5
0.5
1.0
1.5
2.0
Fertility_Generation2_100

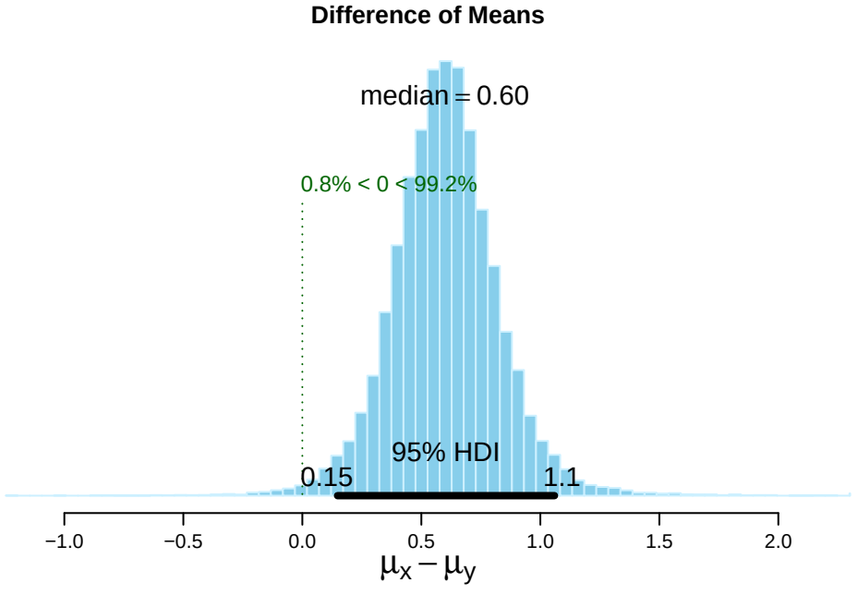
Difference of Means
median = 0.60
0.8% < 0 < 99.2%
95% HDI
0.15
1.1
−1.0
−0.5
0.0
0.5
1.0
1.5
2.0
μx − μy

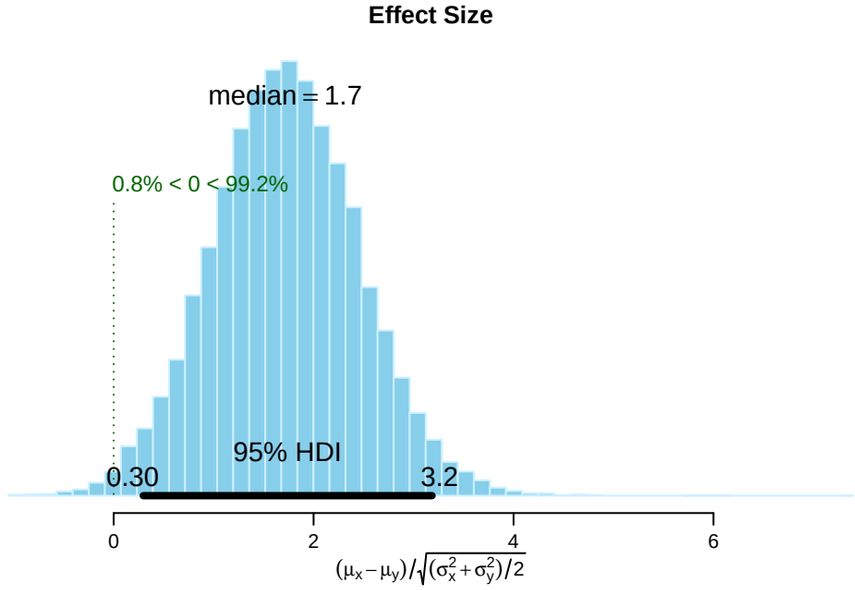
Effect Size
median = 1.7
0.8% < 0 < 99.2%
95% HDI
0.30
3.2
0
2
4
6
(μx − μy)/√((σx² + σy²)/2)

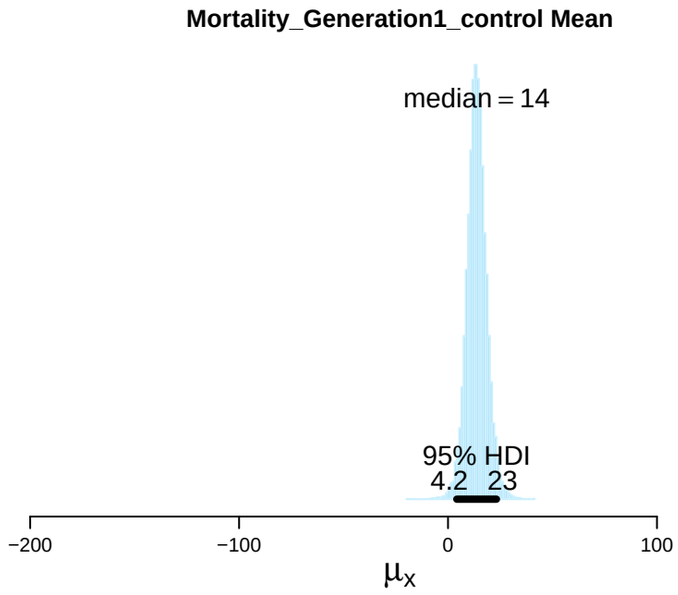
Mortality_Generation1_control Mean
median = 14
95% HDI
4.2 23
−200
−100
0
100
μx

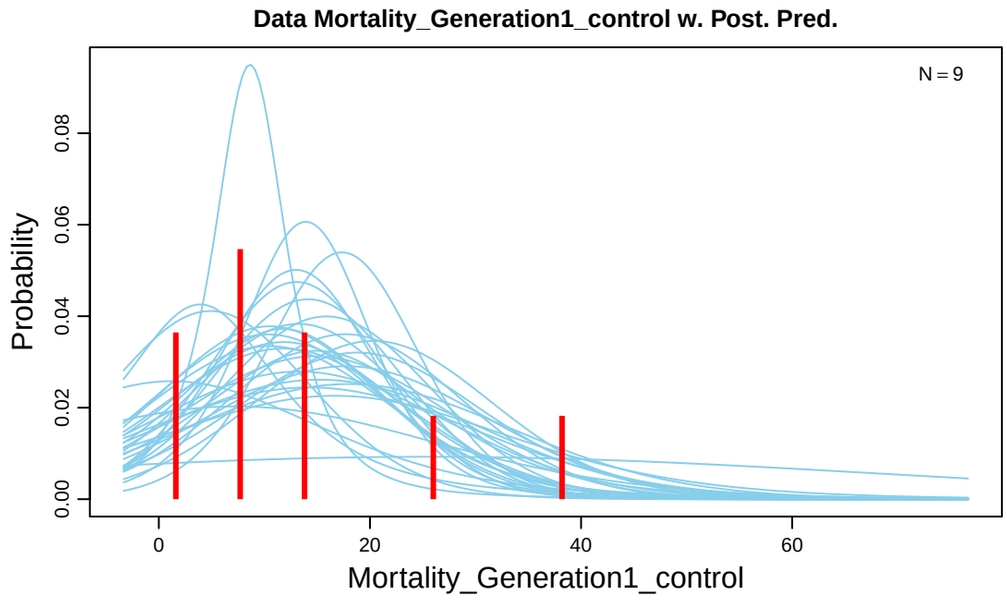
Data Mortality_Generation1_control w. Post. Pred.
N = 9
Probability
0.00
0.02
0.04
0.06
0.08
0
20
40
60
Mortality_Generation1_control

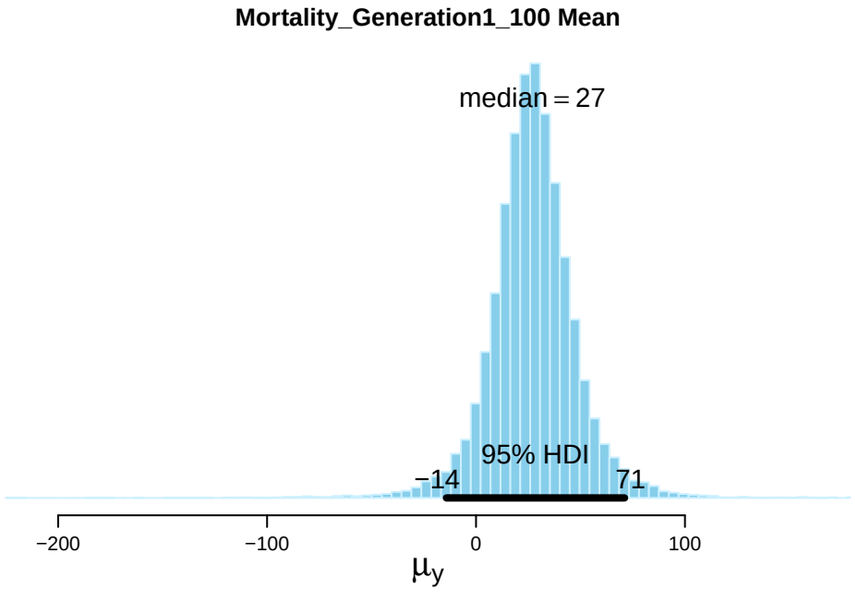
Mortality_Generation1_100 Mean
median = 27
95% HDI
−14
71
−200
−100
0
100
μy

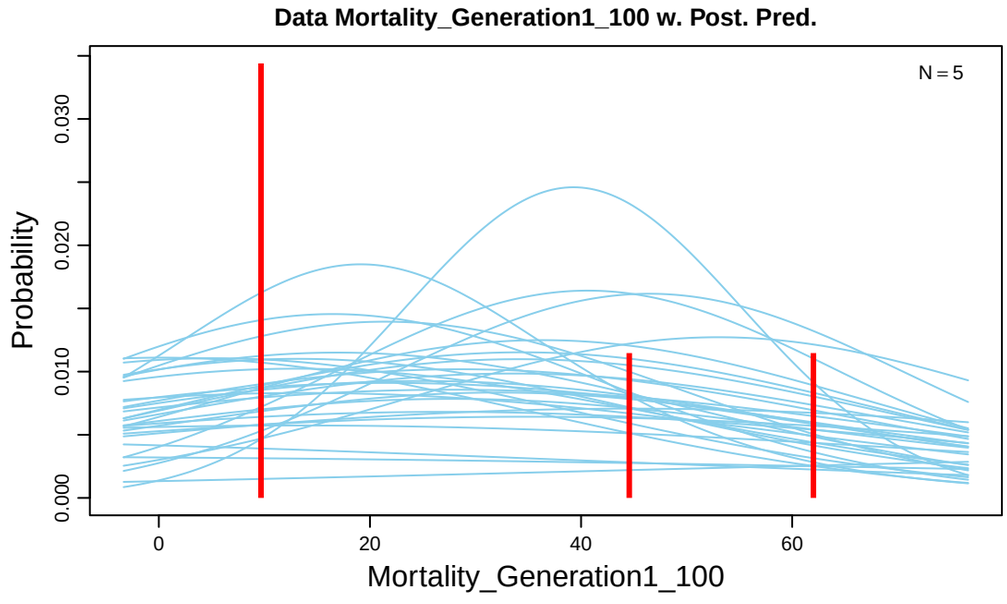
Data Mortality_Generation1_100 w. Post. Pred.
N = 5
Probability
0.000
0.010
0.020
0.030
0
20
40
60
Mortality_Generation1_100

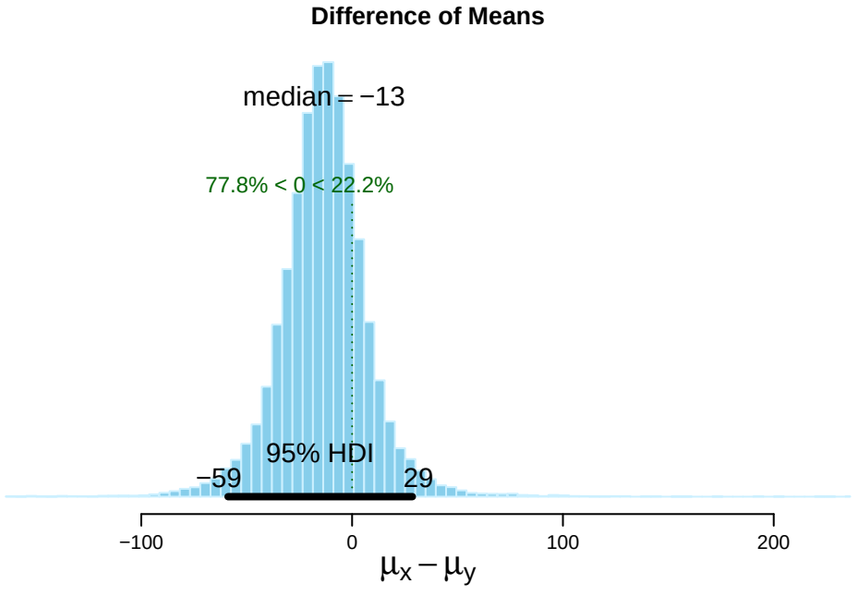
Difference of Means
median = −13
77.8% < 0 < 22.2%
95% HDI
−59
29
−100
0
100
200
μx − μy

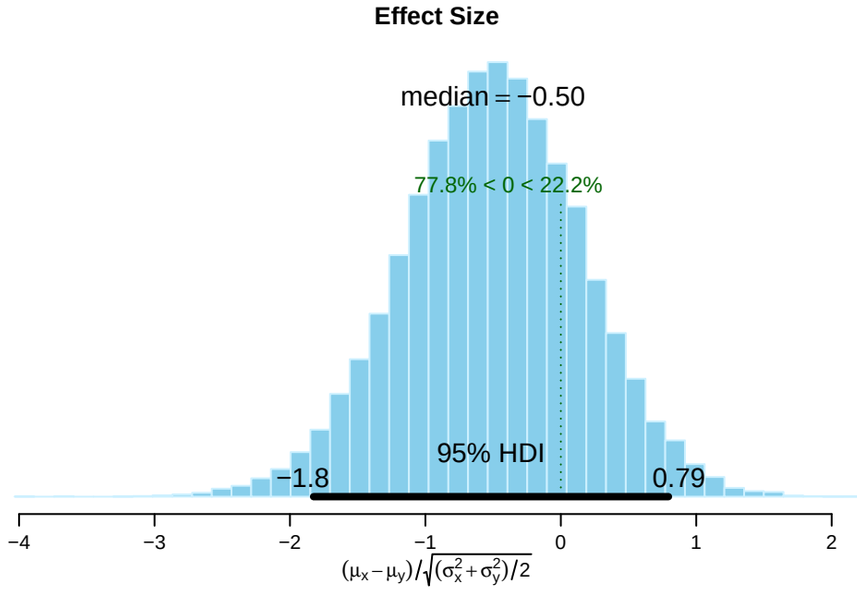
Effect Size
median = −0.50
77.8% < 0 < 22.2%
95% HDI
−1.8
0.79
−4
−3
−2
−1
0
1
2
(μx − μy)/√((σx² + σy²)/2)

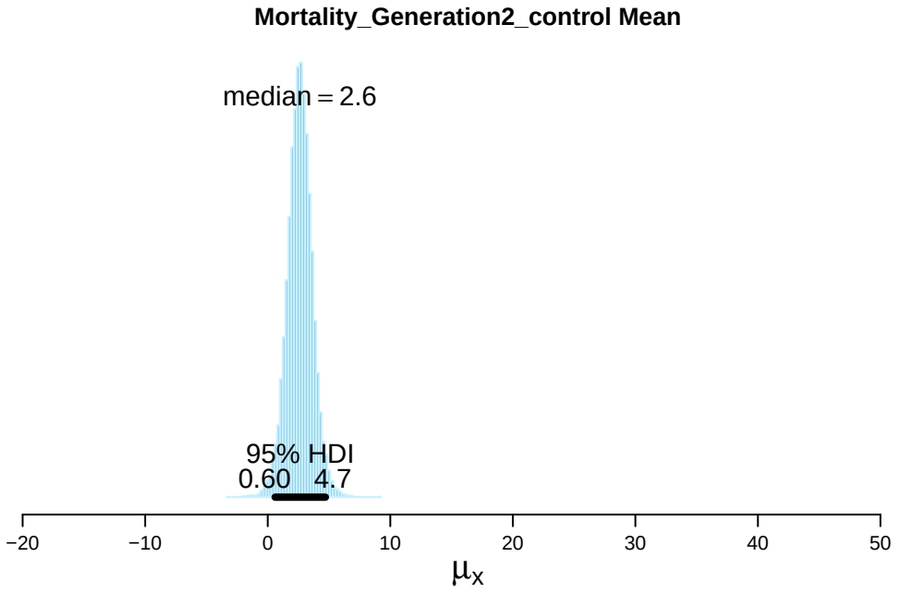
Mortality_Generation2_control Mean
median = 2.6
95% HDI
0.60 4.7
−20 −10 0 10 20 30 40 50
μx

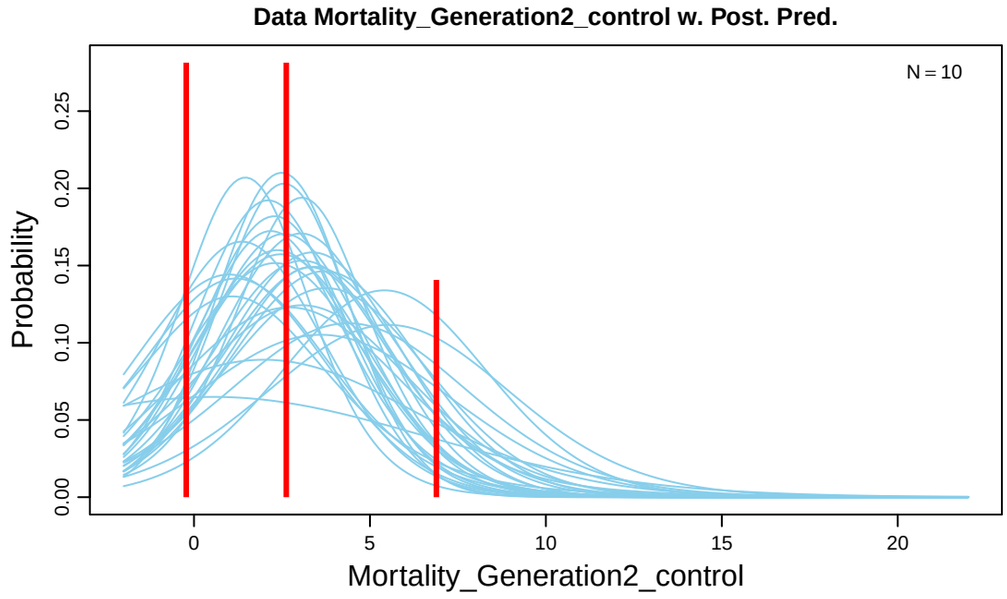
Data Mortality_Generation2_control w. Post. Pred.
N = 10
Probability
0.00 0.05 0.10 0.15 0.20 0.25
0 5 10 15 20
Mortality_Generation2_control

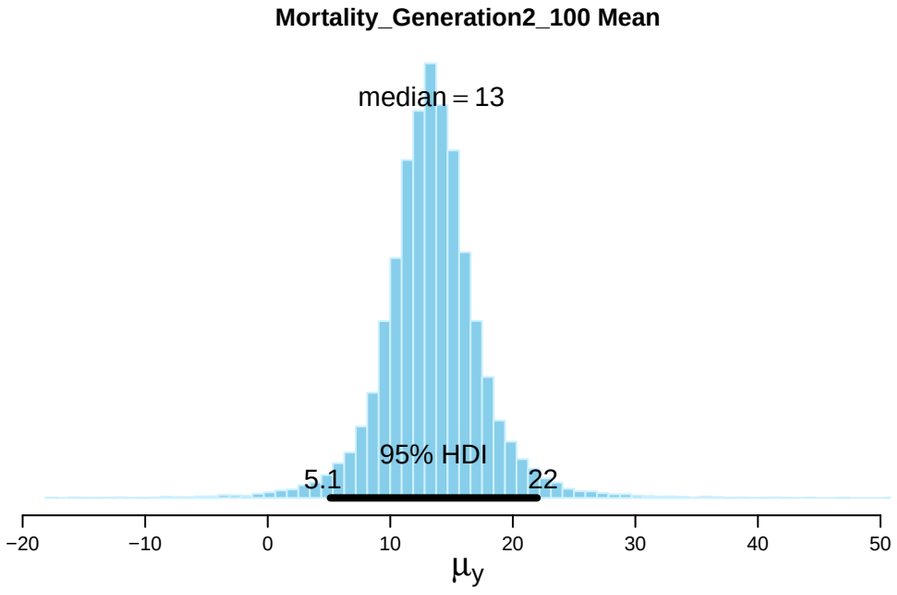
Mortality_Generation2_100 Mean
median = 13
95% HDI
5.1 22
−20 −10 0 10 20 30 40 50
μy

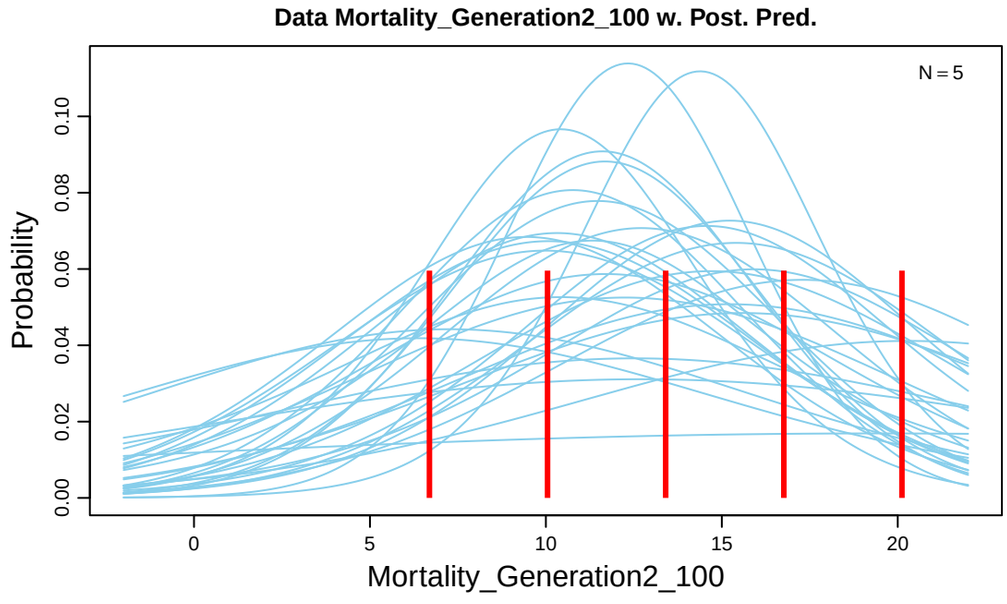
Data Mortality_Generation2_100 w. Post. Pred.
N = 5
Probability
0.00 0.02 0.04 0.06 0.08 0.10
0 5 10 15 20
Mortality_Generation2_100

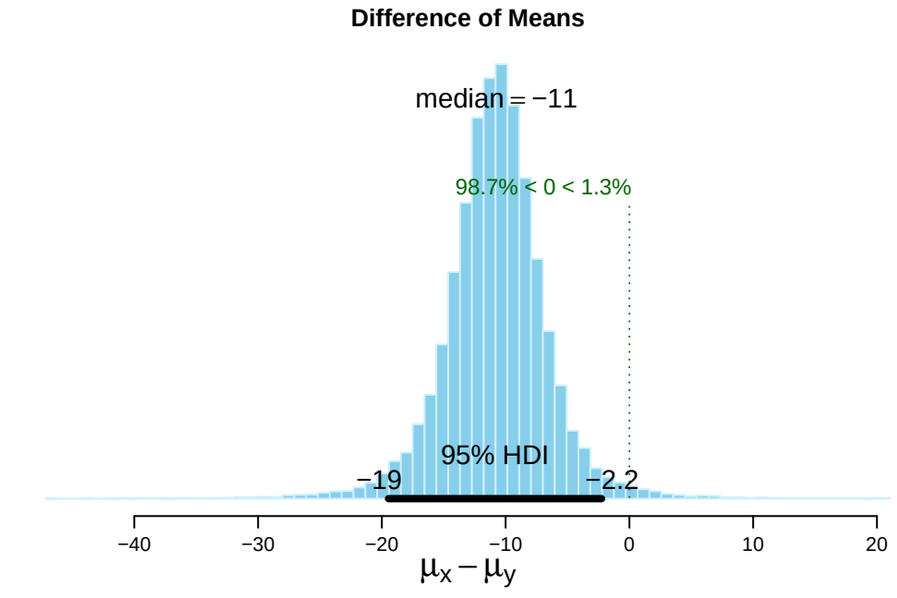
Difference of Means
median = −11
98.7% < 0 < 1.3%
95% HDI
−19 −2.2
−40 −30 −20 −10 0 10 20
μx − μy

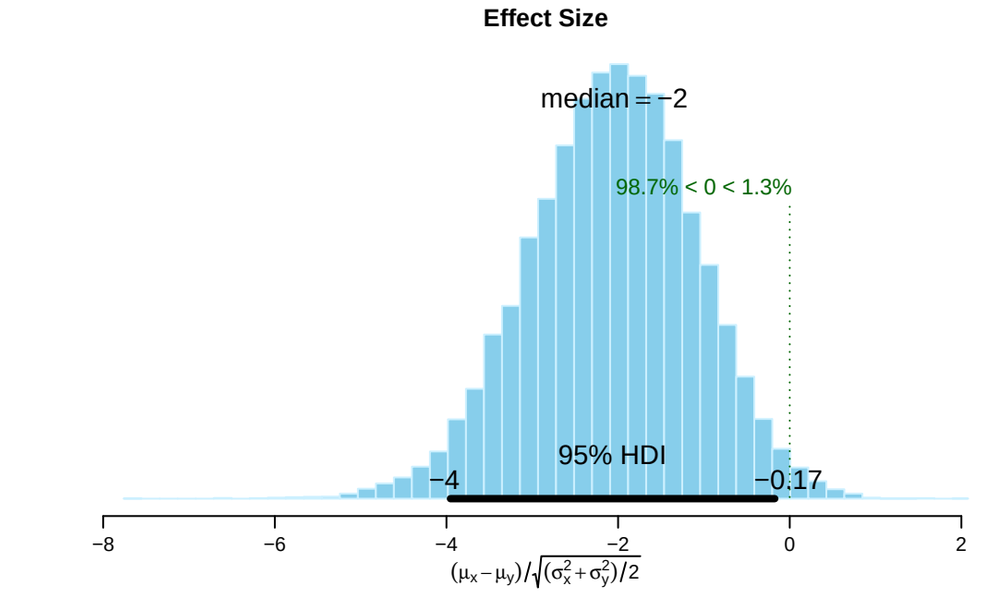
Effect Size
median = −2
98.7% < 0 < 1.3%
95% HDI
−4 −0.17
−8 −6 −4 −2 0 2
(μx − μy)/√((σx² + σy²)/2)

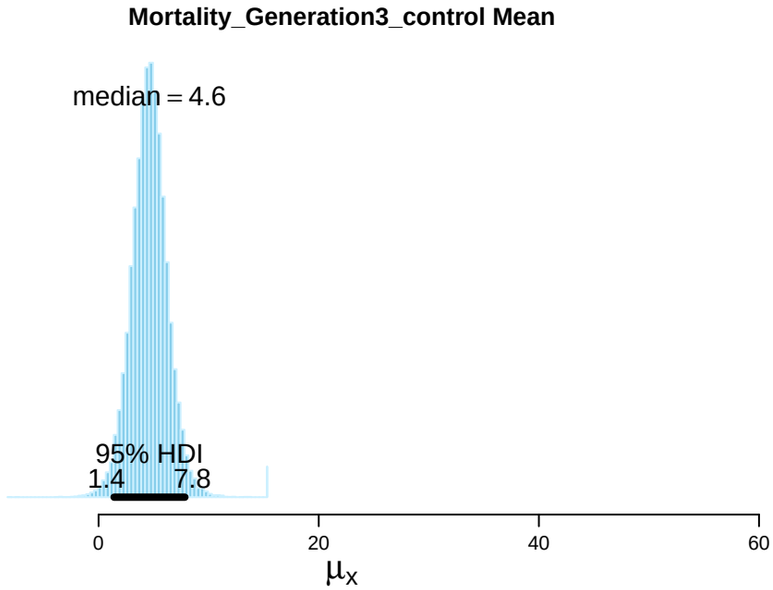
Mortality_Generation3_control Mean
median = 4.6
95% HDI
1.4
7.8
0
20
40
60
μx

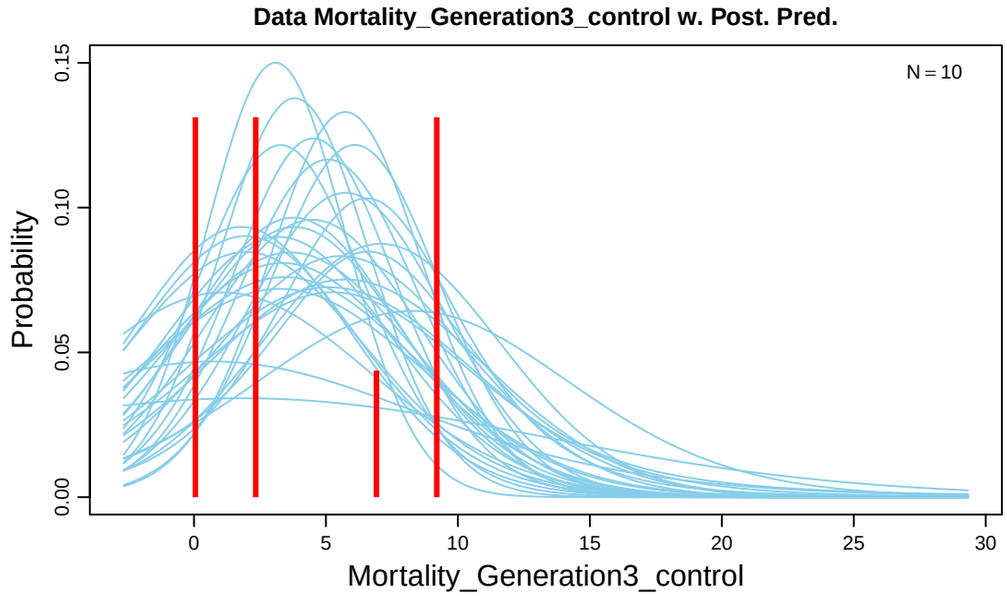
Data Mortality_Generation3_control w. Post. Pred.
N = 10
Probability
0.00
0.05
0.10
0.15
0
5
10
15
20
25
30
Mortality_Generation3_control

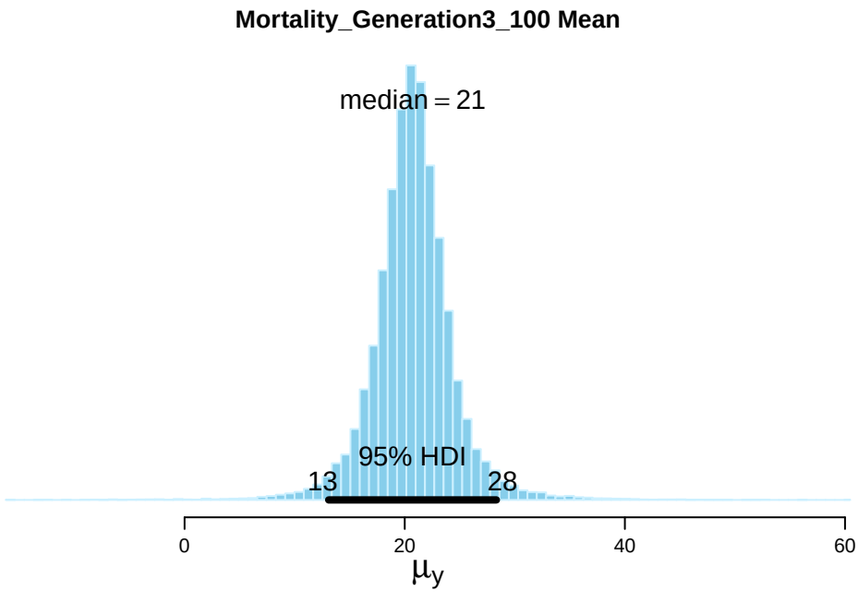
Mortality_Generation3_100 Mean
median = 21
95% HDI
13
28
0
20
40
60
μy

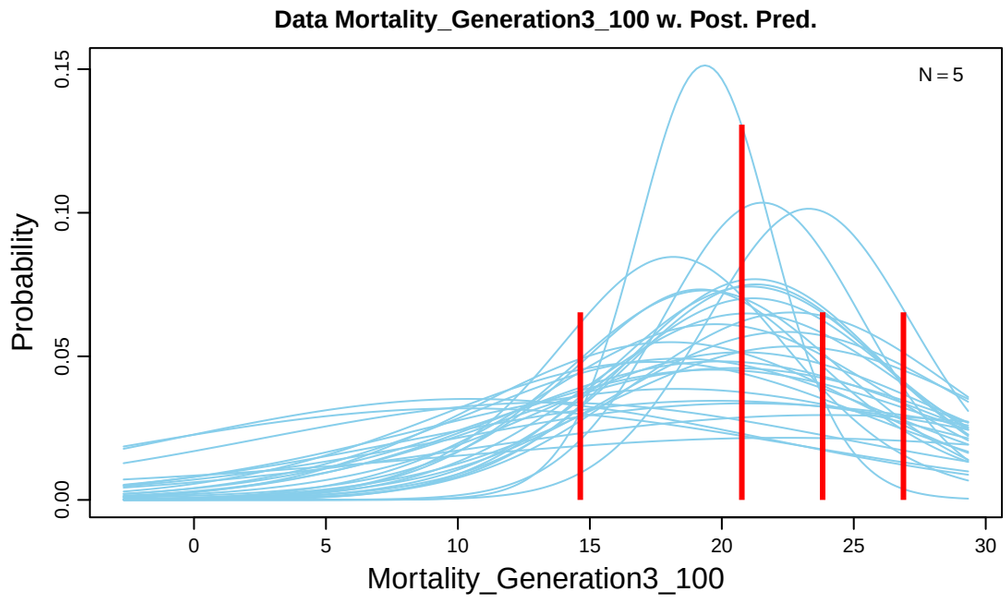
Data Mortality_Generation3_100 w. Post. Pred.
N = 5
Probability
0.00
0.05
0.10
0.15
0
5
10
15
20
25
30
Mortality_Generation3_100

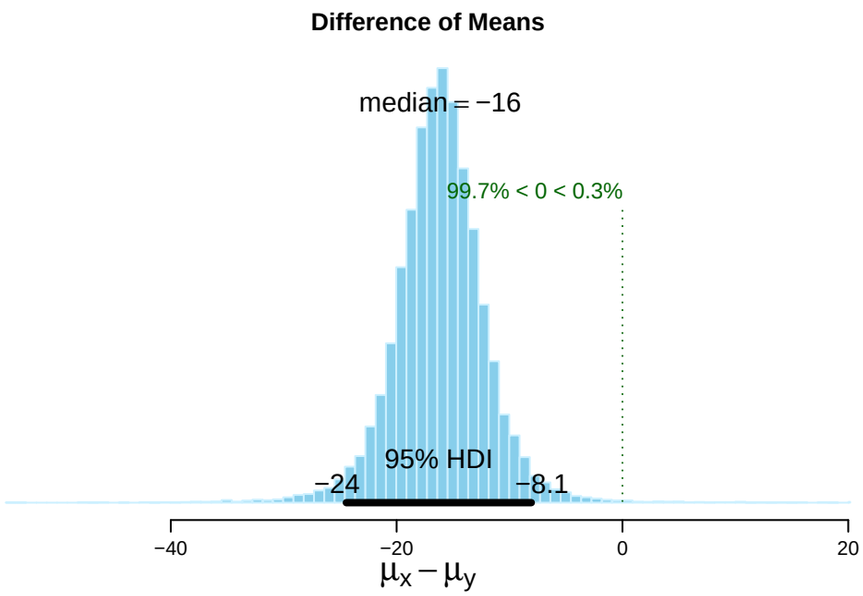
Difference of Means
median = −16
99.7% < 0 < 0.3%
95% HDI
−24
−8.1
−40
−20
0
20
μx − μy

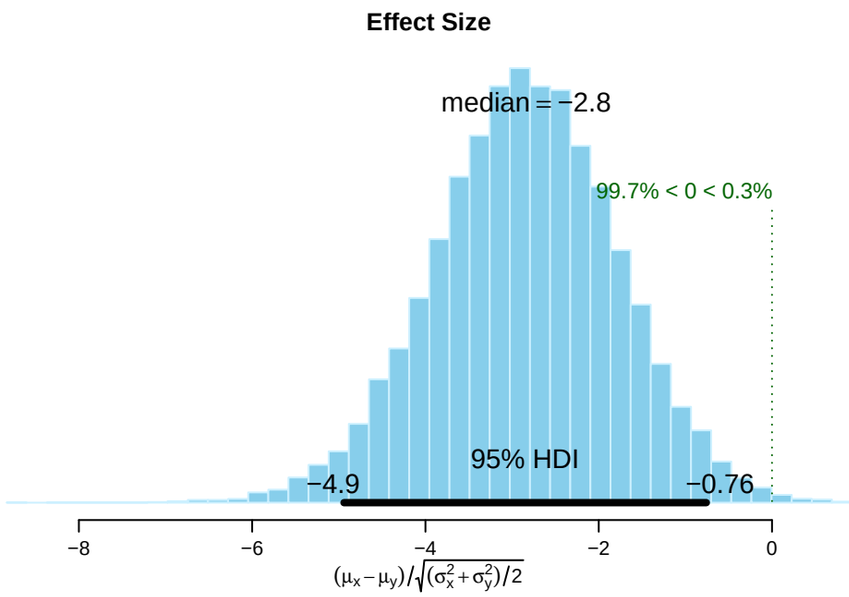
Effect Size
median = −2.8
99.7% < 0 < 0.3%
95% HDI
−4.9
−0.76
−8
−6
−4
−2
0
(μx − μy)/√((σx² + σy²)/2)

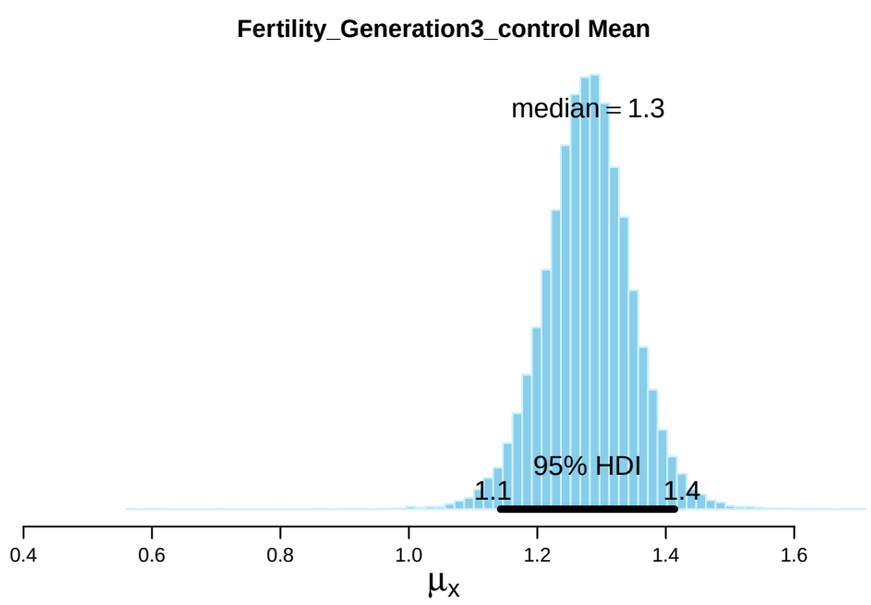
Fertility_Generation3_control Mean
median = 1.3
95% HDI
1.1
1.4
0.4
0.6
0.8
1.0
1.2
1.4
1.6
μx

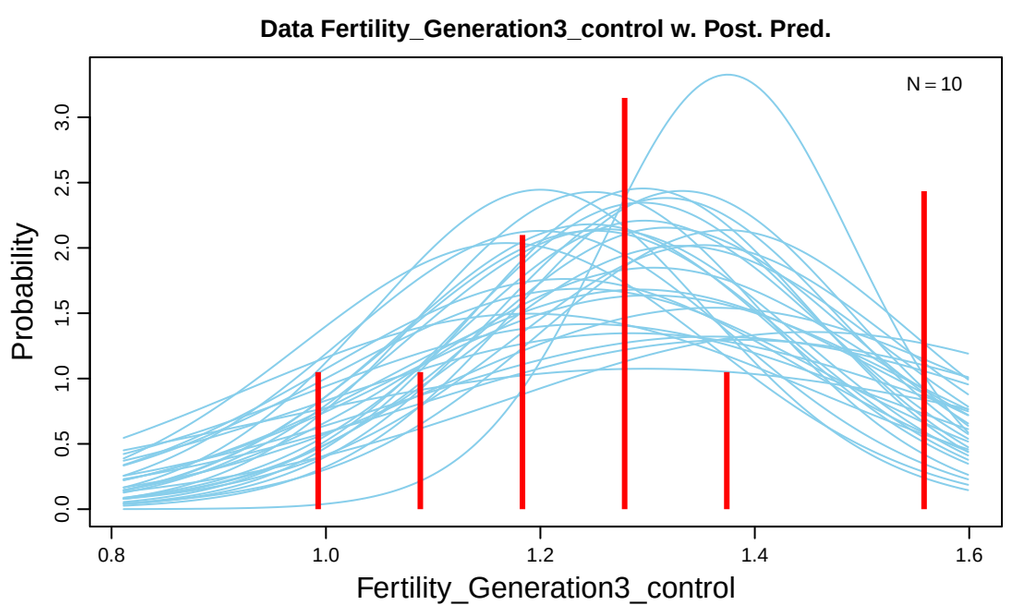
Data Fertility_Generation3_control w. Post. Pred.
N = 10
Probability
0.0
0.5
1.0
1.5
2.0
2.5
3.0
0.8
1.0
1.2
1.4
1.6
Fertility_Generation3_control

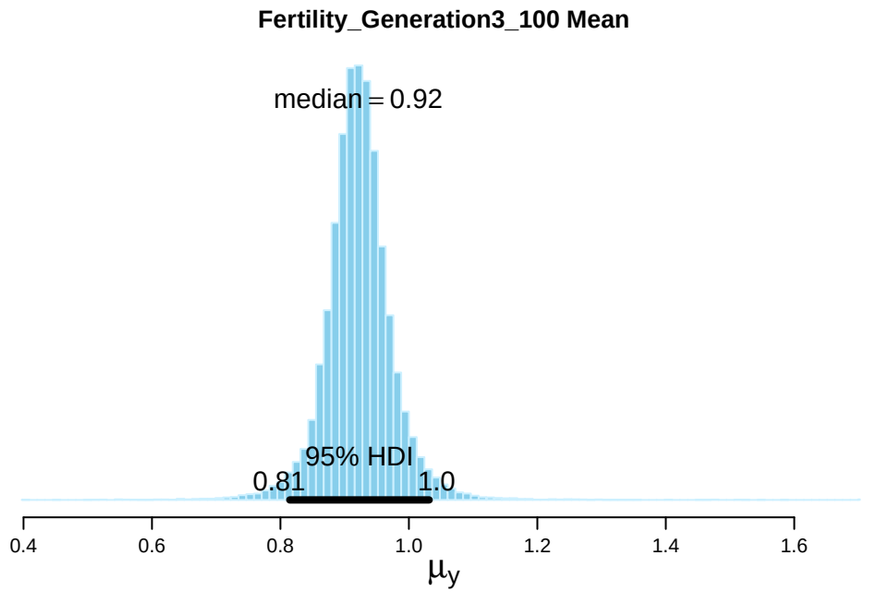
Fertility_Generation3_100 Mean
median = 0.92
95% HDI
0.81
1.0
0.4
0.6
0.8
1.0
1.2
1.4
1.6
μy

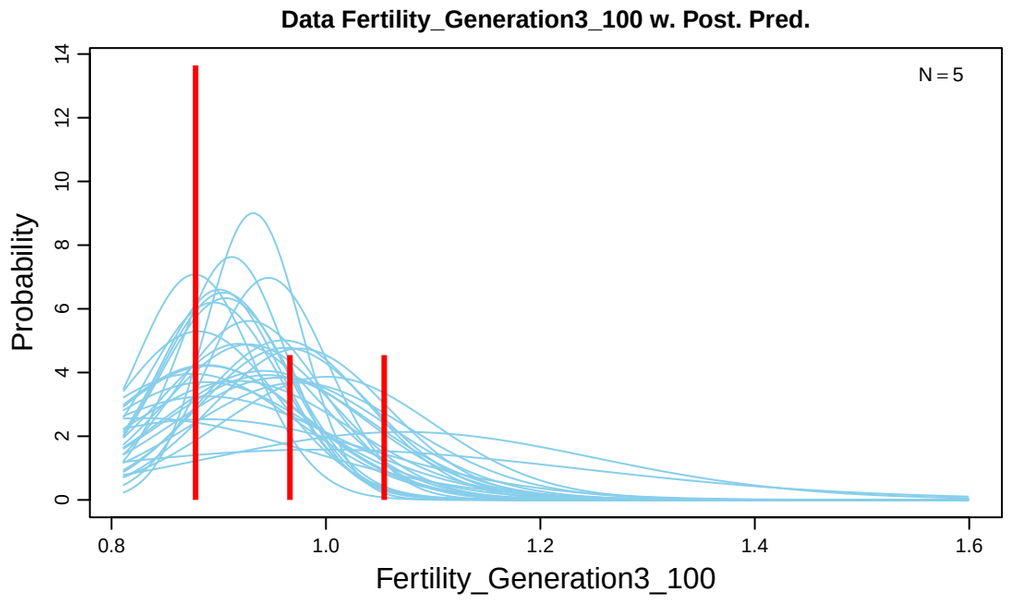
Data Fertility_Generation3_100 w. Post. Pred.
N = 5
Probability
0
2
4
6
8
10
12
14
0.8
1.0
1.2
1.4
1.6
Fertility_Generation3_100

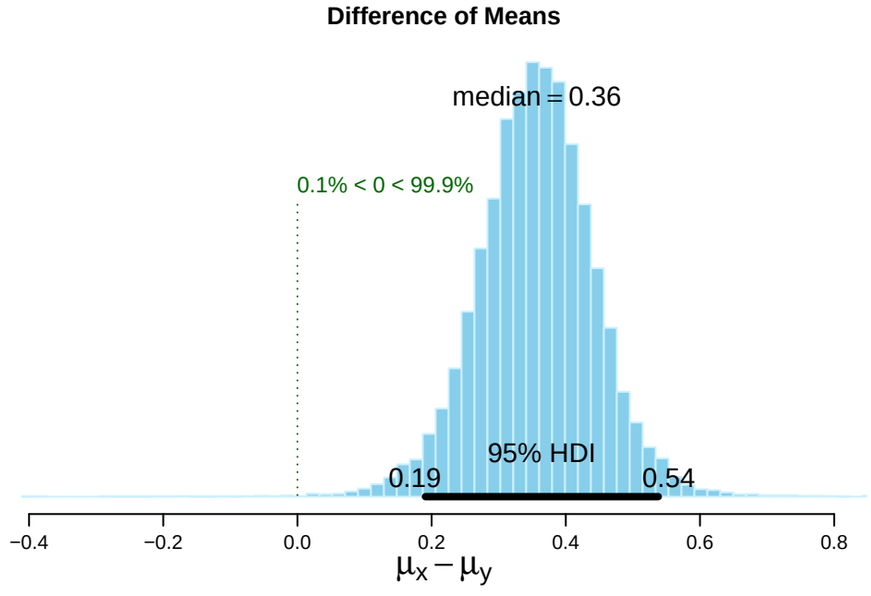
Difference of Means
median = 0.36
0.1% < 0 < 99.9%
95% HDI
0.19
0.54
−0.4
−0.2
0.0
0.2
0.4
0.6
0.8
μx − μy

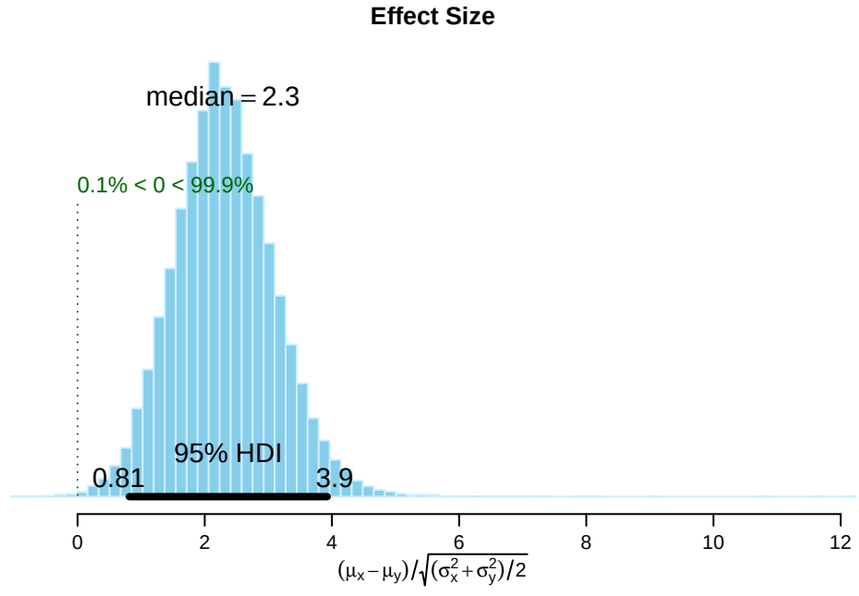
Effect Size
median = 2.3
0.1% < 0 < 99.9%
95% HDI
0.81
3.9
0
2
4
6
8
10
12
(μx − μy)/√((σx² + σy²)/2)

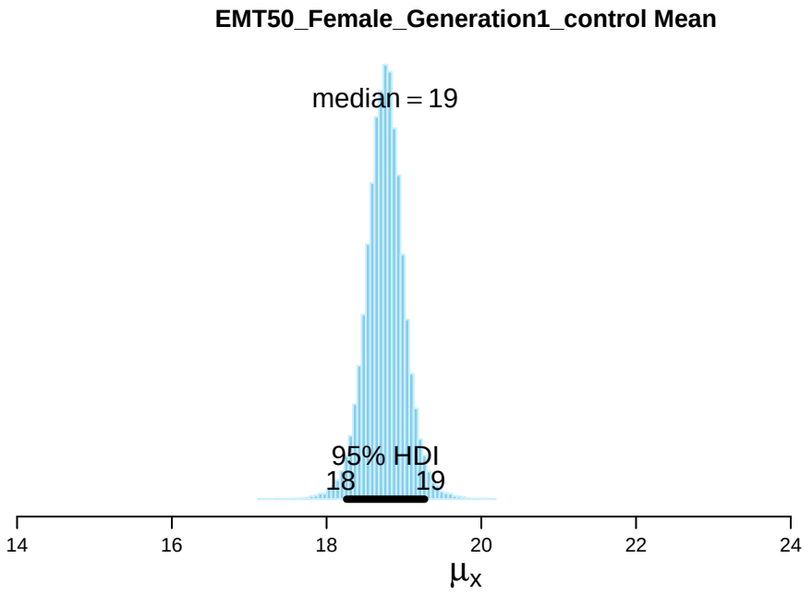
EMT50_Female_Generation1_control Mean
median = 19
95% HDI
18
19
14
16
18
20
22
24
μ_x

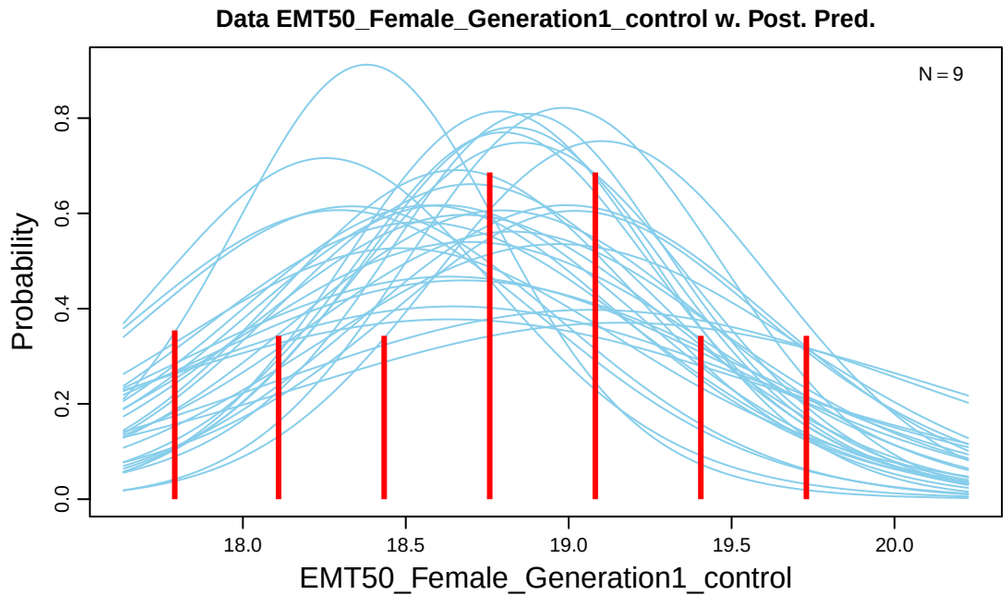
Data EMT50_Female_Generation1_control w. Post. Pred.
N = 9
Probability
0.0
0.2
0.4
0.6
0.8
18.0
18.5
19.0
19.5
20.0
EMT50_Female_Generation1_control

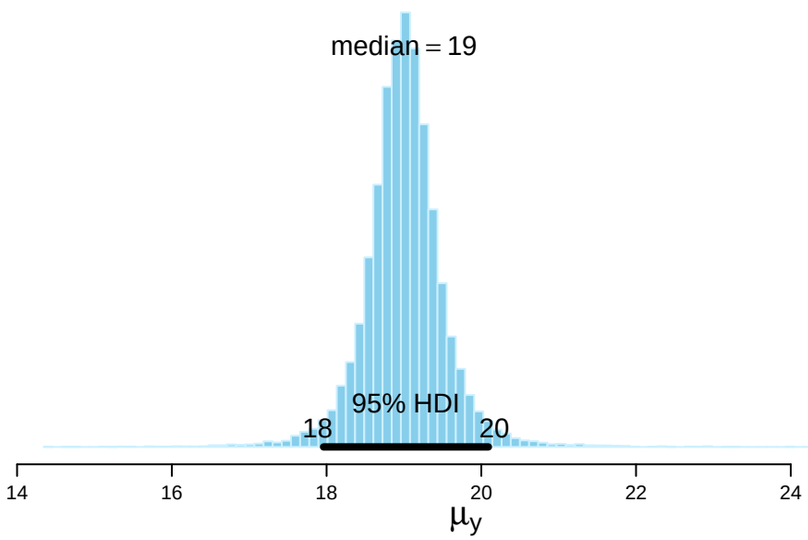
EMT50_Female_Generation1_100 Mean
median = 19
95% HDI
18
20
14
16
18
20
22
24
μ_y

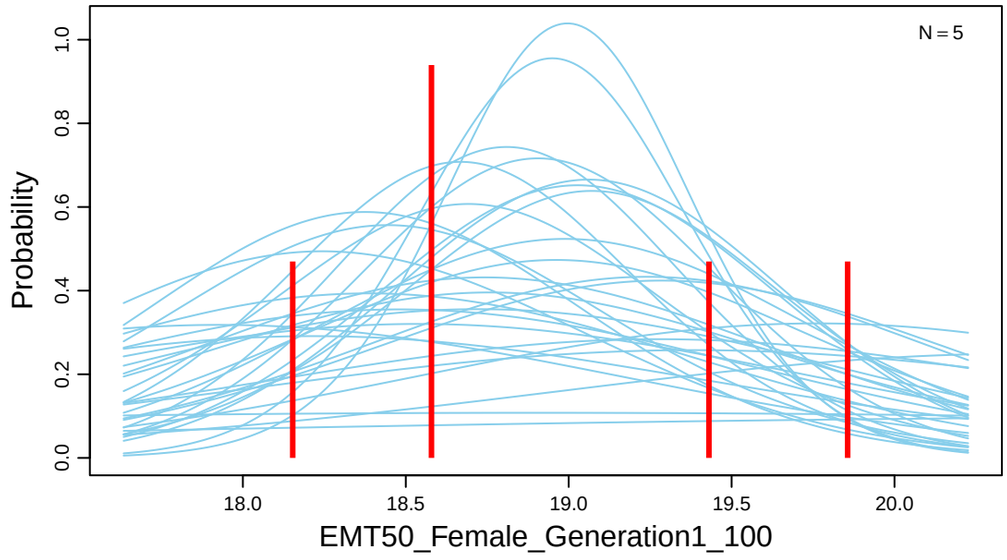
Data EMT50_Female_Generation1_100 w. Post. Pred.
N = 5
Probability
0.0
0.2
0.4
0.6
0.8
1.0
18.0
18.5
19.0
19.5
20.0
EMT50_Female_Generation1_100

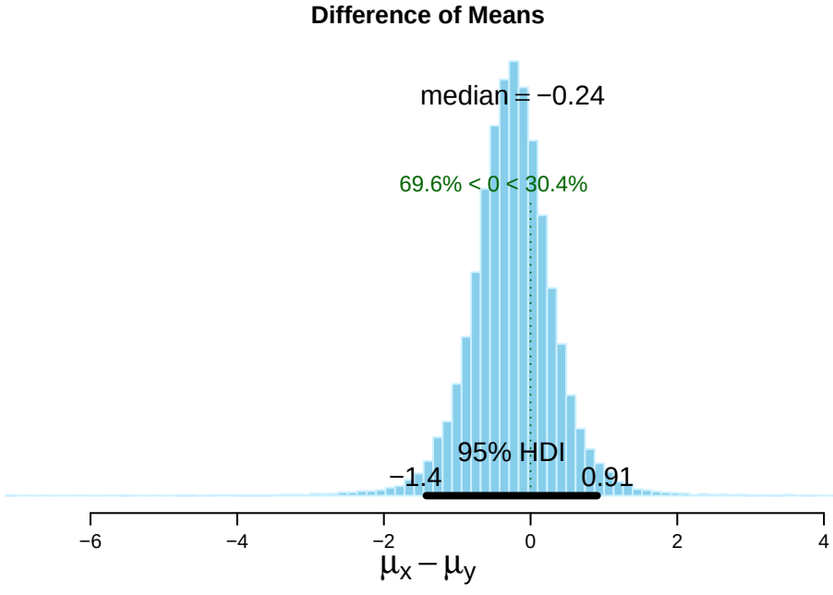
Difference of Means
median = −0.24
69.6% < 0 < 30.4%
95% HDI
−1.4
0.91
−6
−4
−2
0
2
4
$\mu_x - \mu_y$

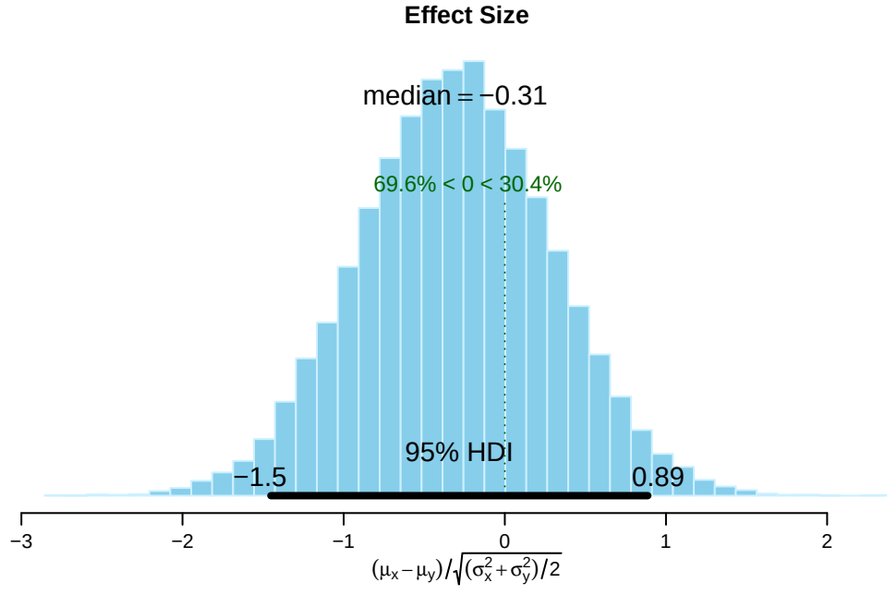
Effect Size
median = −0.31
69.6% < 0 < 30.4%
95% HDI
−1.5
0.89
−3
−2
−1
0
1
2
$(\mu_x - \mu_y)/\sqrt{(\sigma_x^2 + \sigma_y^2)/2}$

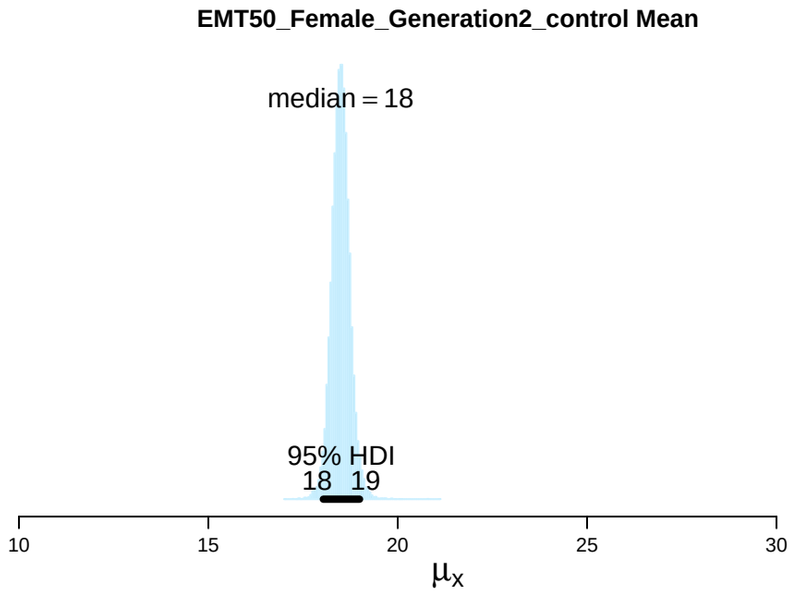
EMT50_Female_Generation2_control Mean
median = 18
95% HDI
18 19
10
15
20
25
30
μx

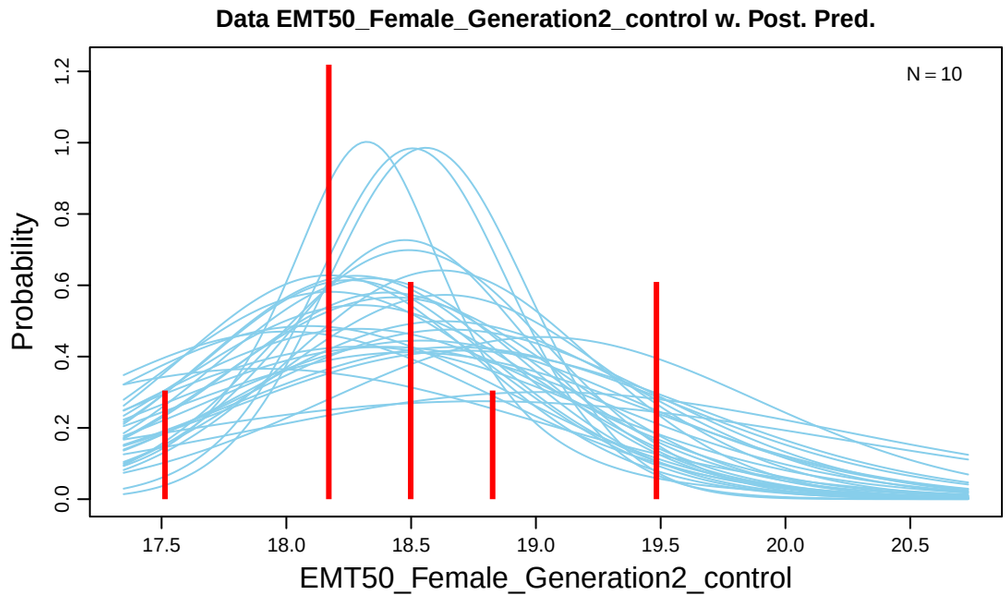
Data EMT50_Female_Generation2_control w. Post. Pred.
N = 10
Probability
0.0
0.2
0.4
0.6
0.8
1.0
1.2
17.5
18.0
18.5
19.0
19.5
20.0
20.5
EMT50_Female_Generation2_control

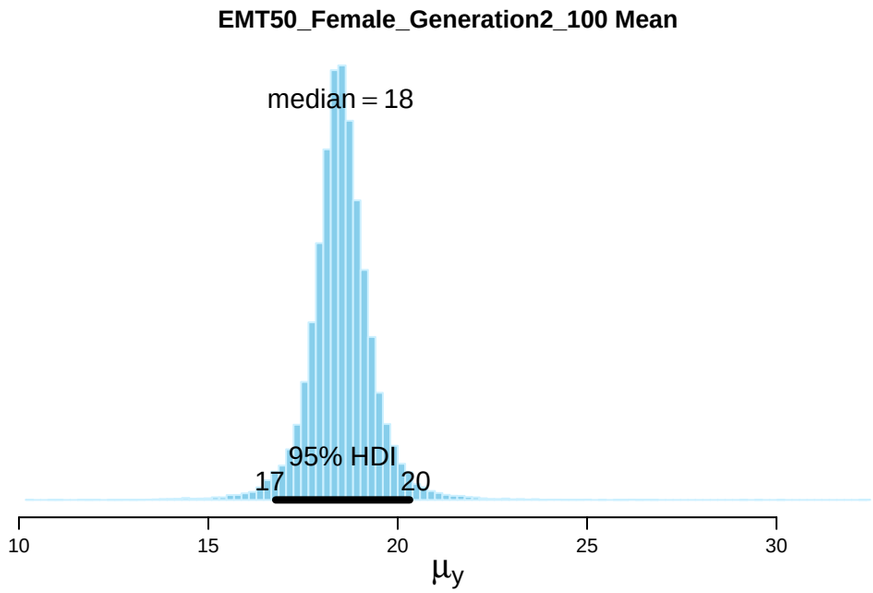
EMT50_Female_Generation2_100 Mean
median = 18
95% HDI
17 20
10
15
20
25
30
μy

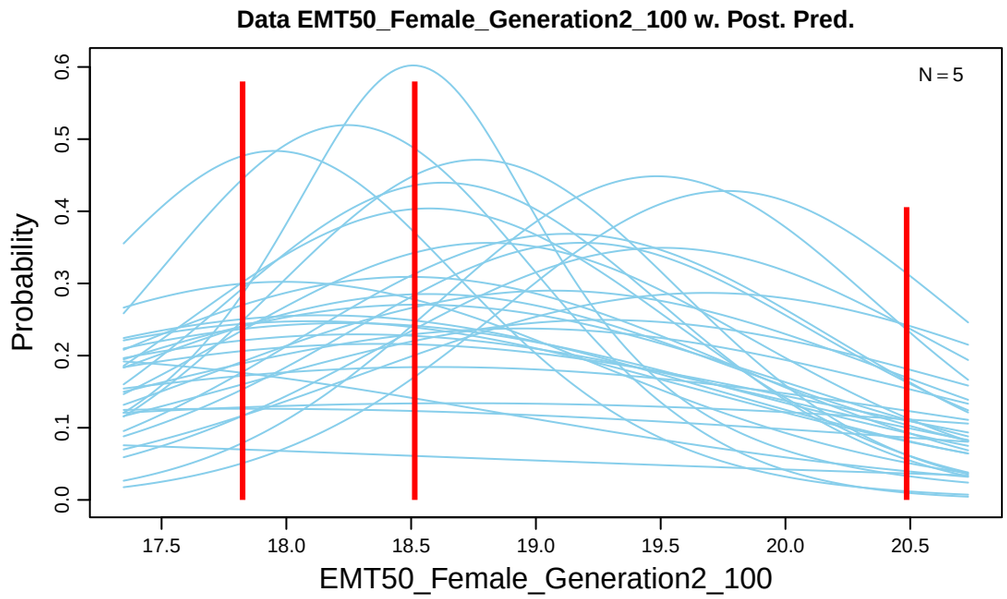
Data EMT50_Female_Generation2_100 w. Post. Pred.
N = 5
Probability
0.0
0.1
0.2
0.3
0.4
0.5
0.6
17.5
18.0
18.5
19.0
19.5
20.0
20.5
EMT50_Female_Generation2_100

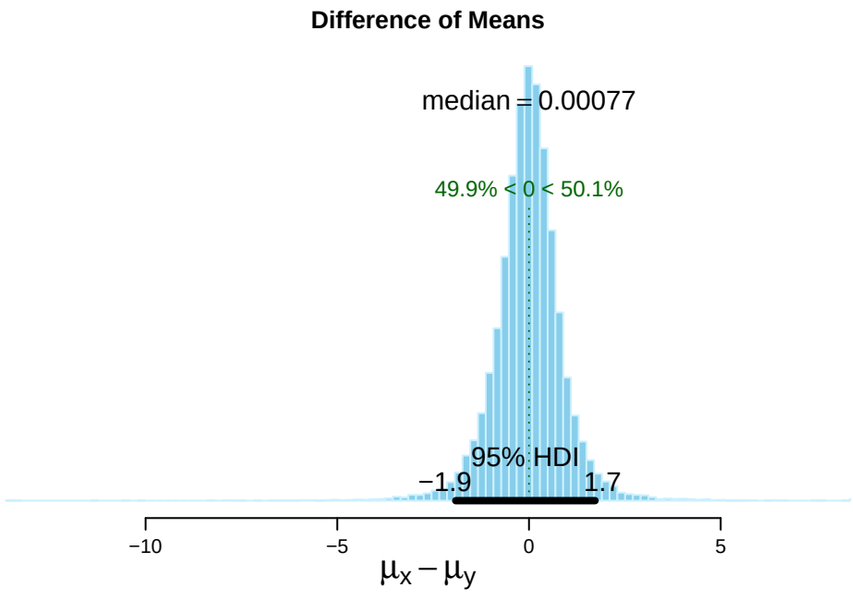
Difference of Means
median = 0.00077
49.9% < 0 < 50.1%
95% HDI
−1.9 1.7
−10
−5
0
5
μx − μy

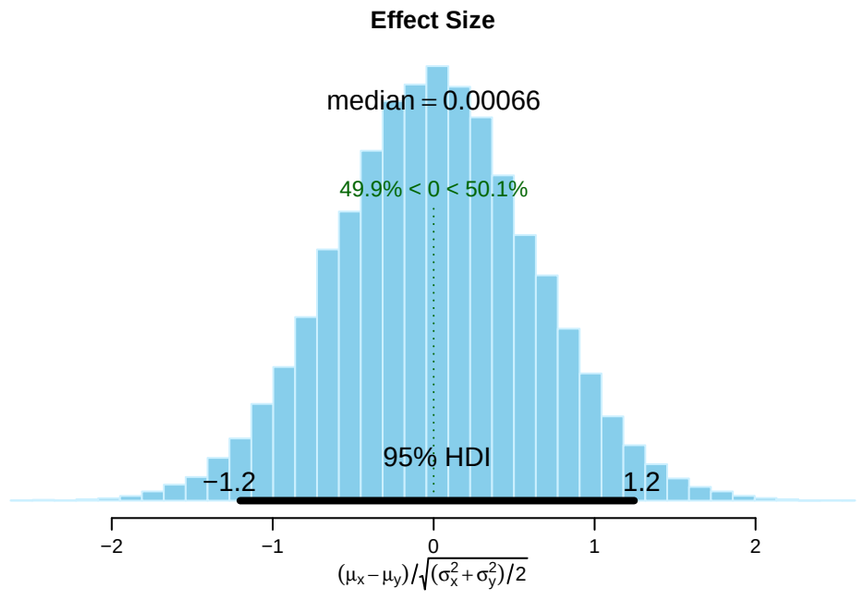
Effect Size
median = 0.00066
49.9% < 0 < 50.1%
95% HDI
−1.2 1.2
−2
−1
0
1
2
(μx − μy)/√((σx² + σy²)/2

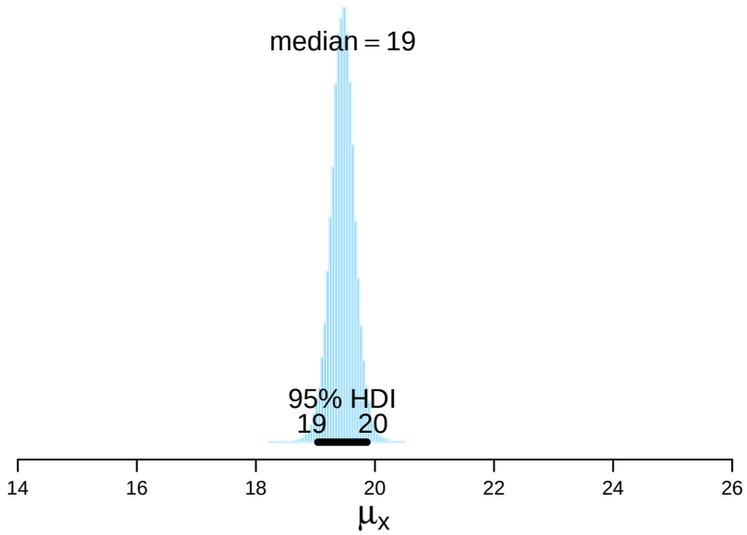
EMT50_Female_Generation3_control Mean
median = 19
95% HDI
19 20
14 16 18 20 22 24 26
μ_x

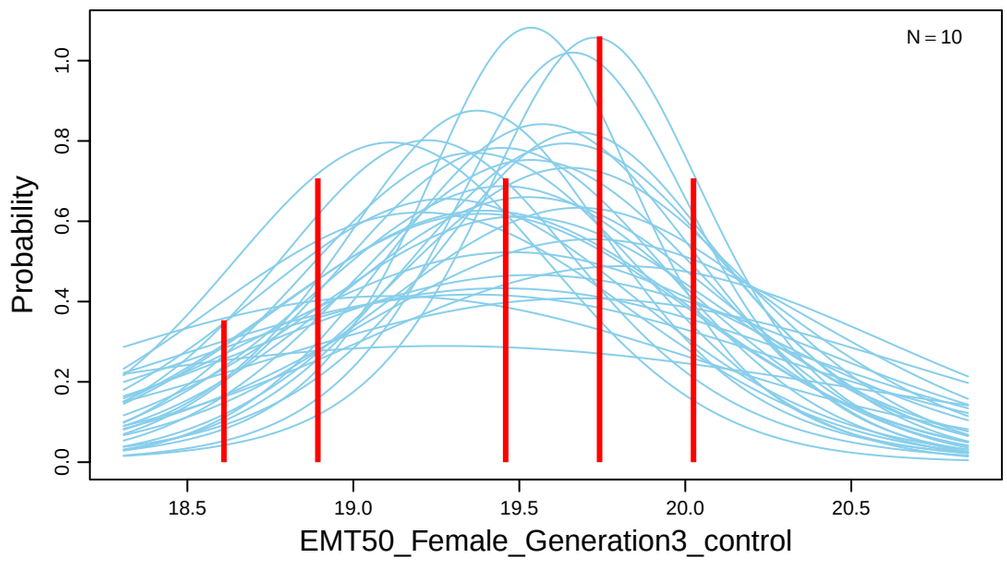
Data EMT50_Female_Generation3_control w. Post. Pred.
N = 10
Probability
0.0 0.2 0.4 0.6 0.8 1.0
18.5 19.0 19.5 20.0 20.5
EMT50_Female_Generation3_control

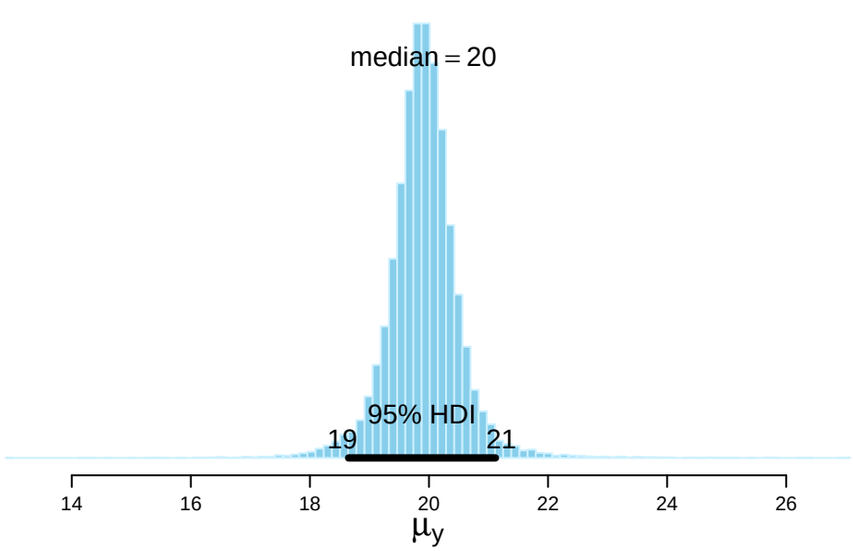
EMT50_Female_Generation3_100 Mean
median = 20
95% HDI
19 21
14 16 18 20 22 24 26
μ_y

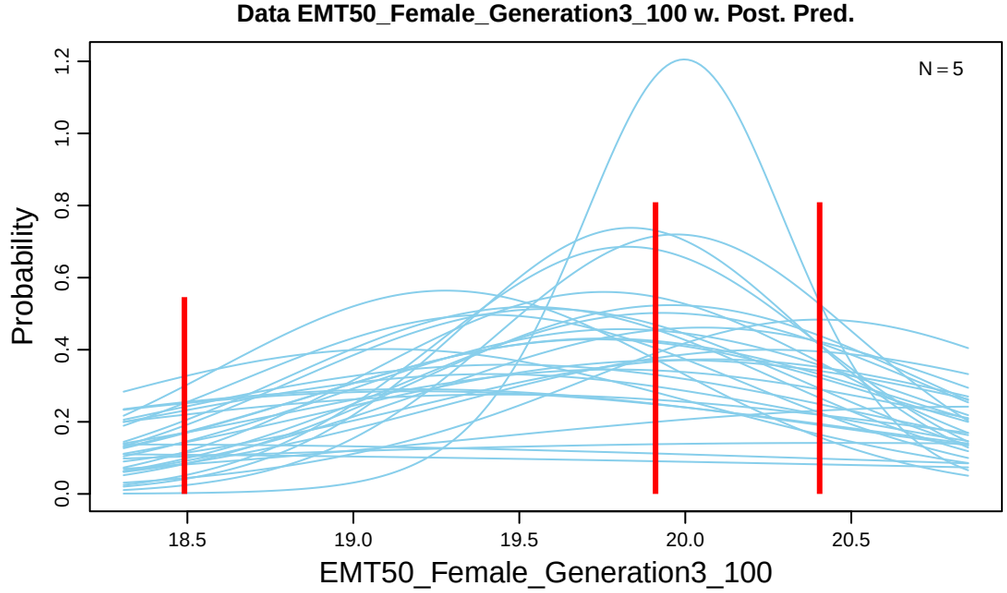
Data EMT50_Female_Generation3_100 w. Post. Pred.
N = 5
Probability
0.0 0.2 0.4 0.6 0.8 1.0 1.2
18.5 19.0 19.5 20.0 20.5
EMT50_Female_Generation3_100

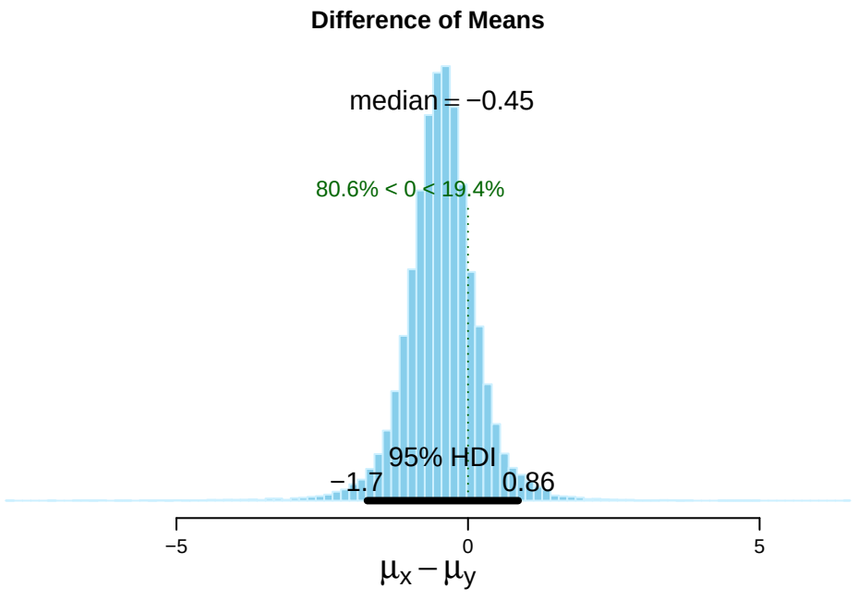
Difference of Means
median = −0.45
80.6% < 0 < 19.4%
95% HDI
−1.7 0.86
−5 0 5
$\mu_x - \mu_y$

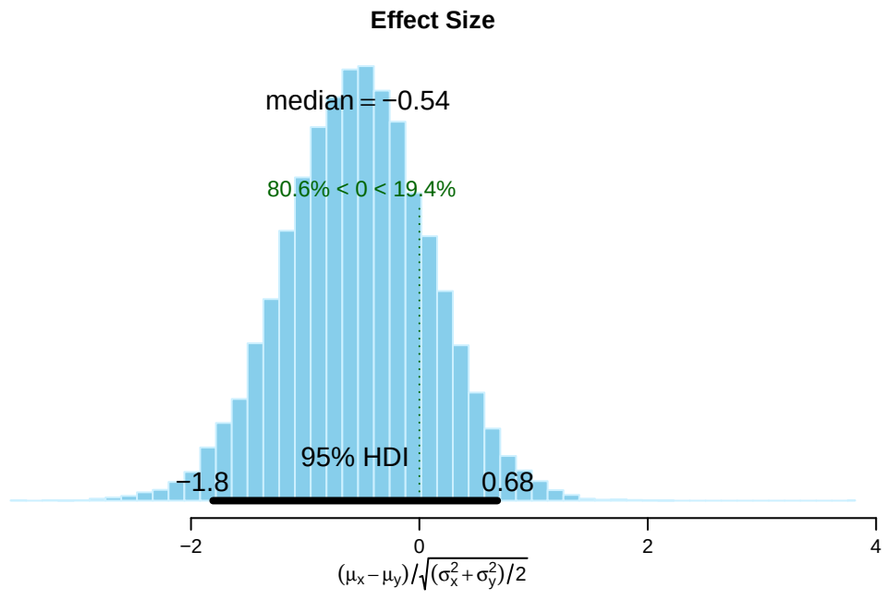
Effect Size
median = −0.54
80.6% < 0 < 19.4%
95% HDI
−1.8 0.68
−2 0 2 4
$(\mu_x - \mu_y)/\sqrt{(\sigma_x^2 + \sigma_y^2)/2}$

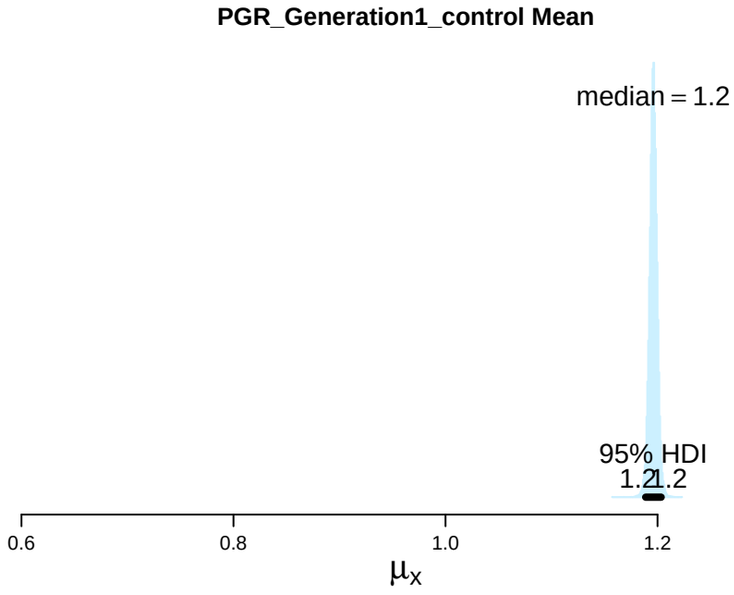
PGR_Generation1_control Mean
median = 1.2
95% HDI
1.2 1.2
0.6
0.8
1.0
1.2
μ_x

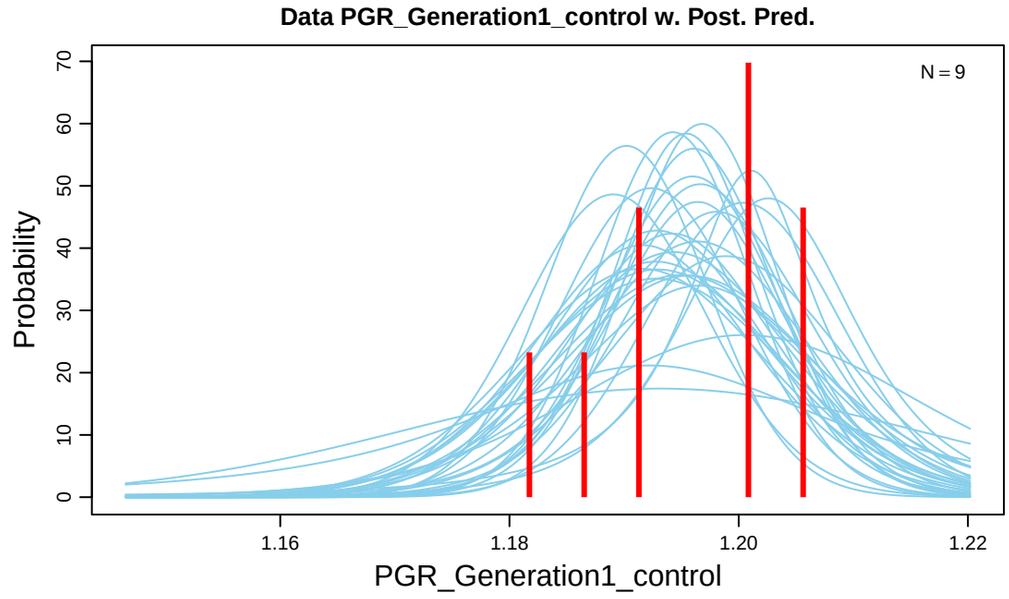
Data PGR_Generation1_control w. Post. Pred.
N = 9
Probability
0
10
20
30
40
50
60
70
1.16
1.18
1.20
1.22
PGR_Generation1_control

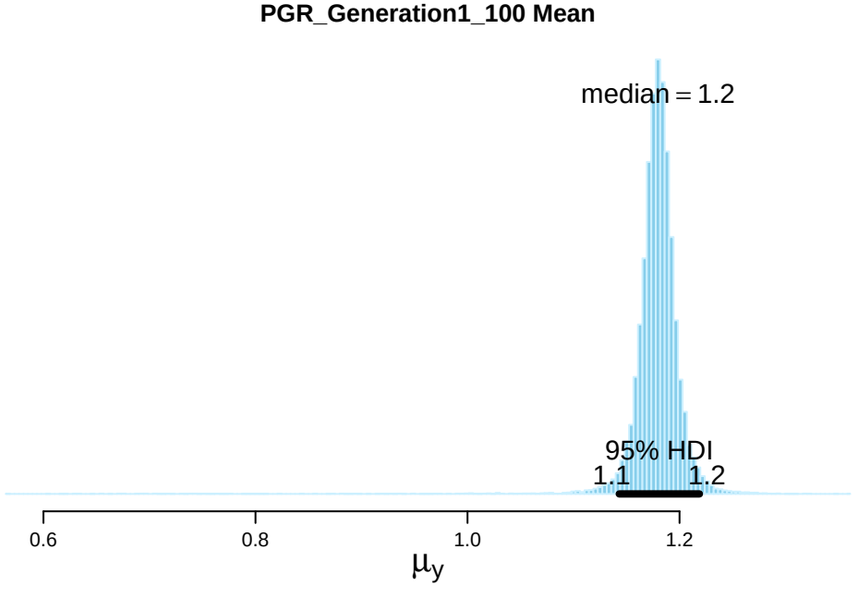
PGR_Generation1_100 Mean
median = 1.2
95% HDI
1.1 1.2
0.6
0.8
1.0
1.2
μ_y

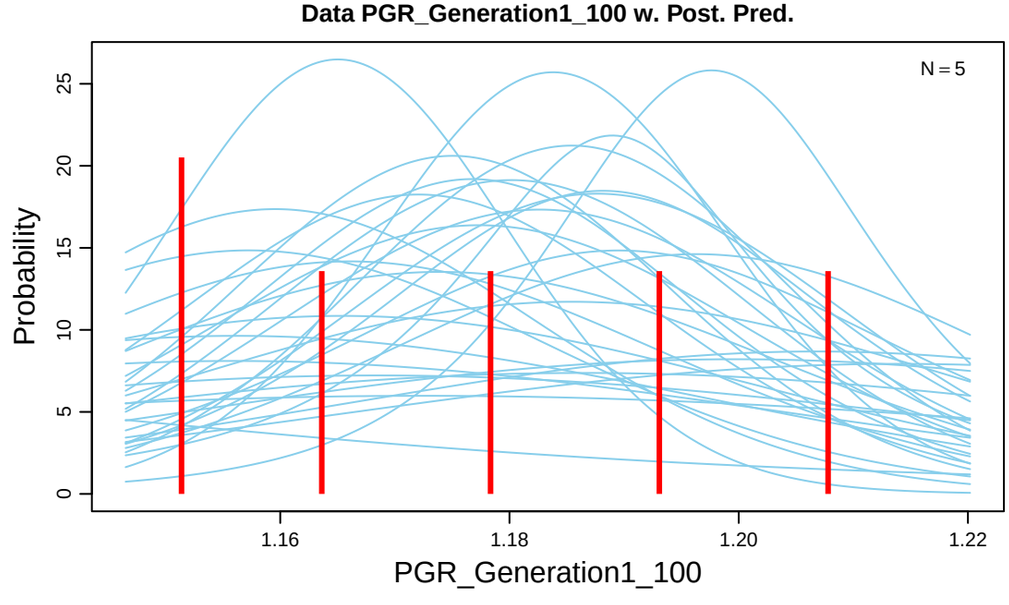
Data PGR_Generation1_100 w. Post. Pred.
N = 5
Probability
0
5
10
15
20
25
1.16
1.18
1.20
1.22
PGR_Generation1_100

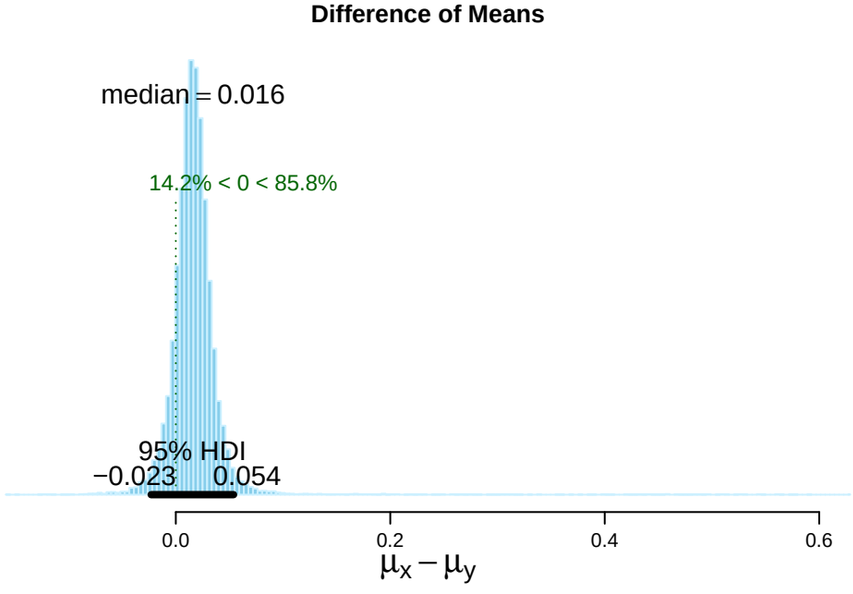
Difference of Means
median = 0.016
14.2% < 0 < 85.8%
95% HDI
−0.023 0.054
0.0
0.2
0.4
0.6
$\mu_x - \mu_y$

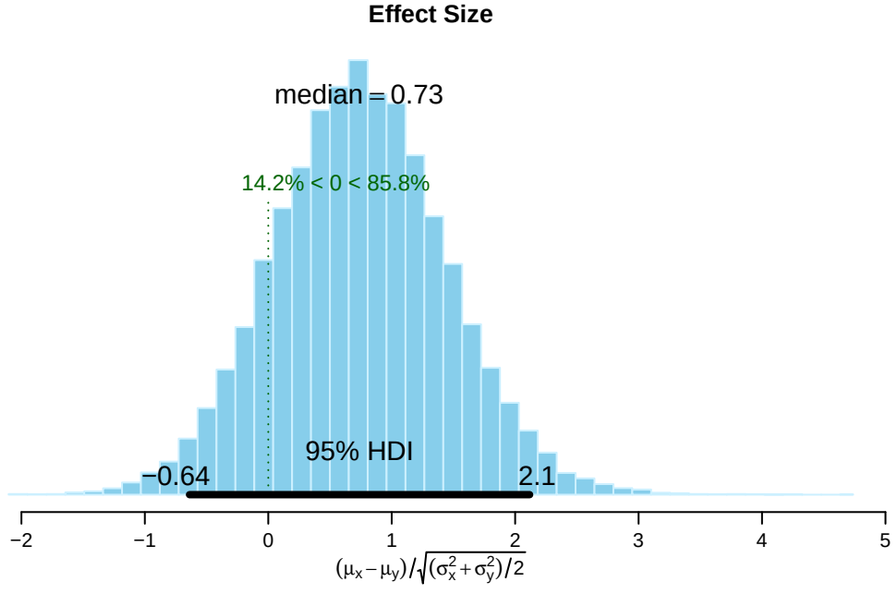
Effect Size
median = 0.73
14.2% < 0 < 85.8%
95% HDI
−0.64 2.1
−2
−1
0
1
2
3
4
5
$(\mu_x - \mu_y)/\sqrt{(\sigma_x^2 + \sigma_y^2)/2}$

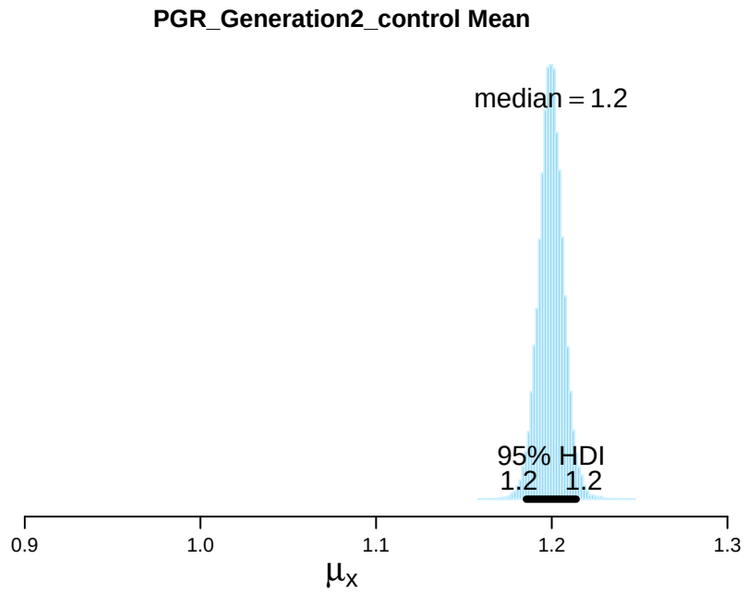
PGR_Generation2_control Mean
median = 1.2
95% HDI
1.2 1.2
0.9
1.0
1.1
1.2
1.3
μ_x

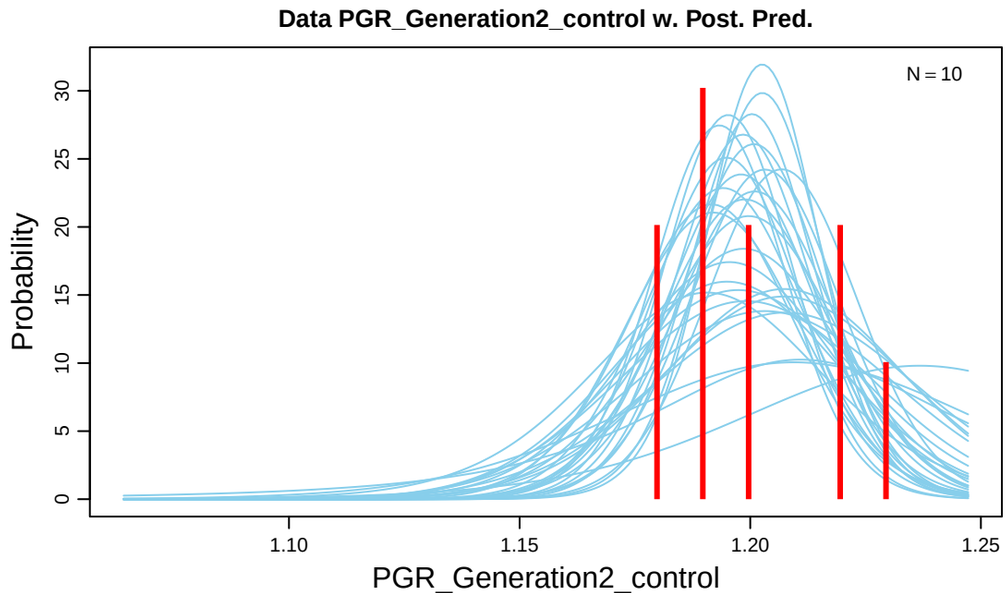
Data PGR_Generation2_control w. Post. Pred.
N = 10
Probability
0
5
10
15
20
25
30
1.10
1.15
1.20
1.25
PGR_Generation2_control

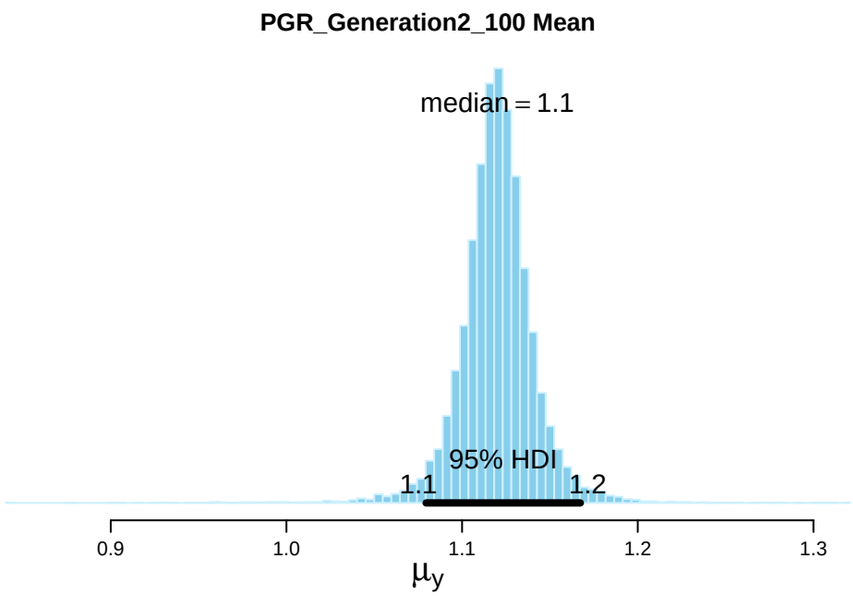
PGR_Generation2_100 Mean
median = 1.1
95% HDI
1.1 1.2
0.9
1.0
1.1
1.2
1.3
μ_y

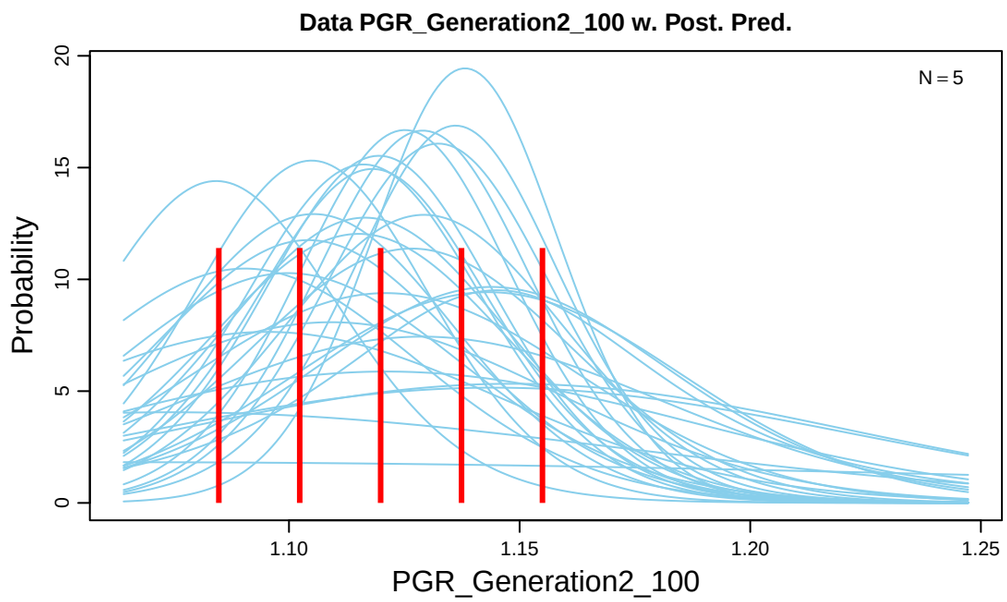
Data PGR_Generation2_100 w. Post. Pred.
N = 5
Probability
0
5
10
15
20
1.10
1.15
1.20
1.25
PGR_Generation2_100

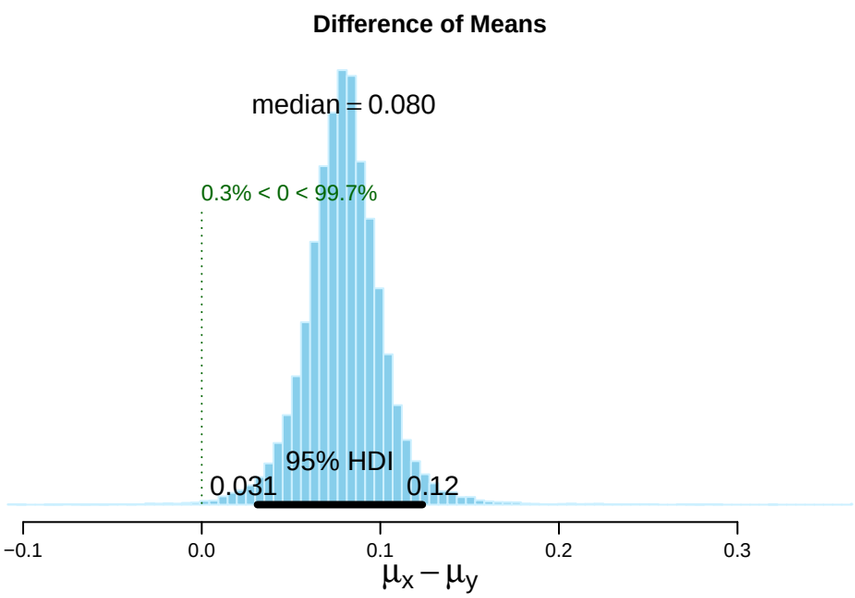
Difference of Means
median = 0.080
0.3% < 0 < 99.7%
95% HDI
0.031 0.12
−0.1
0.0
0.1
0.2
0.3
$\mu_x - \mu_y$

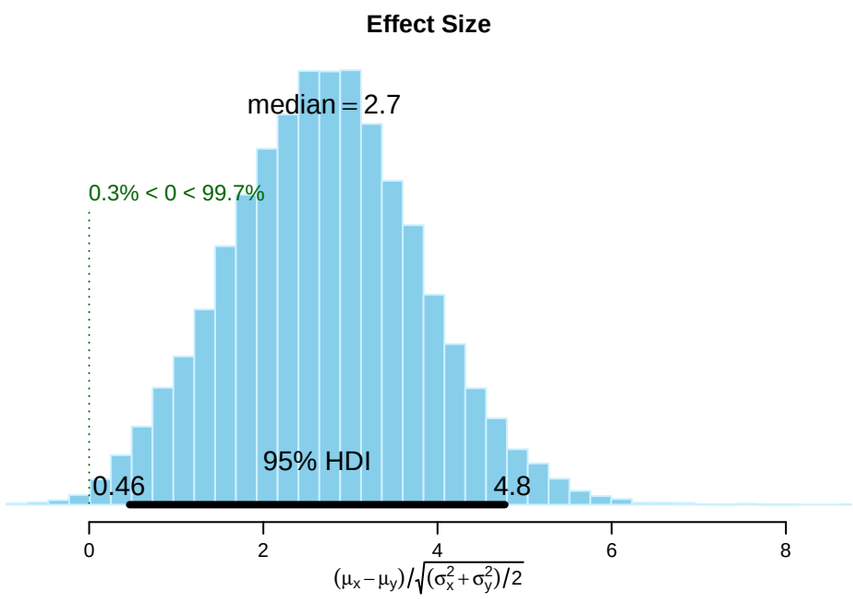
Effect Size
median = 2.7
0.3% < 0 < 99.7%
95% HDI
0.46 4.8
0
2
4
6
8
$(\mu_x - \mu_y)/\sqrt{(\sigma_x^2 + \sigma_y^2)/2}$

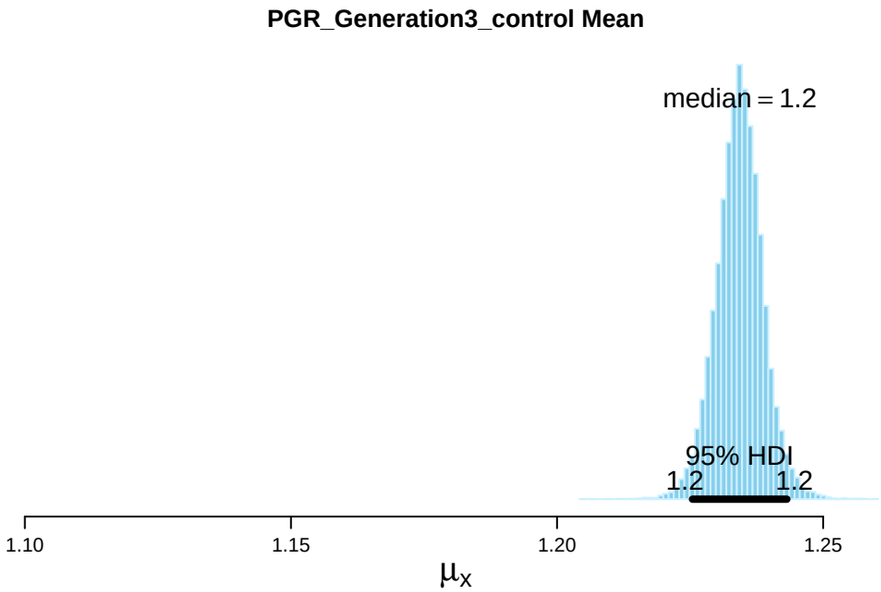
PGR_Generation3_control Mean
median = 1.2
95% HDI
1.2
1.2
1.10
1.15
1.20
1.25
μx

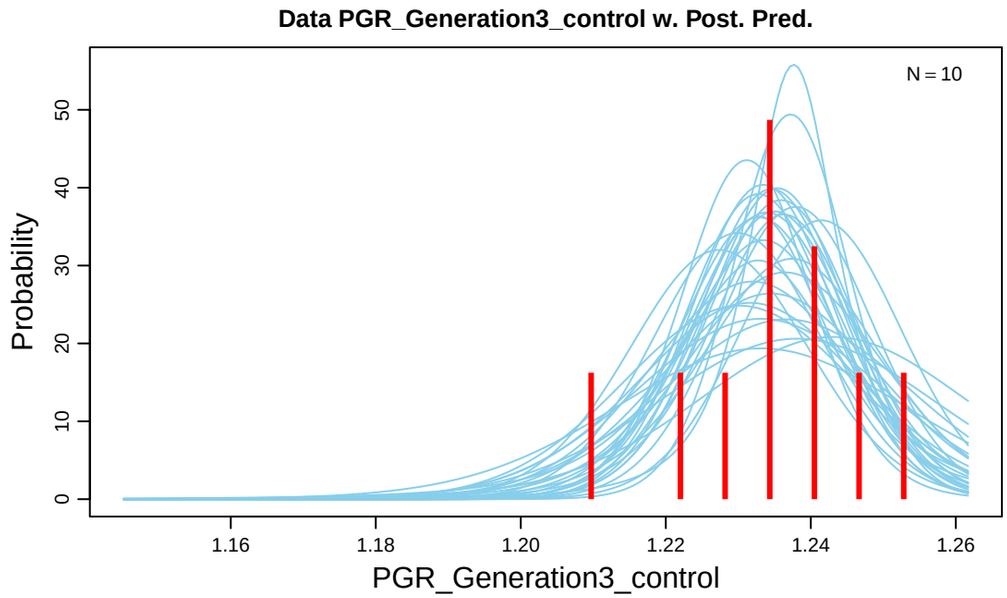
Data PGR_Generation3_control w. Post. Pred.
N = 10
Probability
0
10
20
30
40
50
1.16
1.18
1.20
1.22
1.24
1.26
PGR_Generation3_control

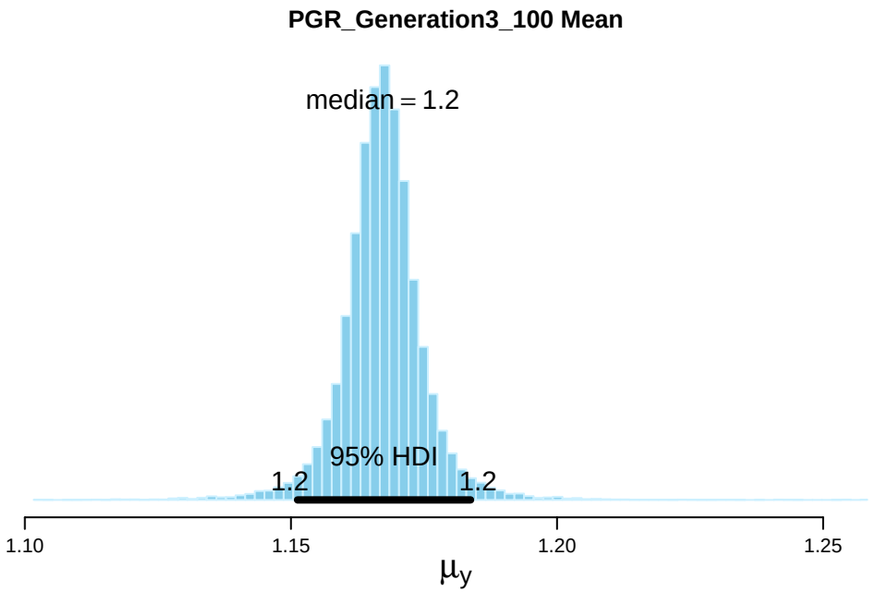
PGR_Generation3_100 Mean
median = 1.2
95% HDI
1.2
1.2
1.10
1.15
1.20
1.25
μy

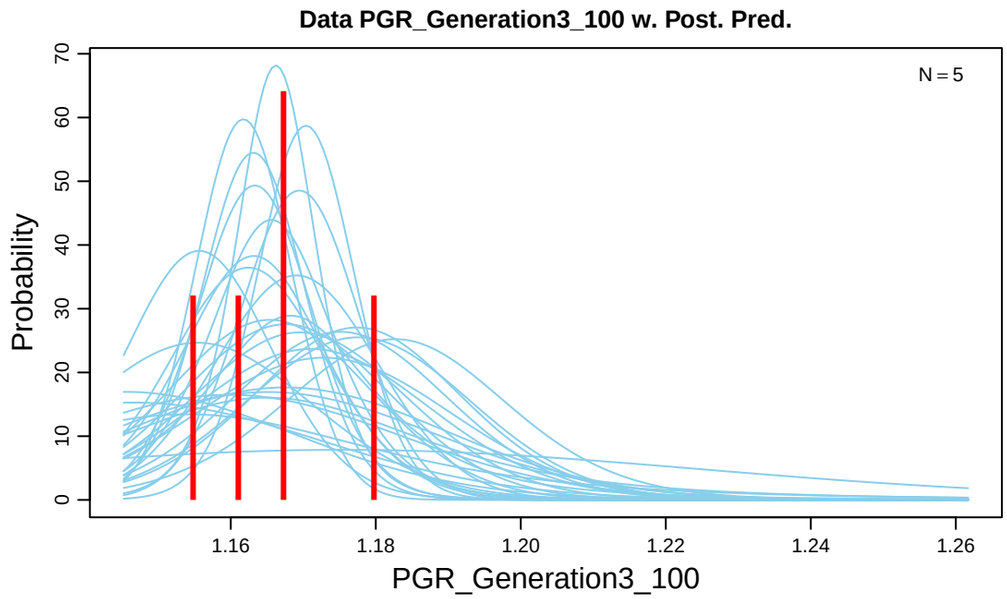
Data PGR_Generation3_100 w. Post. Pred.
N = 5
Probability
0
10
20
30
40
50
60
70
1.16
1.18
1.20
1.22
1.24
1.26
PGR_Generation3_100

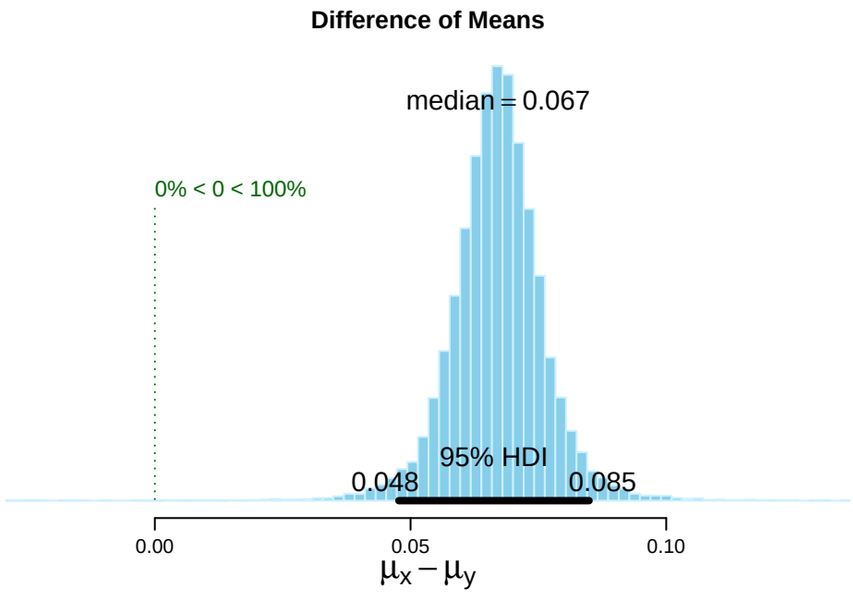
Difference of Means
median = 0.067
0% < 0 < 100%
95% HDI
0.048
0.085
0.00
0.05
0.10
μx − μy

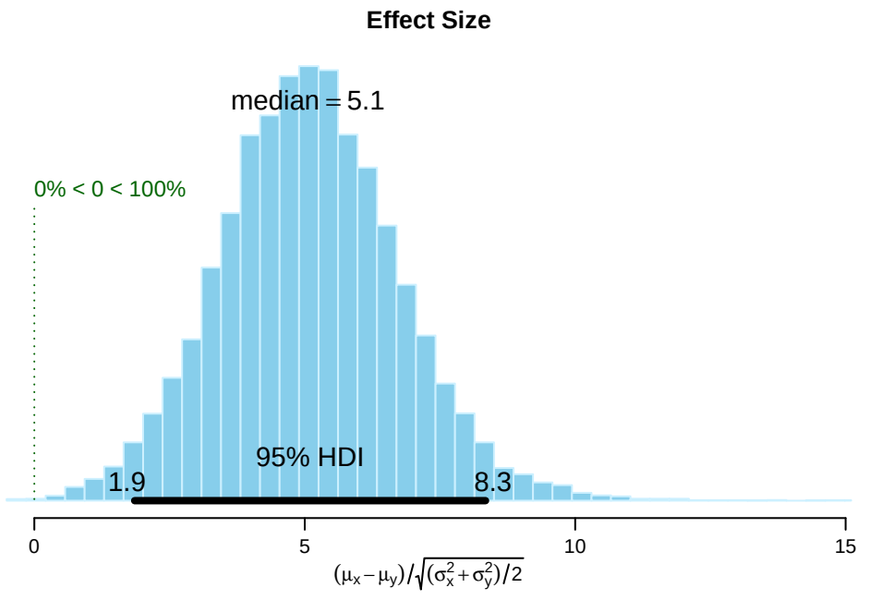
Effect Size
median = 5.1
0% < 0 < 100%
95% HDI
1.9
8.3
0
5
10
15
(μx − μy)/√((σx² + σy²)/2

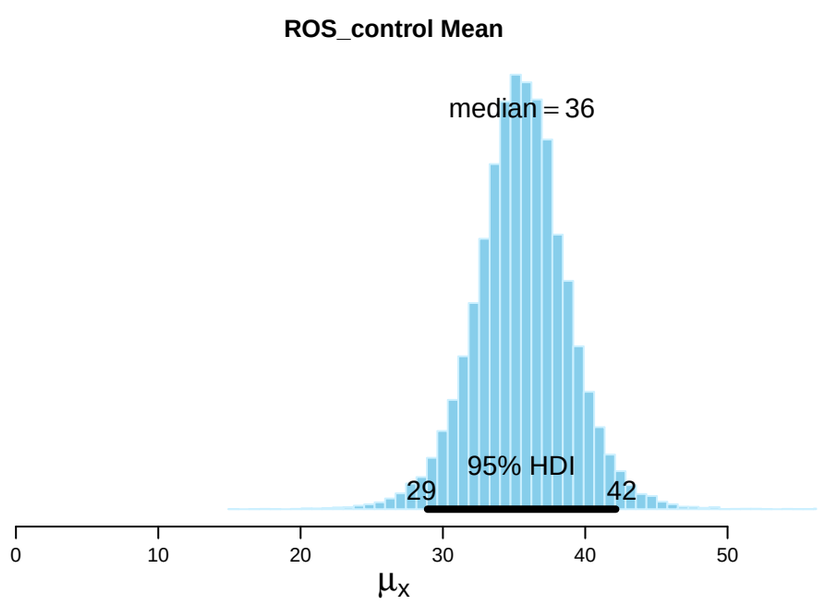
ROS_control Mean
median = 36
95% HDI
29
42
0
10
20
30
40
50
μ_x

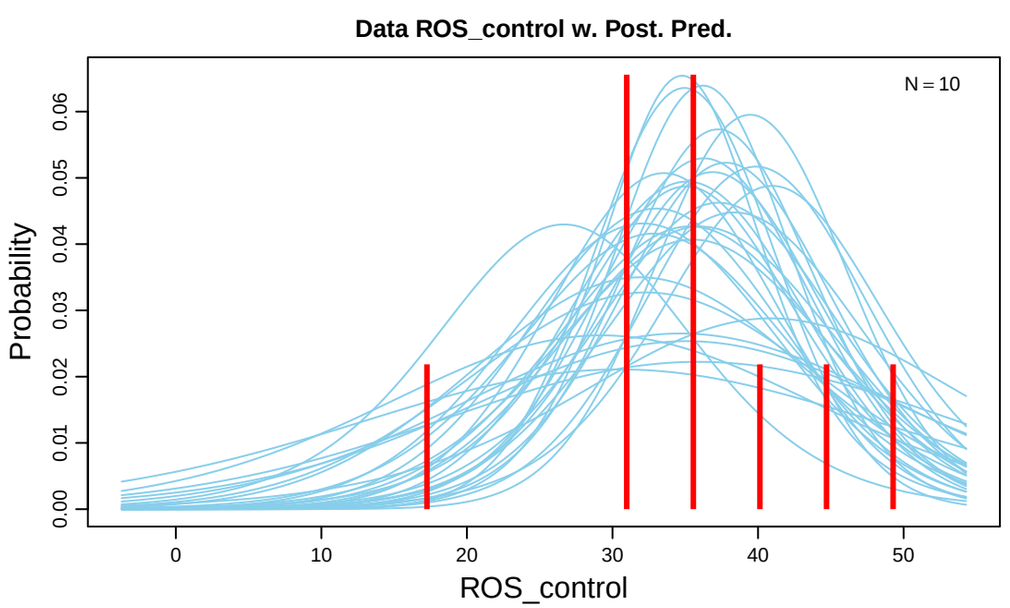
Data ROS_control w. Post. Pred.
N = 10
Probability
0.00
0.01
0.02
0.03
0.04
0.05
0.06
0
10
20
30
40
50
ROS_control

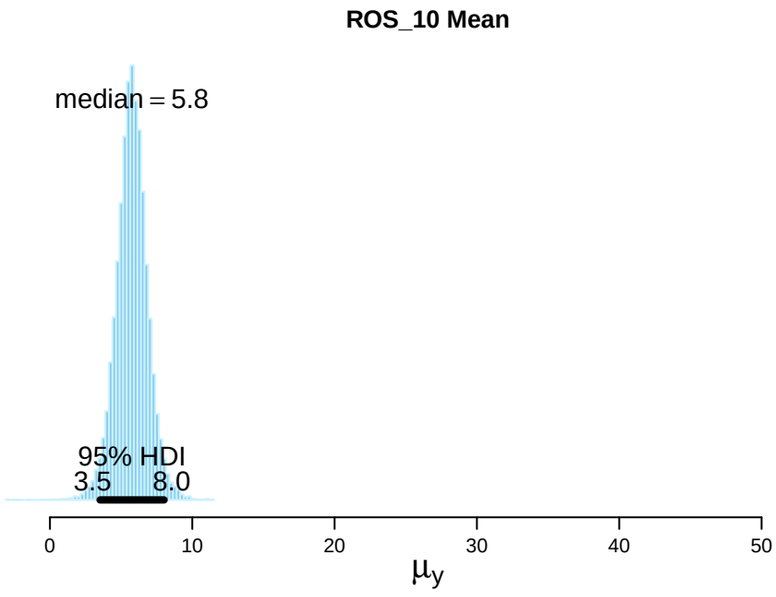
ROS_10 Mean
median = 5.8
95% HDI
3.5
8.0
0
10
20
30
40
50
μ_y

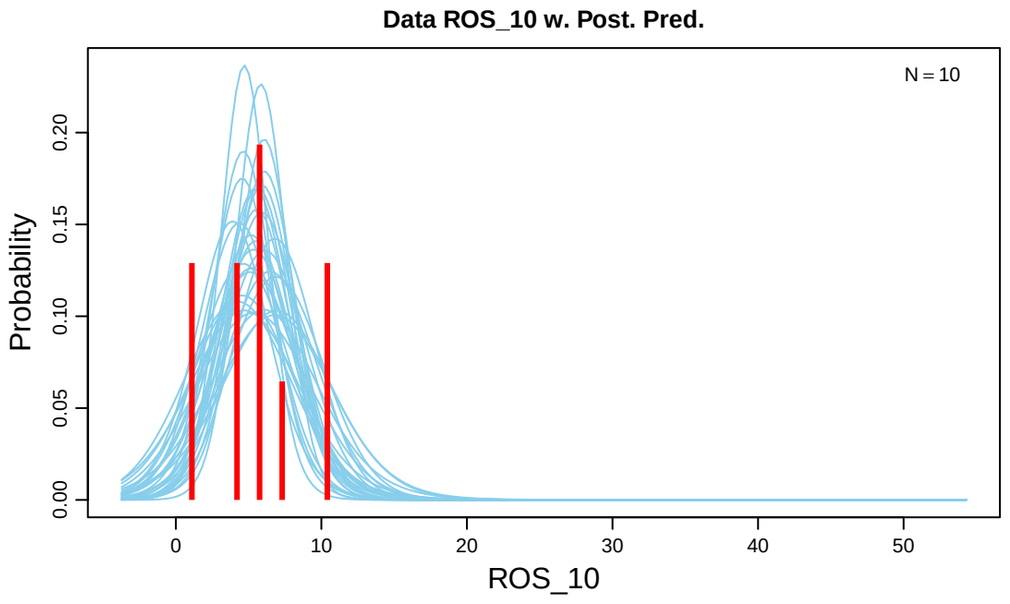
Data ROS_10 w. Post. Pred.
N = 10
Probability
0.00
0.05
0.10
0.15
0.20
0
10
20
30
40
50
ROS_10

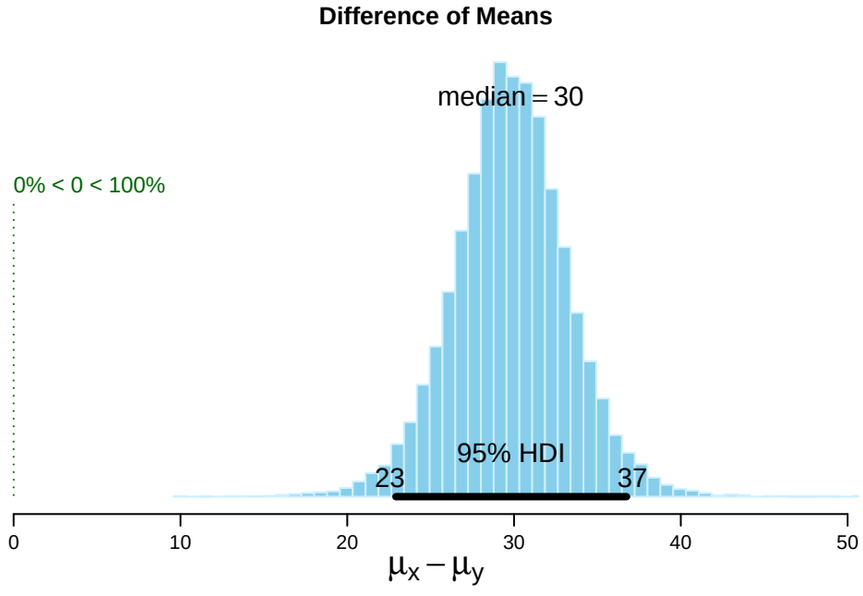
Difference of Means
median = 30
0% < 0 < 100%
95% HDI
23
37
0
10
20
30
40
50
$\mu_x - \mu_y$

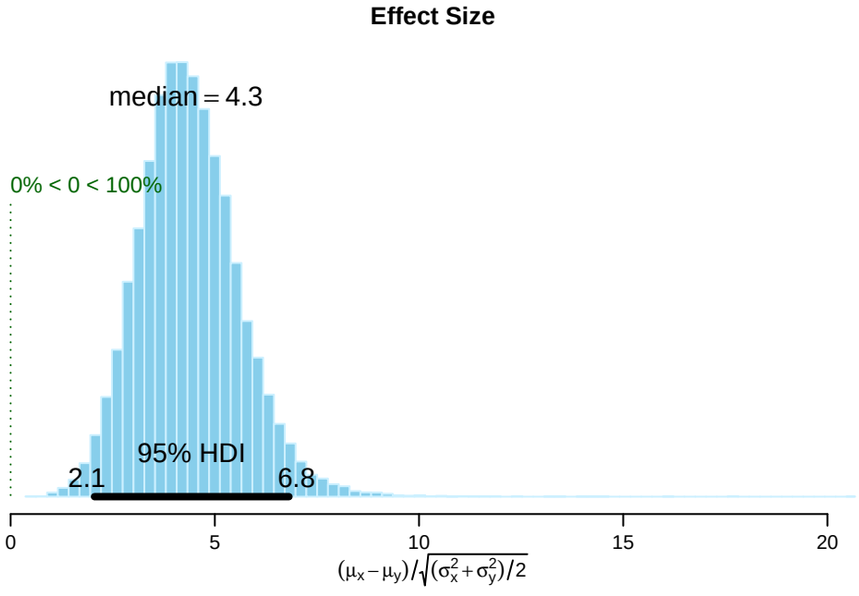
Effect Size
median = 4.3
0% < 0 < 100%
95% HDI
2.1
6.8
0
5
10
15
20
$(\mu_x - \mu_y)/\sqrt{(\sigma_x^2 + \sigma_y^2)/2}$

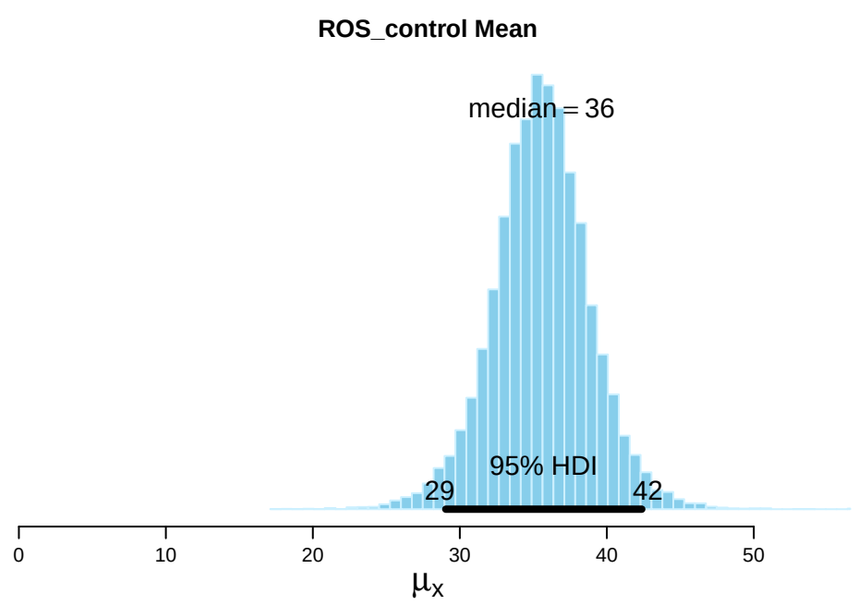
ROS_control Mean
median = 36
95% HDI
29
42
0
10
20
30
40
50
μ_x

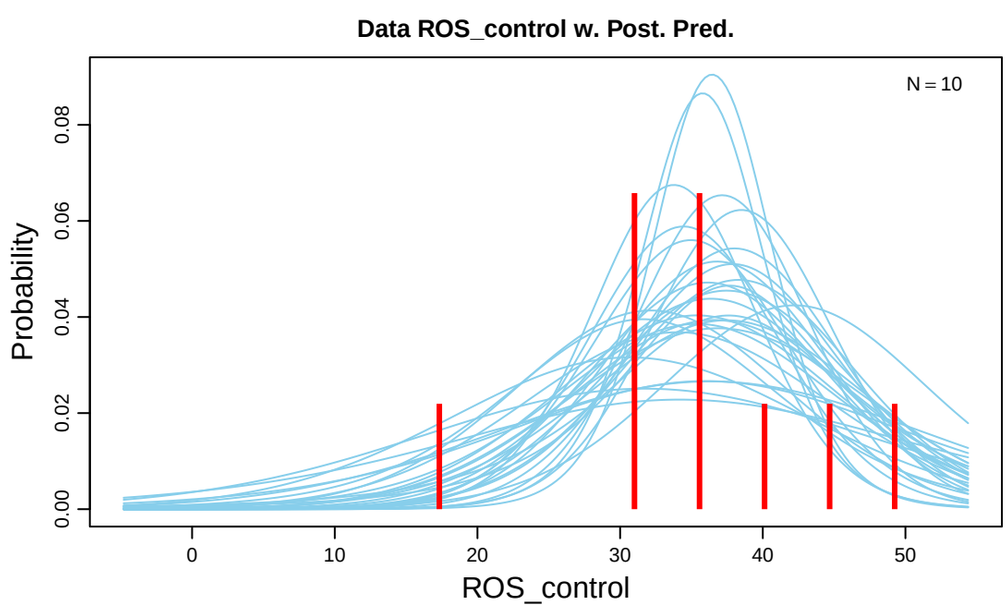
Data ROS_control w. Post. Pred.
N = 10
Probability
0.00
0.02
0.04
0.06
0.08
0
10
20
30
40
50
ROS_control

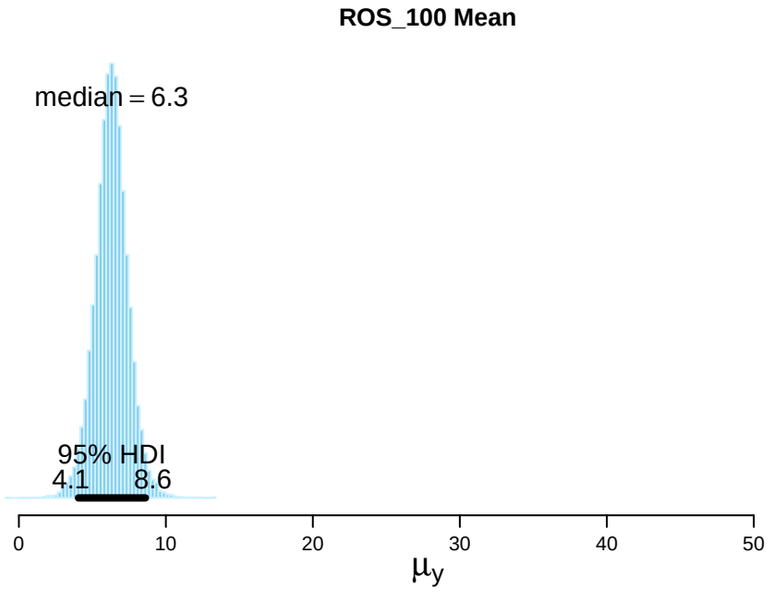
ROS_100 Mean
median = 6.3
95% HDI
4.1
8.6
0
10
20
30
40
50
μ_y

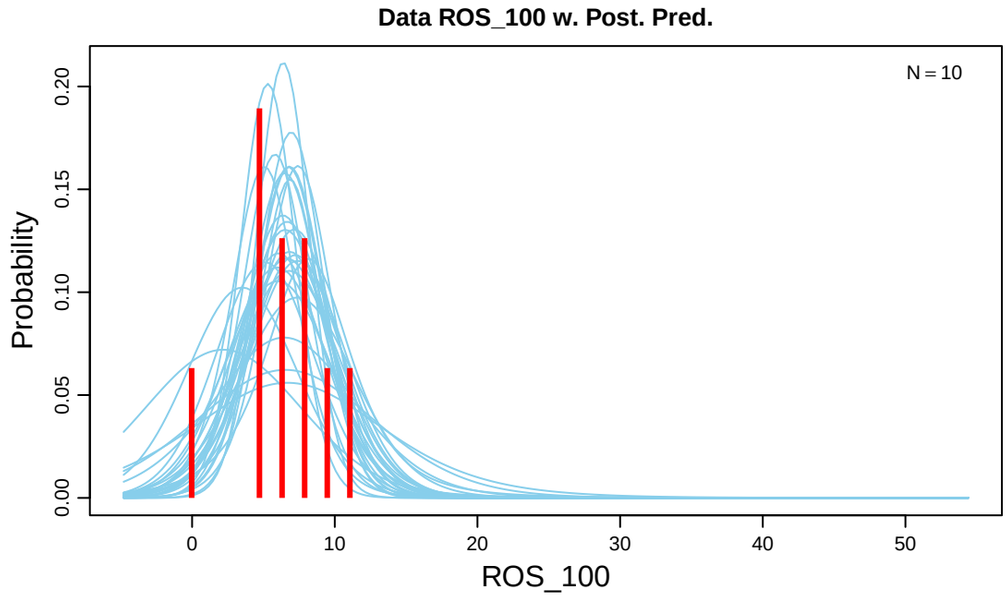
Data ROS_100 w. Post. Pred.
N = 10
Probability
0.00
0.05
0.10
0.15
0.20
0
10
20
30
40
50
ROS_100

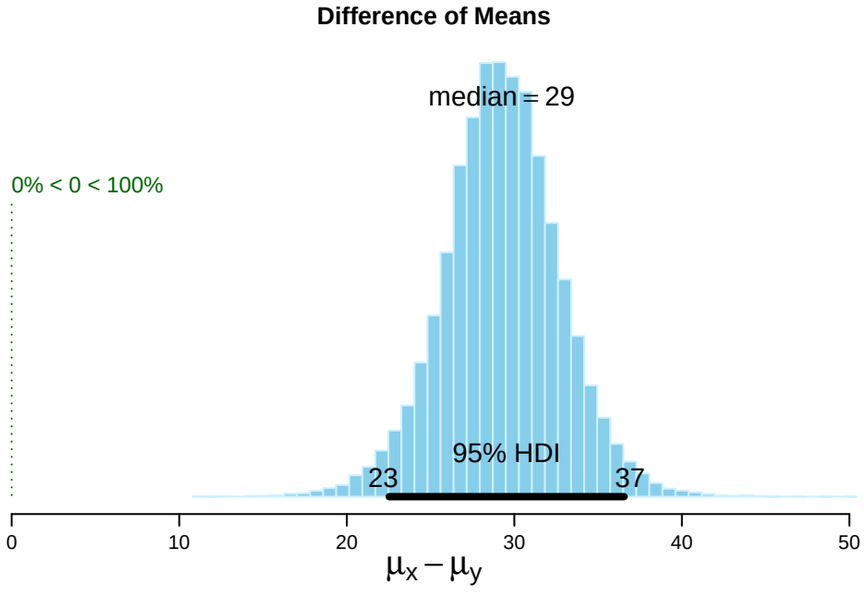
Difference of Means
median = 29
0% < 0 < 100%
95% HDI
23
37
0
10
20
30
40
50
$\mu_x - \mu_y$

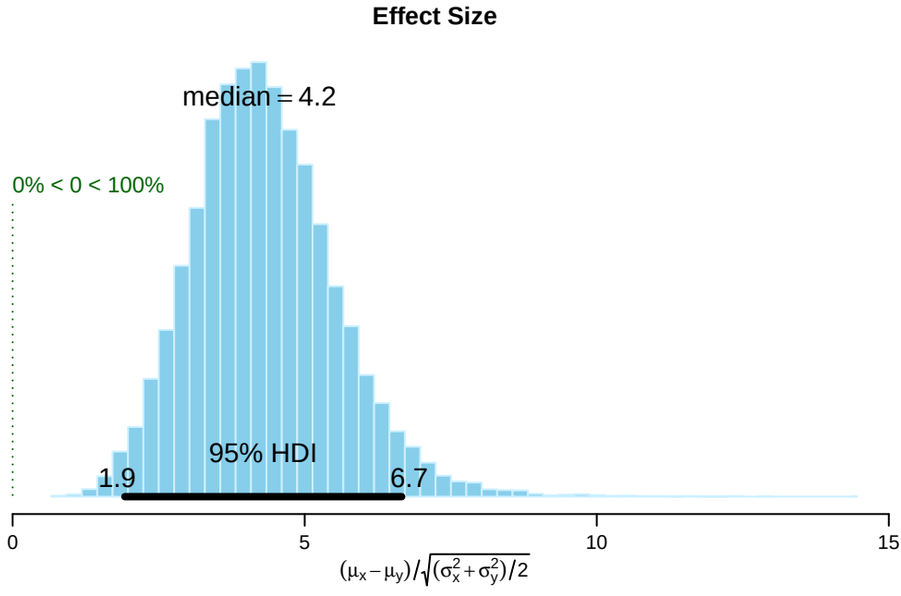
Effect Size
median = 4.2
0% < 0 < 100%
95% HDI
1.9
6.7
0
5
10
15
$(\mu_x - \mu_y)/\sqrt{(\sigma_x^2 + \sigma_y^2)/2}$

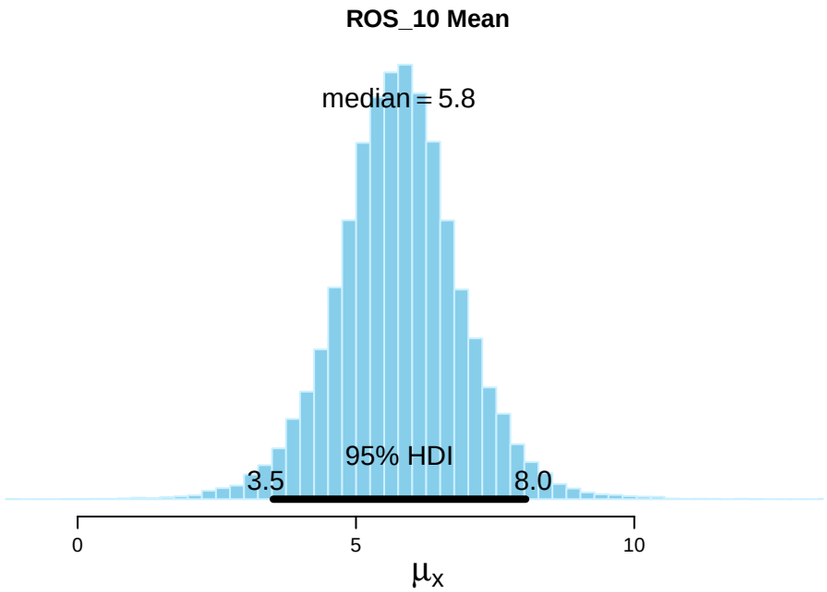
ROS_10 Mean
median = 5.8
95% HDI
3.5
8.0
0
5
10
μ_x

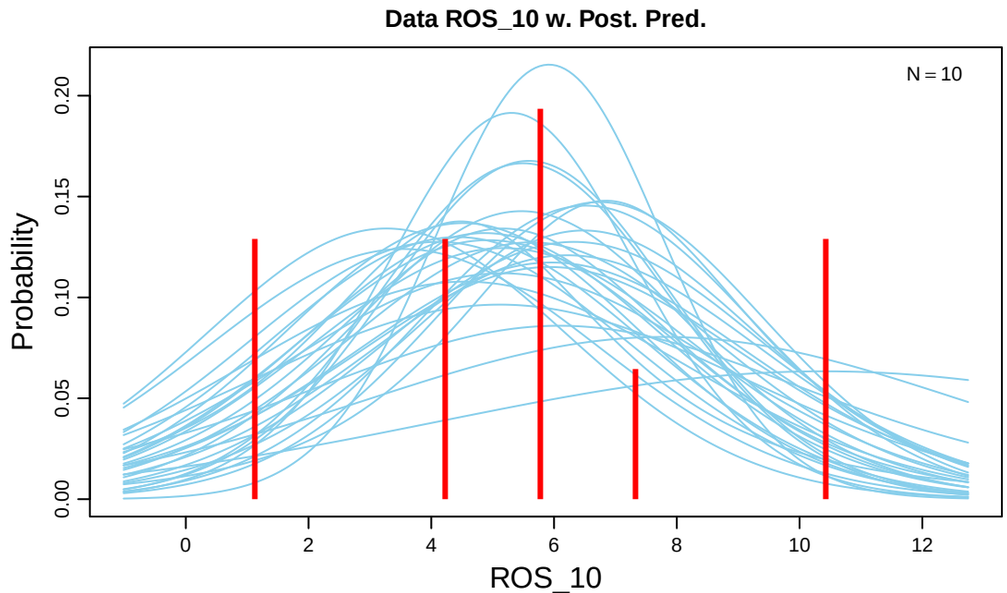
Data ROS_10 w. Post. Pred.
N = 10
Probability
0.00
0.05
0.10
0.15
0.20
0
2
4
6
8
10
12
ROS_10

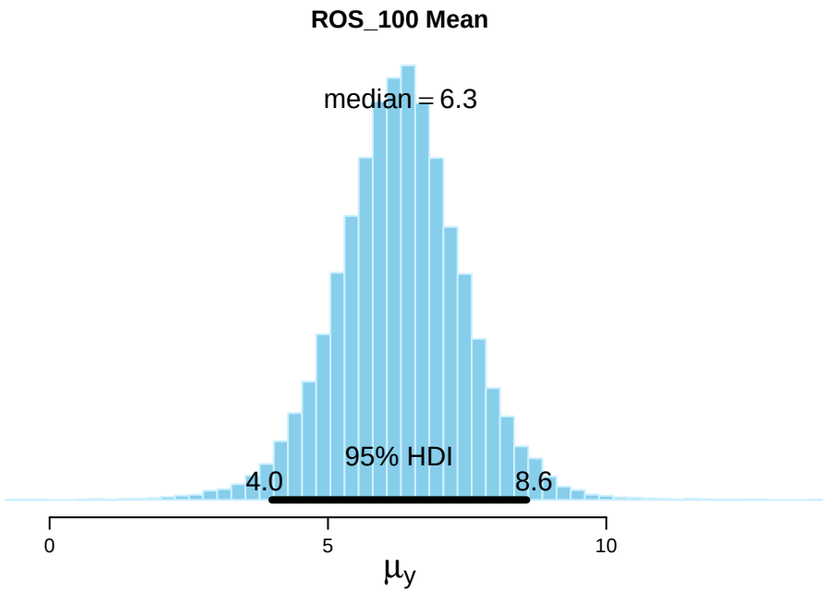
ROS_100 Mean
median = 6.3
95% HDI
4.0
8.6
0
5
10
μ_y

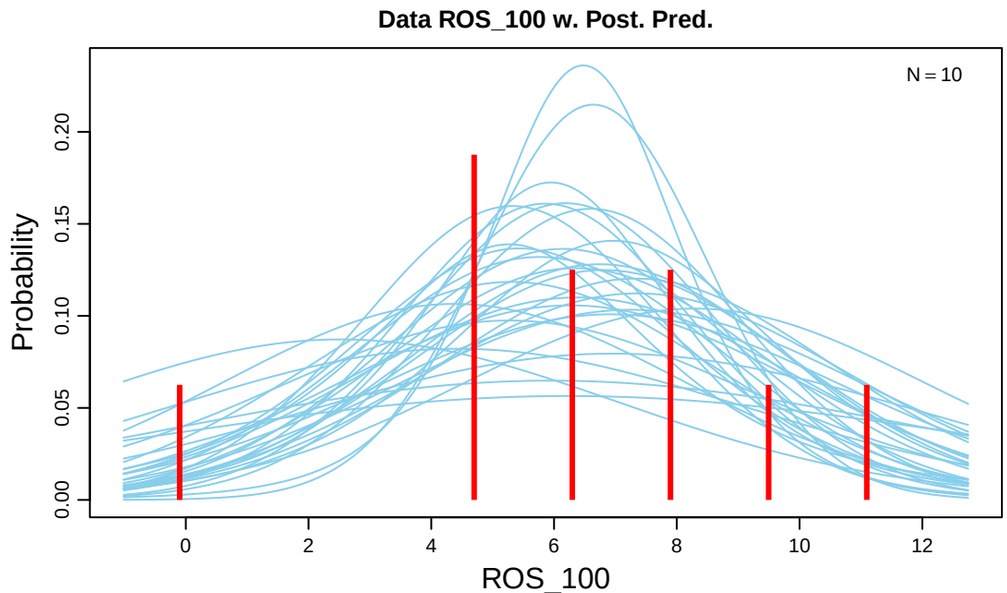
Data ROS_100 w. Post. Pred.
N = 10
Probability
0.00
0.05
0.10
0.15
0.20
0
2
4
6
8
10
12
ROS_100

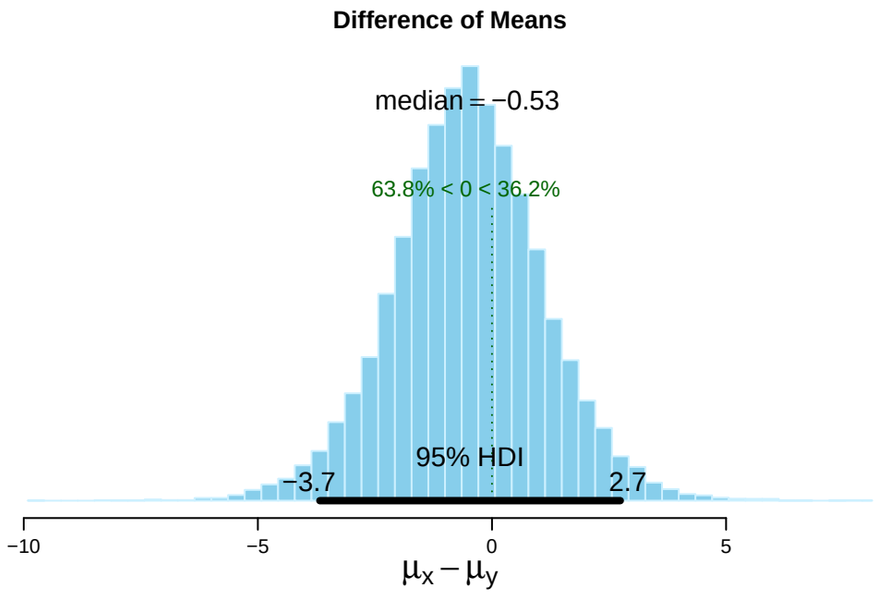
Difference of Means
median = −0.53
63.8% < 0 < 36.2%
95% HDI
−3.7
2.7
−10
−5
0
5
$\mu_x - \mu_y$

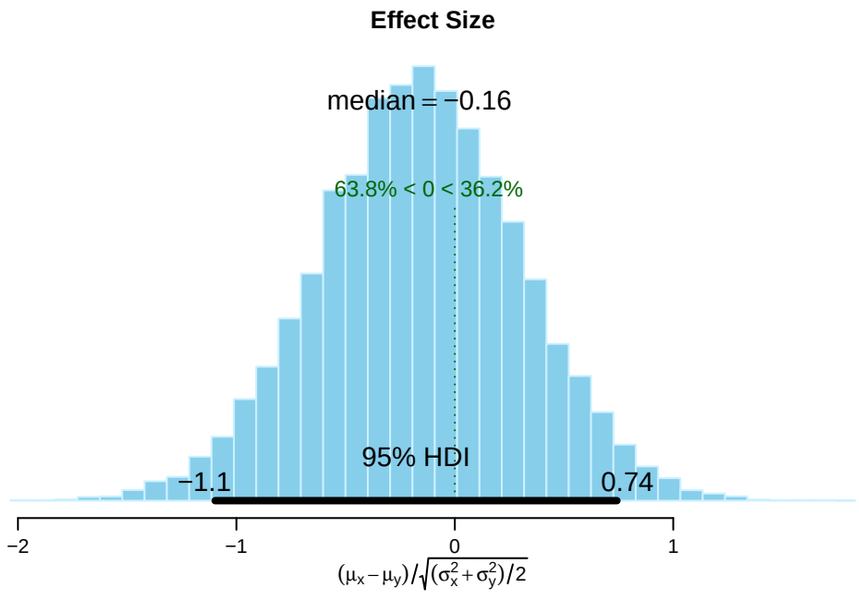
Effect Size
median = −0.16
63.8% < 0 < 36.2%
95% HDI
−1.1
0.74
−2
−1
0
1
$(\mu_x - \mu_y)/\sqrt{(\sigma_x^2 + \sigma_y^2)/2}$

General Discussion

Introduction: Deconstructing the Mutational Phenotype

For decades, the germline mutation rate (μ) was treated as a static species-specific constant, a view formalized by Drake's Rule and foundational to the molecular clock hypothesis (Drake, 1991; Zuckerkandl and Pauling, 1965). However, the accumulation of high-fidelity genomic data has dismantled this paradigm, revealing that μ is a highly plastic, quantitative trait that fluctuates significantly in response to metabolic demands, developmental tempo, and environmental stress (Baer et al., 2007). While current theoretical frameworks, notably the Drift-Barrier Hypothesis, successfully provide a population-genetic explanation for the ultimate lower limit of μ by linking replication fidelity to effective population size (N_e), they do not specify the proximate mechanistic pathways through which this equilibrium is realised.

This thesis bridges the gap between ultimate evolutionary constraints and proximate physiological drivers. It demonstrates that the realised mutation rate is not a random deviation but the mechanistic outcome of physiological constraints, biochemical specificity, and environmental novelty. By systematically deconstructing the drivers of mutagenesis in the model ectotherm *Chironomus riparius*, this work reveals that mutation rate variation is mechanistically structured:

a. Intrinsic Constraints: Shaped by the optimization of life-history traits (Generation Time).

b. Natural Modulation: Driven by the specificity of oxidative stress (Temperature).

c. Anthropogenic Disruption: Caused by mechanistic novelty (Chemical Pollutants).

To elucidate this hierarchy, the following discussion synthesises the empirical findings into three conceptual layers. **Section 1** integrates findings from Chapters 1 and 2 to propose the "Convergence of Optima" hypothesis, suggesting that organisms concentrate their life history within ecological windows where molecular damage is inherently minimized. **Section 2** deconstructs the molecular fingerprints of distinct mutagenic drivers, contrasting the signatures of replication- and time-dependent errors, the differential oxidative signatures characterizing both cold and warm extremes, and the mechanistically distinct pathway of anthropogenic adduction. Finally, **Section 3** explores the evolutionary implications of this framework, contrasting the organism's resilience to recurrent natural challenges against its vulnerability to evolutionarily novel pollutants.

1. The Convergence of Optima

Within the evolutionary ceiling imposed by the Drift-Barrier, realised mutation rates can vary substantially in response to immediate physiological and environmental conditions (Lynch, 2010; Lynch et al., 2016). Organisms operate across a range of developmental tempos and thermal environments, each imposing distinct physiological demands on cellular machinery (Angilletta and M. J., 2009; Gillooly et al., 2001). Some conditions minimize the mutation rate (μ), while others elevate it through increased replication errors, oxidative damage, or metabolic dysfunction (Pyo et al., 2025). Throughout this section, I distinguish between the fitness optimum (conditions maximizing survival and reproductive output) and the mutation rate minimum (conditions yielding the lowest μ). An "optimum" in the context of mutation rate refers to the environmental or physiological state where mutation rate is minimized, not through evolved improvements in repair

machinery per se, but through reproductive schedules concentrated within conditions that reduce the damage burden on existing repair systems (Chatterjee and Walker, 2017).

Ectotherms exhibit thermal performance relationships where physiological traits are maximised within a narrow thermal range and decline at both cold and warm extremes (Angilletta Jr., 2009; Huey and Stevenson, 1979). While endotherms also show thermal sensitivity, the effect is most pronounced in ectotherms whose body temperature tracks ambient conditions directly. For mutation rate specifically, this framework raises a critical question: when multiple independent environmental factors modulate μ (e.g., generation time and temperature), do their respective minima align? If the generation time that minimizes μ also corresponds to the thermal window where oxidative stress is minimal, this convergence would suggest that organisms concentrate reproductive activity under conditions where multiple mutagenic pressures are simultaneously reduced. Such convergence could arise through two non-exclusive mechanisms: (1) organisms have adapted their DNA repair machinery to function optimally under locally prevalent conditions, exhibiting population-specific repair kinetics tuned to the thermal and developmental regime, or (2) organisms concentrate reproductive activity within thermal and developmental windows where damage input to existing, evolutionarily constrained repair systems is minimized.

For ectotherms, temperature modulates germline mutation rates through two pathways: an indirect pathway (temperature determines developmental tempo and thus generation time) and a direct pathway (temperature alters ROS production and metabolic efficiency). Chapters 1 and 2 were designed to partition these effects: **Chapter 1** isolated generation time variation at constant temperature (20°C), while **Chapter 2** measured ROS production across an ecologically relevant thermal gradient (4-28°C). Together, these approaches reveal how developmental tempo and thermal physiology independently constrain mutation rate.

1.1 The Ecological Reproductive Window

The empirical findings from Chapters 1 and 2 reveal a striking convergence between two mutagenic mechanisms that, although deeply entangled in nature, were experimentally partitioned to isolate their distinct contributions. Under natural conditions, temperature simultaneously modulates both generation time (the indirect pathway) and cellular oxidative stress (the direct pathway); consequently, these effects become indistinguishable in wild populations. The mean generation time (26.4 days) identified under laboratory conditions at 20°C and the thermal window where ROS production is minimized (12-18 °C), both coincide with the May-September reproductive period when *C. riparius* concentrates reproductive effort in temperate habitats (Oppold et al., 2016; Pfenninger and Nowak, 2008). This convergence predicts that total germline μ, arising from replication-dependent errors, time-dependent damage, and oxidative stress, is minimized during the periods and under the conditions where natural populations actively reproduce. The developmental axis isolates intrinsic life-history constraints on replication fidelity versus damage accumulation, while the physiological axis isolates extrinsic thermal effects on ROS production. Together, these axes reveal that mutation rate variation below the Drift-Barrier ceiling reflects organism-environment interactions across multiple independent physiological dimensions (Figure 2).

This convergence does not imply that μ minimization is the direct target of natural selection. Rather, it reflects the fact that selection acts on immediate fitness components such as survival, growth rate, fecundity, which are themselves mechanistically constrained by the same physiological processes governing μ (Lande and Arnold, 1983; Lynch, 2010). Furthermore, oxidative stress imposes direct

fitness costs independent of mutagenesis: ROS damages cellular proteins, lipids, and membranes, impairing metabolic efficiency, reducing locomotor performance, and increasing mortality risk (Metcalfe and Alonso-Alvarez, 2010; P. Monaghan et al., 2009). Similarly, thermal extremes impose direct fitness costs through impaired enzyme kinetics, disrupted osmoregulation, and oxygen limitation, all of which reduce survival and reproductive output regardless of their impact on germline μ (Pörtner, 2002; Verberk et al., 2016). In the lab population, originated from Hasselbach, peak reproductive success occurs at 20°C with modal generation times of 25.3-28.3 days. Natural selection favors this reproductive timing because these conditions maximise survival, growth rate, and fecundity. While the μ minimum is a correlated outcome as a mechanistic byproduct of the physiological optima that selection directly targets (Lande and Arnold, 1983), mutational load does impose fitness costs, meaning some component of selection acts to reduce μ as part of the broader optimization of life-history traits under these conditions.

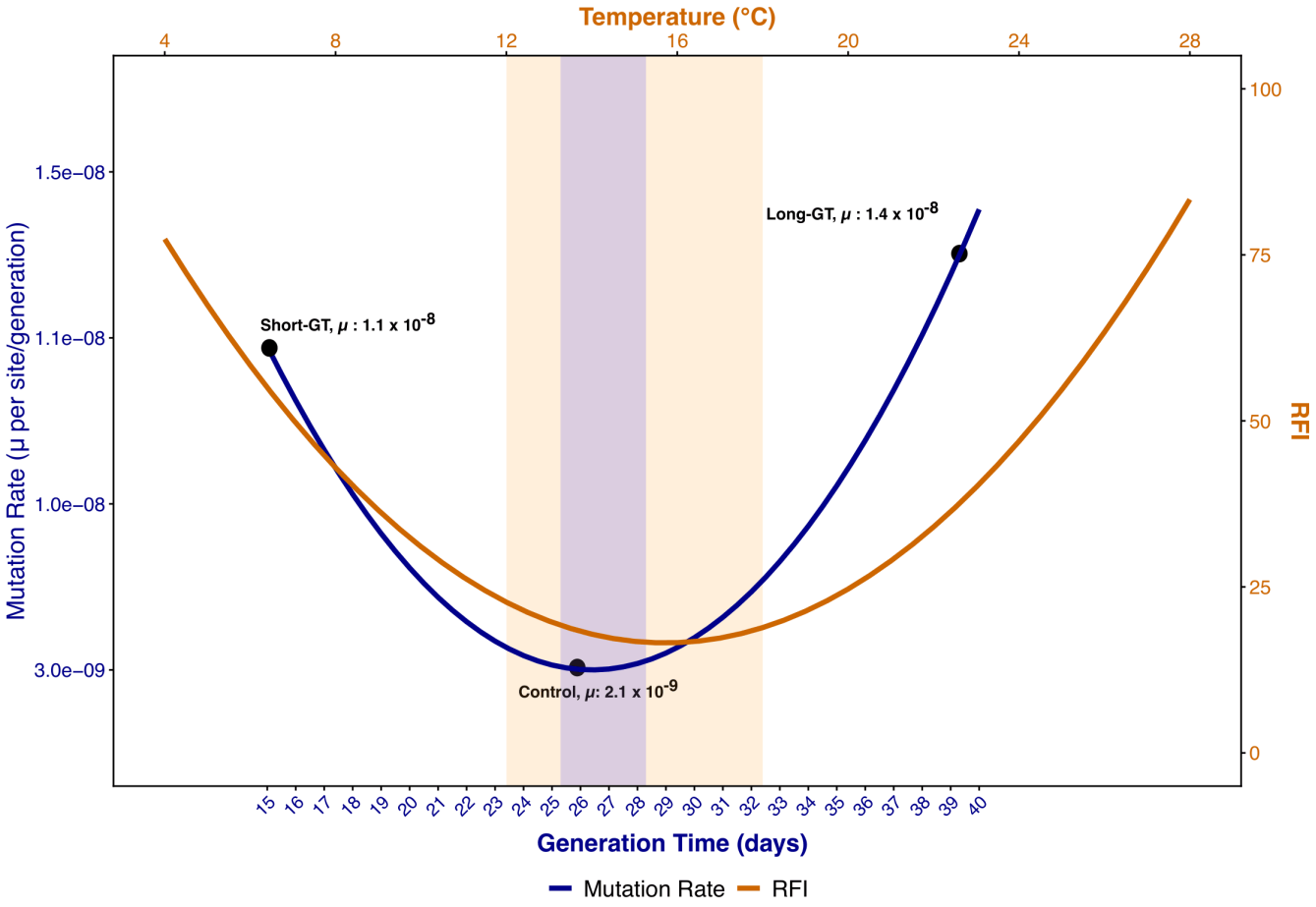

Figure 2: The Convergence of Optima. Overlay of the U-shaped profiles of the de novo germline mutation rate (dark blue line, bottom and left axes) and physiological reactive oxygen species, measured as Relative Fluorescence Intensity (RFI) (orange line, top and right axes), in *Chironomus riparius*. The orange shaded area represents the thermal range where ROS production is at its lowest, whereas the blue shaded area highlights the peak reproductive days. The graph illustrates the alignment of the minimum points of two independently tested mutagenic drivers: generation time constraints (Chapter 1) and temperature-dependent ROS production (Chapter 2). This convergence suggests that the mutation rate does not merely fluctuate randomly below the evolutionary Drift-Barrier ceiling; rather, it reflects an ecological optimization where organisms concentrate their reproductive activities under environmental and

developmental conditions that simultaneously minimize multiple sources of mutagenic damage and metabolic load.

This distinction resolves an apparent paradox with the Drift-Barrier hypothesis. The Drift-Barrier predicts that direct selection on mutation rate is too weak to overcome genetic drift in populations with finite effective size, preventing the evolution of arbitrarily low mutation rates through further refinements in replication fidelity and DNA repair machinery (Lynch, 2010; Lynch et al., 2016). Yet we observe that our *C. riparius* laboratory population concentrates reproduction under conditions where μ is demonstrably minimized. The resolution is that populations do not just evolve lower mutation rates through genetic refinement of repair machinery, but may also exhibit reproductive schedules concentrated within ecological and phenological windows where the mutagenic burden on existing repair systems is reduced. This ecological optimization operates below the Drift-Barrier ceiling: the organism cannot evolve better repair machinery, but it can reduce the damage load by concentrating activity within favorable environmental conditions. Thus, μ variation below the Drift-Barrier ceiling reflects organism-environment interactions rather than adaptive refinement of repair machinery itself. This corresponds to mechanism (2) proposed earlier: rather than evolving population-specific repair machinery tuned to local conditions (mechanism 1), organisms may reduce μ by concentrating reproduction within environmental windows where damage input is minimized. Distinguishing between these mechanisms requires different experimental approaches. Evidence for mechanism (1) would come from comparing repair enzyme kinetics, proofreading fidelity, or antioxidant capacity across populations adapted to different thermal regimes. Our current data cannot evaluate this mechanism. While the current data are consistent with mechanism (2), it cannot exclude mechanism (1) operating simultaneously.

It is critical to note that the convergence patterns documented here reflect the German laboratory population (originally sourced from Hasselbach, Hesse, Germany, (50°12′N, 8°37′E), and regularly refreshed with field-collected individuals). This population is adapted to temperate Central European thermal regimes, where May-September water temperatures naturally range from 13-18°C. High-latitude populations (e.g., Swedish populations experiencing colder, shorter summers) and low-latitude populations (e.g., Spanish populations experiencing warmer, longer summers) would be expected to exhibit shifted modal generation times, thermal optima, and seasonal reproductive schedules corresponding to their local climatic conditions (Foucault et al., 2019; Nieto-Blázquez et al., 2025). Whether the convergence between mutation rate minima and reproductive timing is maintained across these geographically divergent populations (suggesting a general principle of μ optimization) or whether different populations exhibit distinct optima reflecting local adaptation of repair machinery, remains an open question requiring comparative common-garden experiments across latitudinal gradients.

While the convergence between the mean generation time (~26 days), the mutational minimum, and the ROS minimum is striking, it is critical to acknowledge the correlational rather than causal nature of this relationship as currently demonstrated. Chapter 1 isolated generation time variation under constant thermal conditions (20 °C), while Chapter 2 characterised ROS production across a thermal gradient (4-28 °C) without direct measurement of generation time-dependent ROS variation within individuals. Consequently, I have not yet directly tested whether Short-GT individuals at 20°C actually exhibit elevated ROS levels, nor whether Long-GT individuals at 20°C experience increased oxidative stress despite extended development.

Two alternative interpretations must be considered. First, the U-shaped relationships observed for mutation rate (as a function of GT) and ROS (as a function of temperature) may reflect independent optimization processes that coincidentally converge at similar norms without direct mechanistic linkage. Second, the observed patterns may genuinely reflect a unified physiological optimum, but proving this requires direct experimental integration: measuring ROS levels specifically in short-GT versus Long-GT individuals reared at identical temperatures, or alternatively, tracking both mutation rates and ROS production simultaneously across a combined GT × temperature matrix. Until such integrative experiments are conducted, the 'Convergence of Optima' hypothesis should be interpreted as a compelling pattern warranting mechanistic validation rather than as conclusive evidence of optimised life-history integration. Future work should prioritise closing this experimental gap to establish whether generation time and thermal optima are mechanistically coupled or represent parallel but independent axes of physiological constraint.

Regardless of which interpretation proves correct, the mechanistic framework developed here (partitioning direct thermal effects from indirect generation-time effects) resolves a long-standing puzzle in the U-shaped relationship between temperature and germline μ observed by Waldvogel & Pfenninger (2021) in *C. riparius* across 12-26°C. At the warm extreme, elevated mutation rates are readily explained by direct oxidative stress, as high temperatures increase metabolic rate and ROS production. The cold extreme, however, presents an apparent paradox: **Chapter 2** demonstrated that ROS levels at 12°C are within the minimal range observed across the thermal gradient, yet Waldvogel & Pfenninger observed significantly elevated mutation rates at this temperature. The resolution lies in the indirect pathway. Cold temperatures drastically prolong generation time (43 days at 12°C versus 17 days at 26°C), and **Chapter 1** demonstrated that Long-GT lines accumulate proportionally more mutations per generation due to extended chronological exposure to time-dependent damage. Critically, mutational spectrum analysis provides direct empirical support for this indirect mechanism: the spectra of Long-GT individuals clustered with the 12°C treatment, while Short-GT spectra clustered with the moderately elevated 23°C treatment. In contrast, control populations and intermediate optimal temperatures (14°C, 17°C) formed a distinct cluster, separated along the primary axis of spectral variation from both extremes. This pattern reveals that deviation from the optimal generation time, whether imposed intrinsically through life-history variation or extrinsically through thermal modulation of developmental tempo, produces similar mutational signatures. Importantly, this spectral similarity between moderate thermal elevation (23°C) and intrinsic acceleration (Short-GT) challenges the hypothesis that ROS-mediated oxidative stress is the primary driver of μ increases at moderately elevated temperatures. While the other effects of temperature on cell physiology cannot be neglected, the dominant mutagenic pathway at moderate thermal deviations appears to be the indirect effect of temperature. This demonstrates that even in the absence of direct experimental integration between Chapters 1 and 2, the partitioning approach yields novel insights into the mechanistic basis of thermal effects on germline mutation rates.

2. Distinct Molecular Routes to Mutagenesis

The evolutionary persistence of high germline μ despite strong selection against deleterious mutations remains a central puzzle in evolutionary genetics. Drift-Barrier framework provides a population-genetic explanation for this paradox, predicting that multiple independent DNA repair pathways, each constrained by finite effective population size, contribute additively to the total mutation rate (Lynch, 2010; Lynch et al., 2016). This prediction rests on the observation that DNA repair involves numerous semi-independent pathways, each specialised for distinct classes of DNA

lesions, and that the evolutionary optimization of each pathway is limited by genetic drift (Baer et al., 2007). Consequently, reductions in one component of the mutation rate may have minimal impact on the overall rate if other pathways remain unchanged (Schrider et al., 2013). While this multi-pathway architecture is well established at the molecular level, and recent studies have demonstrated mutational spectrum variation across environments in yeast (Bae et al., 2015), stress conditions in bacteria (Maharjan and Ferenci, 2017), and genotoxic exposures in nematodes (Machado et al., 2025), integrating mechanistically distinct mutagenic axes (life-history variation, natural physiological stress, and anthropogenic chemical exposure) within a single ecological model organism remains rare. Such integration is critical for testing pathway fragmentation as it operates across various range of mutagenic pressures experienced by natural populations, where confounding effects of divergent genetic backgrounds, life histories, and repair machinery evolution are controlled.

The mechanistic basis for pathway fragmentation lies in the lesion-specific recognition and processing by distinct repair systems. DNA repair pathways have evolved to handle different classes of damage: mismatch repair (MMR) corrects base to base mismatches and small insertion-deletion loops that arise during DNA replication, base excision repair (BER) removes chemically altered bases such as those produced by oxidation or spontaneous deamination, nucleotide excision repair (NER) excises bulky helix-distorting adducts, and translesion synthesis (TLS) employs specialised error-prone polymerases to bypass lesions that stall replicative polymerases (Kunkel and Erie, 2015; Sale et al., 2012; Schärer and O. D., 2013; Wallace, 2014). These pathways operate with substantial independence: repair of oxidative lesions by BER does not enhance the correction of replication errors by MMR, nor does improved NER capacity reduces the mutagenic burden imposed by endogenous oxidative damage. Critically, this specialization can be seen in different mutagenic sources leave distinct molecular fingerprints in the mutational spectrum. Replication errors are characterised by transition-biased spectra and elevated indel frequencies, reflecting polymerase misincorporation and slippage during DNA synthesis (Kunkel, 2004b; Streisinger et al., 1966). Oxidative damage, by contrast, produces transversion-enriched signatures, (Hahm et al., 2022; Shibutani et al., 1991). Bulky adduct-forming mutagens generate highly specific signatures dictated by the chemistry of the adduct and the fidelity of translesion polymerases recruited for bypass (Pfeiffer and Kirkegaard, 2005). Recent experimental work has confirmed that mutational signatures reflect the joint influence of DNA damage type and the efficiency of pathway-specific repair, with different lesions induced by the same genotoxin being processed by separate repair pathways, thereby producing complex but interpretable spectral shifts (Huang and Zhou, 2021). This framework suggests that experimentally partitioning mutagenic sources within a single organism should reveal distinct molecular signatures corresponding to the engagement of different repair pathways.

However, empirical tests of pathway fragmentation face complementary methodological challenges. Between-species comparisons confound the source of mutagenic pressure with species-specific differences in genetic architecture, life history, and repair machinery evolution (Baer et al., 2007), making it difficult to determine whether observed differences reflect distinct mutagenic mechanisms or adaptive differences in repair capacity. Second, while recent within-species studies have successfully isolated specific mutagenic axes, these studies typically focus on a single class of mutagenic pressure (e.g., exogenous chemical mutagens, metabolic stresses, or environmental shifts) and often employ genetic manipulation of repair pathways to reveal signatures. What remains lacking is an integrated assessment across mechanistically distinct mutagenic axes within

a single organism. To address this gap, I systematically characterised molecular fingerprints arising from three mechanistically distinct mutagenic axes within a single organism, *Chironomus riparius*: intrinsic variation in organismal generation time (Chapter 1), thermal effects on ROS production (Chapter 2), and exposure to the anthropogenic PAH, BaP (Chapter 3). By examining these axes within the same species under controlled laboratory conditions, this design minimizes confounding from genetic architecture and repair machinery evolution while capturing the diversity of mutagenic sources relevant to ecological and evolutionary dynamics.

The following sections explore the evolutionary implications of this fragmentation. Section 2.1 examines how pathway independence constrains multi-pathway optimization under the Drift-Barrier framework and limits cross-protection against combined mutagenic pressures. Section 2.2 discusses the consequences for molecular clock assumptions in phylogenetic inference, where generation time does not equal evolutionary time.

2.1 Pathway Independence and Limited Cross-Protection

The mechanistic fragmentation documented above implies that total germline mutation rate represents the sum of contributions from distinct mutagenic axes: $\mu_{total} = \mu_{replication} + \mu_{oxidative} + \mu_{adduct}$. Generation time variation demonstrates this additivity directly: Short-GT cohorts accumulate mutations primarily through replication errors (transition-biased, elevated indels), whereas Long-GT cohorts accumulate mutations through time-dependent oxidative damage (transversion-enriched, reduced indels). The shift in mutational spectrum reflects a shift in the balance between these two components, not a simple increase or decrease in a single mutagenic process. BaP exposure reveals a second, chemically independent axis: bulky adduct formation elevates μ through a pathway that operates independently of oxidative stress, as demonstrated by reduced ROS levels in BaP-exposed larvae despite elevated mutation rates (Chapter 3). Thermal stress adds a third axis: cold and heat extremes generate compositionally distinct ROS profiles that impose oxidative damage through different molecular routes, as evidenced by oxidant-specific transcriptomic responses (Chapter 2). Critically, these three mutagenic axes engage distinct repair machinery (Mao and Wyrick, 2019).

Because these repair pathways operate independently, improving fidelity along one axis provides only limited protection against damage from other sources. This creates an evolutionary constraint with diminishing returns: selection on μ must simultaneously optimise multiple repair systems, but enhancing one pathway reduces only that component of the total mutation rate. For example, if $\mu_{replication} = 3\times10^{-9}$, $\mu_{oxidative} = 3\times10^{-9}$, and $\mu_{adduct} = 2\times10^{-9}$, then total $\mu = 8\times10^{-9}$. A 50% improvement in MMR fidelity, which halves replication errors to 1.5×10^{-9}, would lower total μ to only 6.5×10^{-9}, representing a 19% reduction in the overall mutation rate. The oxidative and adduct components remain unchanged, continuing to contribute 5.5×10^{-9} to the mutational load. This limited cross-protection has been predicted theoretically (Baer et al., 2007; Schrider et al., 2013), but this empirical demonstration across three pathways within a single organism provides direct support for this prediction. The implication is that even substantial improvements in one repair system yield only modest reductions in total mutation rate, because multiple independent pathways continue to contribute to the mutational input (Baer et al., 2007; Gifford et al., 2024).

Under the Drift-Barrier framework, each repair pathway evolves toward a fidelity optimum where the selection coefficient for further improvement falls below the threshold at which genetic drift dominates, approximately $s \sim 1/(2Ne)$ (Lynch, 2010; Lynch et al., 2016). For *C. riparius*, with an

estimated effective population size of $N_e \sim 10^6$, this threshold is big enough to allow individual pathways to approach their theoretical minima (Lynch and Marinov, 2015; Sari, 2026). MMR can be refined to near-maximal proofreading fidelity, BER can be tuned to excise oxidative lesions efficiently, and NER can be optimised to recognize bulky adducts with high specificity. However, in order to reduce μ substantially, optimizing all pathways simultaneously presents a fundamentally different challenge (Baer et al., 2007; Lynch, 2011). The fixation of beneficial mutations at multiple independent loci requires that alleles improving MMR, BER, and NER must either all arise and fix sequentially in the same lineage, or arise in different lineages and then be brought together through recombination (Barton and Turelli, 1989; Lynch et al., 2016). Because fixation probabilities are multiplicative rather than additive (Lynch, 2010), the compound probability P_total = P_MMR × P_BER × P_NER decreases sharply as the number of pathways increases. This creates a system-level drift barrier that is effectively stronger than the drift barrier acting on any single pathway (Lynch, 2020; Schiffman and Ralph, 2022). Bacteria, with N_e approaching $\sim 10^9$, can efficiently fix beneficial mutations across dozens of repair pathways simultaneously, achieving μ as low as 10^{-10} per site per generation (Sung et al., 2012). In contrast, even organisms like *C. riparius*, with $N_e \sim 10^6$ that is high among metazoans, while large enough to optimise individual pathways, cannot simultaneously refine all pathways with the same efficiency. The result is that spontaneous mutation rate remains relatively high, approximately 2.1×10^{-9} per site per generation (Oppold and Pfenninger, 2017; Waldvogel and Pfenninger, 2021), because it sums multiple independently constrained components, each equilibrating near its own drift-limited ceiling but not simultaneously pushed lower.

This multi-mutational-pathway structure has two broad evolutionary consequences. First, it creates diminishing returns for selection on μ: improving fidelity in one pathway yields only modest reductions in total μ because other pathways continue to contribute substantially to the mutational load (Baer et al., 2007). This helps to explain why multicellular eukaryotes with moderate N_e maintain germline mutation rates orders of magnitude higher than those of large-Ne microbes, despite the strong fitness costs of deleterious mutations (Lynch, 2011; Schrider et al., 2013). Second, and more importantly for contemporary environmental change, it implies that adaptation to one mutagenic regime does not automatically confer protection against others. **Section 1** demonstrated that *C. riparius* minimizes damage input by concentrating reproduction under conditions where both replication errors and oxidative stress are reduced. However, this ecological optimization strategy provides no defence against evolutionarily novel mutagens. Mechanisms that optimise replication fidelity and buffer endogenous oxidative stress do not mitigate the additional burden imposed by adduct-forming pollutants such as BaP. Populations experiencing combined stressors therefore face compounded mutational loads delivered through distinct molecular routes. From a predictive perspective, this means that risk assessments or evolutionary forecasts that consider stressors in isolation will systematically underestimate the long-term mutational and fitness costs experienced by natural populations, particularly in Anthropocene environments where recurrent natural drivers and anthropogenic mutagens act simultaneously.

2.2 Implications for Molecular Clock Assumptions

The molecular clock hypothesis, rooted in the neutral theory of molecular evolution, posits that genetic divergence accumulates at a roughly constant rate over time (Kimura, 1968; Zuckerkandl and Pauling, 1965), enabling the inference of divergence dates from sequence data when calibrated with fossil evidence or biogeographic events (Bromham and Penny, 2003; Ho and Duchêne, 2014). This framework has become foundational to evolutionary biology, underpinning

thousands of studies that date the Tree of Life (Blais and Archibald, 2021). However, classical molecular clock models implicitly assume that mutations arise from a single, uniform process whose rate scales predictably with life-history traits such as generation time (Ohta, 1995). While relaxed-clock methods have been developed to accommodate rate variation among lineages, these approaches treat such variation as a statistical phenomenon rather than as a consequence of distinct mutational mechanisms (Drummond et al., 2006). The Section 2 findings challenge this view by demonstrating that μ variation reflects the shifting balance among multiple, mechanistically distinct mutational pathways, each responding differently to environmental and physiological conditions.

The identification of three mechanistically distinct mutagenic pathways reveals that substitution rates do not simply scale with time or cell divisions, but instead reflect the relative contributions of pathway-specific processes. Critically, the balance among these pathways shifts with environmental context, as discussed earlier. This mechanistic heterogeneity poses a fundamental challenge to phylogenetic inference, because closely related lineages occupying different thermal niches or pollution gradients will accrue substitutions at different rates not due to demographic history or selection, but due to exposure-dependent shifts in mutational input. Current models, which attribute rate variation to factors like N_e or diversification dynamics, may therefore systematically misattribute pathway-driven rate differences to other evolutionary processes (Bromham, 2009; Bromham et al., 1996).

This pathway-dependent rate heterogeneity directly explains a long-standing puzzle in molecular clock calibration: the non-linear relationship between generation time and substitution rate. Classical molecular clock models assume that mutation rates scale inversely with generation time, predicting that organisms with shorter generation times should accumulate proportionally fewer mutations per unit of chronological time (Gremer, 2023; Stearns, 1980). However, empirical observations reveal substantial deviations. Chapter 1 provides a concrete illustration: individuals with 15-day generation times exhibited a mutation rate of 1.1×10^{-8} per site per generation, while those with 37.7-day generation times exhibited a rate of 1.4×10^{-8} per site per generation, representing a 1.27-fold increase despite a 2.5-fold difference in generation time. When scaled to annual rates, the pattern inverts: 15-day individuals complete approximately 24 generations per year, yielding an annual mutation rate of 2.67×10^{-7} per site per year, whereas 37.7-day individuals complete only 10 generations per year, yielding an annual rate of 1.36×10^{-7} per site per year. This demonstrates a two-fold difference in annual mutation rate in the opposite direction relative to generation-time scaling assumptions: shorter generation times lead to higher annual mutation rates, not lower rates as classical models predict (Thomas et al., 2010). This generation time does not equal evolutionary time. This pattern is robustly confirmed by recent meta-analyses across eukaryotes. Lewin and Eyre-Walker (2025), analysing 133 species spanning arthropods to mammals, found a strong negative correlation between μ/year and generation time, with doubling generation time reducing annual mutation rate by approximately 39%. This relationship is consistent across all phylogenetic groups, from fungi to vertebrates (Lewin and Eyre-Walker, 2025; Wang and Obbard, 2023). This pattern demands mechanistic explanation and raises a critical question for phylogenetic inference: if generation time does not equal evolutionary time, what processes drive this decoupling, and how do they bias molecular clock estimates?

The mechanistic basis for this decoupling lies in the pathway fragmentation documented in Section 2.1. As demonstrated in Chapter 1, generation time determines not merely the total mutation rate but the mechanistic source of mutations. Organisms with shorter generation times accumulate

proportionally more replication-associated errors, while those with longer generation times accumulate proportionally more time-dependent oxidative damage. Critically, these distinct mutational sources scale with time differently: replication-driven mutations accumulate proportionally to cell divisions (tracking generational time), whereas oxidative damage accumulates proportionally to chronological exposure (tracking absolute time independent of reproductive cycles). This mechanistic heterogeneity means that lineages with different generation times are accumulating different types of mutations that integrate into the genome through distinct temporal processes. Consequently, phylogenetic models that assume a uniform mutational process will systematically misattribute rate variation arising from shifts in pathway-specific contributions.

It is critical to acknowledge that these mutation rates were measured under controlled laboratory conditions at a single, benign temperature of 20°C. In natural populations, organisms experience multiple simultaneous mutagenic pressures: thermal fluctuations that modulate both generation time and ROS production, exposure to ultraviolet radiation, background pollutants, and nutritional stress, all of which can elevate mutation rates through pathway-specific mechanisms. The additivity principle established in Section 2.1 predicts that these contributions sum: $\mu_{total} = \mu_{replication} + \mu_{oxidative} + \mu_{adduct} + \mu_{other}$. Consequently, annual mutation rates in wild populations are likely substantially higher than laboratory estimates, as multiple stressors act simultaneously rather than in isolation. This has profound implications for molecular clock calibration: divergence time estimates derived from laboratory-measured mutation rates will systematically underestimate the true mutational input experienced by natural populations, particularly for lineages inhabiting thermally variable or polluted environments. Furthermore, the relative contribution of each pathway may vary across lineages depending on local environmental conditions, body size, and metabolic strategy, introducing systematic bias into phylogenetic inference that cannot be corrected by simple generation-time scaling (Bromham, 2011; Bromham et al., 1996). Relaxed molecular clock models, which allow substitution rates to vary across branches, were developed to accommodate such rate heterogeneity (Drummond et al., 2006). However, these models treat rate variation as a statistical phenomenon rather than as a consequence of distinct mutational mechanisms operating under different environmental regimes. These findings suggest that accurate divergence time estimation requires not merely allowing rates to vary, but explicitly modelling the mechanistic sources of that variation. Molecular clock models that assume rate variation reflects only demographic or selective factors risk systematically misattributing pathway-driven differences, leading to biased divergence time estimates across lineages with divergent life histories, thermal regimes, or pollution exposures (Bromham, 2009; Ho and Duchêne, 2014).

3. Evolved Plasticity and Asymmetric Vulnerability: Recurrent vs. Novel Selective Pressures

Evolutionary responses depend fundamentally on the temporal history of exposure. Organisms facing repeated selective pressures can evolve anticipatory defences through two interacting mechanisms (Ghalambor et al., 2007; Via et al., 1995). First, populations can maintain standing genetic variation, meaning segregating alleles at fitness relevant loci that are already present before a particular bout of selection begins (Barrett and Schluter, 2008; Hermisson and Pennings, 2017). In fluctuating environments, this variation is repeatedly filtered and reshuffled, so alleles that are advantageous under one set of conditions can increase in frequency when those conditions recur. Second, populations can optimise coordinated stress responses through refinement of regulatory architectures (Pigliucci et al., 2006). When selection persists across generations, this combination enables rapid evolutionary shifts through allele frequency change rather than waiting for beneficial mutations that arise only after the environment has changed (Messer and Petrov, 2013; Taus et al.,

2017). Crucially, maintaining such variation requires selection strong enough to counteract genetic drift, especially in moderate and small populations (Barrett and Schluter, 2008). Predictable fluctuations can also favour phenotypic plasticity, the capacity to adjust phenotype without genetic change (DeWitt and Scheiner, 2004). In some cases, consistently beneficial plastic responses may become more constitutive over time through genetic assimilation (Pigliucci et al., 2006).

Novel stressors present a contrasting scenario. Populations may lack genetic variation for substrate specific recognition, which can force reliance on generalist mechanisms that may fail to maintain fitness (Bell and Collins, 2008; Hendry et al., 2017). By definition, these pressures have not persisted long enough to build and refine specialised response architectures (Ghalambor et al., 2007; Pigliucci et al., 2006). Adaptation must then proceed through slower routes, including selection on rare alleles at low ancestral frequency or *de novo* mutations arising after exposure begins (Hermisson and Pennings, 2017). Generalist pathways can sometimes be co-opted from unrelated stress contexts (Moczek et al., 2011; Yeh et al., 2004). However, such co-option often lacks the substrate specific optimization that characterises systems shaped by persistent selection. When generalist responses are insufficient, populations can decline even when stress pathways are strongly activated. This pattern reflects evolutionary lag, where environmental conditions shift faster than adaptive evolution can proceed (Hoffmann and Sgrò, 2011). The distinction explored in this section is therefore not whether organisms respond, but whether evolutionary history has optimised those responses to maintain fitness under challenge (DeWitt and Scheiner, 2004).

3.1 Temperature and Generation Time as Recurrent Challenges

Temperature and developmental timing represent recurrent challenges because both vary predictably across seasons and habitats, imposing continuous selection over millions of years (Angilletta Jr., 2009). This evolutionary history shapes the specificity of organismal responses (Tomanek, 2015). In Chapter 2, *C. riparius* deployed distinct antioxidant defences matching specific ROS profiles at thermal extremes. These are not generalised stress responses but oxidant specific regulatory systems that recognize compositional shifts in the oxidative environment and deploy appropriate protection (Abele et al., 2002). Similarly, Chapter 1 revealed that generation time variation is maintained as a persistent life history polymorphism, with the populations mean generation time of approximately 26 days converging with a mutational minimum where both per day and per generation mutation rates are jointly reduced. This alignment suggests that recurrent selection on developmental timing has shaped reaction norms balancing speed fidelity trade-offs, predation risk, resource availability, and seasonal constraints (Roff and D. A., 2002; Stearns and S. C., 1992). The key evolutionary insight is that these systems reflect millions of generations of refinement, not passive physiological tolerance (Pörtner, 2002).

In fluctuating environments, alleles conferring thermal tolerance or developmental plasticity are repeatedly selected through natural selection, so beneficial variants remain available (Hermisson and Pennings, 2017). Crucially, adaptation often proceeds through quantitative shifts in allele frequencies and regulatory tuning rather than requiring qualitative innovations that arise only after selection begins (Messer and Petrov, 2013). For traits with polygenic architecture like developmental timing, where Chapter 1 showed that generation time exhibits continuous variation rather than discrete states, this means selection can act on segregating variation to shift population means without waiting for *de novo* mutations (Barrett and Schluter, 2008). The implication is that when environmental conditions fall within the recurrent range, organisms can respond rapidly because the underlying genetic and regulatory machinery is already present and has been

optimised by long-term selection (Ghalambor et al., 2007). Recent work demonstrates that this standing variation includes cryptic genetic variation (CGV) as heritable diversity phenotypically silent under standard conditions but expressed under stress, which is selectively maintained at loci subject to recurrent environmental fluctuations (Pfenninger et al., 2025). In *C. riparius*, genes under fluctuating thermal selection are significantly enriched for both plasticity and CGV, providing a reservoir of genetic diversity that can be rapidly mobilized when thermal stress intensifies beyond typical ranges.

3.2 BaP as Evolutionary Novelty

Novel stressors constrain adaptation because populations lack genetic variation for substrate specific recognition, forcing reliance on generalist mechanisms that often fail to maintain fitness (Hendry et al., 2017; Sih et al., 2011). PAHs as a chemical class have been present at low background levels from wildfires and volcanic activity over evolutionary time (Abdel-Shafy and Mansour, 2016; Lundstedt et al., 2007). However, industrialization has increased PAH loads in urban sediments by orders of magnitude above pre industrial background, creating exposure regimes that are evolutionarily unprecedented in their scale (Nacci et al., 2010; Reid et al., 2016). On the last two centuries since large scale fossil fuel combustion began, populations have not had sufficient time to build standing variation for BaP specific recognition or repair proteins (Nacci et al., 2010). This addresses a critical distinction: standing genetic variation maintain for traits under recurrent selection, like thermal tolerance, where fluctuating temperatures have maintained allelic diversity at relevant loci over millions of years (Angilletta Jr., 2009; Pedrosa et al., 2017). In contrast, BaP specific tolerance would require variation at loci conferring enhanced recognition of BPDE-dG adducts. Chapter 3 demonstrated that *C. riparius* lacks such substrate specific defences: BaP elevated germline mutation rates 1.2-fold at 100 µg/L while decreased ROS levels, confirming that mutagenesis proceeded through a pathway mechanistically distinct from oxidative damage (Reid et al., 2016) (Chapter 3). The absence of adaptive response over three generations suggests that alleles conferring BaP-specific tolerance are either absent or at extremely low frequency in this population.

The mechanistic basis for this constraint lies in the distinction between specialist and generalist repair pathways (Wallace, 2014). As established in Section 2, BPDE-dG adducts are processed by NER and TLS, which recognize helix distorting lesions rather than specific chemical structures (Schärer, 2003). This makes NER a generalist pathway that can accommodate a diverse array of bulky lesions but lacks the substrate specific optimization characteristic of BER (Leibeling et al., 2006). Building a BaP specific recognition system analogous to the oxidant specific defences would require coordinated modifications across sensor proteins, metabolic enzymes, and repair machinery (Nebert and Dalton, 2006). These are complex polygenic changes that unlikely to arise through single mutations (Messer and Petrov, 2013). Furthermore, Section 2 demonstrated that pathway independence creates limited cross protection: populations adapted to oxidative DNA damage through refined BER and antioxidant systems gain no benefit against adduct forming mutagens that operate through NER (Schrider et al., 2013). This explains why the composition specific ROS defences in *C. riparius*, despite their sophistication, provides no protection against BaP mutagenesis (Chapter 3).

Atlantic killifish populations provide an instructive contrast that clarifies what conditions permit adaptation to novel chemical stressors (Whitehead et al., 2011). *Fundulus heteroclitus* populations inhabiting PAH and PCB contaminated estuaries have evolved heritable tolerance to normally lethal

pollutant levels (Nacci et al., 2010). Genomic analyses reveal convergent evolution through modifications of AHR signalling pathways, with distinct molecular variants underlying adaptation in independent populations (Reid et al., 2016). However, three critical features distinguish killifish adaptation from my *C. riparius* experiment. First, tolerant populations experienced decades of continuous contamination, corresponding to many tens of generations under field conditions where complex pollutant mixtures imposed strong and consistent selection. Second, these populations were already resident in contaminated habitats before severe pollution began, allowing selection to act on standing genetic variation present within locally adapted gene pools. Third, adaptation-imposed fitness costs: resistant populations show reduced performance in clean environments, indicating evolutionary trade-offs rather than cost free improvements (Meyer and Di Giulio, 2003). Our experiment tested a laboratory population across three generations at a high BaP concentration (Chapter 3). The tested population likely lacked standing variation for BaP tolerance, and the three-generation timeframe was insufficient for polygenic adaptation to proceed through rare alleles or *de novo* mutations (Barrett and Schluter, 2008). The lesson from killifish is clear: adaptation to novel mutagens is possible but requires abundant standing variation, many generations of strong selection, and imposes evolutionary costs that constrain performance under alternative conditions (Meyer and Di Giulio, 2003).

However, several lines of evidence suggest an alternative interpretation: at environmentally relevant concentrations, existing generalist defences may be sufficient to protect the genome, rendering specialised adaptation unnecessary, though this protection comes at a severe metabolic cost. First, BaP exposure at 10 µg/L produced no detectable mutagenic effect, and even the extreme concentration of 100 µg/L elevated mutation rates only 1.2-fold. This is substantially less mutagenic than ecologically relevant thermal variation, which yielded 2.79- to 4.54-fold increases (Waldvogel and Pfenninger, 2021). This suggests that generalist DNA repair pathways (such as NER) are adequately counteracting the DNA damage, meaning BaP does not impose a strong enough mutational load to drive selection for substrate-specific repair mechanisms in *C. riparius*. Second, the observed decrease in ROS levels under BaP exposure strongly indicates the deployment of a mismatched, generalist stress response. Literature shows that BaP exposure triggers a transient upregulation of antioxidant genes at 24 hours, which returns to baseline by 48 hours (Vicentini et al., 2017). Crucially, as demonstrated in Chapter 2, when an organism faces a true, continuous oxidative stressor (like thermal extremes), ROS levels remain high despite the upregulation of antioxidant defences. The fact that ROS levels decreased here implies that BaP is not primarily generating ROS; rather, because *C. riparius* lacks a substrate-specific sensor for BaP, the organism blindly deploys its broad-spectrum stress defences, including antioxidants, which inappropriately scavenge baseline ROS. Third, this unoptimised deployment of generalist defences directly explains the observed fitness costs. Over three generations, the primary fitness impacts were reduced fertility and increased mortality. Activating and maintaining broad, generalist stress mechanisms is highly energetically demanding. Because the organism cannot mount a tailored, efficient response, it is forced to reallocate energy away from normal cellular processes and life-history traits (e.g., reproduction) to sustain these generalist defences (Lynch, 2011). Therefore, the lack of a massive mutational spike combined with a severe fitness decline indicates that current defence mechanisms are sufficient to protect the genome, but because they lack substrate-specific optimization, they drain the organism's energy budget. Ultimately, natural selection may not be targeting specialised BaP defences because the generalist pathways prevent catastrophic genome degradation, even though they impose a heavy metabolic consequence (Lynch, 2012). Nevertheless, these hypotheses require further validation, and the limitations of this study

(specifically the restriction to a three-generation timeframe and the absence of direct transcriptomic data under BaP exposure) must be acknowledged.

3.3 Implications for Ecotoxicology and Evolutionary Risk Assessment

The asymmetry documented in the preceding sections has direct implications for predicting evolutionary responses under rapid environmental change (Hendry et al., 2017). While populations can adapt rapidly to recurrent challenges like temperature and generation time variation, they exhibit severe asymmetric vulnerability when confronted with novel, industrial-scale stressors for which no substrate-specific defences exist (Nacci et al., 2010; Whitehead et al., 2011). The most vulnerable natural populations face a "triple threat": exposure to evolutionarily novel mutagens, small effective population sizes that limit the efficiency of purifying selection, and low genetic diversity that reduces the substrate for any adaptive response (Hoffmann and Sgrò, 2011). These factors create a compounded vulnerability that current conservation frameworks rarely anticipate (Oziolor et al., 2019). As discussed, while environmentally relevant concentrations of pollutants (e.g., 10 µg/L BaP) may not immediately overwhelm the genome due to the deployment of generalist defences, this apparent resilience is precarious. The true evolutionary threat emerges when the organism's energy budget, already drained by sustaining these unoptimised generic defences, is forced to cope synergistically with other environmental stressors (Relyea, 2009).

Because natural populations face thermal stress, altered generation times, and anthropogenic chemicals simultaneously, the mutational and metabolic burdens of these stressors compound (Holmstrup et al., 2010). As established in Section 2, mutagenic pathways are mechanistically independent: replication errors, targeted oxidative damage, and bulky adducts engage distinct repair machinery. Therefore, their contributions to the total germline mutation rate are additive rather than redundant (Baer et al., 2007). Crucially, thermal tolerance does not confer chemical resilience (Chapter 3). Chapter 2 documented composition-specific antioxidant defences that successfully buffer oxidative stress at thermal extremes, yet Chapter 3 demonstrated that these same defences provided no protection against BaP-induced mutagenesis, which operates through an independent adduction pathway. This limited cross-protection means that populations adapted to variable thermal environments gain no evolutionary advantage against novel chemical mutagens (Sih et al., 2011). When an organism is forced to simultaneously endure thermal extremes and chemical pollution, the additive metabolic cost of running both targeted antioxidant defences and generalist DNA repair systems can lead to energetic exhaustion, precipitating a collapse in overall genomic maintenance and severe fitness declines.

Consequently, toxicological risk assessment frameworks that evaluate stressors in isolation systematically underestimate the mutational and fitness costs experienced by wild populations (Relyea, 2009). Extrapolating from single-compound laboratory exposures and assuming that general stress tolerance predicts pollutant resistance obscures the long-term evolutionary burden of combined stressors (Oziolor et al., 2019; Whitehead et al., 2011). To directly test the "energy allocation" and additive mutation hypotheses proposed here, future experimental designs must embrace multi-stressor complexity. A critical next step would involve exposing *C. riparius* to environmentally relevant BaP concentrations while simultaneously rearing them at stressful thermal extremes over an extended evolutionary timeframe. Pairing comprehensive fitness tracking with whole-transcriptome sequencing would reveal whether the targeted, highly optimised thermal antioxidant response falters when the organism is forced to concurrently sustain metabolically demanding generalist defences against adduction. Only by investigating these proximate drivers in

tandem can we accurately predict the evolutionary resilience of populations facing the compounding genomic threats of the Anthropocene.

4. Conclusion: From Drift-Barrier to Proximate Mechanisms

The Drift-Barrier hypothesis successfully explains why germline mutation rates remain orders of magnitude higher in multicellular eukaryotes than in microbes, defining the ultimate evolutionary floor below which selection becomes too weak to drive further refinements in replication fidelity. This dissertation bridges the gap between ultimate evolutionary constraints and proximate mechanistic drivers of mutation rate variation. While the Drift-Barrier hypothesis sets the minimum mutation rate a species can achieve through optimization of non-mutator alleles, it does not explain the mechanistic processes generating variation within these limits. The realised mutation rate at any moment reflects how cellular machinery responds to immediate physiological demands, a question of proximate causation. The central question this thesis addresses is not why mutation rates cannot evolve lower, but rather how and why they vary so dramatically within the constraints the Drift-Barrier imposes. By systematically deconstructing mutation rate variation into intrinsic life-history constraints, natural environmental modulators, and anthropogenic stressors, this work reveals that the germline mutation rate is not a fixed parameter but a mechanistically structured and environmentally plastic trait.

The first implication of this work concerns how organisms manage their mutational load when the Drift-Barrier prevents further genetic refinement of DNA repair machinery. Section 1 suggests that the realised μ does not simply rest at a fixed physiological baseline, but instead reflects the conditions under which natural selection has optimised immediate fitness components such as survival, growth rate, and fecundity. The striking convergence between the modal generation time of the *C. riparius* laboratory population and the thermal range of minimal ROS production which both converging with the natural reproductive season in temperate habitats, is consistent with this interpretation. Because selection favours the thermal and developmental conditions that maximise fitness, and because these same conditions happen to minimize the mutagenic burden imposed on existing repair systems, μ minimization emerges as a correlated byproduct of fitness optimization rather than as a direct target of selection. Crucially, however, this convergence is correlational rather than causally demonstrated: Chapters 1 and 2 were conducted under separate experimental conditions, and direct mechanistic integration has not yet been tested. Whether this pattern reflects a general principle operating across ectotherm life histories or a population-specific outcome of local adaptation in the German *C. riparius* population remains an open question requiring comparative, multi-stressor experimental designs.

The second implication concerns the mechanistic structure of mutation rate variation and its consequences for the molecular clock. Section 2 demonstrates that distinct environmental stressors act through mechanistically independent pathways, each generating characteristic molecular fingerprints in the mutational spectrum. Because these pathways respond differently to environmental and physiological conditions, substitution rates in natural populations reflect not simply the tempo of reproduction, but the shifting balance among multiple pathway-specific mutagenic inputs. This has direct consequences for phylogenetic inference: closely related lineages occupying distinct ecological regimes which are differing in thermal exposure, developmental tempo, or pollution history, will accrue substitutions at different rates not due to divergence time or selection, but due to proximate differences in mutagenic exposure. Molecular clock frameworks that assume rate variation scales predictably with generation time or metabolic rate will systematically

misattribute this pathway-driven heterogeneity, potentially biasing divergence time estimates and reconstructions of ancestral mutagenic environments.

The third implication is that standard laboratory estimates of μ, obtained under single-stressor, near-optimal conditions, likely underestimate the mutational and fitness costs experienced by wild populations. Because the mutagenic pathways operate independently, their contributions to the total germline mutation rate are additive: $\mu_{total} = \mu_{replication} + \mu_{oxidative} + \mu_{adduct}$. Consequently, adaptive optimization of one pathway confers no cross-protection against damage arising from others. As demonstrated in this thesis, the composition-specific antioxidant defences that buffer oxidative stress during thermal extremes provides no protection against BaP-induced adduct formation. Moreover, at environmentally relevant BaP concentrations, generalist repair pathways appear sufficient to prevent catastrophic mutational increases, yet the observed fitness declines suggest that maintaining these unoptimised defences imposes a substantial metabolic cost, though this energy allocation hypothesis requires direct transcriptomic validation. Taken together, these findings indicate that toxicological risk assessments and evolutionary forecasts based on single-stressor laboratory experiments will systematically underestimate the compounded mutational and fitness burdens experienced by populations facing simultaneous natural and anthropogenic challenges.

Taken together, this dissertation demonstrates that the germline mutation rate is not a passive reflection of evolutionary history, but a dynamic trait which mechanistically structured by the interaction between the organism's life history, its physiological environment, and the evolutionary novelty of the stressors it faces. To formally test the predictions arising from this framework, future research should prioritise three experimental directions. First, multi-stressor mutation accumulation designs are essential to determine whether pathway-specific mutational contributions are strictly additive or exhibit synergistic interactions, and whether the energy allocation costs of generalist defences can be directly measured through whole-transcriptome profiling. Second, field-based mutation accumulation studies across latitudinal gradients would test whether the convergence between life-history and thermal optima documented here is a general principle of ectotherm biology or a population-specific outcome of local adaptation. Third, developing phylogenetic models that explicitly account for pathway-specific mutational contributions, rather than assuming a single, uniform mutation rate would reduce systematic biases in molecular clock calibration and improve divergence time estimation across lineages with divergent ecologies. Ultimately, the central message of this thesis is this: understanding mutation rate variation requires knowing ***why it arises***, as a correlated byproduct of ecological fitness optimization operating beneath Drift-Barrier constraints, ***how it operates***, through mechanistically independent additive pathways that offer no cross-protection, and ***which populations*** are most exposed to those encountering evolutionarily novel stressors for which no optimised defence exists. Without this mechanistic foundation, neither evolutionary forecasting nor toxicological risk assessment can be fully grounded in biological reality.

References

Abdel-Shafy, H.I., Mansour, M.S.M., 2016. A review on polycyclic aromatic hydrocarbons: Source, environmental impact, effect on human health and remediation. Egypt. J. Pet. 25, 107–123. https://doi.org/10.1016/j.ejpe.2015.03.011

Abele, D., Heise, K., Pörtner, H.O., Puntarulo, S., 2002. Temperature-dependence of mitochondrial function and production of reactive oxygen species in the intertidal mud clam *Mya arenaria*. J. Exp. Biol. 205, 1831–1841. https://doi.org/10.1242/jeb.205.13.1831

Agarwal, I., Fuller, Z.L., Myers, S.R., Przeworski, M., 2023. Relating pathogenic loss-of-function mutations in humans to their evolutionary fitness costs. eLife. https://doi.org/10.7554/eLife.83172

Agrawal, A.F., Whitlock, M.C., 2012. Mutation Load: The Fitness of Individuals in Populations Where Deleterious Alleles Are Abundant. Annu. Rev. Ecol. Evol. Syst. 43, 115–135. https://doi.org/10.1146/annurev-ecolsys-110411-160257

Alexandrov, L.B., Nik-Zainal, S., Wedge, D.C., Aparicio, S.A.J.R., Behjati, S., Biankin, A.V., Bignell, G.R., Bolli, N., Borg, A., Børresen-Dale, A.-L., Boyault, S., Burkhardt, B., Butler, A.P., Caldas, C., Davies, H.R., Desmedt, C., Eils, R., Eyfjörd, J.E., Foekens, J.A., Greaves, M., Hosoda, F., Hutter, B., Ilicic, T., Imbeaud, S., Imielinski, M., Jäger, N., Jones, D.T.W., Jones, D., Knappskog, S., Kool, M., Lakhani, S.R., López-Otín, C., Martin, S., Munshi, N.C., Nakamura, H., Northcott, P.A., Pajic, M., Papaemmanuil, E., Paradiso, A., Pearson, J.V., Puente, X.S., Raine, K., Ramakrishna, M., Richardson, A.L., Richter, J., Rosenstiel, P., Schlesner, M., Schumacher, T.N., Span, P.N., Teague, J.W., Totoki, Y., Tutt, A.N.J., Valdés-Mas, R., van Buuren, M.M., van 't Veer, L., Vincent-Salomon, A., Waddell, N., Yates, L.R., Zucman-Rossi, J., Andrew Futreal, P., McDermott, U., Lichter, P., Meyerson, M., Grimmond, S.M., Siebert, R., Campo, E., Shibata, T., Pfister, S.M., Campbell, P.J., Stratton, M.R., 2013. Signatures of mutational processes in human cancer. Nature 500, 415–421. https://doi.org/10.1038/nature12477

Ames, B.N., 1983. Dietary carcinogens and anticarcinogens. Oxygen radicals and degenerative diseases. Science 221, 1256–1264. https://doi.org/10.1126/science.6351251

Angilletta Jr., M.J., 2009. Thermal Adaptation: A Theoretical and Empirical Synthesis. Oxford University Press. https://doi.org/10.1093/acprof:oso/9780198570875.001.1

Angilletta, M. J., 2009. . Therm. Adapt. Theor. Empir. Synth. Oxf. Univ. Press.

Aravind, L., Walker, D.R., Koonin, E.V., 1999. Conserved domains in DNA repair proteins and evolution of repair systems. Nucleic Acids Res. 27, 1223–1242. https://doi.org/10.1093/nar/27.5.1223

Bae, J.-H., Hyun Sung, B., Kim, H.-J., Park, S.-H., Lim, K.-M., Kim, M.-J., Lee, C.-R., Sohn, J.-H., 2015. An Efficient Genome-Wide Fusion Partner Screening System for Secretion of Recombinant Proteins in Yeast. Sci. Rep. 5, 12229. https://doi.org/10.1038/srep12229

Baer, C.F., Miyamoto, M.M., Denver, D.R., 2007. Mutation rate variation in multicellular eukaryotes: causes and consequences. Nat. Rev. Genet. 8, 619–631. https://doi.org/10.1038/nrg2158

Baird, W.M., Hooven, L.A., Mahadevan, B., 2005. Carcinogenic polycyclic aromatic hydrocarbon-DNA adducts and mechanism of action. Environ. Mol. Mutagen. 45, 106–114. https://doi.org/10.1002/em.20095

Balaban, R.S., Nemoto, S., Finkel, T., 2005. Mitochondria, oxidants, and aging. Cell 120, 483–495. https://doi.org/10.1016/j.cell.2005.02.001

Balmer, B., Ylitalo, G., Watwood, S., Quigley, B., Bolton, J., Mullin, K., Rosel, P., Rowles, T., Speakman, T., Wilcox, L., Zolman, E., Schwacke, L., 2019. Comparison of persistent organic pollutants (POPs) between small cetaceans in coastal and estuarine waters of the northern Gulf of Mexico. Mar. Pollut. Bull. 145, 239–247. https://doi.org/10.1016/j.marpolbul.2019.05.017

Barrett, R.D.H., Schluter, D., 2008. Adaptation from standing genetic variation. Trends Ecol. Evol. 23, 38–44. https://doi.org/10.1016/j.tree.2007.09.008

Barton, N.H., Turelli, M., 1989. Evolutionary quantitative genetics: how little do we know? Annu. Rev. Genet. 23, 337–370. https://doi.org/10.1146/annurev.ge.23.120189.002005

Beichman, A.C., Zhu, L., Harris, K., 2024. The Evolutionary Interplay of Somatic and Germline Mutation Rates. Annu. Rev. Biomed. Data Sci. 7, 83–105. https://doi.org/10.1146/annurev-biodatasci-102523-104225

Bell, G., Collins, S., 2008. Adaptation, extinction and global change. Evol. Appl. 1, 3–16. https://doi.org/10.1111/j.1752-4571.2007.00011.x

Bestion, E., Teyssier, A., Richard, M., Clobert, J., Cote, J., 2015. Live Fast, Die Young: Experimental Evidence of Population Extinction Risk due to Climate Change. PLOS Biol. 13, e1002281. https://doi.org/10.1371/journal.pbio.1002281

Bickham, J.W., Sandhu, S., Hebert, P.D.N., Chikhi, L., Athwal, R., 2000. Effects of chemical contaminants on genetic diversity in natural populations: implications for biomonitoring and ecotoxicology. Mutat. Res. Mutat. Res. 463, 33–51. https://doi.org/10.1016/S1383-5742(00)00004-1

Blais, C., Archibald, J.M., 2021. The past, present and future of the tree of life. Curr. Biol. 31, R314–R321. https://doi.org/10.1016/j.cub.2021.02.052

Bromham, L., 2011. The genome as a life-history character: why rate of molecular evolution varies between mammal species. Philos. Trans. R. Soc. B Biol. Sci. https://doi.org/10.1098/rstb.2011.0014

Bromham, L., 2009. Why do species vary in their rate of molecular evolution? Biol. Lett. 5, 401–404. https://doi.org/10.1098/rsbl.2009.0136

Bromham, L., Leys, R., 2005. Sociality and the rate of molecular evolution. Mol. Biol. Evol. 22, 1393–1402. https://doi.org/10.1093/molbev/msi133

Bromham, L., Penny, D., 2003. The modern molecular clock. Nat. Rev. Genet. 4, 216–224. https://doi.org/10.1038/nrg1020

Bromham, L., Rambaut, A., Harvey, P.H., 1996. Determinants of rate variation in mammalian DNA sequence evolution. J. Mol. Evol. 43, 610–621. https://doi.org/10.1007/BF02202109

Burczynski, M.E., McMillian, M., Ciervo, J., Li, L., Parker, J.B., Dunn, R.T., Hicken, S., Farr, S., Johnson, M.D., 2000. Toxicogenomics-based discrimination of toxic mechanism in

HepG2 human hepatoma cells. Toxicol. Sci. Off. J. Soc. Toxicol. 58, 399–415. https://doi.org/10.1093/toxsci/58.2.399

Bush, S.J., Goriely, A., 2023. Fine-tuning germline mutation rates across evolution. Trends Genet. 39, 598–599. https://doi.org/10.1016/j.tig.2023.05.001

Chatterjee, N., Walker, G.C., 2017. Mechanisms of DNA damage, repair and mutagenesis. Environ. Mol. Mutagen. 58, 235–263. https://doi.org/10.1002/em.22087

Coop, G., Bullaughey, K., Luca, F., Przeworski, M., 2008. The Timing of Selection at the Human FOXP2 Gene. Mol. Biol. Evol. 25, 1257–1259. https://doi.org/10.1093/molbev/msn091

Costantini, D., 2014. Oxidative Stress and Hormesis in Evolutionary Ecology and Physiology: A Marriage Between Mechanistic and Evolutionary Approaches. Springer Berlin Heidelberg, Berlin, Heidelberg. https://doi.org/10.1007/978-3-642-54663-1

Crow, J.F., 1970. Genetic Loads and the Cost of Natural Selection. Math. Top. Popul. Genet. https://doi.org/10.1007/978-3-642-46244-3_5

Cucchi, D., Gibson, A., Martin, S. a, n.d. The emerging relationship between metabolism and DNA repair. Cell Cycle 20, 943–959. https://doi.org/10.1080/15384101.2021.1912889

D'Autréaux, B., Toledano, M.B., 2007. ROS as signalling molecules: mechanisms that generate specificity in ROS homeostasis. Nat. Rev. Mol. Cell Biol. 8, 813–824. https://doi.org/10.1038/nrm2256

David, S.S., O'Shea, V.L., Kundu, S., 2007a. Base-excision repair of oxidative DNA damage. Nature 447, 941–950. https://doi.org/10.1038/nature05978

de Souza, A.M., da Silva Junior, F.C., Dantas, É.D., Galvão-Pereira, M.C., de Medeiros, S.R.B., Luchiari, A.C., 2025. Temperature effects on development and lifelong behavior in zebrafish. Sci. Total Environ. 973, 179172. https://doi.org/10.1016/j.scitotenv.2025.179172

de Vries, H., 1914. The Principles of the Theory of Mutation. Science 40, 77–84. https://doi.org/10.1126/science.40.1020.77

DeWitt, T.J., Scheiner, S.M. (Eds.), 2004. Phenotypic Plasticity: Functional and Conceptual Approaches. Oxford University Press. https://doi.org/10.1093/oso/9780195138962.001.0001

Dohnalová, H., Matoušková, E., Lankaš, F., 2024. Temperature-dependent elasticity of DNA, RNA, and hybrid double helices. Biophys. J. 123, 572–583. https://doi.org/10.1016/j.bpj.2024.01.032

Douzery, E., Lebreton, J.-D., Catzeflis, F.M., 1995. Testing the generation time hypothesis using DNA/DNA hybridization between artiodactyls. J. Evol. Biol. 8, 511–529. https://doi.org/10.1046/j.1420-9101.1995.8040511.x

Drake, J.W., 1991. A constant rate of spontaneous mutation in DNA-based microbes. Proc. Natl. Acad. Sci. https://doi.org/10.1073/pnas.88.16.7160

Drummond, A.J., Ho, S.Y.W., Phillips, M.J., Rambaut, A., 2006. Relaxed Phylogenetics and Dating with Confidence. PLOS Biol. 4, e88. https://doi.org/10.1371/journal.pbio.0040088

Ellegren, H., 2006. Characteristics, causes and evolutionary consequences of male-biased mutation. Proc. R. Soc. B Biol. Sci. 274, 1–10. https://doi.org/10.1098/rspb.2006.3720

Eyre-Walker, A., Woolfit, M., Phelps, T., 2006. The Distribution of Fitness Effects of New Deleterious Amino Acid Mutations in Humans. Genetics. https://doi.org/10.1534/genetics.106.057570

Fitzsimmons, W.J., Woods, R.J., McCrone, J.T., Woodman, A., Arnold, J.J., Yennawar, M., Evans, R., Cameron, C.E., Lauring, A.S., 2018. A speed-fidelity trade-off determines the mutation rate and virulence of an RNA virus. PLoS Biol. 16, e2006459. https://doi.org/10.1371/journal.pbio.2006459

Foucault, Q., Wieser, A., Waldvogel, A., Pfenninger, M., 2019. Establishing laboratory cultures and performing ecological and evolutionary experiments with the emerging model species *Chironomus riparius*. J. Appl. Entomol. 143, 584–592. https://doi.org/10.1111/jen.12606

Fridovich, I., 1995. Superoxide radical and superoxide dismutases. Annu. Rev. Biochem. 64, 97–112. https://doi.org/10.1146/annurev.bi.64.070195.000525

Gao, Z., Wyman, M.J., Sella, G., Przeworski, M., 2016. Interpreting the Dependence of Mutation Rates on Age and Time. PLOS Biol. 14, e1002355. https://doi.org/10.1371/journal.pbio.1002355

Geacintov, N.E., Broyde, S., Buterin, T., Naegeli, H., Wu, M., Yan, S., Patel, D.J., 2002. Thermodynamic and structural factors in the removal of bulky DNA adducts by the nucleotide excision repair machinery. Biopolymers 65, 202–210. https://doi.org/10.1002/bip.10239

Ghalambor, C.K., McKAY, J.K., Carroll, S.P., Reznick, D.N., 2007. Adaptive versus non-adaptive phenotypic plasticity and the potential for contemporary adaptation in new environments. Funct. Ecol. 21, 394–407. https://doi.org/10.1111/j.1365-2435.2007.01283.x

Gifford, D.R., Bhattacharyya, A., Geim, A., Marshall, E., Krašovec, R., Knight, C.G., 2024. Environmental and genetic influence on the rate and spectrum of spontaneous mutations in Escherichia coli. Microbiology 170, 001452. https://doi.org/10.1099/mic.0.001452

Gillooly, J.F., Brown, J.H., West, G.B., Savage, V.M., Charnov, E.L., 2001. Effects of Size and Temperature on Metabolic Rate. Science 293, 2248–2251. https://doi.org/10.1126/science.1061967

Green, R., Wang, H., Botchey, C., Zhang, S.N.N., Wadsworth, C., Tyrrell, F., Letton, J., McBain, A.J., Paszek, P., Krašovec, R., Knight, C.G., 2024. Collective peroxide detoxification determines microbial mutation rate plasticity in E. coli. PLOS Biol. 22, e3002711. https://doi.org/10.1371/journal.pbio.3002711

Gremer, J.R., 2023. Looking to the past to understand the future: linking evolutionary modes of response with functional and life history traits in variable environments. New Phytol. 237, 751–757. https://doi.org/10.1111/nph.18605

Hahm, J.Y., Park, J., Jang, E.-S., Chi, S.W., 2022. 8-Oxoguanine: from oxidative damage to epigenetic and epitranscriptional modification. Exp. Mol. Med. 54, 1626–1642. https://doi.org/10.1038/s12276-022-00822-z

Haldane, J.B.S., 1937. A Dialectical Account of Evolution. Sci. Soc. 1, 473–486. https://doi.org/10.1177/003682373700100403

Halligan, D.L., Keightley, P.D., 2009. Spontaneous Mutation Accumulation Studies in Evolutionary Genetics. Annu. Rev. Ecol. Evol. Syst. 40, 151–172. https://doi.org/10.1146/annurev.ecolsys.39.110707.173437

Halliwell, B., Gutteridge, J.M., 1990. Role of free radicals and catalytic metal ions in human disease: an overview. Methods Enzymol. 186, 1–85. https://doi.org/10.1016/0076-6879(90)86093-b

Halliwell, B., Gutteridge, J.M.C., 2015. Free Radicals in Biology and Medicine. Oxford University Press. https://doi.org/10.1093/acprof:oso/9780198717478.001.0001

Hendry, A. P., Schoen, D. J., Wolak, M. E., Reid, J. M., 2017. https://doi.org/10.1146/annurev-ecolsys-110316-023054

Hermisson, J., Pennings, P.S., 2017. Soft sweeps and beyond: understanding the patterns and probabilities of selection footprints under rapid adaptation. Methods Ecol. Evol. 8, 700–716. https://doi.org/10.1111/2041-210X.12808

Hess, M.T., Gunz, D., Luneva, N., Geacintov, N.E., Naegeli, H., 1997. Base pair conformation-dependent excision of benzo[a]pyrene diol epoxide-guanine adducts by human nucleotide excision repair enzymes. Mol. Cell. Biol. 17, 7069–7076. https://doi.org/10.1128/MCB.17.12.7069

Hewitt, O.H., Degnan, S.M., 2023. Antioxidant enzymes that target hydrogen peroxide are conserved across the animal kingdom, from sponges to mammals. Sci. Rep. 13, 2510. https://doi.org/10.1038/s41598-023-29304-6

Ho, S.Y.W., Duchêne, S., 2014. Molecular-clock methods for estimating evolutionary rates and timescales. Mol. Ecol. 23, 5947–5965. https://doi.org/10.1111/mec.12953

Hodgkinson, A., Eyre-Walker, A., 2011. Variation in the mutation rate across mammalian genomes. Nat. Rev. Genet. 12, 756–766. https://doi.org/10.1038/nrg3098

Hoeijmakers, J.H., 2001. Genome maintenance mechanisms for preventing cancer. Nature 411, 366–374. https://doi.org/10.1038/35077232

Hoffmann, A.A., Hercus, M.J., 2000. Environmental Stress as an Evolutionary Force. BioScience 50, 217–226. https://doi.org/10.1641/0006-3568(2000)050%255B0217:ESAAEF%255D2.3.CO;2

Hoffmann, A.A., Sgrò, C.M., 2011. Climate change and evolutionary adaptation. Nature 470, 479–485. https://doi.org/10.1038/nature09670

Holmstrup, M., Bindesbøl, A.-M., Oostingh, G.J., Duschl, A., Scheil, V., Köhler, H.-R., Loureiro, S., Soares, A.M.V.M., Ferreira, A.L.G., Kienle, C., Gerhardt, A., Laskowski, R., Kramarz, P.E., Bayley, M., Svendsen, C., Spurgeon, D.J., 2010. Interactions between effects of environmental chemicals and natural stressors: A review. Sci. Total Environ., Cumulative Stressors - Risk assessment of mixtures of chemicals and combinations of chemicals and natural stressors 408, 3746–3762. https://doi.org/10.1016/j.scitotenv.2009.10.067

Hopfield, J.J., 1974. Kinetic proofreading: a new mechanism for reducing errors in biosynthetic processes requiring high specificity. Proc. Natl. Acad. Sci. U. S. A. 71, 4135–4139. https://doi.org/10.1073/pnas.71.10.4135

Huang, R., Zhou, P.-K., 2021. DNA damage repair: historical perspectives, mechanistic pathways and clinical translation for targeted cancer therapy. Signal Transduct. Target. Ther. 6, 254. https://doi.org/10.1038/s41392-021-00648-7

Huey, R.B., Stevenson, R.D., 1979. Integrating Thermal Physiology and Ecology of Ectotherms: A Discussion of Approaches. Am. Zool. 19, 357–366. https://doi.org/10.1093/icb/19.1.357

Katju, V., Bergthorsson, U., 2019. Old Trade, New Tricks: Insights into the Spontaneous Mutation Process from the Partnering of Classical Mutation Accumulation Experiments with High-Throughput Genomic Approaches. Genome Biol. Evol. 11, 136–165. https://doi.org/10.1093/gbe/evy252

Keightley, P.D., Lynch, M., 2003. Toward a realistic model of mutations affecting fitness. Evol. Int. J. Org. Evol. 57, 683–685; discussion 686-689. https://doi.org/10.1111/j.0014-3820.2003.tb01561.x

Keightley, P.D., Trivedi, U., Thomson, M., Oliver, F., Kumar, S., Blaxter, M.L., 2009. Analysis of the genome sequences of three Drosophila melanogaster spontaneous mutation accumulation lines. Genome Res. 19, 1195–1201. https://doi.org/10.1101/gr.091231.109

Kimura, M., 1983. The Neutral Theory of Molecular Evolution. Cambridge University Press, Cambridge. https://doi.org/10.1017/CBO9780511623486

Kimura, M., 1968. Evolutionary Rate at the Molecular Level. Nature 217, 624–626. https://doi.org/10.1038/217624a0

Kirkwood, T.B.L., 1977. Evolution of ageing. Nature 270, 301–304. https://doi.org/10.1038/270301a0

Kirschner, M., Gerhart, J., 1998. Evolvability. Proc. Natl. Acad. Sci. 95, 8420–8427. https://doi.org/10.1073/pnas.95.15.8420

Kondrashov, A.S., 2003. Accumulation of Dobzhansky-Muller incompatibilities within a spatially structured population. Evol. Int. J. Org. Evol. 57, 151–153. https://doi.org/10.1111/j.0014-3820.2003.tb00223.x

Kondrashov, F.A., Kondrashov, A.S., 2010. Measurements of spontaneous rates of mutations in the recent past and the near future. Philos. Trans. R. Soc. B Biol. Sci. 365, 1169–1176. https://doi.org/10.1098/rstb.2009.0286

Kong, A., Frigge, M.L., Masson, G., Besenbacher, S., Sulem, P., Magnusson, G., Gudjonsson, S.A., Sigurdsson, A., Jonasdottir, Aslaug, Jonasdottir, Adalbjorg, Wong, W.S.W., Sigurdsson, G., Walters, G.B., Steinberg, S., Helgason, H., Thorleifsson, G., Gudbjartsson, D.F., Helgason, A., Magnusson, O.T., Thorsteinsdottir, U., Stefansson, K., 2012. Rate of de novo mutations and the importance of father's age to disease risk. Nature 488, 471–475. https://doi.org/10.1038/nature11396

Krašovec, R., Richards, H., Gifford, D.R., Hatcher, C., Faulkner, K.J., Belavkin, R.V., Channon, A., Aston, E., McBain, A.J., Knight, C.G., 2017. Spontaneous mutation rate is a plastic trait associated with population density across domains of life. PLOS Biol. 15, e2002731. https://doi.org/10.1371/journal.pbio.2002731

Kucab, J.E., Zou, X., Morganella, S., Joel, M., Nanda, A.S., Nagy, E., Gomez, C., Degasperi, A., Harris, R., Jackson, S.P., Arlt, V.M., Phillips, D.H., Nik-Zainal, S., 2019. A

Compendium of Mutational Signatures of Environmental Agents. Cell 177, 821-836.e16. https://doi.org/10.1016/j.cell.2019.03.001

Kunkel, T.A., 2004a. DNA replication fidelity. J. Biol. Chem. 279, 16895–16898. https://doi.org/10.1074/jbc.R400006200

Kunkel, T.A., 2004b. DNA replication fidelity. J. Biol. Chem. 279, 16895–16898. https://doi.org/10.1074/jbc.R400006200

Kunkel, T.A., Erie, D.A., 2015. Eukaryotic Mismatch Repair in Relation to DNA Replication. Annu. Rev. Genet. 49, 291–313. https://doi.org/10.1146/annurev-genet-112414-054722

Lande, R., Arnold, S.J., 1983. The Measurement of Selection on Correlated Characters. Evolution 37, 1210–1226. https://doi.org/10.1111/j.1558-5646.1983.tb00236.x

Lankoff, A., Sochacki, J., Spoof, L., Meriluoto, J., Wojcik, A., Wegierek, A., Verschaeve, L., 2008. Nucleotide excision repair impairment by nodularin in CHO cell lines due to ERCC1/XPF inactivation. Toxicol. Lett. 179, 101–107. https://doi.org/10.1016/j.toxlet.2008.04.008

Leibeling, D., Laspe, P., Emmert, S., 2006. Nucleotide excision repair and cancer. J. Mol. Histol. 37, 225–238. https://doi.org/10.1007/s10735-006-9041-x

Lesecque, Y., Keightley, P.D., Eyre-Walker, A., 2012. A Resolution of the Mutation Load Paradox in Humans. Genetics. https://doi.org/10.1534/genetics.112.140343

Lewin, L., Eyre-Walker, A., 2025. Estimates of the Mutation Rate per Year Can Explain Why the Molecular Clock Depends on Generation Time. Mol. Biol. Evol. 42, msaf069. https://doi.org/10.1093/molbev/msaf069

Lindahl, T., 1993. Instability and decay of the primary structure of DNA. Nature 362, 709–715. https://doi.org/10.1038/362709a0

Lundstedt, S., White, P.A., Lemieux, C.L., Lynes, K.D., Lambert, I.B., Oberg, L., Haglund, P., Tysklind, M., 2007. Sources, fate, and toxic hazards of oxygenated polycyclic aromatic hydrocarbons (PAHs) at PAH-contaminated sites. Ambio 36, 475–485. https://doi.org/10.1579/0044-7447(2007)36%255B475:sfatho%255D2.0.co;2

Luria, S.E., Delbrück, M., 1943. MUTATIONS OF BACTERIA FROM VIRUS SENSITIVITY TO VIRUS RESISTANCE. Genetics. https://doi.org/10.1093/genetics/28.6.491

Lushchak, V.I., Bagnyukova, T.V., Lushchak, O.V., Storey, J.M., Storey, K.B., 2005. Hypoxia and recovery perturb free radical processes and antioxidant potential in common carp (Cyprinus carpio) tissues. Int. J. Biochem. Cell Biol. 37, 1319–1330. https://doi.org/10.1016/j.biocel.2005.01.006

Lynch, M., 2020. The evolutionary scaling of cellular traits imposed by the drift barrier. Proc. Natl. Acad. Sci. 117, 10435–10444. https://doi.org/10.1073/pnas.2000446117

Lynch, M., 2012. Evolutionary layering and the limits to cellular perfection. Proc. Natl. Acad. Sci. 109, 18851–18856. https://doi.org/10.1073/pnas.1216130109

Lynch, M., 2011. The Lower Bound to the Evolution of Mutation Rates. Genome Biol. Evol. https://doi.org/10.1093/gbe/evr066

Lynch, M., 2010. Evolution of the mutation rate. Trends Genet. TIG 26, 345–352. https://doi.org/10.1016/j.tig.2010.05.003

Lynch, M., Ackerman, M.S., Gout, J.-F., Long, H., Sung, W., Thomas, W.K., Foster, P.L., 2016. Genetic drift, selection and the evolution of the mutation rate. Nat. Rev. Genet. 17, 704–714. https://doi.org/10.1038/nrg.2016.104

Lynch, M., Blanchard, J., Houle, D., Kibota, T., Schultz, S., Vassilieva, L., Willis, J., 1999. Perspective: Spontaneous Deleterious Mutation. Evolution 53, 645–663. https://doi.org/10.1111/j.1558-5646.1999.tb05361.x

Lynch, M., Marinov, G.K., 2015. The bioenergetic costs of a gene. Proc. Natl. Acad. Sci. U. S. A. 112, 15690–15695. https://doi.org/10.1073/pnas.1514974112

Machado, R.A.R., Muller, A., Hiltmann, A., Bhat, A.H., Půža, V., Malan, A.P., Castaneda-Alvarez, C., San-Blas, E., Duncan, L.W., Shapiro-Ilan, D., Karimi, J., Lalramliana, Lalramnghaki, H.C., Baimey, H., 2025. Genome-wide analyses provide insights into genetic variation, phylo- and co-phylogenetic relationships, and biogeography of the entomopathogenic nematode genus *Heterorhabditis*. Mol. Phylogenet. Evol. 204, 108284. https://doi.org/10.1016/j.ympev.2025.108284

Maharjan, R.P., Ferenci, T., 2017. A shifting mutational landscape in 6 nutritional states: Stress-induced mutagenesis as a series of distinct stress input-mutation output relationships. PLoS Biol. 15, e2001477. https://doi.org/10.1371/journal.pbio.2001477

Makarova, K.S., Aravind, L., Koonin, E.V., 1999. A superfamily of archaeal, bacterial, and eukaryotic proteins homologous to animal transglutaminases. Protein Sci. Publ. Protein Soc. 8, 1714–1719. https://doi.org/10.1110/ps.8.8.1714

Maki, H., 2002. Origins of spontaneous mutations: specificity and directionality of base-substitution, frameshift, and sequence-substitution mutageneses. Annu. Rev. Genet. 36, 279–303. https://doi.org/10.1146/annurev.genet.36.042602.094806

Mao, P., Wyrick, J.J., 2019. Organization of DNA Damage, Excision Repair, and Mutagenesis in Chromatin: a Genomic Perspective. DNA Repair 81, 102645. https://doi.org/10.1016/j.dnarep.2019.102645

Marteijn, J.A., Lans, H., Vermeulen, W., Hoeijmakers, J.H.J., 2014. Understanding nucleotide excision repair and its roles in cancer and ageing. Nat. Rev. Mol. Cell Biol. 15, 465–481. https://doi.org/10.1038/nrm3822

Martin, A.P., Palumbi, S.R., 1993. Body size, metabolic rate, generation time, and the molecular clock. Proc. Natl. Acad. Sci. U. S. A. 90, 4087–4091. https://doi.org/10.1073/pnas.90.9.4087

Messer, P.W., Petrov, D.A., 2013. Population genomics of rapid adaptation by soft selective sweeps. Trends Ecol. Evol. 28, 659–669. https://doi.org/10.1016/j.tree.2013.08.003

Metcalfe, N.B., Alonso-Alvarez, C., 2010. Oxidative stress as a life-history constraint: the role of reactive oxygen species in shaping phenotypes from conception to death. Funct. Ecol. 24, 984–996. https://doi.org/10.1111/j.1365-2435.2010.01750.x

Meyer, J.N., Di Giulio, R.T., 2003. Heritable Adaptation and Fitness Costs in Killifish (fundulus Heteroclitus) Inhabiting a Polluted Estuary. Ecol. Appl. 13, 490–503. https://doi.org/10.1890/1051-0761(2003)013%255B0490:HAAFCI%255D2.0.CO;2

Miller, G., Suzuki, N., Ciftci-Yilmaz, S., Mittler, R., 2010. Reactive oxygen species homeostasis and signalling during drought and salinity stresses. Plant Cell Environ. 33, 453–467. https://doi.org/10.1111/j.1365-3040.2009.02041.x

Moczek, A.P., Sultan, S., Foster, S., Ledón-Rettig, C., Dworkin, I., Nijhout, H.F., Abouheif, E., Pfennig, D.W., 2011. The role of developmental plasticity in evolutionary innovation. Proc. Biol. Sci. 278, 2705–2713. https://doi.org/10.1098/rspb.2011.0971

Monaghan, P., Metcalfe, N.B., Torres, R., 2009. . Oxidative Stress Mediat. Life Hist. Trade-Mech. Meas. Interpret. Ecol. Lett. 121 75-92.

Monaghan, P., Metcalfe, N.B., Torres, R., 2009. Oxidative stress as a mediator of life history trade-offs: mechanisms, measurements and interpretation. Ecol. Lett. 12, 75–92. https://doi.org/10.1111/j.1461-0248.2008.01258.x

Monroe, J.G., 2023. Potential and limits of (mal)adaptive mutation rate plasticity in plants. New Phytol. 237, 2020–2026. https://doi.org/10.1111/nph.18640

Murphy, M.P., 2009. How mitochondria produce reactive oxygen species. Biochem. J. 417, 1–13. https://doi.org/10.1042/BJ20081386

Nacci, D.E., Champlin, D., Jayaraman, S., 2010. Adaptation of the Estuarine Fish Fundulus heteroclitus (Atlantic Killifish) to Polychlorinated Biphenyls (PCBs). Estuaries Coasts 33, 853–864.

Nathan, C., Cunningham-Bussel, A., 2013. Beyond oxidative stress: an immunologist's guide to reactive oxygen species. Nat. Rev. Immunol. 13, 349–361. https://doi.org/10.1038/nri3423

Nauman, C.H., Schairer, L.A., Sparrow, A.H., 1978. Influence of temperature on spontaneous and radiation-induced somatic mutations in tradescantia stamen hairs. Mutat. Res. 50, 207–218. https://doi.org/10.1016/0027-5107(78)90025-8

Nebert, D.W., Dalton, T.P., 2006. The role of cytochrome P450 enzymes in endogenous signalling pathways and environmental carcinogenesis. Nat. Rev. Cancer 6, 947–960. https://doi.org/10.1038/nrc2015

Niccum, B.A., Lee, H., MohammedIsmail, W., Tang, H., Foster, P.L., 2018. The Spectrum of Replication Errors in the Absence of Error Correction Assayed Across the Whole Genome of Escherichia coli. Genetics 209, 1043–1054. https://doi.org/10.1534/genetics.117.300515

Nieto-Blázquez, M.E., Caliendo, C., Pettrich, L.C., Waldvogel, A.-M., Pfenninger, M., 2025. Influence of geography, seasonality and experimental selection on Chironomus riparius recombination rates. https://doi.org/10.1101/2025.06.04.657814

OECD, 2010. Test No. 233: Sediment-Water Chironomid Life-Cycle Toxicity Test Using Spiked Water or Spiked Sediment. OECD Guidel. Test. Chem. Sect. 2. https://doi.org/10.1787/9789264090910-en

Ohta, T., 1995. Synonymous and nonsynonymous substitutions in mammalian genes and the nearly neutral theory. J. Mol. Evol. 40, 56–63. https://doi.org/10.1007/BF00166595

Ohta, T., 1992. The Nearly Neutral Theory of Molecular Evolution. Annu. Rev. Ecol. Syst. 23, 263–286.

Oman, M., Alam, A., Ness, R.W., 2022. How Sequence Context-Dependent Mutability Drives Mutation Rate Variation in the Genome. Genome Biol. Evol. https://doi.org/10.1093/gbe/evac032

Oppold, A.-M., Pedrosa, J.A.M., Bálint, M., Diogo, J.B., Ilkova, J., Pestana, J.L.T., Pfenninger, M., 2016. Support for the evolutionary speed hypothesis from intraspecific population genetic data in the non-biting midge *Chironomus riparius*. Proc. R. Soc. B Biol. Sci. 283, 20152413. https://doi.org/10.1098/rspb.2015.2413

Oppold, A.-M., Pfenninger, M., 2017. Direct estimation of the spontaneous mutation rate by short-term mutation accumulation lines in Chironomus riparius. Evol. Lett. 1, 86–92. https://doi.org/10.1002/evl3.8

Oziolor, E.M., Reid, N.M., Yair, S., Lee, K.M., Guberman VerPloeg, S., Bruns, P.C., Shaw, J.R., Whitehead, A., Matson, C.W., 2019. Adaptive introgression enables evolutionary rescue from extreme environmental pollution. Science 364, 455–457. https://doi.org/10.1126/science.aav4155

Pak, M., 2008. Stochastic stability and time-dependent mutations. Games Econ. Behav., Special Issue in Honor of Michael B. Maschler 64, 650–665. https://doi.org/10.1016/j.geb.2008.01.010

Parsons, D.W., Wang, T.-L., Samuels, Y., Bardelli, A., Cummins, J.M., DeLong, L., Silliman, N., Ptak, J., Szabo, S., Willson, J.K.V., Markowitz, S., Kinzler, K.W., Vogelstein, B., Lengauer, C., Velculescu, V.E., 2005. Mutations in a signalling pathway. Nature 436, 792–792. https://doi.org/10.1038/436792a

Pedrosa, J., Campos, D., Cocchiararo, B., Nowak, C., Soares, A.M.V.M., Barata, C., L T Pestana, J., 2017. Evolutionary consequences of historical metal contamination for natural populations of Chironomus riparius (Diptera: Chironomidae). Ecotoxicology 26, 534–546. https://doi.org/10.1007/s10646-017-1784-5

Petljak, M., Alexandrov, L.B., 2016. Understanding mutagenesis through delineation of mutational signatures in human cancer. Carcinogenesis 37, 531–540. https://doi.org/10.1093/carcin/bgw055

Pettrich, L.C., Waldvogel, A.-M., 2025. The interplay of recombination landscape and a transposable element in European populations of Chironomus riparius. BMC Genomics 26, 1002. https://doi.org/10.1186/s12864-025-12130-7

Pfeifer, G.P., Denissenko, M.F., Olivier, M., Tretyakova, N., Hecht, S.S., Hainaut, P., 2002. Tobacco smoke carcinogens, DNA damage and p53 mutations in smoking-associated cancers. Oncogene 21, 7435–7451. https://doi.org/10.1038/sj.onc.1205803

Pfeiffer, J.K., Kirkegaard, K., 2005. Increased fidelity reduces poliovirus fitness and virulence under selective pressure in mice. PLoS Pathog. 1, e11. https://doi.org/10.1371/journal.ppat.0010011

Pfenninger, M., Nieto-Blazquez, M.-E., Schell, T., Geiss, M., Bulut, B., Eberhardt, L., Feldmeyer, B., 2025. Pervasive and dynamic release of Cryptic Genetic Variation in Chironomus riparius: Rethinking adaptation in fluctuating environments. https://doi.org/10.1101/2025.07.01.661462

Pfenninger, M., Nowak, C., 2008. Reproductive Isolation and Ecological Niche Partition among Larvae of the Morphologically Cryptic Sister Species Chironomus riparius and C. piger. PLOS ONE 3, e2157. https://doi.org/10.1371/journal.pone.0002157

Pigliucci, M., Murren, C.J., Schlichting, C.D., 2006. Phenotypic plasticity and evolution by genetic assimilation. J. Exp. Biol. 209, 2362–2367. https://doi.org/10.1242/jeb.02070

Poetsch, A.R., 2020. The genomics of oxidative DNA damage, repair, and resulting mutagenesis. Comput. Struct. Biotechnol. J. 18, 207–219. https://doi.org/10.1016/j.csbj.2019.12.013

Pohl, F.M., Thomae, R., Karst, A., 1982. Temperature dependence of the activity of DNA-modifying enzymes: endonucleases and DNA ligase. Eur. J. Biochem. 123, 141–152. https://doi.org/10.1111/j.1432-1033.1982.tb06510.x

Pörtner, H.O., 2002. Climate variations and the physiological basis of temperature dependent biogeography: systemic to molecular hierarchy of thermal tolerance in animals. Comp. Biochem. Physiol. A. Mol. Integr. Physiol. 132, 739–761. https://doi.org/10.1016/s1095-6433(02)00045-4

Prakash, S., Johnson, R.E., Prakash, L., 2005. Eukaryotic translesion synthesis DNA polymerases: specificity of structure and function. Annu. Rev. Biochem. 74, 317–353. https://doi.org/10.1146/annurev.biochem.74.082803.133250

Pyo, A.G.T., Yu, Q., Merkenschlager, J., Wingreen, N.S., 2025. Evolutionary Benefits of Fitness-Dependent Mutation Rates. Phys. Rev. Lett. 135, 048402. https://doi.org/10.1103/szpk-sx1c

Raynes, Y., Sniegowski, P.D., 2014. Experimental evolution and the dynamics of genomic mutation rate modifiers. Heredity 113, 375–380. https://doi.org/10.1038/hdy.2014.49

Reid, N.M., Proestou, D.A., Clark, B.W., Warren, W.C., Colbourne, J.K., Shaw, J.R., Karchner, S.I., Hahn, M.E., Nacci, D., Oleksiak, M.F., Crawford, D.L., Whitehead, A., 2016. The genomic landscape of rapid repeated evolutionary adaptation to toxic pollution in wild fish. Science 354, 1305–1308. https://doi.org/10.1126/science.aah4993

Relyea, R.A., 2009. A cocktail of contaminants: how mixtures of pesticides at low concentrations affect aquatic communities. Oecologia 159, 363–376. https://doi.org/10.1007/s00442-008-1213-9

Rhee, S.G., Chae, H.Z., Kim, K., 2005. Peroxiredoxins: a historical overview and speculative preview of novel mechanisms and emerging concepts in cell signaling. Free Radic. Biol. Med. 38, 1543–1552. https://doi.org/10.1016/j.freeradbiomed.2005.02.026

Roff, D. A., 2002. . Life Hist. Evol. Sinauer Assoc.

Sale, J.E., Lehmann, A.R., Woodgate, R., 2012. Y-family DNA polymerases and their role in tolerance of cellular DNA damage. Nat. Rev. Mol. Cell Biol. 13, 141–152. https://doi.org/10.1038/nrm3289

Sari, A., 2026. Intraspecific genetic diversity and population structure of the non-biting midge Chironomus riparius (Diptera: Chironomidae) in Türkiye. Zool. Middle East 72, 36–50. https://doi.org/10.1080/09397140.2025.2599002

Schärer, O. D., 2013. https://doi.org/10.1101/cshperspect.a012609

Schärer, O.D., 2003. Chemistry and Biology of DNA Repair. Angew. Chem. Int. Ed. 42, 2946–2974. https://doi.org/10.1002/anie.200200523

Schiffman, J.S., Ralph, P.L., 2022. System drift and speciation. Evolution 76, 236–251. https://doi.org/10.1111/evo.14356

Schrider, D.R., Houle, D., Lynch, M., Hahn, M.W., 2013. Rates and Genomic Consequences of Spontaneous Mutational Events in *Drosophila melanogaster*. Genetics 194, 937–954. https://doi.org/10.1534/genetics.113.151670

Shibutani, S., Takeshita, M., Grollman, A.P., 1991. Insertion of specific bases during DNA synthesis past the oxidation-damaged base 8-oxodG. Nature 349, 431–434. https://doi.org/10.1038/349431a0

Shokolenko, I., Venediktova, N., Bochkareva, A., Wilson, G.L., Alexeyev, M.F., 2009. Oxidative stress induces degradation of mitochondrial DNA. Nucleic Acids Res. 37, 2539–2548. https://doi.org/10.1093/nar/gkp100

Sies, H., 2017. Hydrogen peroxide as a central redox signaling molecule in physiological oxidative stress: Oxidative eustress. Redox Biol. 11, 613–619. https://doi.org/10.1016/j.redox.2016.12.035

Sih, A., Ferrari, M.C.O., Harris, D.J., 2011. Evolution and behavioural responses to human-induced rapid environmental change. Evol. Appl. 4, 367–387. https://doi.org/10.1111/j.1752-4571.2010.00166.x

Sniegowski, P., 1997. Evolution: Setting the mutation rate. Curr. Biol. 7, R487–R488. https://doi.org/10.1016/S0960-9822(06)00244-2

Sniegowski, P.D., Gerrish, P.J., Johnson, T., Shaver, A., 2000. The evolution of mutation rates: separating causes from consequences. BioEssays News Rev. Mol. Cell. Dev. Biol. 22, 1057–1066. https://doi.org/10.1002/1521-1878(200012)22:12%253C1057::AID-BIES3%253E3.0.CO;2-W

Stearns, S. C., 1992. . Evol. Life Hist. Oxf. Univ. Press.

Stearns, S.C., 1980. A New View of Life-History Evolution. Oikos 35, 266–281. https://doi.org/10.2307/3544434

Streisinger, G., Okada, Y., Emrich, J., Newton, J., Tsugita, A., Terzaghi, E., Inouye, M., 1966. Frameshift mutations and the genetic code. This paper is dedicated to Professor Theodosius Dobzhansky on the occasion of his 66th birthday. Cold Spring Harb. Symp. Quant. Biol. 31, 77–84. https://doi.org/10.1101/sqb.1966.031.01.014

Sung, W., Ackerman, M.S., Miller, S.F., Doak, T.G., Lynch, M., 2012. Drift-barrier hypothesis and mutation-rate evolution. Proc. Natl. Acad. Sci. https://doi.org/10.1073/pnas.1216223109

Surai, P.F., Fisinin, V.I., Karadas, F., 2016. Antioxidant systems in chick embryo development. Part 1. Vitamin E, carotenoids and selenium. Anim. Nutr. 2, 1–11. https://doi.org/10.1016/j.aninu.2016.01.001

Taus, T., Futschik, A., Schlötterer, C., 2017. Quantifying Selection with Pool-Seq Time Series Data. Mol. Biol. Evol. 34, 3023–3034. https://doi.org/10.1093/molbev/msx225

Thomas, J.A., Welch, J.J., Lanfear, R., Bromham, L., 2010. A Generation Time Effect on the Rate of Molecular Evolution in Invertebrates. Mol. Biol. Evol. 27, 1173–1180. https://doi.org/10.1093/molbev/msq009

Tomanek, L., 2015. Proteomic responses to environmentally induced oxidative stress. J. Exp. Biol. 218, 1867–1879. https://doi.org/10.1242/jeb.116475

Turrens, J.F., 2003. Mitochondrial formation of reactive oxygen species. J. Physiol. 552, 335–344. https://doi.org/10.1113/jphysiol.2003.049478

Uchimura, A., Higuchi, M., Minakuchi, Y., Ohno, M., Toyoda, A., Fujiyama, A., Miura, I., Wakana, S., Nishino, J., Yagi, T., 2015. Germline mutation rates and the long-term phenotypic effects of mutation accumulation in wild-type laboratory mice and mutator mice. Genome Res. 25, 1125–1134. https://doi.org/10.1101/gr.186148.114

Verberk, W.C.E.P., Overgaard, J., Ern, R., Bayley, M., Wang, T., Boardman, L., Terblanche, J.S., 2016. Does oxygen limit thermal tolerance in arthropods? A critical review of current evidence. Comp. Biochem. Physiol. A. Mol. Integr. Physiol. 192, 64–78. https://doi.org/10.1016/j.cbpa.2015.10.020

Via, S., Gomulkiewicz, R., De Jong, G., Scheiner, S.M., Schlichting, C.D., Van Tienderen, P.H., 1995. Adaptive phenotypic plasticity: consensus and controversy. Trends Ecol. Evol. 10, 212–217. https://doi.org/10.1016/S0169-5347(00)89061-8

Vicentini, M., Morais, G.S., Rebechi-Baggio, D., Richardi, V.S., Santos, G.S., Cestari, M.M., Navarro-Silva, M.A., 2017. Benzo(a)pyrene Exposure Causes Genotoxic and Biochemical Changes in the Midge Larvae of Chironomus sancticaroli Strixino & Strixino (Diptera: Chironomidae). Neotrop. Entomol. 46, 658–665. https://doi.org/10.1007/s13744-017-0505-3

Vogt, C., Pupp, A., Nowak, C., Jagodzinski, L., Baumann, J., Jost, D., Oetken, M., Oehlmann, J., 2007. Interaction between genetic diversity and temperature stress on life-cycle parameters and genetic variability in midge Chironomus riparius populations. Clim. Res. 33, 207–214. https://doi.org/10.3354/cr033207

Waldvogel, A.-M., Pfenninger, M., 2021. Temperature dependence of spontaneous mutation rates. Genome Res. 31, 1582–1589. https://doi.org/10.1101/gr.275168.120

Wallace, S.S., 2014. Base excision repair: A critical player in many games. DNA Repair 19, 14–26. https://doi.org/10.1016/j.dnarep.2014.03.030

Wang, Y., Obbard, D.J., 2023. Experimental estimates of germline mutation rate in eukaryotes: a phylogenetic meta-analysis. Evol. Lett. 7, 216–226. https://doi.org/10.1093/evlett/qrad027

Waters, L.S., Minesinger, B.K., Wiltrout, M.E., D'Souza, S., Woodruff, R.V., Walker, G.C., 2009. Eukaryotic translesion polymerases and their roles and regulation in DNA damage tolerance. Microbiol. Mol. Biol. Rev. MMBR 73, 134–154. https://doi.org/10.1128/MMBR.00034-08

Wei, W., Ho, W.-C., Behringer, M.G., Miller, S.F., Bcharah, G., Lynch, M., 2022. Rapid evolution of mutation rate and spectrum in response to environmental and population-genetic challenges. Nat. Commun. 13, 4752. https://doi.org/10.1038/s41467-022-32353-6

Whitehead, A., Roach, J.L., Zhang, S., Galvez, F., 2011. Genomic mechanisms of evolved physiological plasticity in killifish distributed along an environmental salinity gradient. Proc. Natl. Acad. Sci. 108, 6193–6198. https://doi.org/10.1073/pnas.1017542108

Wong, H.-S., Dighe, P.A., Mezera, V., Monternier, P.-A., Brand, M.D., 2017. Production of superoxide and hydrogen peroxide from specific mitochondrial sites under different bioenergetic conditions. J. Biol. Chem. 292, 16804–16809. https://doi.org/10.1074/jbc.R117.789271

Xue, W., Warshawsky, D., 2005. Metabolic activation of polycyclic and heterocyclic aromatic hydrocarbons and DNA damage: A review. Toxicol. Appl. Pharmacol. 206, 73–93. https://doi.org/10.1016/j.taap.2004.11.006

Yeh, P. J., Price, T. D., 2004. https://doi.org/10.1086/423825

Zuckerkandl, E., Pauling, L., 1965. Molecules as documents of evolutionary history. J. Theor. Biol. 8, 357–366. https://doi.org/10.1016/0022-5193(65)90083-4